

Justus-Liebig-Universität Giessen
Institut für Anorganische und Analytische Chemie



Investigations on Reactions of Metal Complexes with N-donor Ligands towards Hydrogen Peroxide

Inaugural-Dissertation

Zur Erlangung des Doktorgrades der Naturwissenschaften im Fachbereich Biologie
und Chemie der Justus-Liebig-Universität Gießen

vorgelegt von

Thomas Nebe

aus

Eisenach

Erstgutachter:

Professor Dr. Siegfried Schindler

Zweitgutachter:

Professor Dr. Richard Göttlich

Datum der Abgabe der Dissertation im Prüfungsamt:

Datum der mündlichen Prüfung:

For my family

ACKNOWLEDGEMENTS

Acknowledgements

The work described in this thesis was carried out between October 2005 and February 2010 at the Institute for Inorganic and Analytical Chemistry at the Justus-Liebig University of Gießen under supervision of Professor Dr. Siegfried Schindler.

I would like to thank Professor Dr. Siegfried Schindler for his excellent guidance, the useful scientific discussions and the financial support during these years.

Furthermore I wish to thank my colleagues, friends and labmates Alexander Beitat, Tobias Hoppe, Dr. Sabrina Turba, Dr. Anja Henß, Jörg Müller, Sandra Kisslinger, Dr. Christian Würtele, Sabrina Schäfer, Jenny Friebe, Dr. Jörg Astner, Cornelius Brombach, Janina Heck, Janine Will, Jonathan Becker, Lars Valentin, Sabine Löw, Frank Mehlich, Janine Capell, Melanie Jopp, Dr. Jing-Yuan Xu and Dr. Ildikó Kerezsi for the pleasant atmosphere in this research group.

I am very grateful to Alexander Beitat, Dr. Christian Würtele and Günther Koch for their great support in the handling of the X-ray crystallographic measurements.

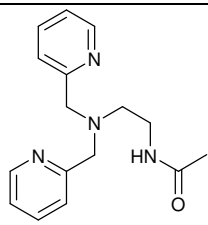
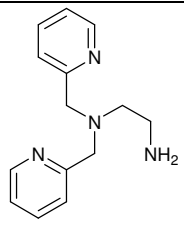
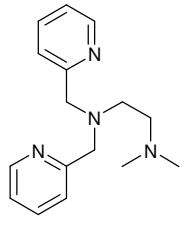
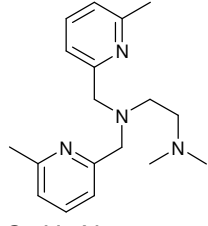
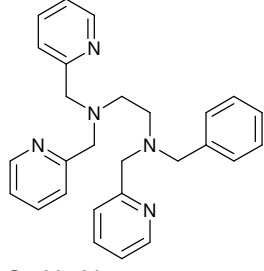
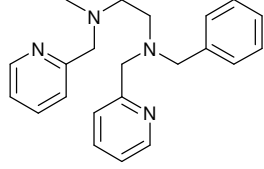
Special thanks go to Dr. Carlos Dücker-Benfer from University of Erlangen-Nürnberg for his great help with high pressure kinetic studies.

I also want to thank all the people of the chemical department at the Justus-Liebig University of Gießen for their support of my work.

Very special thanks go to my wife Julia and my family for their great support and endless patience during all this years.

LIGANDS USED

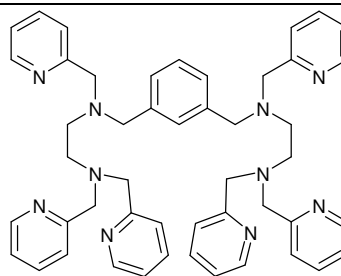
Ligands Used

Name	Abbreviation	Structure and Formula	Molar Mass [g mol ⁻¹]
N-Acetyl-N',N'-bis(2-pyridylmethyl)ethylenediamine	acetyl-uns-penp	 <chem>CC(=O)NCCN(Cc1ccncc1)Cc2ccncc2</chem> $C_{16}H_{20}N_4O$	284.36
N,N-bis(2-pyridylmethyl)ethylenediamine	uns-penp	 <chem>NCCN(Cc1ccncc1)Cc2ccncc2</chem> $C_{14}H_{18}N_4$	242.32
N,N-Dimethyl-N',N'-bis(2-pyridylmethyl)ethylenediamine	Me ₂ -uns-penp	 <chem>CN(C)CCN(Cc1ccncc1)Cc2ccncc2</chem> $C_{16}H_{22}N_4$	270.37
N,N-Dimethyl-N',N'-bis(6-methyl-2-pyridylmethyl)ethylenediamine	Me ₄ -uns-penp	 <chem>CN(C)CCN(Cc1cc(C)cn1)Cc2cc(C)cn2</chem> $C_{18}H_{26}N_4$	298.43
N-benzyl-N,N',N'-tris(2-pyridylmethyl)ethylenediamine	bztpen	 <chem>C1=CC=C(C=C1)CN(Cc2ccncc2)Cc3ccncc3</chem> $C_{27}H_{29}N_5$	423.55
N-methyl-N,N'-N'-tris(2-pyridylmethyl)ethylenediamine	metpen	 <chem>CN(Cc1ccncc1)CCN(Cc2ccncc2)Cc3ccncc3</chem> $C_{22}H_{26}N_4$	346.47

LIGANDS USED

1,3-bis(N,N,N'-tris(2-pyridylmethyl-))
diaminoethyl-benzene

bz-b-tpen

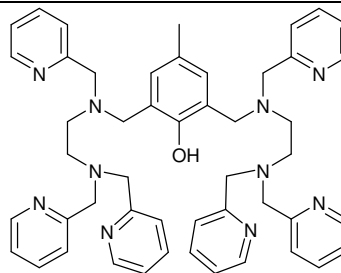


768.99

$C_{48}H_{52}N_{10}$

2,6-bis(N,N,N'-tris(2-pyridylmethyl-))
diaminoethyl-4-methyl-phenol

pC-b-tpen



799.02

$C_{49}H_{54}N_{10}O$

ABBREVIATIONS

Abbreviations

ATR	attenuated total reflectance
BPh ₄	tetraphenylborate
bz	benzyl
d	doublet (NMR)
DNA	deoxyribonucleic acid
δ	chemical shift (NMR)
e. g.	for example (Latin: <i>exempli gratia</i>)
ESI	electro spray ionization
EXAFS	extended X-ray absorption fine structure
EtOH	ethanol
IR	infrared
m	multiplet
MeOH	methanol
MeCN	acetonitrile
me	methyl
MS	mass spectrometry
NAD(P)H	nicotinamide adenine dinucleotide phosphate
NMR	nuclear magnetic resonance
OAc	acetate
OTf	triflate (Trifluoromethanesulfonate)
pC	para cresole
RNR R2 X	ribonucleotide reductase intermediate X
RT	room temperature
s	singlet (NMR)
t	triplet (NMR)
TauD J	α-ketoglutarate dioxygenase intermediate J
UV/Vis	ultraviolet-visible

TABLE OF CONTENTS

Table of Contents

Acknowledgements	I
Ligands Used.....	II
Abbreviations.....	IV
Table of Contents	V
Table of Figures.....	XII
1 Introduction.....	1
1.1 Motivation.....	1
1.2 The Element Cobalt.....	1
1.3 Cobalt–Oxygen Complexes.....	2
1.4 The Element Iron.....	5
1.5 Heme Iron Proteins	6
1.6 Methane Monooxygenase	7
1.7 “Iron-Oxygen” Adduct Complexes	9
1.8 Dinuclear Iron Peroxido Complexes.....	10
1.9 Tripodal Tetradentate Ligands and Derivatives.....	12
1.10 The Ligand Uns-penp.....	14
1.11 Mononuclear Iron Peroxido Complexes	17
1.12 Iron Oxido Complexes.....	20
1.13 Model Complexes for Methane Monooxygenase	21
1.14 Projects	23
1.14.1 Reactions of Metal Complexes with the Ligand bztpen and Derivatives towards Hydrogen Peroxide	23
1.14.2 Kinetic Investigations on Hydroperoxido Complex Formation	24
1.14.3 Metal Complexes with Uns-penp and Derivatives	24
2 Theory of Reaction Kinetics.....	26
2.1 The Reaction Rate	26

TABLE OF CONTENTS

2.2	First Order Dependence.....	27
2.3	Second Order Dependence.....	28
2.4	Reactions in Equilibria.....	29
2.5	Consecutive Reactions.....	29
2.6	Determination of the Activation Enthalpy ΔH^\ddagger , the Activation Entropy ΔS^\ddagger , and the Activation Volume ΔV^\ddagger	31
3	A reinvestigation of the formation of mononuclear Fe(III) peroxides using high pressure kinetics.....	33
3.1	Abstract.....	33
3.2	Introduction	33
3.3	Experimental	35
3.3.1	Materials and Techniques	35
3.3.2	Kinetic Measurements.....	36
3.3.3	X-ray Crystallography.....	36
3.3.4	Syntheses	37
3.3.4.1	Bztpen (1)	37
3.3.4.2	[Fe(bztpen)(OAc)]BPh ₄ (2).....	37
3.3.4.3	[Co(bztpen)Cl]BF ₄ (3).....	37
3.3.4.4	[Co(metpen)Cl]SbF ₆ (4)	37
3.3.4.5	[Co(bztpen)(OAc)]BPh ₄ (5)	38
3.3.4.6	[Fe(bztpen)NO](triflate) ₂ (6)	38
3.4	Results and Discussion.....	38
3.4.1	Syntheses, Characterization and Reactivity of Complexes	38
3.4.1.1	Reactivity towards Nitric Oxide	43
3.4.1.2	Kinetic Studies	45
3.5	Conclusion	48
4	Supporting Information for Chapter 3 and unpublished Results	49
4.1	Supporting Material for Chapter 3	49
4.1.1	Oxidation of [Fe(bztpen)Cl]ClO ₄	49

TABLE OF CONTENTS

4.1.2	Formation of $[\text{Fe}(\text{bztpen})\text{OOH}]^{2+}$	51
4.1.3	High Pressure Kinetics.....	53
4.2	Unpublished Results related to Chapter 3.....	55
4.2.1	Experimental	55
4.2.1.1	Materials and Reagents	55
4.2.1.2	Physical Measurement.....	55
4.2.1.3	Syntheses	55
4.2.2	Results and Discussion.....	57
4.2.2.1	Crystal Structure of $[\text{Fe}(\text{bztpen})\text{Cl}]\text{OCH}_3 \times 4 \text{H}_2\text{O}$ (7).....	57
4.2.2.2	Stopped Flow Investigation on the Reaction of $[\text{Co}(\text{bztpen})\text{Cl}]\text{BF}_4$ with Hydrogen Peroxide.....	58
4.2.2.3	ESIMS Solution Studies of Cobalt Rtpen Complexes and their Reaction with Hydrogen Peroxide.....	60
4.2.2.4	Reactions of Iron(II) and Cobalt(II) Bztpen Complexes with Nitric Oxide	63
4.2.2.5	Stopped Flow Investigations on the Reactions of Cobalt(II) Bztpen Complex Solutions with Nitric Oxide	65
5	Iron Complexes with the bridging Ligands bz-b-tpen and pC-b-tpen.....	66
5.1	Experimental	66
5.1.1	Materials and Reagents	66
5.1.2	Physical Measurements	66
5.1.3	Syntheses of the Ligand bz-b-tpen.....	66
5.1.3.1	Formation of the Schiff-Base.....	66
5.1.3.2	Reduction of the Schiff-Base.....	67
5.1.3.3	Reductive Amination	67
5.1.4	Syntheses of the Ligand pC-b-tpen.....	68
5.1.4.1	Formation of the Schiff-Base.....	68
5.1.4.2	Reduction of the Schiff-base	68
5.1.4.3	Reductive Amination	69
5.1.5	Syntheses of the Complexes.....	69

TABLE OF CONTENTS

5.1.5.1	[Fe ₂ (bz-b-tpen)](SbF ₆) ₄	69
5.1.5.2	[Fe ₂ (bz-b-tpen)](PF ₆) ₄	69
5.1.5.3	Fe ₂ (bz-b-tpen)](BPh ₄) ₄	69
5.1.5.4	[Fe ₂ (bz-b-tpen)](triflate) ₄	70
5.1.5.5	[Fe ₂ (bz-b-tpen)](BF ₄) ₄	70
5.1.5.6	[Fe ₂ (bz-b-tpen)](ClO ₄) ₄	70
5.1.5.7	[Fe ₂ (pC-b-tpen)Cl ₂](ClO ₄) ₂	70
5.1.5.8	[Fe ₂ (pC-b-tpen)Cl ₂](ClO ₄) ₄	70
5.2	Results	71
5.2.1	Synthesis of the Iron(II)complexes.....	71
5.2.2	Reaction with of Iron (II) and Iron(III) bz-b-tpen Complex Solutions with Hydrogen Peroxide / Triethylamine	71
5.2.3	Reaction of the Iron(II) pC-b-tpen Complex with Air.....	72
6	Iron and Cobalt Complexes with the Ligand (2-amino-ethyl)-bis(2-pyridylmethyl)amine (uns-penp) and Derivatives.....	74
6.1	Abstract.....	74
6.2	Introduction	74
6.3	Experimental	76
6.3.1	Materials	76
6.3.2	Physical Measurements	76
6.3.3	Syntheses	77
6.3.3.1	Ligand Syntheses	77
6.3.3.2	[Co(uns-penp)Cl ₂]SbF ₆ x C ₃ H ₆ O (9).....	77
6.3.3.3	[Fe(Me ₂ -uns-penp)Cl ₂]ClO ₄ (10).....	77
6.3.3.4	[Fe ₂ (Me ₂ -uns-penp) ₂ Cl ₂ O](BPh ₄) ₂ (11).....	78
6.3.3.5	[Fe(Me ₂ -uns-penp)Cl(CH ₃ CN)]BPh ₄ (12)	78
6.3.3.6	[Co(Me ₂ -uns-penp)Cl]ClO ₄ (13).....	78
6.3.3.7	[Co(Me ₄ -uns-penp)Cl]BF ₄ (14).....	78
6.3.3.8	[Fe ₂ (acetyl-uns-penp) ₂ Cl ₂ (CH ₃ OH) ₂](ClO ₄) ₂ x 2 CH ₃ OH (15).....	79

TABLE OF CONTENTS

6.3.3.9	[Co ₂ (acetyl-uns-penp) ₂ Cl ₂](BF ₄) ₂ x C ₃ H ₆ O (16)	79
6.3.3.10	[Fe ₂ (acetyl-uns-penp) ₂ (triflate) ₂ (CH ₃ OH) ₂](ClO ₄) ₂ (17)	79
6.3.3.11	[Fe ₂ (acetyl-uns-penp) ₂ OH](ClO ₄) ₂ x 3 C ₃ H ₆ O (18)	79
6.3.3.12	[Fe ₂ (acetyl-uns-penp) ₂ (DMF) ₂ O](ClO ₄) ₄ x CH ₃ CN (19)	80
6.3.3.13	[Co(acetyl-uns-penp)Cl(H ₂ O)]Cl x H ₂ O (20)	80
6.3.3.14	[Co(acetyl-uns-penp)CO ₃] (21)	80
6.4	Results and Discussion	80
6.4.1	Uns-penp	81
6.4.1.1	[Co(uns-penp)Cl ₂]SbF ₆ x C ₃ H ₆ O (9)	81
6.4.2	Me ₂ -uns-penp	83
6.4.2.1	[Fe(Me ₂ -uns-penp)Cl ₂]ClO ₄ (10)	83
6.4.2.2	[Fe ₂ (Me ₂ -uns-penp) ₂ Cl ₂ O](BPh ₄) ₂ (11)	84
6.4.2.3	[Fe(Me ₂ -uns-penp)Cl(CH ₃ CN)]BPh ₄ (12)	85
6.4.2.4	[Co(Me ₂ -uns-penp)Cl]ClO ₄ (13)	87
6.4.3	Me ₄ -uns-penp	88
6.4.3.1	[Co(Me ₄ -uns-penp)Cl]BF ₄ (14)	88
6.4.4	Acetyl-uns-penp	89
6.4.4.1	[Fe ₂ (acetyl-uns-penp) ₂ Cl ₂ (CH ₃ OH) ₂](ClO ₄) ₂ x 2 CH ₃ OH (15)	90
6.4.4.2	[Co ₂ (acetyl-uns-penp)Cl ₂](BF ₄) ₂ x C ₃ H ₆ O (16)	90
6.4.4.3	[Fe ₂ (acetyl-uns-penp) ₂ (triflate) ₂ (CH ₃ OH) ₂](ClO ₄) ₂ (17)	92
6.4.4.4	[Fe ₂ (acetyl-uns-penp) ₂ OH](ClO ₄) ₂ x 3 C ₃ H ₆ O (18)	93
6.4.4.5	[Fe ₂ (acetyl-uns-penp) ₂ (DMF) ₂ O](ClO ₄) ₂ x CH ₃ CN (19)	96
6.4.4.6	[Co(acetyl-uns-penp)Cl(H ₂ O)]Cl x H ₂ O (20)	97
6.4.4.7	[Co(acetyl-uns-penp)CO ₃] (21)	98
6.5	Conclusion	100
6.6	Supplementary Material	100
7	Unpublished Results related to Chapter 6	101
7.1	Experimental	101

TABLE OF CONTENTS

7.1.1	Reagents and Materials	101
7.1.2	Physical Measurements	101
7.1.3	Syntheses	101
7.1.3.1	[Fe ₂ (acetyl -uns-penp) ₂ (OH)](triflate) ₂ x C ₃ H ₆ O x H ₂ O (22)	101
7.1.3.2	[Fe ₂ (uns-penp) ₂ Cl ₂ O]S ₂ O ₆ x 2 H ₂ O (23)	102
7.1.3.3	Complexes used for ESI-MS and UV/ Vis Studies	102
7.1.3.4	[Fe(CH ₃ CN) ₂ (triflate) ₂]	102
7.1.3.5	[Fe(CH ₃ CN) ₆](BF ₄) ₂	102
7.1.3.6	[Fe(CH ₃ CN) ₆](SbF ₆) ₂	103
7.2	Results and Discussion	104
7.2.1	Acetyl-uns-penp	104
7.2.1.1	Crystal Structure of [Fe ₂ (acetyl-uns-penp) ₂ (OH)](triflate) ₂ x C ₃ H ₆ O x H ₂ O (22)	104
7.2.2	Uns-penp	106
7.2.2.1	Crystal Structure of [Fe(uns-penp) ₂ Cl ₂ O]S ₂ O ₆ x 2 H ₂ O (23)	106
7.3	Solution Studies of Cobalt Complexes with Uns-penp, Acetyl-uns-penp, Me ₂ -uns-penp and Me ₄ -uns-penp and their Reactions with hydrogen peroxide. 107	
7.3.1	ESI-MS Solution Studies	107
7.3.1.1	[Co(uns-penp)Cl ₂]SbF ₆ (9)	107
7.3.1.2	[Co(Me ₂ -uns-penp)Cl]BF ₄	108
7.3.1.3	[Co(Me ₄ -uns-penp)Cl]BF ₄ (14)	109
7.3.1.4	[Co ₂ (acetyl-uns-penp) ₂ Cl ₂](BF ₄) ₂ x C ₃ H ₆ O (16)	110
7.3.2	UV/ Vis Studies on the Reaction of Cobalt Complexes with Hydrogen Peroxide 111	
7.3.2.1	[Co(Me ₂ -uns-penp)Cl]BF ₄	111
7.3.2.2	[Co(Me ₄ -uns-penp)Cl]BF ₄ (14)	112
7.3.3	ATR-IR Spectroscopy of the Iron(II) Acetonitrile Complexes	112
8	Summary	115
9	Zusammenfassung	120

TABLE OF CONTENTS

List of Crystal Structures	125
Publications	131
Presentations.....	131
Bibliography.....	132

TABLE OF FIGURES

Table of Figures

Figure 1-1: Structure of cobalamines. Coenzyme B12 R = 5'-Desoxyadenosyl; Cyanidocobalamine R = CN; Hydroxidocobalamin R = OH; Methylcobalamin R = CH ₃	2
Figure 1-2: Crystal structure of Werner's green (left) and Werner's red (right).	2
Figure 1-3: Ortep plot of the cobalt superoxido complex with the ligand salmdpt based on the structural data reported in Ref. 27. The co-crystallized nonoxygenated cobalt(II) complex cation is omitted for clarity.	4
Figure 1-4: Selection of structurally characterized cobalt oxygen adduct complexes.	4
Figure 1-5: Ortep plot of the cobalt hydroperoxido complex cation based on the structural data reported in Ref. 44.	5
Figure 1-6: Structure of heme b.	6
Figure 1-7: Proposed structure of Fe-bleomycine. ⁴⁹	7
Figure 1-8: The active center of soluble methane monooxygenase in its reduced (left) and its oxidized form (right).	8
Figure 1-9: Principal intermediates during the catalytic cycle of MMOH.....	9
Figure 1-10: Dinuclear iron-peroxido complexes with the ligands HTPMP, HPTP and Et-HPTB.	11
Figure 1-11: Tetradentate pyridyl ligands described in the text.	13
Figure 1-12: Postulated mechanism for the reaction of [Fe(tmpa)(dbc)]B(C ₆ H ₅) ₄ with dioxygen.	14
Figure 1-13: The ligand uns-penp and derivatives.....	15
Figure 1-14: Dimeric solid state structure of the complex cation [Fe(acetyl-uns-penp) ₂ O]-(ClO ₄) ₂ x H ₂ O. Ortep plot was made with crystallographic data from Ref. 91	16
Figure 1-15: Solid state structure of the complex [Fe(acetyl-uns-penp)(tcc)] ₂ O. Ortep plot was made with crystallographic data published in Ref. 91	16
Figure 1-16: The ligands bppa and H ₆ 1.	18
Figure 1-17: Time resolved UV/Vis spectra for the formation of the purple [Fe(bztpen)OOH](ClO ₄) ₂	18
Figure 1-18: Attempt to stabilize either the hydroperoxido or peroxido intermediate by secondary hydrogen bonding interaction in the complexes [Fe(etOHtpen)OOH] ²⁺ /[Fe(etOHtpen)OO] ⁺	19

TABLE OF FIGURES

Figure 1-19: Proposed structures for high-valent intermediates of TauD J (α -Ketoglutarate Dioxygenase Intermediate J)(1), MMO Q (2) and RNR R2 X (Ribonucleotide Reductase Intermediate X) (3). ⁶⁸	20
Figure 1-20: Ortep plot of $[\text{Fe}^{\text{IV}}(\text{O})(\text{TMC})(\text{MeCN})]^{2+}$ based on structural data reported in Ref. 108 (left) and Ortep plot of $[\text{Fe}^{\text{IV}}(\text{O})(\text{N4Py})]^{2+}$ based on the structural data reported in Ref. 112 (right)	21
Figure 1-21: Selected ligands that support the formation of iron(IV)-oxido species. 21	
Figure 1-22: Proposed structure for the $\text{Fe}^{\text{IV}}_2(\mu\text{-O})_2$ tmpa diamond core.....	22
Figure 1-23: bz-b-tpen and pC-b-tpen.	24
Figure 1-24: uns-penp and derivatives used in this work.....	25
Figure 3-1: The ligands Rtpen.	34
Figure 3-2: Ortep plot of bztpen (1). The thermal ellipsoids are shown at 30% probability. Hydrogen atoms are omitted for clarity.	39
Figure 3-3: Ortep plot of the complex cation $[\text{Fe}(\text{bztpen})(\text{OAc})]^+$ (2). The thermal ellipsoids are shown at 30% probability. Hydrogen atoms are omitted for clarity.	39
Figure 3-4: Ortep plot of the complex cation $[\text{Co}(\text{bztpen})\text{Cl}]^+$ (3). The thermal ellipsoids are shown at 30% probability. Hydrogen atoms are omitted for clarity.	40
Figure 3-5: Ortep plot of the complex cation $[\text{Co}(\text{metpen})\text{Cl}]^+$ (4). The thermal ellipsoids are shown at 30% probability. Hydrogen atoms are omitted for clarity.	42
Figure 3-6: Ortep plot of the complex cation $[\text{Co}(\text{bztpen})\text{OAc}]^+$ (5). The thermal ellipsoids are shown at 30% probability. Hydrogen atoms are omitted for clarity.	42
Figure 3-7: Time resolved spectra for the formation of $[\text{Fe}(\text{bztpen})\text{NO}]^{2+}$ in methanol (-40°C , $\Delta t = 300$ ms). Insert: absorbance vs. time trace at 550 nm (data and fit to one exponential function).	44
Figure 3-8: Ortep plot of the cation $[\text{Fe}(\text{bztpen})\text{NO}]^+$ (6) (30% probability displacement ellipsoids, hydrogen atoms omitted for clarity).....	44
Figure 3-9: Time resolved spectra for the oxidation reaction of $[\text{Fe}(\text{bztpen})(\text{Cl})]\text{ClO}_4$ ($c = 0.2$ mM) with hydrogen peroxide ($c = 0.25$ M) in methanol ($T = -40^\circ\text{C}$, $\Delta t = 1.5$ ms). Insert: absorbance vs. time trace at 393 nm (data and fit to one exponential function). Because of instrument reasons the spectra do not show a clean isosbestic point and some drift at longer wavelengths (>600 nm).....	46

TABLE OF FIGURES

Figure 3-10: Time resolved spectra for the formation of $[\text{Fe}(\text{bztpen})\text{OOH}]^{2+}$ ($c = 0.2$ mM) with hydrogen peroxide ($c = 0.1$ M) in methanol ($T = 25^\circ\text{C}$, $\Delta t = 100$ ms). Insert: absorbance vs. time trace at 550 nm (data and fit to one exponential function). The black line shows the spectrum of the starting complex. Inset: absorbance vs. time trace at 550 nm (data and fit to single exponential function). Because of instrument reasons the spectra do not show a clean isosbestic point and some drift at longer wavelengths (>600 nm).....	47
Figure 3-11: Plot of $\ln k_{\text{obs}}$ versus pressure for determination of the activation volume of the formation reaction of $[\text{Fe}(\text{bztpen})\text{OOH}]^{2+}$	48
Figure 4-1: k_{obs} vs. $[\text{H}_2\text{O}_2]$ for the oxidation of $[\text{Fe}(\text{bztpen})\text{Cl}]\text{ClO}_4$ by H_2O_2 in methanol.....	49
Figure 4-2: k_{obs} vs. $[\text{H}_2\text{O}_2]$ to calculate the initial slopes and intercepts of the curved plots in Figure 4-1.....	50
Figure 4-3: “Eyring-Plot” for the oxidation of $[\text{Fe}(\text{bztpen})\text{Cl}]\text{ClO}_4$ in methanol.	50
Figure 4-4: “Eyring plot” for the back reaction of the oxidation of $[\text{Fe}(\text{bztpen})\text{Cl}]\text{ClO}_4$ in methanol.....	51
Figure 4-5: k_{obs} vs. $[\text{H}_2\text{O}_2]$ for the formation of $[\text{Fe}(\text{bztpen})\text{OOH}]^{2+}$	52
Figure 4-6: “Eyring plot” for the formation of $[\text{Fe}(\text{bztpen})\text{OOH}]^{2+}$	52
Figure 4-7: “Eyring plot” for the back reaction of the formation of $[\text{Fe}(\text{bztpen})\text{OOH}]^{2+}$	53
Figure 4-8: k_{obs} vs. $[\text{H}_2\text{O}_2]$ for the formation under high pressure conditions of $[\text{Fe}(\text{bztpen})\text{OOH}]^{2+}$ at 27°C (every data point is average over all pressures).....	54
Figure 4-9: Ortep plot of the cation $[\text{Fe}(\text{bztpen})\text{Cl}]^+$ (7) (30% probability displacement ellipsoids, hydrogen atoms omitted for clarity).....	57
Figure 4-10: Reaction of 1 mM solution of $[\text{Co}(\text{bztpen})\text{Cl}]^+$ with 1 M hydrogen peroxide in methanol at -40°C . Insert: time trace at 550 nm measurement data and fit to one exponential function.	58
Figure 4-11: Reaction of a 2 mM solution of $\text{Co}(\text{BF}_4)_2 \times 6 \text{H}_2\text{O}$ and bztpen in methanol with 0,2 M hydrogen peroxide in methanol at 24°C . Insert: time trace at 560 nm measurement data and fit to one exponential function.	59
Figure 4-12: ESIMS of a solution of $[\text{Co}(\text{bztpen})\text{Cl}]\text{BF}_4$ in methanol.....	60
Figure 4-13: ESIMS spectrum of $[\text{Co}(\text{bztpen})(\text{OAc})]\text{ClO}_4$ in methanol.....	60
Figure 4-14: ESIMS spectrum of $[\text{Co}(\text{bztpen})(\text{OAc})]\text{ClO}_4$ with an excess of hydrogen peroxide in methanol.	61
Figure 4-15: ESIMS spectrum of $[\text{Co}(\text{metpen})\text{Cl}]\text{SbF}_6$ in methanol.....	62
Figure 4-16: ESIMS spectrum of $[\text{Co}(\text{metpen})\text{Cl}]\text{triflate}$ in methanol.	62

TABLE OF FIGURES

Figure 4-17: ESIMS spectrum of [Co(metpen)Cl]triflate in methanol with an excess of hydrogen peroxide.....	63
Figure 4-18: Ortep plot of the cation [Fe(bztpen)NO ₂] ⁺ (8) (30% probability displacement ellipsoids, hydrogen atoms omitted for clarity).....	63
Figure 4-19: Time resolved spectra of the reaction of 2 mM solution of Co(BF ₄) ₂ x 6 H ₂ O and bztpen with a saturated solution of nitric oxide in methanol (T = -40 °C, Δt = 10 ms). Insert: absorbance vs. time trace at 675 nm (data and fit to one exponential function).	65
Figure 5-1: UV/ Vis-spectra of the iron(III)bz-b-tpen complex in methanol (green line) and after reaction with hydrogen peroxide (black line) and hydrogen peroxide/ triethylamine (red line) r.t.....	72
Figure 5-2: UV/ Vis spectra of iron(II)-pC-b-tpen in methanol (black line) and after reaction with air (red line) at r.t.	73
Figure 6-1: Molecular structure of the cation of 9 with hydrogen atoms omitted for clarity. Thermal ellipsoids are shown at 30 % probability levels.	81
Figure 6-2: Molecular structure of the cation of 10 with hydrogen atoms omitted for clarity. Thermal ellipsoids are shown at 30 % probability levels.	83
Figure 6-3: Molecular structure of the cation of 11 with hydrogen atoms omitted for clarity. Thermal ellipsoids are shown at 30 % probability levels.	85
Figure 6-4: Molecular structure of the cation of 12 with hydrogen atoms omitted for clarity. Thermal ellipsoids are shown at 30% probability levels.	87
Figure 6-5: Molecular structure of the cation of 13 with hydrogen atoms omitted for clarity. Thermal ellipsoids are shown at 30 % probability levels.	88
Figure 6-6: Molecular structure of the cation of 14 with hydrogen atoms omitted for clarity. Thermal ellipsoids are shown at 30 % probability levels.	89
Figure 6-7: Molecular structure of the cation of 15 with hydrogen atoms omitted for clarity. Thermal ellipsoids are shown at 30 % probability levels.	90
Figure 6-8: Molecular structure of the cation of 16 with hydrogen atoms omitted for clarity. Thermal ellipsoids are shown at 30 % probability levels.	92
Figure 6-9: Molecular structure of the cation of 17 with hydrogen atoms omitted for clarity. Thermal ellipsoids are shown at 30 % probability levels.	93
Figure 6-10: Molecular structure of the cation of 18 with hydrogen atoms omitted for clarity. Thermal ellipsoids are shown at 30 % probability levels.	94
Figure 6-11: Molecular structure of the cation of 19 with hydrogen atoms omitted for clarity. Thermal ellipsoids are shown at 30 % probability levels.	96

TABLE OF FIGURES

Figure 6-12: Molecular structure of 20 with hydrogen atoms omitted for clarity, except the hydrogen atoms of the coordinated water molecule. Thermal ellipsoids are shown at 30 % probability levels.....	98
Figure 6-13: Molecular structure of 21 with hydrogen atoms omitted for clarity. Thermal ellipsoids are shown at 30 % probability levels.....	99
Figure 7-1: Crystal structure of 22 with hydrogen atoms omitted for clarity. Thermal ellipsoids are shown at 30 % probability levels.....	104
Figure 7-2: Crystal structure of 23 with hydrogen atoms omitted for clarity. Thermal ellipsoids are shown at 30 % probability levels.....	106
Figure 7-3: ESIMS of a solution of [Co(uns-penp)Cl ₂][SbF ₆] (9) in methanol.	107
Figure 7-4: ESIMS of a solution of [Co(Me ₂ -uns-penp)Cl]BF ₄ in methanol.....	108
Figure 7-5: ESIMS of a solution of [Co(Me ₂ -uns-penp)Cl]BF ₄ in methanol with an excess of hydrogen peroxide.....	108
Figure 7-6: ESIMS of a solution of 14 in methanol.	109
Figure 7-7: ESIMS of a solution of 14 in methanol with an excess of hydrogen peroxide.....	109
Figure 7-8: ESIMS of a solution of [Co ₂ (acetyl-uns-penp) ₂ Cl ₂](BF ₄) ₂ (16) in methanol.	110
Figure 7-9: ESIMS of a solution of [Co ₂ (acetyl-uns-penp) ₂ Cl ₂](BF ₄) ₂ (16) in methanol with an excess of hydrogen peroxide.	110
Figure 7-10: UV/ Vis spectra of a solution of [Co(Me ₂ -uns-penp)Cl]BF ₄ in methanol (black line) and after addition of hydrogen peroxide (red and green lines).....	111
Figure 7-11: UV/ Vis spectra of a solution of 14 in methanol (black line) and after addition of hydrogen peroxide (red, green, blue and turquoise lines).....	112
Figure 7-12: ATR-IR-spectrum of [Fe(CH ₃ CN) ₂ (triflate) ₂].....	113
Figure 7-13: ATR-IR-spectrum of [Fe(CH ₃ CN) ₆](BF ₄) ₂	113
Figure 7-14: ATR-IR-spectrum, of [Fe(CH ₃ CN) ₆](SbF ₆) ₂	114
Figure 8-1: The ligand bztpen.....	115
Figure 8-2: left: molecular structure of the cation [Fe(bztpen)NO] ²⁺ (6) right: time-resolved UV/ Vis Spectra for the reaction of iron(II) bztpen complex with nitric oxide in methanol at -40 °C. (insert: absorbance vs. time at 550 nm and fit to one exponential function).	117
Figure 8-3: The ligands acetyl-uns-penp and uns-penp.	118
Figure 8-4: Molekülstruktur des Kations von [Fe ₂ (acetyl-uns-penp) ₂ (OH)](ClO ₄) ₂ (18).	118

1 Introduction

This chapter includes selected parts of the previously published book chapter: *Iron Complexes and Dioxygen Activation*, Thomas Nebe, Jing-Yuan Xu, Siegfried Schindler in *Activating Unreactive Substrates*, Carsten Bolm, Ekkehardt Hahn (editors), Wiley VCH, Weinheim, 2009, p. 39-51.

1.1 Motivation

The fact that dioxygen activation mainly is observed at transition metal sites is important for the understanding of catalytic and selective oxidations of organic substrates using dioxygen (air) as the oxidant. Whereas it is easy to completely oxidize (burn) unreactive hydrocarbons such as methane to carbon dioxide and water, it is quite a challenge to partially oxidize hydrocarbons selectively to alcohols, for example methanol. In contrast, the iron enzyme soluble methane monooxygenase (MMO) easily accomplishes this reaction at ambient conditions.^{1,2} Therefore, investigations of non-heme iron enzymes as well as their model compounds have gained a lot of interest during the last decades.³⁻⁵ Iron compounds in general play an important role in biological electron transfer reactions, most likely because of the combination of their ready availability and their ability to easily change oxidation states. Knowing about the mechanisms of dioxygen activation of iron-containing enzymes (oxidases and oxygenases) therefore is important for understanding (and suppressing) free radical pathways of oxidative damage in biological systems as well as for the synthesis of new selective oxidation catalysts. In this respect, dioxygen and, to a lesser extent, hydrogen peroxide are ideal oxidants for the chemical industry because they are readily available and ecologically beneficial. It is necessary to investigate the mechanisms of these reactions by detailed kinetic measurements for a better understanding of dioxygen activation at the iron sites and the subsequent reactions.^{5,6} If possible, important intermediates should be characterized through their structural, electronic and spectroscopic properties.³⁻⁶

1.2 The Element Cobalt

The ferromagnetic metal cobalt does not occur in elemental form in nature. In its minerals it is frequently associated with nickel.⁷ In biology, the element cobalt plays an important role as a trace element. It is part of the active center of coenzymes,

which are called cobalamines. These coenzymes can be found in all multicell organisms. For mammals the cobalamine vitamin B12 (see Figure 1-1) is essential.⁸

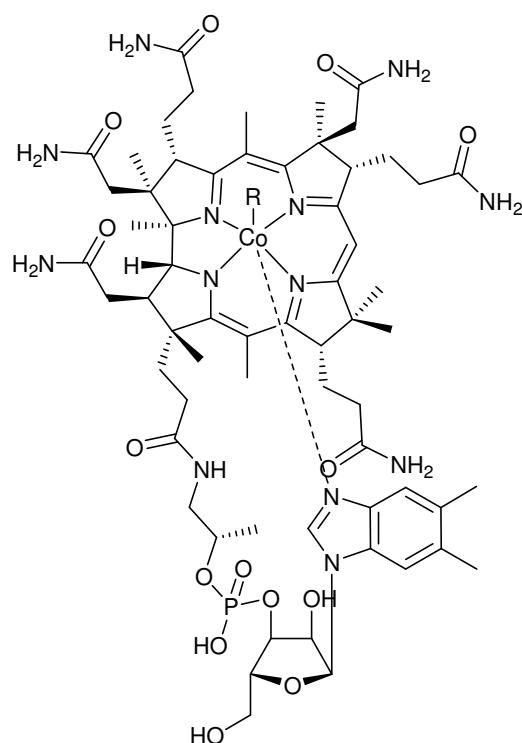


Figure 1-1: Structure of cobalamines. Coenzyme B12 R = 5'-Desoxyadenosyl; Cyanidocobalamine R = CN; Hydroxidocobalamin R = OH; Methylcobalamin R = CH₃.

1.3 Cobalt–Oxygen Complexes

So far Cobalt ions were not observed in oxygen activating enzymes but the reactivity of cobalt complexes towards dioxygen makes them to excellent model compounds for dioxygen activation. Therefore, cobalt complexes and their reaction with dioxygen have been of great interest for coordination chemists. They have a high potential as oxygen carriers⁹ and oxidation catalysts.¹⁰⁻¹⁴ The fact that solutions of cobalt(II) salts turn brown in aqueous ammonia solutions when exposed to dioxygen was discovered already in the 19th century.¹⁵

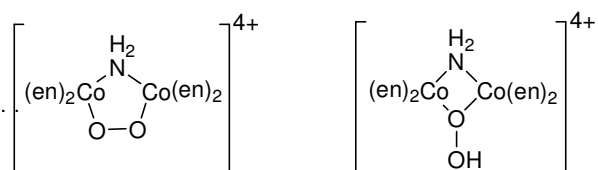
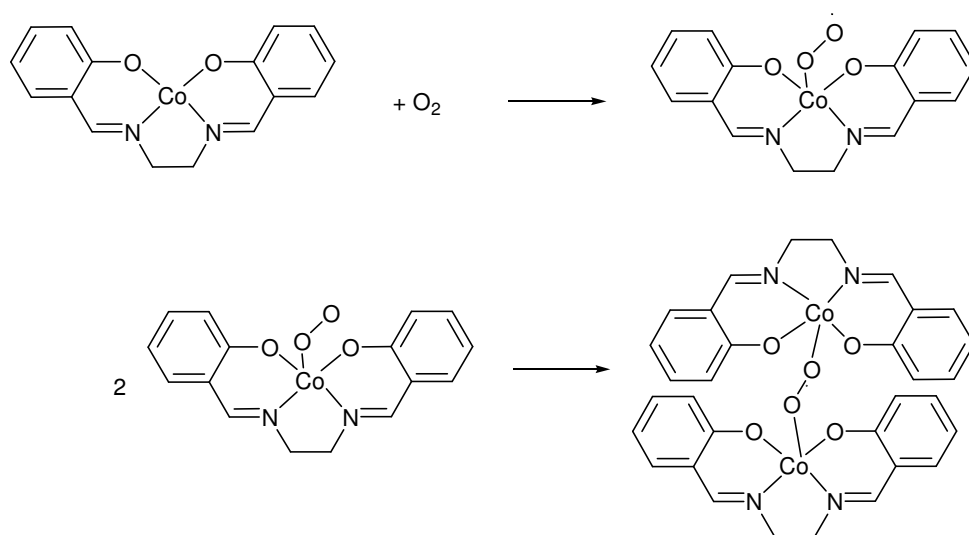


Figure 1-2: Crystal structure of Werner's green (left) and Werner's red (right).

The earliest known synthetic dioxygen complexes were $[(\text{NH}_3)_{10}\text{Co}_2\text{O}_2]^{4+}$ and derivatives prepared by Werner and co-workers.^{16,17} The crystal structures of these

complexes (e.g. The dinuclear peroxido complex Werner's green and the dinuclear hydroperoxido complex Werner's red) could be determined later and are presented in Figure 1-2.^{18,19}

In 1938 Tsumaki reported the ability of the cobalt(II)salen complex to bind dioxygen reversibly.²⁰⁻²³ Its ability to carry dioxygen made it to the first synthetic model for the reactivity of hemoglobin. Studies were directed towards military applications as a system for oxygen storage in submarines.^{21,24-26} Scheme 1-1 shows the reaction of cobalt salen with dioxygen. When the Co^{II} salen complex is oxygenated, in a first step an end-on-bound superoxido species is formed, however, in a second step the formation of a dimeric μ -peroxido bridged species follows immediately. Salen derivatives, which offer additional donor atoms and / or sterical hinderance can stabilize the initial superoxido species.



Scheme 1-1

This superoxido cobalt(III) complex with the ligand salmdpt ((N,N'-(3,3'-dipropylmethylamine)bis(salicylideneamine)) and derivatives could be isolated and was characterized by X-ray crystallographic analysis (Figure 1-3).^{27,28}

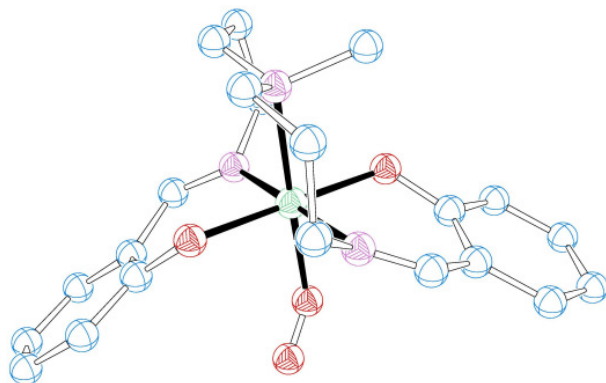


Figure 1-3: Ortep plot of the cobalt superoxido complex with the ligand salmdpt based on the structural data reported in Ref. 27. The co-crystallized nonoxygenated cobalt(II) complex cation is omitted for clarity.

Today there is a large number of well-characterized cobalt oxygen complexes.^{9,13,18,19,27,29-43} Figure 1-4 shows examples for the different binding modes of oxygen in structurally characterized cobalt complexes.

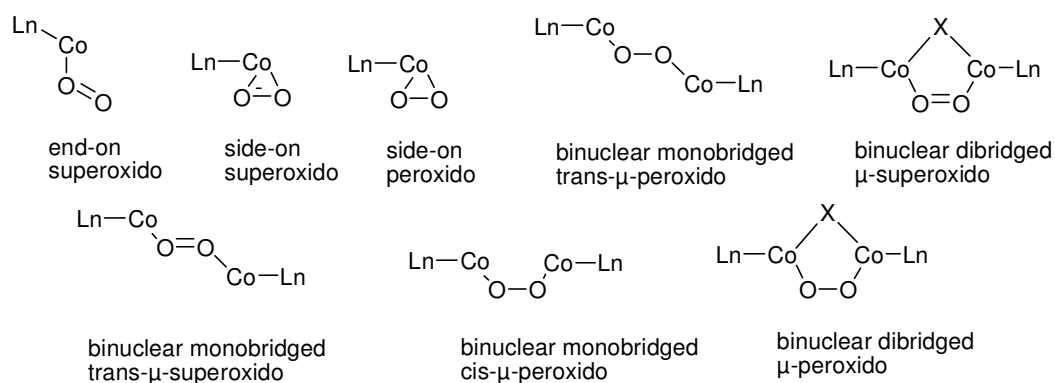


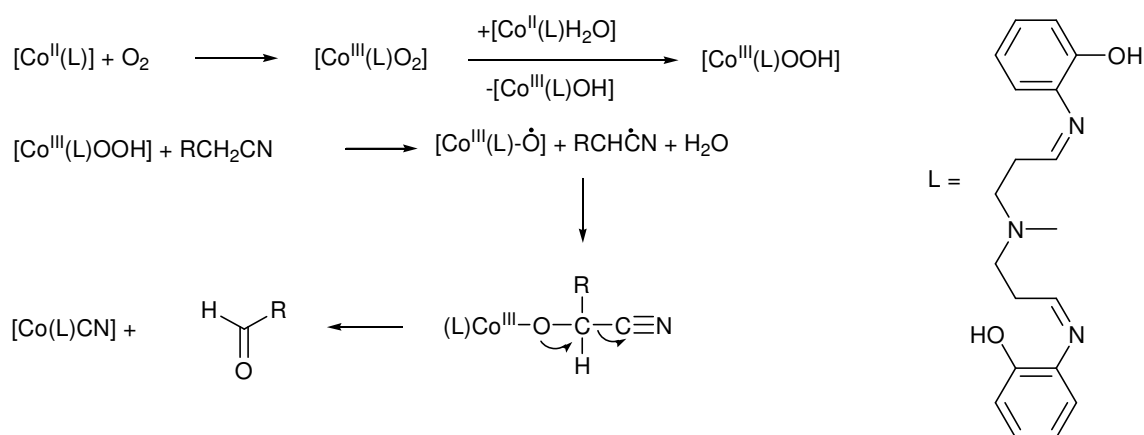
Figure 1-4: Selection of structurally characterized cobalt oxygen adduct complexes.

As described above cobalt complexes with salmdpt can be used for dioxygen activation and are capable to form stable superoxido adducts. The Schindler group demonstrated that cobalt dioxygen adduct complexes could be used to perform unusual chemical transformations from nitriles to aldehydes.¹⁴

The postulated mechanism of this reaction is presented in Scheme 1-2. The first product of the reaction of the cobalt(II) complex with dioxygen is the cobalt(III) superoxido complex, which is well known (see above), but which has not been observed in the reaction mixture so far. A cobalt(III) hydroperoxido complex is formed in the next step by reaction with a water containing cobalt(II) complex. Until now this intermediate has also not been detected in the reaction mixture, but the hydroxido complex, which is the co-product of this reaction step, was isolated and structurally characterized.

The occurrence of cobalt hydroperoxido complexes is known and one example for such a compound was described previously.⁴⁴ Figure 1-5 shows this structurally characterized mononuclear end-on cobalt-hydroperoxido complex with a macrocyclic cyclam based ligand. A possible decomposition reaction of cobalt hydroperoxides is the formation of a cobalt oxido intermediate as presented in Scheme 1-2. ($\text{Co}^{\text{IV}}=\text{O} \leftrightarrow \text{Co}^{\text{III}}-\text{O}^\cdot$) These intermediates are supposed to be highly reactive, in analogy to well known iron(IV) oxido complexes, which are strong oxidizing agents that can attack C-H bonds in hydrocarbons (see chapter 1.13).

It would be of great interest to isolate such a species for spectroscopic, structural and reactivity studies.



Scheme 1-2: L = salmdpt

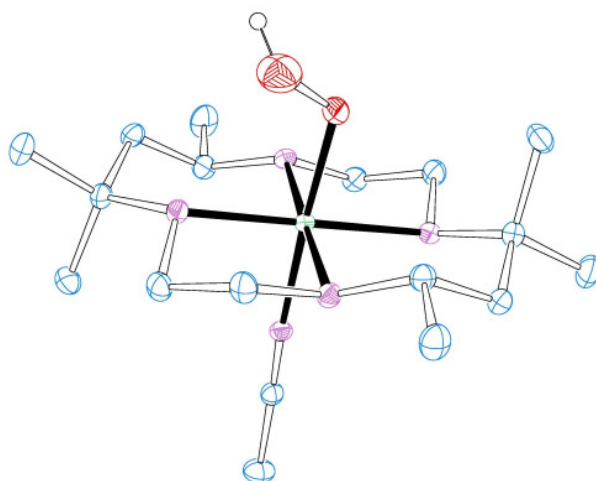


Figure 1-5: Ortep plot of the cobalt hydroperoxido complex cation based on the structural data reported in Ref. 44.

1.4 The Element Iron

Iron is formed in the final act of the “burning” of elements in massive stars. It is believed to be the sixth most abundant element in the universe. 35% of the earth

mass is believed to be iron caused by its core of an iron-nickel alloy. But only 5% of the earth crust is iron. Here iron is mostly bound in oxygen minerals like hematite (Fe_2O_3) or magnetite (Fe_3O_4). Metallic iron is found in iron-nickel meteorites.⁷

Iron is an essential element for living species and is generally stored in ionic form in metalloproteins, because “free” iron is toxicant. This fact is caused by its ability to catalyze the production of free radicals.⁸

1.5 Heme Iron Proteins

Iron containing proteins play an important role in biology. The best known and investigated systems are the heme-proteins, which contain one or more iron-porphyrine units.⁴⁵ Figure 1-6 shows the structure of the most common prosthetic group protoheme IX (heme b). Oxygen carriers like hemoglobin and myoglobin belong to the heme-protein family.⁴⁶ Also the enzymes of the cytochrome p450 family, which are catalyzing hydrocarbon hydroxylation reactions are heme-enzymes.⁴⁷

Proteins without a porphyrine unit are called non-heme-iron proteins. A large number of this protein-family are molecules that are responsible for the bonding, activation and transfer of dioxygen similar to the porphyrin systems in biology.⁴⁵

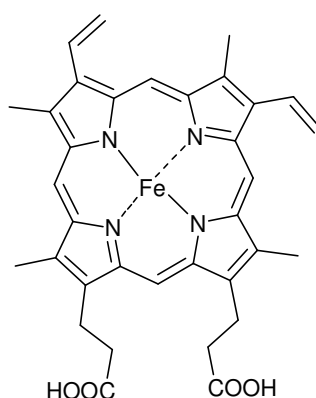


Figure 1-6: Structure of heme b.

These non-heme-iron-enzymes (NHE) can be classified into two groups. On the one hand there are the mononuclear NHE, which contain only one metal ion in their active sites. On the other hand there are the dinuclear NHE whose metal atoms are linked with a bridging ligand.^{5,45}

A simple example for a mononuclear iron system is bleomycin, which can be used as an anti-tumor drug, because of its capability to cut DNA-chains. For this reaction the

activation of dioxygen at its active iron site is essential. The reaction sequence of the DNA cutting process includes the binding of dioxygen on the iron(II) site (shown in Figure 1-7), the formation of the so called "active bleomycin" by single electron transfer and the generation of a hydroperoxido intermediate, which interacts with the DNA substrate.⁴⁸

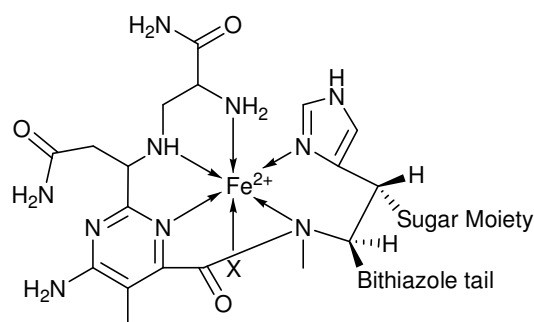
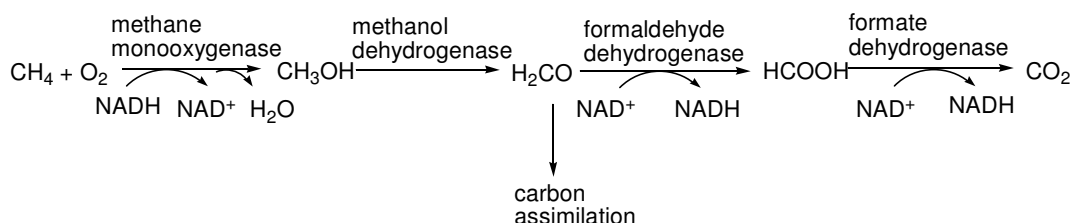


Figure 1-7: Proposed structure of Fe-bleomycin.⁴⁹

Dinuclear iron enzymes that are bridged by carboxylates are an important group of iron containing proteins. The oxygen carrier hemerythrin, which is responsible for the dioxygen transport in some marine organisms belongs to this group.⁵ Another very interesting NHE, the methane monooxygenase (MMO) is described below in more detail.

1.6 Methane Monooxygenase

Oxygen transferring enzymes can be classified in different groups. Monooxygenases enzymes are mixed functional oxidases. One atom of the dioxygen molecule is transferred to the substrate molecule. The other oxygen atom is also reduced and forms water. There are also dioxygenases, which are able to transfer both oxygen atoms of dioxygen to a substrate molecule. Furthermore, there are enzymes called oxidases which catalyze the 4 electron reduction from dioxygen to water.^{4,50}



Scheme 1-3

Methane monooxygenases exist in two distinctive forms: a particulate, membrane bound form, which contains copper and a soluble form, which contains iron in the active sites.^{1,4,51} Soluble methane monooxygenases (sMMO) are found in some

methanotroph soil bacteria. Two of the better characterized systems are isolated from *Methylococcus capsulatus* (Bath) and *Methyosinus trichosporium* (OB3b).⁵² In the first step of the metabolic pathway of methanotrophs, methane monooxygenase converts methane into methanol. Methanotrophs use methane as carbon and dioxygen energy source.^{45,53-55} The metabolic pathway for methane oxidation in *Methylococcus capsulatus* is presented in Scheme 1-3. Crystal structures for the iron containing enzymes as well as for the copper containing enzymes are described in the literature.^{51,56-61}

The reaction system of the methane monooxygenase consists of three components. On the one hand there are two non-heme iron atoms containing the hydroxylase component (MMOH), which transfers the oxygen atom to the substrate,⁴ on the other hand there is the reductase component, which includes a 2Fe2S-cluster and a Flavine-Adenine-dinucleotide (FAD). As a third component of the reaction system is the so called protein B that catalyzes the electron transfer between the hydroxylase and the reductase part.⁴

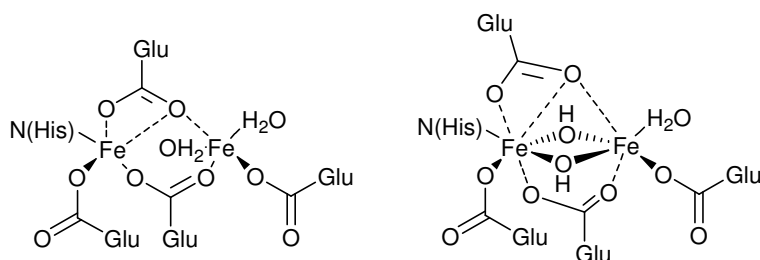


Figure 1-8: The active center of soluble methane monooxygenase in its reduced (left) and its oxidized form (right).

The two iron ions on the active site of the hydroxylase component, shown in Figure 1-8, are coordinated to four glutamate- and two histidine-residues. The reduced form contains iron(II) ions whereas the oxidized form is an iron(III) unit bridged by two hydroxido ligands.

The minimal core transformations in the catalytic cycle of MMOH are depicted in Figure: 1-9. The resting state of the enzyme is the diferric component (Fe^{III}_2),⁶² which has to be reduced to the active diferrous form (Fe^{II}_2) to bind dioxygen.⁶³

This reaction needs two electrons that are provided by NAD(P)H. The two electrons are transferred solely by MMOR into the active metal atom of MMOH.⁶⁴ In the following compound P* (Fe^{III}_2 or $\text{Fe}^{\text{II}}/\text{Fe}^{\text{III}}$), dioxygen is coordinated in form of a bridging peroxide.⁶⁵ Protonation leads to the intermediate P, which is transformed by

O-O bond scission to the kinetically intermediate Q, which oxygenates methane and other substrates.⁶⁶ The resulting alcohol is bound to the intermediate T.⁶⁷ The release of the product leads back to the beginning of the catalytic cycle.

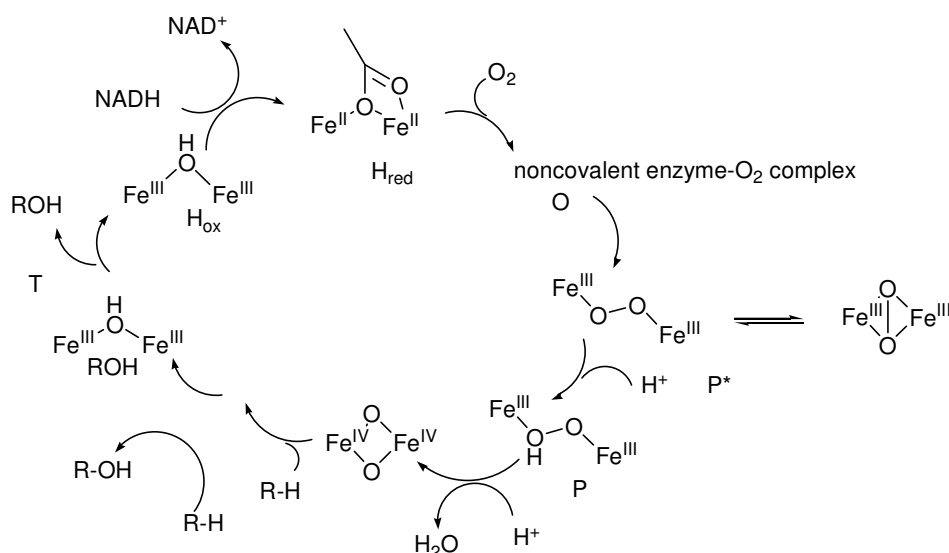
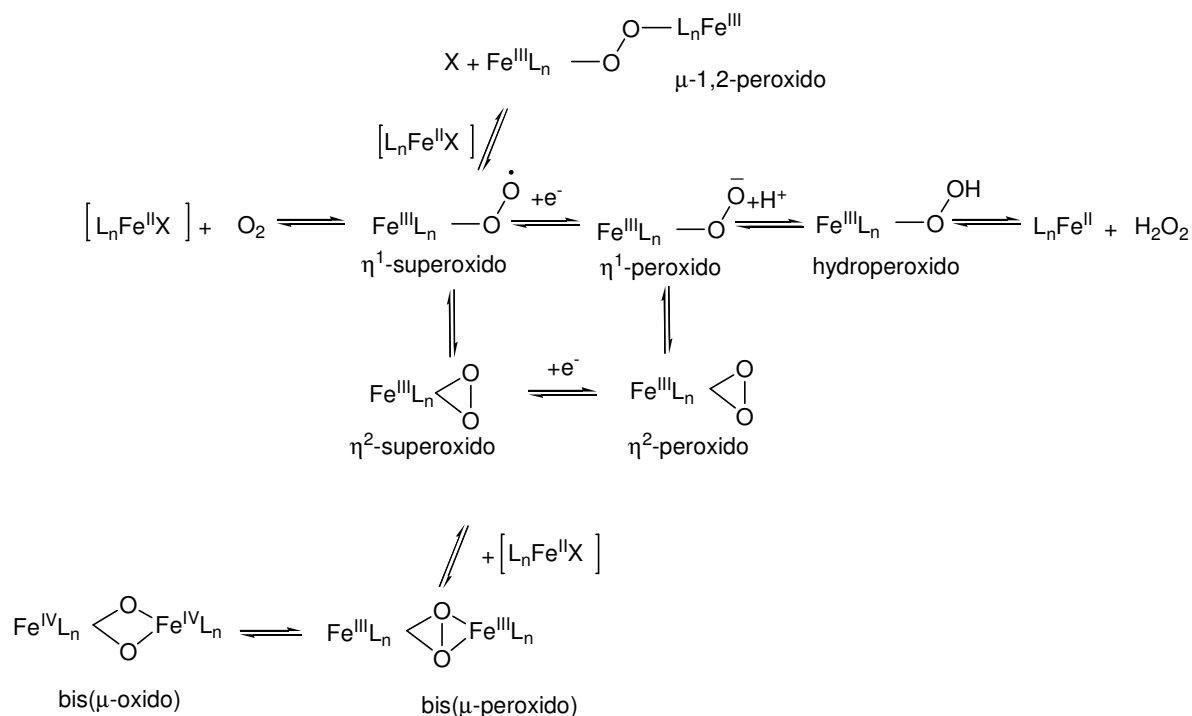


Figure 1-9: Principal intermediates during the catalytic cycle of MMOH.

1.7 “Iron-Oxygen” Adduct Complexes

A general reaction sequence for the reaction of a mononuclear iron(II) complex with dioxygen is presented in Scheme 1-4.³⁻⁵ These reactions can be easily extended to dinuclear or polynuclear complexes as well, but reaction rates in these reactions can be quite different because of the pre-organization of some of the complexes, thus making their formation much more facile. Furthermore, additional bridging groups can be present and inter- and intramolecular reactions are possible.



Scheme 1-4

The mechanisms of iron dioxygen-activating enzymes depend on the number of metal atoms. Dinuclear systems, such as MMO (described above), that utilize a $\text{Fe}^{\text{IV}}_2/\text{Fe}^{\text{III}}_2$ redox couple for a formally two-electron oxidation of methane, take advantage of both iron atoms in catalysis.² In addition to electron and charge delocalization over two irons, which stabilize high-valent intermediates, the second metal ion can also be important for substrate coordination at the dinuclear core. While observable iron oxygen intermediates can be generated from iron(II) complexes and dioxygen according to Scheme 1-4, it is also possible to obtain these species from reactions with superoxide, hydrogen peroxide, alkyl hydroperoxides, peroxoacids, iodosobenzene, etc.^{3-5,68}

1.8 Dinuclear Iron Peroxido Complexes

In contrast to analogous studies on model compounds for copper proteins, only a few of the “oxygen adduct” iron complexes shown in Scheme 1-4 could be structurally characterized.^{3-5,68} Dinuclear iron peroxide complexes shown in Figure 1-10 could be analyzed in great detail and were studied independently mainly by the research groups of Que and Lippard.⁶⁹⁻⁷³

The kinetic studies of the Schindler group in cooperation with the Lippard group using low-temperature and high-pressure stopped-flow techniques, allowed to perform a

detailed mechanistic analysis of the binding of dioxygen to the iron(II) compounds to form the dinuclear peroxido complexes depicted in Figure 1-10.⁷⁴

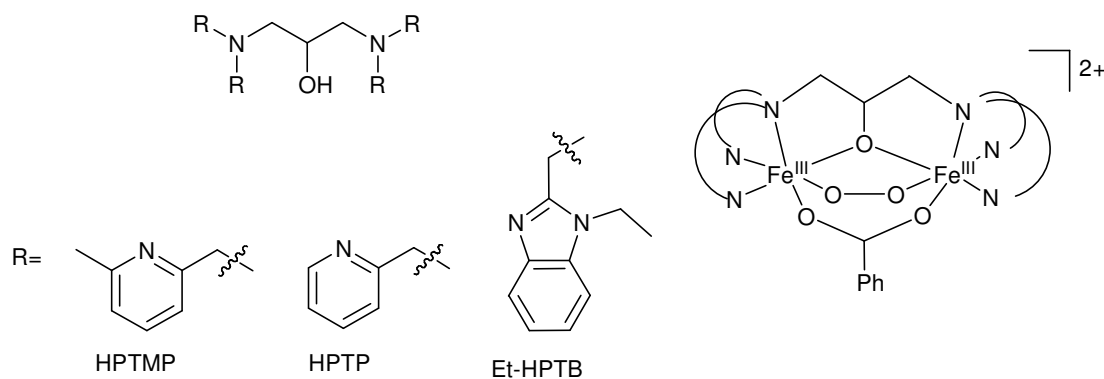
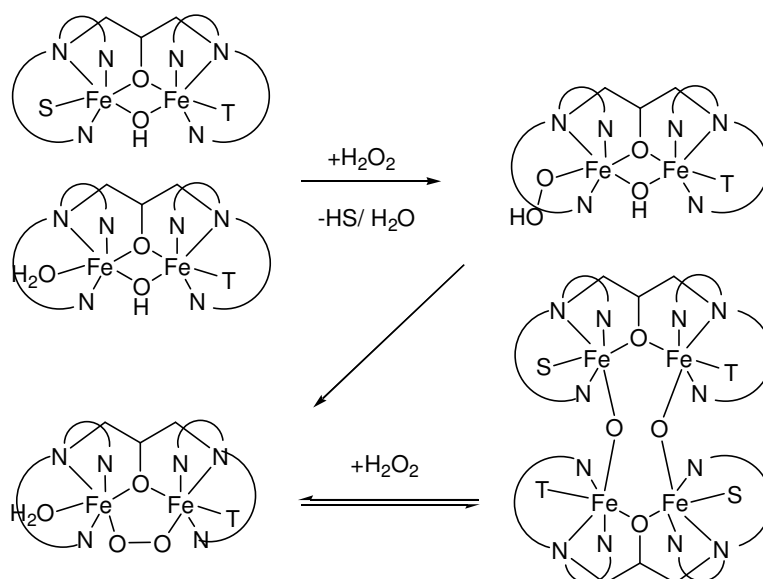


Figure 1-10: Dinuclear iron-peroxido complexes with the ligands HTPMP, HPTP and Et-HPTB.

Cooperating with the Krebs group, the Schindler group was able to show that the same complexes can be prepared much more easily from the relevant iron(III) complexes and hydrogen peroxide.⁷⁵ These reactions could be investigated in protic solvents at ambient temperatures, and it turned out that the product complexes were much more persistent under these conditions (hours in contrast to seconds). This surprising effect could be explained in a detailed kinetic analysis, and the proposed mechanism is shown in Scheme 1-5 (S and T are additional ligands such as nitrate or solvent molecules, e.g. acetonitrile).⁷⁵ Formation of peroxido-complexes is irreversible and does not depend on the way of its formation. Therefore, differences between the reaction pathways of the iron(II) complexes with dioxygen and those of the iron(III) complexes with hydrogen peroxide could not be the reason for the different stabilities. Instead, it was proposed that the final products of the decomposition reactions of the peroxido complexes are responsible for this effect. These products are tetranuclear oxido-bridged iron(III) complexes that can react again with hydrogen peroxide to reform the blue peroxide compounds. This reaction is reversible, and therefore peroxido complexes prepared from an excess of hydrogen peroxide and iron(III) complexes are stable for hours in contrast to those prepared from iron(II) complexes and dioxygen. If no hydrogen peroxide is present, the peroxido complexes decompose very fast. Preliminary studies also demonstrated that the formed peroxido complexes could be used to oxidize alkanes, even methane, to alkyl hydroperoxides as a major product if certain amino acids were added.⁷⁶ However, this reaction in general would need further optimization.



Scheme 1-5

1.9 Tripodal Tetradentate Ligands and Derivatives

Tetradentate tripodal ligands have attracted great interest during recent years.⁷⁷ Especially tris((2-pyridyl)methyl)amine (= tmpa, also abbreviated as tpa in literature, Figure 1-11) has been used successfully in the bioinorganic chemistry of copper⁷⁸⁻⁸⁰ and to quite a large extent in experimental studies to model iron enzymes (see also chapter 1-14).³⁻⁵

Que and coworkers showed that the iron(III) complex of tmpa is one of the most efficient biomimetic model compounds for intradiol-cleaving catechol dioxygenases.^{3,81} Que and coworkers postulated a mechanism for the reaction of $[\text{Fe}(\text{tmpa})(\text{dbc})]\text{BPh}_4$ (dbc = 3,5-di-tert-butyl-catecholate anion) with dioxygen (Figure 1-12). However, a quantitative kinetic study of this important reaction was lacking.^{3,81} Schindler and coworkers hoped to observe one of the postulated reactive intermediates using low-temperature stopped-flow methods (an approach that has been used by the Schindler group and others successfully in copper dioxygen chemistry),⁸² but such a species could not be detected spectroscopically.⁸³

Temperature dependence studies allowed the calculation of the activation parameter from the Eyring equation as $\Delta H^\ddagger = 23 \pm 1 \text{ kJmol}^{-1}$ and $\Delta S^\ddagger = -199 \pm 4 \text{ Jmol}^{-1}\text{K}^{-1}$.⁸³ These data are in accordance with related reactions in copper chemistry and indicate that the attack of dioxygen on the catecholates complexes is the rate-determining step. The kinetic data therefore do not contradict the postulated reaction mechanism;

however, they also do not provide additional evidence for the occurrence of the described reaction steps.

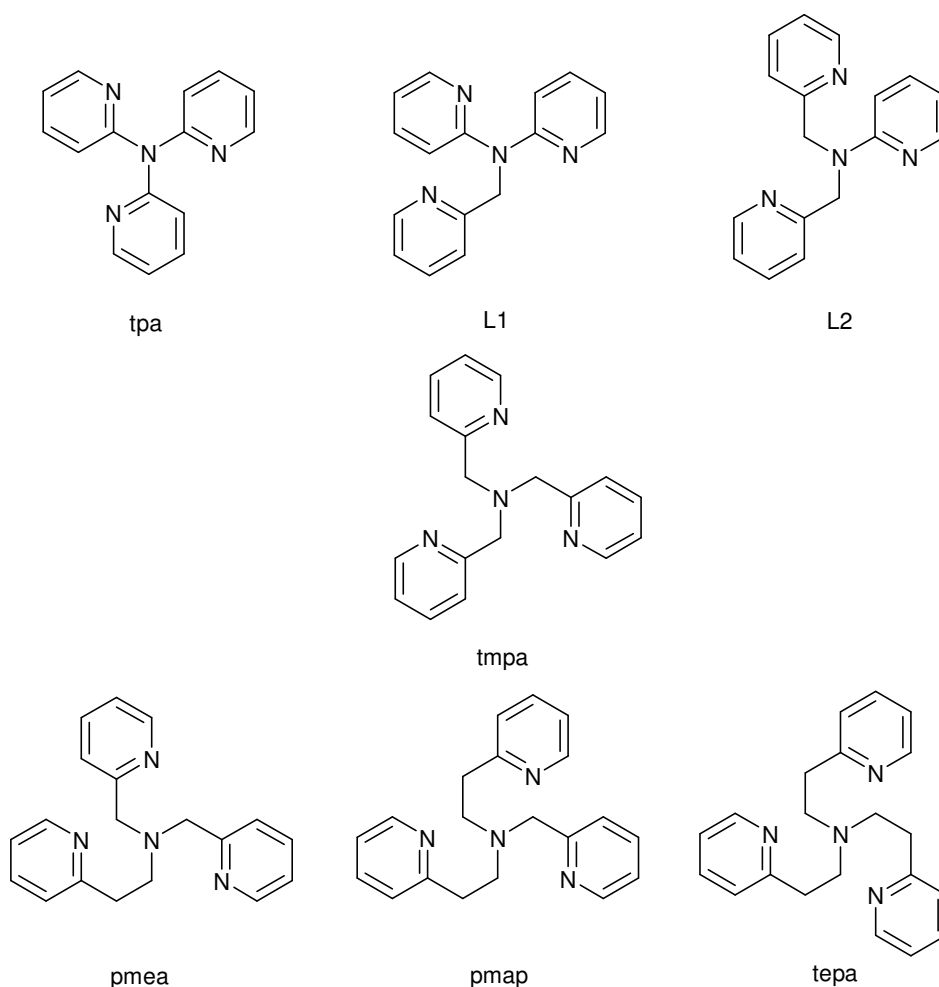


Figure 1-11: Tetradentate pyridyl ligands described in the text.

It can not be determined in a kinetic study at which site the attack takes place without the observation of intermediates. Modifications of the chelate ring sizes could affect the reaction rates and/ or stabilize reactive intermediates (as has been observed previously in kinetic studies on copper complexes).^{84,85}

Therefore, iron(III) complexes with the whole ligand series shown in Figure 1-11 were tested together with different catecholates. Several iron complexes with these ligands could be structurally characterized by the Schindler group, but rates could not be enhanced nor could reaction intermediates be trapped.⁸³

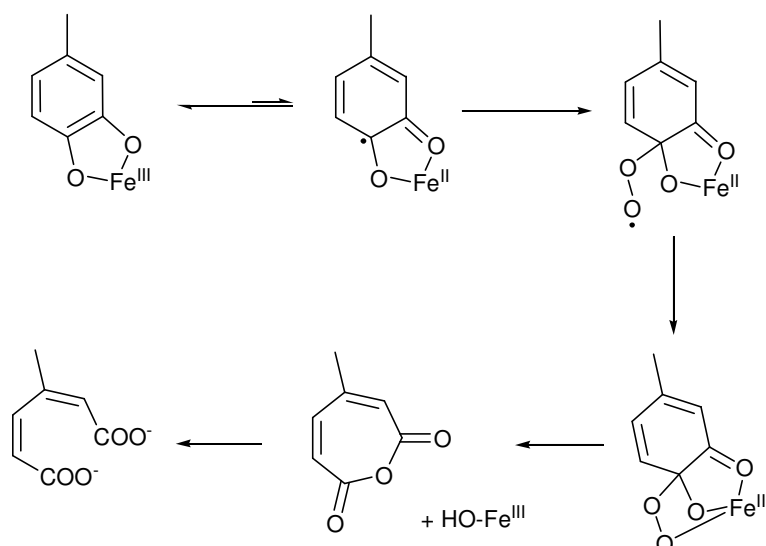


Figure 1-12: Postulated mechanism for the reaction of $[\text{Fe}(\text{tmpa})(\text{dbc})]\text{B}(\text{C}_6\text{H}_5)_4$ with dioxygen.

1.10 The Ligand Uns-penp

In previous studies on the dioxygen activation with copper complexes the Schindler group was quite successful with the systematic approach to substitute pyridyl arms in tmpa through aliphatic amine arms, thus obtaining uns-penp, apme and the commercially available tren ligand (Figure 1-13).^{78,82,86} Uns-penp (N, N-bis[(2-pyridyl)methyl]ethylenediamine) is a very interesting ligand that can be easily modified and different research groups have only recently started to use it in different areas of coordination chemistry (Unfortunately most of the authors do not refer to the original synthesis by Mandel et al.).^{87,88} The Schindler group applied this ligand and derivatives previously in copper coordination chemistry and improved its preparation.⁸⁶ It is remarkable, that up to date only an iron(II) complex of uns-penp has been described in the literature, which was investigated in regard to its spin cross over properties.⁸⁹ Furthermore, very recently an iron(II) complex of a derivative of uns-penp was described.⁹⁰ Apart from that there are no iron(III) complexes described in literature. The Schindler group was able to easily synthesize iron(III) uns-penp complexes and to characterize them by X-ray crystallography.⁹¹ As the catechol 1, 2-dioxygenase activity of this complex system again was lower than with tmpa and it was therefore not investigated further.

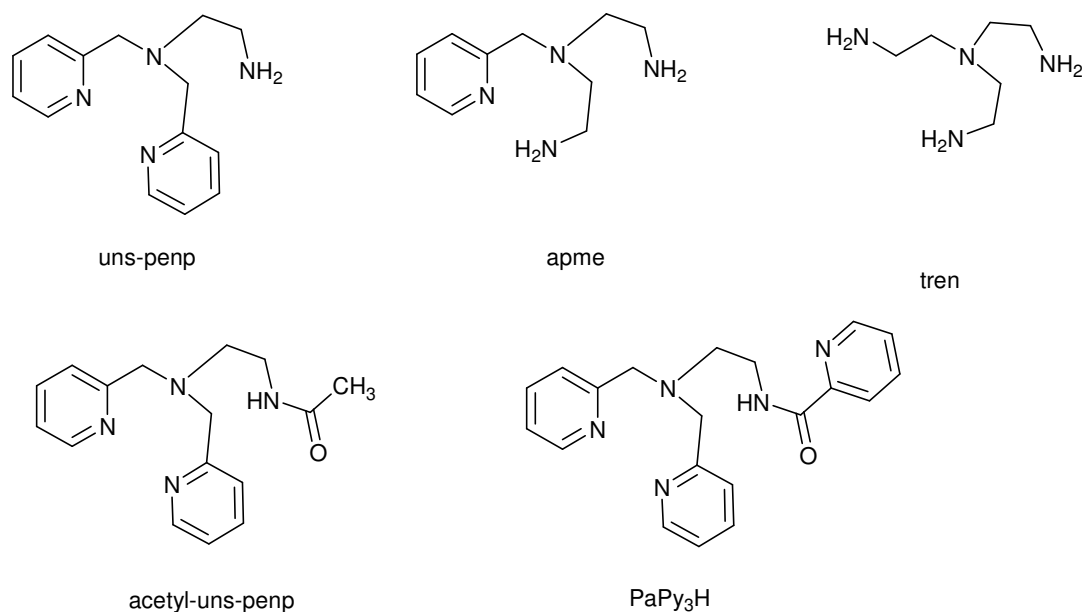


Figure 1-13: The ligand uns-penp and derivatives.

During the synthesis of uns-penp, its acetyl amide derivative, acetyl-uns-penp (N-acetyl-N',N'-bis[2-(pyridyl)methyl]ethylenediamine, Figure 1-13) was prepared, an interesting compound/ligand itself.^{87,91} In the solid state it forms a dimer that could be structurally characterized and the efforts to synthesize the mononuclear deprotonated iron(III) complex $[\text{Fe}(\text{acetyl-uns-penp})](\text{ClO}_4)_2$ led to the formation of the dinuclear complex $[\text{Fe}_2(\text{acetyl-uns-penp})_2\text{O}](\text{ClO}_4)_2 \times \text{H}_2\text{O}$ (Figure 1-14).

It is particularly interesting that the iron complex of the related ligand PaPy₃H described by Mascharak and co-workers is structurally completely different from the compound described by the Schindler group.⁹² In the complex synthesized by Mascharak et al., the oxido-bridge assembles two mononuclear amide complexes (with coordinated deprotonated amide nitrogen atoms whereas the oxygen atoms are not coordinated) to form the dimer (as one would expect). In contrast, the ligand acetyl-uns-penp shows an unusual pentadentate coordination mode displaying deprotonated carboxamido NCO bridging groups. In contrast to the expectations, replacing one pyridyl moiety of the tmpa ligand with a deprotonated carboxamide function again did not improve the oxidation of catecholates relative to the tmpa system.

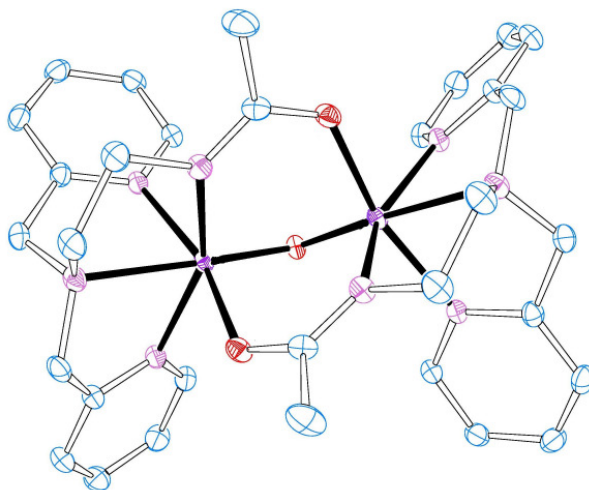


Figure 1-14: Dimeric solid state structure of the complex cation $[\text{Fe}(\text{acetyl-uns-penp})_2\text{O}]-(\text{ClO}_4)_2 \times \text{H}_2\text{O}$. Ortep plot was made with crystallographic data from Ref. 91

However, reactions of iron(III) salts with tetrachlorocatechol ($\text{tcc} =$ tetrachlorocatecholate anion) and triethylamine in solution allowed the isolation and structural characterization of the complex $[\text{Fe}(\text{acetyl-uns-penp})(\text{tcc})_2\text{O}]$ (Figure 1-15).⁹¹

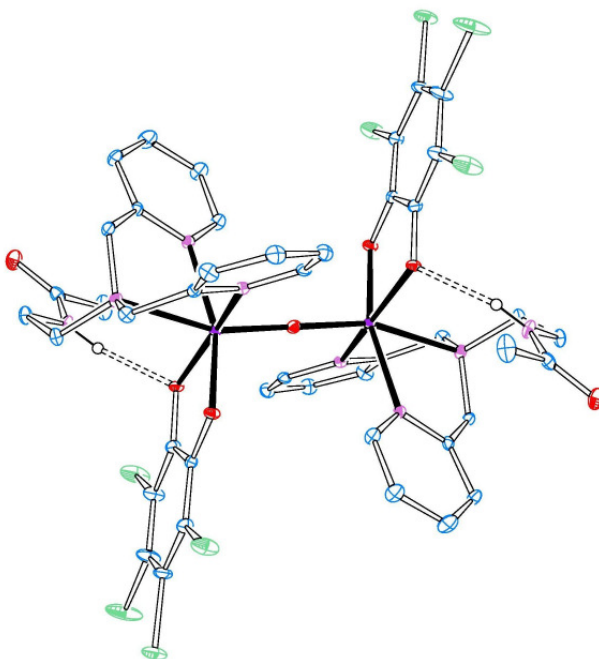


Figure 1-15: Solid state structure of the complex $[\text{Fe}(\text{acetyl-uns-penp})(\text{tcc})_2\text{O}]$. Ortep plot was made with crystallographic data published in Ref. 91

The most striking feature of this complex is that it shows so called secondary interactions, namely intramolecular hydrogen bonds between the carboxamide nitrogen N(4) and O(2) of the catecholate (the donor-acceptor distance has a typical value of 2.755(3) Å and the distance between Fe(1) and N(4) is 3.692 Å). This

intramolecular hydrogen bond between one arm of the tripodal ligand and a coordinated substrate molecule makes this compound an excellent model for the second substrate deprotonation step in the reaction cycle of intradiol cleaving catechol dioxygenases.

1.11 Mononuclear Iron Peroxido Complexes

Efforts by Schindler et al. and other research groups have not been successful in structurally characterizing an end-on superoxido iron complex so far, the first adduct complex that forms during the reaction of an iron(II) complex with dioxygen (Scheme 1-4). Until now, only Que and co-workers reported the spectroscopic characterization of such a species in a dinuclear system.⁹³ In contrast, in cooperation with the research groups of Sundermeyer and Holthausen, Christian Würtele from the Schindler group was able to successfully crystallize an end-on copper superoxido complex and to report its molecular structure previously.⁹⁴ However, it is important to note at this point that it is not always easy to formulate such a transition metal dioxygen adduct complex correctly as a superoxido compound. The real electron density distribution, for example in a copper complex, might not show complete oxidation of the Cu(I) ion to Cu(II) and it might be more correct to describe some of these complexes better as a Cu(III) peroxido species.⁹⁵

Previous investigations and further recent studies on the reported copper superoxido complex as well as on related systems indicate that most likely a hydroperoxido complex is the reactive species. This is further supported through results recently reported by Jörg Müller from the Schindler group on an end-on cobalt superoxido complex (see also chapter 1.3).¹⁴ It is therefore likely, that this reaction in general presents a possible pathway for the oxidation of transition metal complexes with dioxygen. The hydroperoxido complexes are formed as depicted for iron(II) complexes in Scheme 1-4. However, hydroperoxido transition metal complexes can again undergo subsequent reactions and form high-valent mononuclear oxido complexes ($\text{Fe}^{\text{IV}}=\text{O}$, which are discussed for iron compounds in more detail below).^{96,97} Instead of oxidizing the low-valent complexes with dioxygen, hydroperoxido complexes can be obtained more easily from reactions with hydrogen peroxide. Again, in copper chemistry such an end-on hydroperoxido complex could be structurally characterized, by using a ligand (bppa, Figure 1-16) that stabilized this species through secondary interactions by hydrogen bonding.⁹⁸ Also, a mononuclear

spectroscopically and structurally characterized cobalt hydroperoxido complex was described in the literature (see chapter 1.3). This has not yet been achieved in iron chemistry, although Borovik and co-workers obtained a monomeric $\text{Fe}^{\text{III}}=\text{O}$ complex with a deprotonated amide ligand ($\text{H}_6\text{1}$, Figure 1-16) related to bppa, which is also stabilized through hydrogen bonding, which demonstrated the ability of this ligand to stabilise iron-oxygen intermediates.⁹⁹

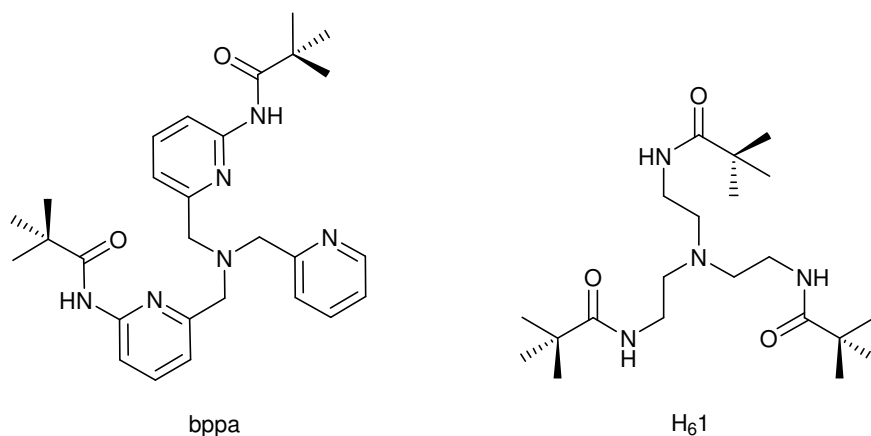


Figure 1-16: The ligands bppa and $\text{H}_6\text{1}$.

As discussed in chapter 1.9, uns-penp is an interesting ligand that can be easily modified at the aliphatic amine arm.

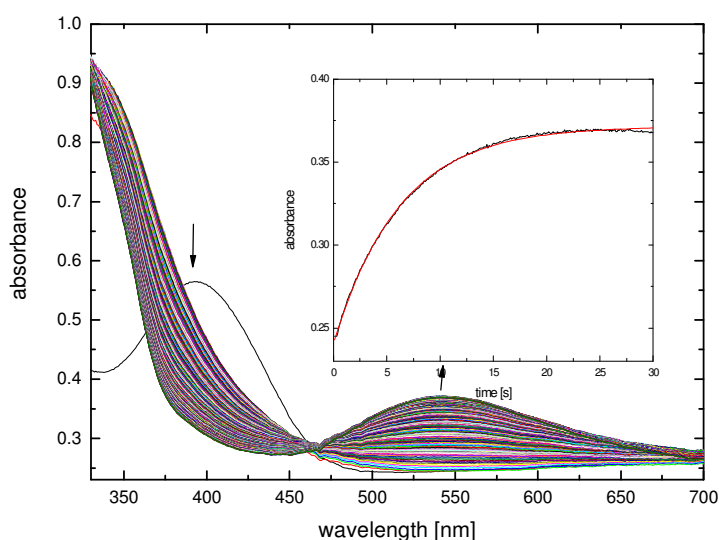
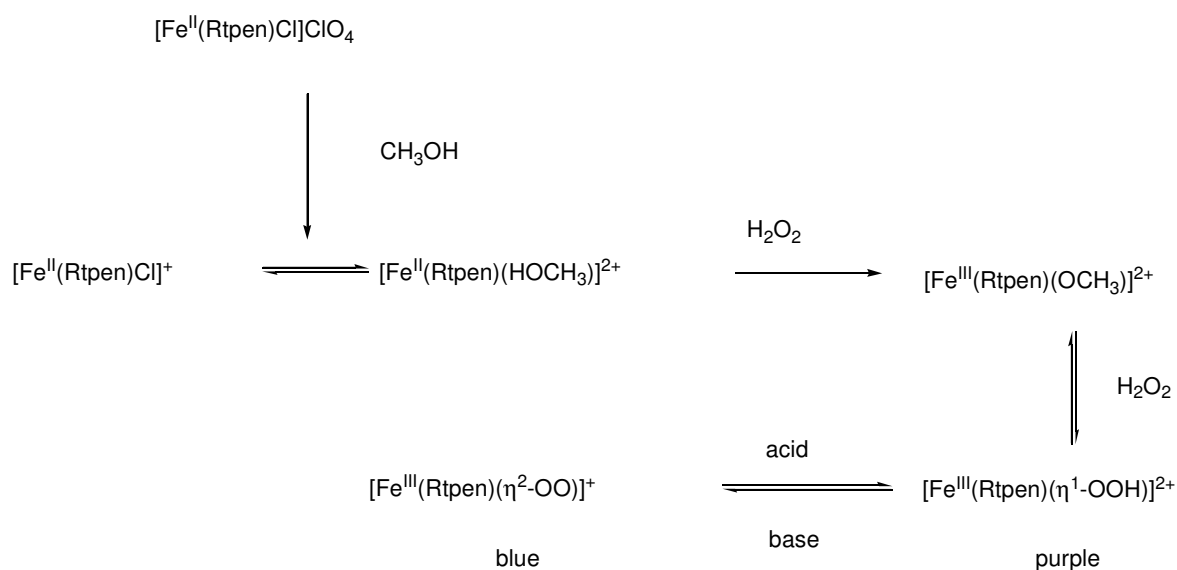


Figure 1-17: Time resolved UV/Vis spectra for the formation of the purple $[\text{Fe}(\text{bztpen})\text{OOH}](\text{ClO}_4)_2$.

Introduction of a further pyridyl group together with different other groups R can be accomplished by facile reductive amination leading to a series of ligands, abbreviated

as Rtpen (Figure 1-13). This method avoids the use of the unpleasant picolyl chloride applied in the original syntheses described.^{100,101} In cooperation with the McKenzie group the Schindler group investigated the reaction of the iron(II) complex $[\text{Fe}^{\text{II}}(\text{bztpen})\text{Cl}]\text{ClO}_4$ (Scheme 1-6) with hydrogen peroxide using stopped-flow techniques.¹⁰² Time-resolved UV/Vis spectra for the formation of $[\text{Fe}(\text{bztpen})\text{OOH}](\text{ClO}_4)_2$ are shown in Figure 1-17.

The mechanism proposed for this reaction is presented in Scheme 1-6. The hydroperoxido complex starts to form immediately after the fast oxidation of Fe^{II} to Fe^{III} .



Scheme 1-6

Deprotonation with base leads to a side-on peroxido iron complex. Unfortunately, so far all efforts to obtain crystals of one of these species for structural characterization have been unsuccessful.

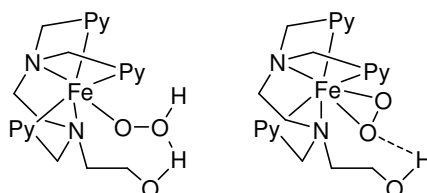


Figure 1-18: Attempt to stabilize either the hydroperoxido or peroxido intermediate by secondary hydrogen bonding interaction in the complexes $[\text{Fe}(\text{etOHtpen})\text{OOH}]^{2+}/[\text{Fe}(\text{etOHtpen})\text{OO}]^+$

In one attempt to stabilize either the hydroperoxido or the peroxido complex through secondary interactions, the ligand Rtpen was used with $\text{R} = \text{EtOH}$ to create a

situation suitable for an intramolecular hydrogen bonding interaction as shown in Figure 1-18. Unfortunately, no significant stabilization was achieved and indeed this complex even decomposed faster than the other derivatives of this complex.

From kinetic studies, a negative activation entropy ($\Delta S^\ddagger = -72 \pm 8 \text{ Jmol}^{-1}\text{K}^{-1}$) was obtained for the formation of $[\text{Fe}(\text{II})(\text{bztpen})\text{OOH}](\text{ClO}_4)_2$, suggesting an associative mechanism. However, this was in contrast to a series of related reactions, which were investigated in the past and which accounted for a pure interchange mechanism.¹⁰³

1.12 Iron Oxido Complexes

Fully characterized high-valent (oxidation states V and VI) iron complexes have been recently described.^{104,105} However, in bioinorganic chemistry iron(IV) oxido species probably play a more important role as active species in most selective substrate oxidations.¹⁰⁶⁻¹⁰⁸ Figure 1-19 shows some examples for iron(IV) intermediates, which are proposed as active species in enzyme reactions.

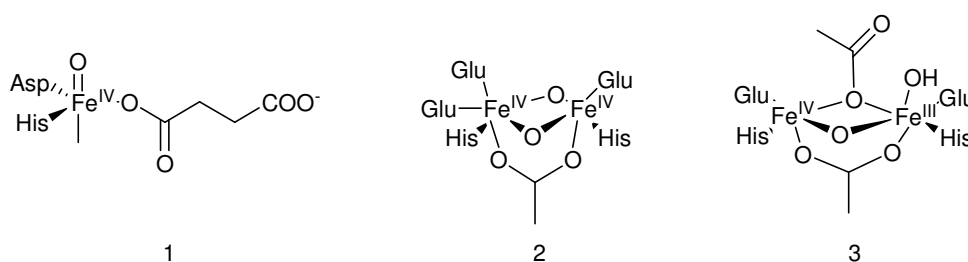


Figure 1-19: Proposed structures for high-valent intermediates of TauD J (α -Ketoglutarate Dioxygenase Intermediate J)(1), MMO Q (2) and RNR R2 X (Ribonucleotide Reductase Intermediate X) (3).⁶⁸

Excellent work by Que and co-workers allowed for the first time the structural characterization of a mononuclear $\text{Fe}^{\text{IV}}=\text{O}$ complex, using a simple macrocycle, methylated cyclam, as ligand (Figure 1-20).^{68,109} From the full spectroscopic description of this system it was easy to spectroscopically detect the occurrence of this species as an intermediate with a series of ligands in solution and quite surprisingly, even in water.^{68,110,111,112-114}

During these studies it could be furthermore demonstrated that an iron complex with different ligands (some examples are depicted in Figure 1-21), for example bztpen as well as the related N4Py (see Figure 1-21), can form iron(IV)oxido compounds and

that these species are able to oxidize substrates, even alkanes such as cyclohexane.^{111,112}

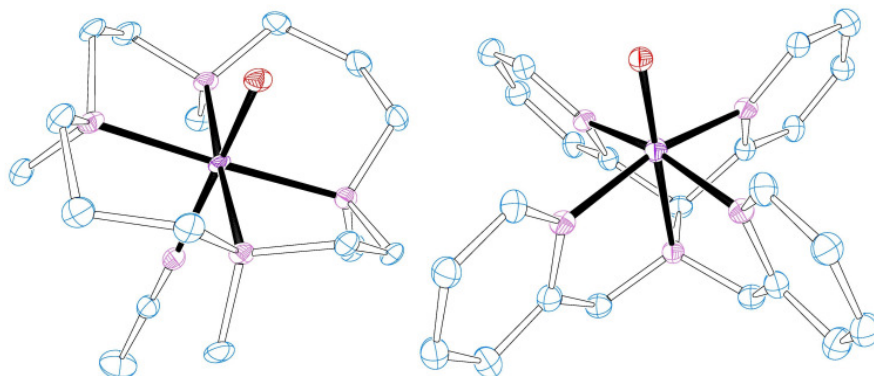


Figure 1-20: Ortep plot of $[\text{Fe}^{\text{IV}}(\text{O})(\text{TMC})(\text{MeCN})]^{2+}$ based on structural data reported in Ref. 108 (left) and Ortep plot of $[\text{Fe}^{\text{IV}}(\text{O})(\text{N4Py})]^{2+}$ based on the structural data reported in Ref. 112 (right)

Most recently, Que and co-workers demonstrated that using the ligand acetyl-uns-penp, described above, leads to quite interesting oxidation reactions of the relevant iron complexes using an oxidant and a substrate (see also chapter 6).

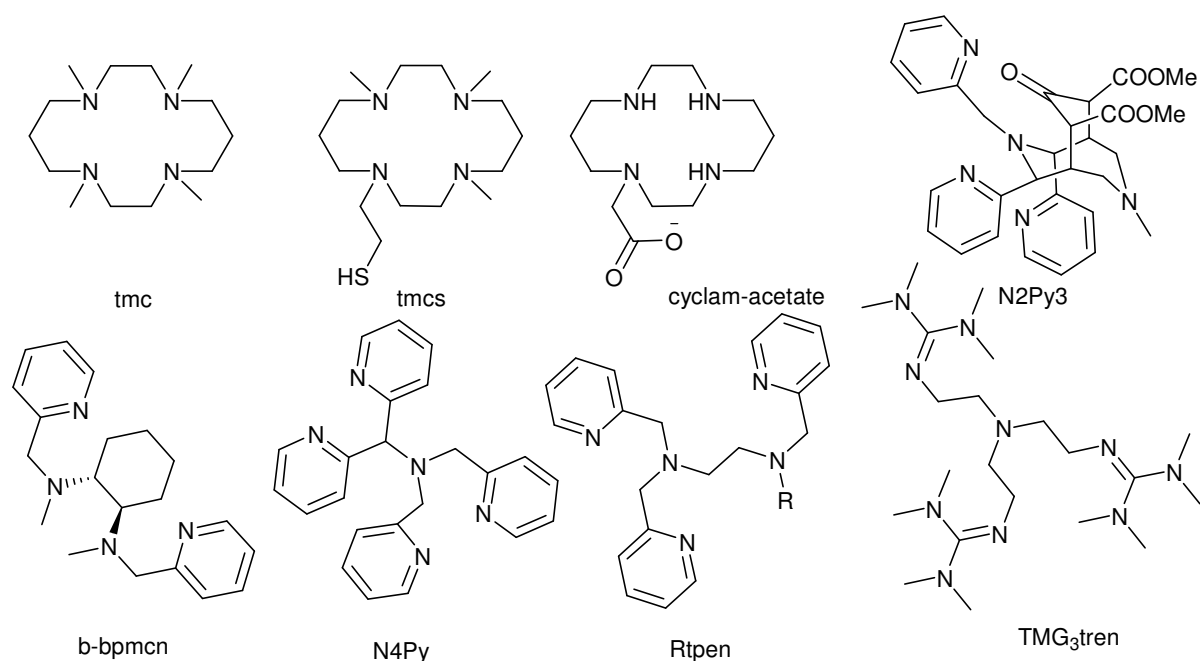


Figure 1-21: Selected ligands that support the formation of iron(IV)-oxido species

1.13 Model Complexes for Methane Monooxygenase

As described in chapter 1.6 as active species of MMO, the intermediate Q consist of an dinuclear iron(IV)oxido diamond core. For further information about the reaction mechanism and to mimic the reactivity of MMO it is necessary to use dinuclear iron model complexes.⁴ Very good model complexes for the MMO-catalytic cycle and other NH enzymes are iron complexes with the tetradentate ligand tmpa (tris-(2-

pyridylmethyl)amine and its derivatives.^{5,115-117} Mononuclear as well as dinuclear iron complexes of these ligands are known, which is important to compare the reactivities of the species directly.

The most interesting aspect of the iron-tmpa system is the formation of the well characterized high-valent $[\text{Fe}^{\text{III}}\text{Fe}^{\text{IV}}-(\mu\text{-O})_2(\text{tmpa})_2]^{3+}$ compound, which is formed by reaction of a (μ -oxido)diiron(III) precursor, which is the one-electron reduced relative to MMO-intermediate Q, with hydrogen peroxide.^{72,118,119} The knowledge of the structure and the spectroscopic properties of such synthetic $\text{Fe}_2(\mu\text{-O})_2$ clusters lead to a better understanding of the behavior of MMOH intermediate Q, which is assumed to have a $\text{Fe}^{\text{IV}}_2(\mu\text{-O})_2$ cluster, on its active site.

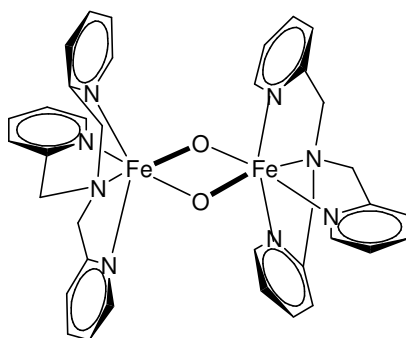


Figure 1-22: Proposed structure for the $\text{Fe}^{\text{IV}}_2(\mu\text{-O})_2$ tmpa diamond core.

L. Que and co-workers claimed to have synthesized a dinuclear complex, which was characterized by EXAFS and resonance Raman spectroscopy as an $[\text{Fe}^{\text{IV}}_2(\mu\text{-O})_2(\beta\text{-BPMCM})_2](\text{OTf})_4$ complex by reaction of a mononuclear iron(II) precursor complex of the ligand BPMCM (N,N'-bis(2-pyridylmethyl)-N,N'-dimethyl-trans-1,2-diaminocyclohexane) with tBuOOH.¹²⁰ Additional data from further investigations led to reformulation of the species as an $\text{Fe}^{\text{IV}}(\text{OH})(\text{OOR})$ species.¹¹⁷ In 2005 the first (μ -oxido)-diiron(IV) complex was structurally and spectroscopically characterized.¹²¹ In this case the high oxidation state was stabilized by the tetraanionic, macrocyclic TAML ligand ("tetra anionic macrocyclic ligand", 3,3,6,6,9,9-hexamethyl-3,4,8,9-tetrahydro-1H-1,4,8,11-benzotetraazacyclotridecine-2,5,7,10(6H,11H)-tetraone). The first $\text{Fe}^{\text{IV}}(\mu\text{-O})_2$ complexes were reported in 2007.¹²² They were synthesized by one-electron reduction of $[\text{Fe}^{\text{III}}\text{Fe}^{\text{IV}}-(\mu\text{-O})_2]^{3+}$ precursors with TMPA-type ligands by bulk electrolysis. These are the first synthetic complexes that mimic the oxidation state and structure of the MMOH Intermediate Q.

1.14 Projects

As discussed above, iron and cobalt complexes are useful as model compounds for dioxygen activation. The characterization of oxygen intermediates is very important for a detailed understanding of these reactions. In copper chemistry most oxygen adducts are known by now and have been structurally characterized.^{78-80,94} In non-heme iron chemistry so far only bridged peroxides and iron(IV) oxido species could be isolated (see chapters 1.9 and 1.13). It would therefore be of great interest to characterize other iron oxygen adducts, which take part in enzymatic reactions.

1.14.1 Reactions of Metal Complexes with the Ligand bztpen and Derivatives towards Hydrogen Peroxide

As described above (chapter 1.12) iron complexes with Rtpen type ligands such as bztpen react with hydrogen peroxide to form mononuclear hydroperoxido intermediates. These complexes can react with bases such as triethylamine to form peroxido complexes. Isolation and characterization of these intermediates at low temperatures would be of great interest. Therefore, the following tasks should be accomplished in detail during this thesis work:

- Synthesis, isolation and characterization of hydroperoxido and peroxido complexes of iron complexes using the ligand bztpen or derivatives.
- Cobalt(II) compounds with Rtpen ligands have not been described so far. Because of the fact that cobalt complexes more easily form hydroperoxido or peroxido complexes, attempts should be made to characterize these complexes in analogy to the iron derivatives.
- The new “bridged” bztpen ligand bz-b-tpen depicted in Figure 1-23 and related iron(II) complexes should be synthesized and characterized. Because of the fact that in MMO intermediate Q a dinuclear complex is formed from two monomers, the application of a preorganized dinucleating ligand would favor the reaction to a diiron diamond core or lead to an additional stabilization of hydrogen peroxide adduct complexes by secondary interactions.

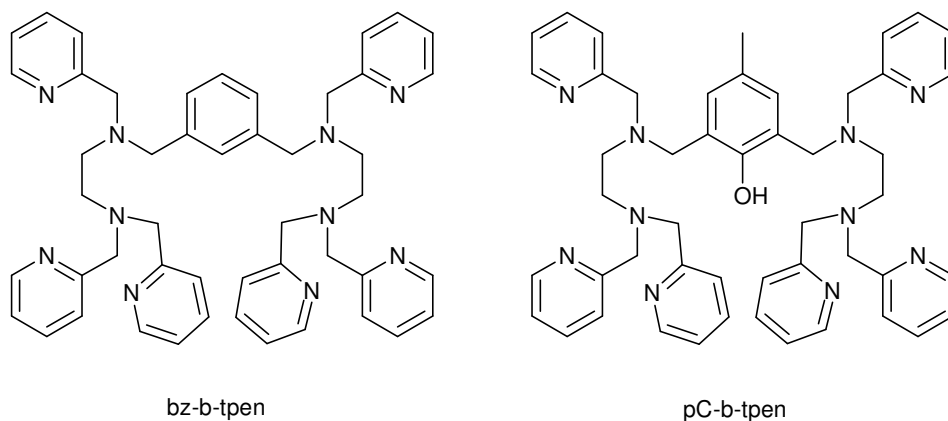


Figure 1-23: bz-b-tpen and pC-b-tpen.

A possible reaction of these intermediates is the intramolecular hydroxylation of an aromatic ring. To have analogue substances for structural and spectroscopic studies, the phenol bridged ligand pC-b-tpen should be synthesized. However, this molecule should also be an interesting ligand in iron coordination chemistry itself.

1.14.2 Kinetic Investigations on Hydroperoxido Complex Formation

The formation of the iron-bztpen hydroperoxido complex was subject of a detailed kinetic study in the past as described in Chapter 1.12. The activation parameters were calculated on the basis of the reactions temperature dependence. The activation entropy indicated an associative mechanism with a seven-fold coordinated transition state for this reaction. Because of conflicts with other results for similar reactions and because of the large experimental error activation entropies, the more reliable activation volumes should be obtained from a pressure dependence of the reaction in this work. That way a better description of the reaction mechanism should be obtained.

1.14.3 Metal Complexes with Uns-penp and Derivatives

As described before, uns-penp and derivatives are very useful ligands that can be utilized for enzyme model complexes. Figure 1-24 shows the derivatives of the uns-penp ligand family that were used for this work. The acetylamide derivative of uns-penp, acetyl-uns-penp was previously used for intensive studies on iron(III) compounds in the Schindler group.

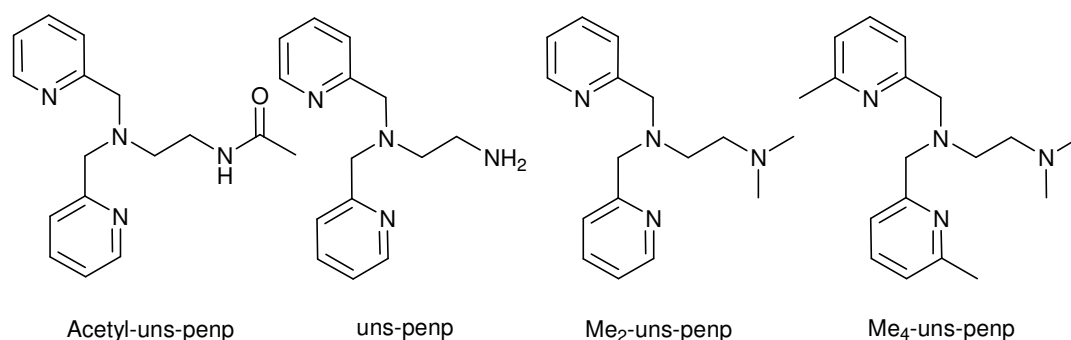


Figure 1-24: uns-penp and derivatives used in this work.

Because of the fact that active species of iron enzymes are in the ferrous oxidation state (see above) the reactivity of iron(II) complexes with acetyl-uns-penp would be of great interest. Therefore iron(II) compounds with acetyl-uns-penp should be characterized in this work. Due to the acidity of the amide function attempts to change the coordination mode and reactivity of the complexes by deprotonation of the ligand were made. The lack of cobalt compounds with the ligand acetyl-uns-penp lead to attempts to synthesize and characterize such complexes.

Other ligands of the uns-penp family are Me₂-uns-penp and Me₄-uns-penp. Here, the properties of the ligand are tuned by systematic substitution of hydrogen atoms by methyl groups. New iron and cobalt compounds with Me₂-uns-penp and Me₄-uns-penp should be synthesized and characterized in this work.

2 Theory of Reaction Kinetics

One main goal of reaction kinetics is the investigation of reaction mechanisms. Here, it is necessary to follow the progress of a chemical reaction with variation of different parameters especially concentration, temperature, pressure and solvent.

The following chapter explains terms and equations of the chemical reaction kinetics, which are important for this work. Further details and complete descriptions of this topic are noted in several textbooks.¹²³⁻¹²⁶

2.1 The Reaction Rate

The change in the concentrations of educts and products in a chemical reaction can be used to characterize the rate of a chemical reaction. Formally a reaction can be described as the differential change of n_i :

$$dn_i = \nu_i \cdot d\zeta \quad [2.1]$$

Herein ζ describes the progress of the reaction; n_i stands for the amount of matter, ν_i are the stoichiometric coefficients. If the volume is constant, a reaction can be described as:

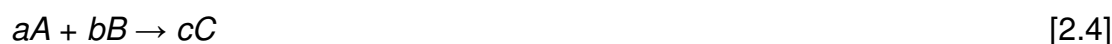
$$\frac{dn_i}{V} = \nu_i \cdot \frac{d\zeta}{V} = \nu_i \cdot d\chi \quad [2.2]$$

with χ as volume based extent of the reaction.

The reaction rate ν_R is defined for a closed system with constant-volume as:

$$\nu_R = \frac{d\chi}{dt} = \frac{1}{\nu_i} \cdot \frac{dc_i}{dt} \quad [2.3]$$

The reaction rate for a general reaction is given as follows:



$$\nu_R = -\frac{1}{a} \frac{d[A]}{dt} = -\frac{1}{b} \frac{d[B]}{dt} = \frac{1}{c} \frac{d[C]}{dt} \quad [2.5]$$

If the reaction rate is only dependent on the concentrations of the educts A and B , the proportionality factor k in the rate law is termed as the rate constant of the reaction:

$$v_R = -\frac{d[A]}{dt} = k[A]^x[B]^y \quad [2.6]$$

The sum of the term x and y determines the order of reaction. For example when $x = 1$ and $y = 2$, the reaction is termed first order in A and second order in B , and the reaction is third order.

2.2 First Order Dependence

Reactions with first order dependence are very common. The reaction rate is only determined by the concentration of one reactant.

The decrease in concentration of A over time can be written as shown in equation 2.7, for a chemical reaction like $A \rightarrow B$. The reaction rate is proportional to the first power of $[A]$:

$$-\frac{d[A]}{dt} = \frac{d[B]}{dt} = k[A] \quad [2.7]$$

The differential form leads to an equivalent integrated expression:

$$\int_{A_0}^A \frac{d[A]}{[A]} = -k \int_0^t dt \Rightarrow \ln \frac{[A]}{[A_0]} = -kt \quad [2.8]$$

To establish first order kinetics for a reaction it is usual to plot concentration versus time. It is common to measure properties like absorbance or conductivity, which are proportional to the concentration of the reactant. The plot of the natural logarithm of concentration of A versus time gives a linear dependence. The slope of the straight line is $-k$. The rate constant for a first order reaction could be calculated from the slope of a plot of the experimental data.

Nowadays, linearization of the experimental data is not necessary, because exponential functions could be directly fitted to the absorbance time traces (iteration) with computer programs.

2.3 Second Order Dependence

Many reactions of complex ions are second order in the reactants. Generally in a reaction between the two reactants A and B , the reaction order is 1 for each reactant, but second order overall, because the rate is proportional to the product of the two concentrations. The second order reaction law for a common reaction is determined by:



$$-\frac{d[A]}{dt} = -\frac{d[B]}{dt} = \frac{d[C]}{dt} = k[A][B] \quad [2.10]$$

Integration leads to:

$$\frac{1}{[A]_0 - [B]_0} \cdot \ln \frac{[B]_0 \cdot [A]}{[A]_0 \cdot [B]} = kt \quad [2.11]$$

It is common and much easier to investigate such reactions under pseudo first order conditions. This means that one of the educts is provided in excess in respect to the other one (minimum 10:1 ratio). In such cases the concentration of the reactant in excess can be regarded as constant and implicated into the rate constant (now pseudo-first order constant). So a first order reaction constant can be obtained from a second order rate equation. Thus it is much easier to obtain the integrated rate equation and the rate constants are again independent of the concentrations. If the concentration of B is much larger than the concentration of A , the rate law can be written as:

$$-\frac{d[A]}{dt} = k_{obs}[A] \quad [2.12]$$

which leads to an expression for the observed rate constant:

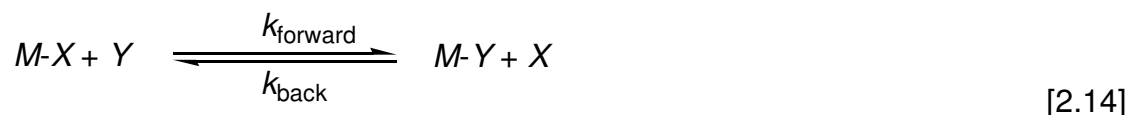
$$k_{obs} = k[B]_0 \quad [2.13]$$

To obtain the rate constant k it is usual to plot k_{obs} versus $[B]_0$

2.4 Reactions in Equilibria

Most chemical reactions such as ligand exchange reactions of coordination compounds are equilibrium reactions, defined by the backward and forward reaction.

This means for a typical reaction in equilibrium:



(M = metal ion; X , Y = ligands)

When the concentrations of the ligands X and Y were kept in great excess with respect to the concentration of the metal complex, it is possible to get pseudo first order conditions concerning k_{forward} and k_{back} . Therefore the reaction rate for this kind of reactions can be expressed as:

$$-\frac{d[M-X]}{dt} = \frac{d[Y]}{dt} = k_{\text{forward}} [M-X][Y] - k_{\text{back}} [M-Y][X] \quad [2.15]$$

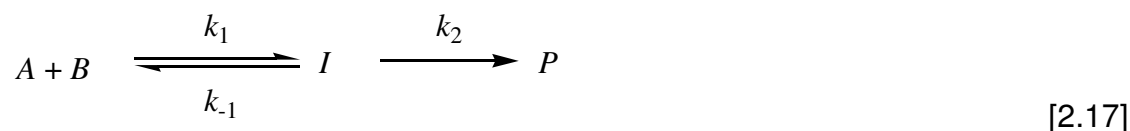
with:

$$k_{\text{obs}} = k_{\text{forward}} [Y] - k_{\text{back}} [X] \quad [2.16]$$

The rate constant k_{obs} is determined as sum of k_{forward} and k_{back} . Both can be obtained by plots of k_{obs} versus $[X]$ or $[Y]$.

2.5 Consecutive Reactions

Many reactions in chemistry include several reaction steps. In this cases all educts, products and intermediates can have influence on the reaction kinetics. In enzyme kinetics this fact is described within the Michaelis-Menten theory as saturation concentration of the enzyme substrate complex. In the simplest case only one intermediate is formed in a reversible reaction step. Several reaction pathways can be observed. In most simple case only one intermediate is formed in a reversible reaction step. The determination of the according rate law is more complex when multiple reversible reaction steps are included. The simple case with one reversible reaction is shown in equation 2.17:



(A, B = educts; I = intermediate; P = product)

The mathematical description of such reactions is quite difficult. So it is common to use approximations to simplify such terms.

One approach can be used if the first step of the reaction is much faster than the second step. In this case k_1 and k_{-1} are much larger than k_2 . Here the intermediate I will be in equilibrium with A and B and will be continually maintained:

$$K = \frac{[I]}{[A][B]} \quad [2.18]$$

A mathematical term for k_{obs} is formed, when equation 2.17 is inserted in equation 2.18.

This is considered to be the solution of the rate law.

An alternative method to simplify such complex reactions is the steady-state approximation. It is supposed that the intermediate reacts very fast to the product, so that the concentration of I is very low in the reaction mixture. In this case the rate of concentration change of I is nearly zero:

$$[I] \ll [A], [B] \quad \frac{d[I]}{dt} \approx 0 \quad [2.19]$$

and therefore:

$$k_1[A][B] - k_{-1}[I] - k_2[I] = 0 \quad [2.20]$$

With this equation it is possible to form a mathematical term for k_{obs} without knowing the exact concentration of I . The steady state approximation facilitates the solution of the differential equation which results from most reaction laws, which lack of analytical solutions.

2.6 Determination of the Activation Enthalpy ΔH^\ddagger , the Activation Entropy ΔS^\ddagger , and the Activation Volume ΔV^\ddagger

The theory of the transition state and the activated complex is described in the Eyring-Polanyi equation. It is the basis for the determination of the activation parameters ΔH^\ddagger , ΔS^\ddagger , and ΔV^\ddagger . The dependence of the reaction rate from temperature is described in equation 2.21. This mathematical term combines transition state theory and basic thermodynamic concepts:

$$k = \frac{k_b T}{h} \cdot e^{\left(\frac{\Delta H^\ddagger}{RT} + \frac{\Delta S^\ddagger}{R} \right)} \quad [2.21]$$

ΔH^\ddagger is the activation enthalpy and ΔS^\ddagger is the activation entropy. This term is known as Eyring equation

From linearization follows:

$$\ln\left(\frac{k}{T}\right) = \ln\left(\frac{k_b}{h}\right) - \frac{\Delta H^\ddagger}{RT} + \frac{\Delta S^\ddagger}{R} \quad [2.22]$$

Variation of reaction temperature allows the determination of the reaction rate. The plot of $\ln(k/T)$ versus $1/T$ gives a straight line and is known as "Eyring-plot". The slope is $-(\Delta H^\ddagger/R)$ from which the activation enthalpy can be derived. The activation entropy can be derived from extrapolation and the intercept of the straight line.

The investigation of the temperature dependence of a reaction provides the value of ΔS^\ddagger , which contains important information about the activated complex. A more ordered transition state is indicated by a large negative value of ΔS^\ddagger . In this case, the degrees of freedom (translation, rotation and vibration) are reduced to the activated complex in comparison with the reactants. Therefore, a quite negative value of ΔS^\ddagger supports an associative mechanism, whereas a positive ΔS^\ddagger indicates a dissociative mechanism.

The determination of ΔS^\ddagger through the "Eyring-plot" usually leads to large errors because the intercept is extrapolated ($T \rightarrow \infty$). The activation volume of a reaction can be obtained in contrast with much smaller errors by investigation of the pressure dependence of a reaction. The high pressure measurements lead to more reliable

data for a mechanistic discussion of a reaction. The pressure dependence is determined as:

$$\left(\frac{\partial G}{\partial p}\right)_T = V \Rightarrow \Delta V^\ddagger = \left(\frac{\partial(\Delta G^\ddagger)}{\partial p}\right)_T \quad [2.23]$$

with $\Delta G = -RT \ln k$ follows

$$\Delta V^\ddagger = -RT \left(\frac{\partial(\ln k)}{\partial p}\right)_T \quad [2.24]$$

The activation volume can be interpreted according to the transition state theory as the difference between the partial molar volumes of the educts and the partial molar volumes of the transition state. When $\ln k$ is plotted versus the pressure p , ΔV^\ddagger , can be determined from the slope.

3 A reinvestigation of the formation of mononuclear Fe(III) peroxides using high pressure kinetics

This chapter has been submitted to Dalton Transactions:

Thomas Nebe, Alexander Beitat, Christian Würtele, Carlos Dücker-Benfer, Rudi van Eldik, Christine J. McKenzie and Siegfried Schindler

3.1 Abstract

Previous stopped flow kinetic experiments indicated an interchange associative mechanism for the ligand substitution reaction, $[\text{Fe}(\text{bztpen})(\text{OMe})]^{2+} + \text{H}_2\text{O}_2 \rightarrow [[\text{Fe}(\text{bztpen})(\text{OMe})(\text{HOOH})]^{2+}]^\ddagger \rightarrow [\text{Fe}(\text{bztpen})(\text{OOH})]^{2+} + \text{CH}_3\text{OH}$ (bztpen = N-benzyl-N, N',N'-tris(2-methylpyridyl)ethylenediamine). Thus a seven coordinated intermediate containing both the leaving methoxide and the incoming hydrogen peroxide ligands was proposed. On the basis of high pressure techniques we can now conclude that this is not the case since the activation volume of the reaction is independent of pressure in the formation of the purple low spin transient hydroperoxide complex, $[\text{Fe}(\text{bztpen})(\text{OOH})]^{2+}$. $[\text{Fe}(\text{bztpen})(\text{OOH})]^{2+}$ is short-lived and has never been isolated and structurally characterized. Thus we pursued characterization of the analogous Co(III) peroxide complexes, which might be expected to be more readily attainable. The Co(II) complexes $[\text{Co}(\text{bztpen})\text{Cl}]\text{BF}_4$, $[\text{Co}(\text{metpen})\text{Cl}]\text{SbF}_6$ and $[\text{Co}(\text{bztpen})(\text{OAc})]\text{BPh}_4$ were structurally characterized. However, these were neither oxygenated, peroxidized or oxidized when exposed to O_2 and H_2O_2 . The new iron(II) complex $[\text{Fe}(\text{bztpen})(\text{OAc})](\text{BPh}_4)$ and the free ligand were also characterized by single crystal X-ray diffraction.

3.2 Introduction

Binding and activating oxygen by metalloenzymes plays a fundamental role for aerobic life. Iron porphyrin based proteins have been intensively studied in the past, more recently non heme iron containing enzymes such as methane monooxygenase (MMO) have attracted great interest.^{4,50,73,127} MMO for example catalyzes the selective oxidation of methane to methanol under ambient conditions using air as an oxidant. In general these selective oxidation reactions of hydrocarbons with dioxygen under ambient conditions are extremely interesting. Chemists would like to perform

these reactions in the lab or in industry using iron complexes as catalysts. Therefore, synthetic iron complexes have been thoroughly investigated as functional model compounds for iron enzymes.^{3-5,68} It is a well known fact that iron superoxido, peroxido, hydroperoxido or oxido complexes are important intermediates during these oxidation reactions. Apart from synthetic investigations kinetic studies have helped to gain better insight into the detailed mechanism of these oxidation reactions.⁵ Often the easiest way to prepare model Fe peroxides or high valent oxides is to react starting complexes with hydrogen peroxide instead of dioxygen and quite a large number of studies have been performed on the reaction of iron complexes with hydrogen peroxide.^{69-71,73,101,118,128-131}

Rtpen type ligands (Figure 1) introduced by the McKenzie group gained a lot of interest in the past due to the fact that their iron complexes form quite stable hydroperoxido and peroxido complexes.^{68,113,132} Furthermore, they can form reactive iron(IV)oxido species, which are able to attack C-H-bonds like those found in cyclohexane.¹³³ The iron complexes of bztpen (Fig. 1: R = Bz; N-benzyl-N,N',N'-tris(2-pyridylmethyl)-1,2-ethylenediamine) have been investigated in most detail.^{100,102,113,132,134,135}

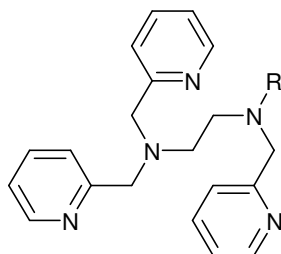


Figure 3-1: The ligands Rtpen.

The iron(II) chloride and iron(III) methoxide complexes of bztpen react with hydrogen peroxide to form a purple end-on hydroperoxido complex. The iron(III) hydroperoxido intermediate is not a strong oxidant,¹³⁶ but hydroperoxides or peroxides are possible precursors for the formation of iron(IV)oxido species.^{108,132} Scheme 1 presents the mechanism of the formation of the hydroperoxido and peroxide complexes postulated from the results of our previous investigations.¹⁰² In a first step the chlorido ligand is exchanged reversibly by a solvent molecule. The solvated complex is oxidized. The resulting iron(III) complex reacts with hydrogen peroxide to form a purple hydroperoxido intermediate. This intermediate can be deprotonated reversibly with bases such as triethylamine. A detailed kinetic study of the reaction of the iron(III) complex with hydrogen peroxide was performed.¹⁰² Activation parameters were

methods.^{101,134,141} $[\text{Fe}(\text{bztpen})\text{Cl}]\text{ClO}_4$ for the kinetic measurements was synthesized according to the literature method.¹⁰² $[\text{Fe}(\text{CH}_3\text{CN})_2(\text{triflate})_2]$ was also synthesized according to a literature method.¹⁴² Nitric oxide was made by reaction of a sulfuric acid/ iron sulfate solution with sodium nitrite under argon-atmosphere. The gas was purified by purging through a 2 M sodium hydroxide solution. If not mentioned otherwise all reactions were performed under ambient conditions and air.

Caution! The perchlorate salts used in this study are potentially explosive and should be handled with care.

3.3.2 Kinetic Measurements

Stopped-flow experiments at ambient pressures were performed with a commercially available Hi Tech (Salisbury, GB), SF-61DX2 instrument. Detailed descriptions on low temperature stopped flow kinetics were published previously.^{5,82} The effect of pressure was measured on a home built high-pressure stopped-flow instrument in the van Eldik group. Details of the instrumentation and measurements were described recently.¹⁴³ Methanol p.a. (from Aldrich) was used for the kinetic measurements without further purification. Solutions were 2×10^{-4} M in the iron complex and the concentrations of the hydrogen peroxide solutions were varied from 0.02 to 0.2 M for hydroperoxido complex formation and from 0.01 to 1.5 M for oxidation of the iron(II) complex (pseudo first order conditions $[\text{H}_2\text{O}_2] \gg [\text{complex}]$). Hydrogen peroxide solutions were made by dilution of p.a. grade 35 % hydrogen peroxide (manganometric titrations were used to determine the exact concentration) with methanol. The water concentration was kept constant by adding small amounts of water. Data from normal pressure kinetic measurements were treated by extracting single absorbance vs. time traces. These traces were fitted to single exponential functions using the integrated Hi Tech software Kinet Assist.¹⁴⁴ High pressure time traces were fitted using Olis and Origin software.^{145,146}

3.3.3 X-ray Crystallography

A STOE IPDS-diffractometer equipped with a low temperature system (Karlsruher Glastechnisches Werk), a graphite monochromator and IP detector system with Mo- K_α radiation ($\lambda = 0.71069 \text{ \AA}$) was used. The frames were integrated with the STOE software package. No absorption corrections were applied.

All structures were solved by direct methods and refined by using fullmatrix least squares in SHELXL software package.^{147,148} All non hydrogen atoms were refined anisotropically. All hydrogen atoms were positioned geometrically.

3.3.4 Syntheses

3.3.4.1 *Bztpen* (**1**)

Single crystals of *bztpen* were obtained by recrystallization of a pure sample from petrol ether.

3.3.4.2 *[Fe(bztpen)(OAc)]BPh₄* (**2**)

42.4 mg (0.1 mmol) of *bztpen* and 11.6 mg (0.095 mmol) $\text{Fe}(\text{OAc})_2$ were dissolved in 1 ml methanol by gently warming to 50 °C. The mixture was allowed to cool down to room temperature. A mixture of 1 ml 0.1 M hydrogen peroxide solution in methanol and 5 mg (0.5 mmol) triethylamine was added. The mixture reacted under heating and a dark brown solution was formed. Small amounts of a precipitate were formed and decanted from the solution. Crystals suitable for X-ray analysis were grown by adding the solution to 51 mg (0.15 mmol) NaBPh_4 . The assay was kept at -30 °C. After 2 months yellow block shaped crystals were formed. Calc. for $\text{C}_{53}\text{H}_{52}\text{BFen}_5\text{O}_2$: C, 74.22; H, 6.11; N, 8.17%. Found: C, 73.20; H, 6.02; N, 7.66%. ESIMS (CH_3CN), m/z (% assignment): 239.59 (75, $[\text{Fe}(\text{bztpen})]^{2+}$), 514.16 (60, $[\text{Fe}(\text{bztpen})\text{Cl}]^+$), 524.12 (100, $[\text{Fe}(\text{bztpen})(\text{HCO}_2)]^+$).

3.3.4.3 *[Co(bztpen)Cl]BF₄* (**3**)

42.4 mg (0.1 mmol) *bztpen* and 23.8 mg (0.1 mmol) $\text{CoCl}_2 \cdot 6 \text{H}_2\text{O}$ were dissolved in 1 ml methanol. This solution was layered with a solution of 11.0 mg (0.1 mmol) NaBF_4 dissolved in 0.5 ml of methanol. Overnight purple block shaped crystals, suitable for X-ray analysis were formed. Calc. for $\text{C}_{27}\text{H}_{29}\text{BClF}_4\text{CoN}_5$: C, 53.62; H, 4.83; N, 11.58%. Found: C, 52.54; H, 4.83; N, 11.32%. ESIMS (CH_3CN), m/z (% assignment): 241.61 (55, $[\text{Co}(\text{bztpen})]^{2+}$), 256.61 (40, $[\text{Co}(\text{bztpen})\text{Cl}]^{2+}$), 518.17 (100, $[\text{Co}(\text{bztpen})\text{Cl}]^+$).

3.3.4.4 *[Co(metpen)Cl]SbF₆* (**4**)

104.2 mg (0.3 mmol) *metpen* and 66.6 mg (0.28 mmol) $\text{CoCl}_2 \cdot 6 \text{H}_2\text{O}$ were dissolved in 1 ml methanol and the resulting brown to violet solution was stirred for 15 min., 37.0 mg (0.14 mmol) NaSbF_6 dissolved in 1.5 ml methanol was added. A purple powder was precipitated by adding the complex solution to diethyl ether. The solution was decanted and the precipitate was dried in air. Redissolving in acetone

and diffusion of diethyl ether into this solution at room temperature yielded after 12 h purple single crystals, suitable for X-ray analysis. Calc. for $C_{21}H_{25}ClF_6CoN_5Sb$: C, 37.22; H, 3.72; N, 10.34%. Found: C, 37.13; H, 3.63; N, 10.57%. ESIMS (CH_3CN), m/z (%), assignment): 203.08 (55, $[Co(metpen)]^{2+}$), 220.58 (40, $[Co(metpen)Cl]^{2+}$), 441.07 (100, $[Co(metpen)Cl]^+$).

3.3.4.5 $[Co(bztpen)(OAc)]BPh_4$ (5)

20.0 mg (0.05 mmol) bztpen and 11.2 mg (0.045 mmol) $Co(OAc)_2 \times 4 H_2O$ were dissolved in 1 ml methanol. A solution of 15.1 mg (0.044 mol) $NaBPh_4$ in 0.5 ml methanol was added. A precipitate was formed immediately, which was redissolved by adding 1.5 ml of dichloromethane. Salmon colored block shaped single crystals were obtained by diffusion of diethyl ether at room temperature after 12 h. $C_{53}H_{52}BCoN_5O_2$: C, 73.95; H, 6.09; N, 8.14%. Found: C, 73.18; H, 6.02; N, 7.78%. ESIMS (CH_3CN), m/z (%), assignment): 241.61 (85, $[Co(bztpen)]^{2+}$), 527.12 (100, $[Co(bztpen)(HCO_2)]^+$), 517.16 (60, $[Co(bztpen)Cl]^+$).

3.3.4.6 $[Fe(bztpen)NO](triflate)_2$ (6)

Nitric oxide was purged for 5 min through 5 ml of a complex solution 211.8 mg (0.5 mmol) of bztpen and 218.0 mg (0.5 mmol) $Fe(CH_3CN)_2(triflate)_2$ in oxygen and water free methanol. The color of the solution from reddish brown changed to dark violet. After 5 min a crystalline precipitate was formed. The reaction mixture was transferred to an argon glove box and the solid was removed by filtration and purple single crystals suitable for X-ray analysis were obtained. ESIMS (CH_3OH), m/z (%), assignment): 628.1 ($[Fe(bztpen)(OTf)]^+$), ATRIR, (cm^{-1}): ν_{NO} 1671.4.

3.4 Results and Discussion

3.4.1 Syntheses, Characterization and Reactivity of Complexes

The previously characterized complex $[Fe(bztpen)(Cl)]ClO_4$ was used for the kinetic studies on the formation of $[Fe(bztpen)(OOH)]^{2+}$ described below.^{102,149} However we made further attempts towards isolation and structural characterization of $[M(bztpen)(OOH)]^{2+}$ ($M = Fe, Co$) or possible derivatives containing oxidized ligands similar to those reported for related iron complexes of pentadentate ligands.¹⁵⁰ Unfortunately this resulted only in the isolation of some new Fe^{II} and Co^{II} complexes of bztpen. Furthermore the free ligand was structurally characterized, Fig. 3-2 (see Table 3-1 for crystallographic data).

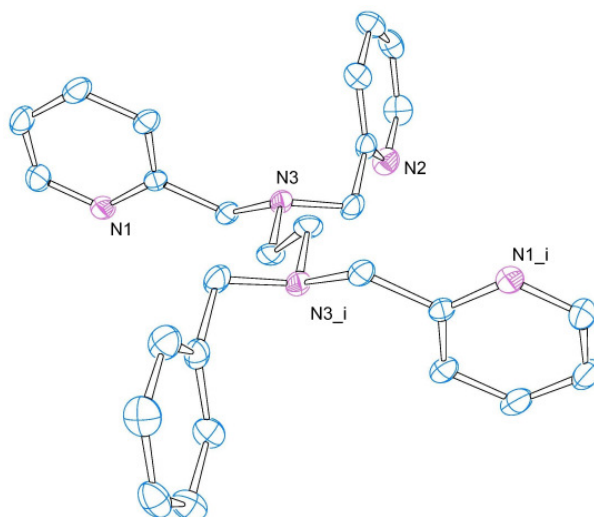


Figure 3-2: Ortep plot of bztpen (1). The thermal ellipsoids are shown at 30% probability. Hydrogen atoms are omitted for clarity.

Although the solution contained hydrogen peroxide single crystals of $[\text{Fe}(\text{bztpen})(\text{OAc})]\text{BPh}_4$ were isolated from the reaction of iron(II)acetate and bztpen in methanol solution. The molecular structure of this complex is presented in Figure 3-3 (crystallographic data are reported in Table 3-1 and Table 3-2). The iron(II) atom in the mono cationic complex is coordinated by the three pyridyl arms and the two amine nitrogen atoms of bztpen. The sixth coordination site is occupied by a monodentate acetate anion. The iron atom shows a distorted octahedral coordination with trans ligand angles of $138.68(9)^\circ$ for N3-Fe-N4 and $150.37(9)^\circ$ for O1-Fe-N1. Moreover the angle for N1-Fe-N3 is $72.09(10)^\circ$, is considerably smaller than 90° and the angle for O1-Fe-N4 is $132.30(9)^\circ$ is significantly larger than 90° .

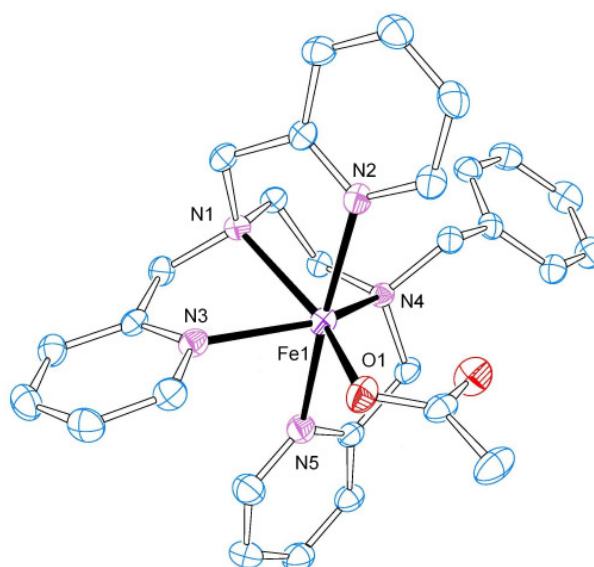


Figure 3-3: Ortep plot of the complex cation $[\text{Fe}(\text{bztpen})(\text{OAc})]^+$ (2). The thermal ellipsoids are shown at 30% probability. Hydrogen atoms are omitted for clarity.

Like in many cases when tripodal ligands form five membered chelate rings the Fe-N_{Py}-bonds (average 2.215 Å) are shorter than the Fe-N_{amine}-bonds (average 2.314 Å). The distance between Fe and O1 (acetate) (2.068(3) Å) is significant shorter than the distance between Fe and O2 (acetate) (2.579(0) Å) which indicates that the acetate ion is bonded by one oxygen atom to the metal center.

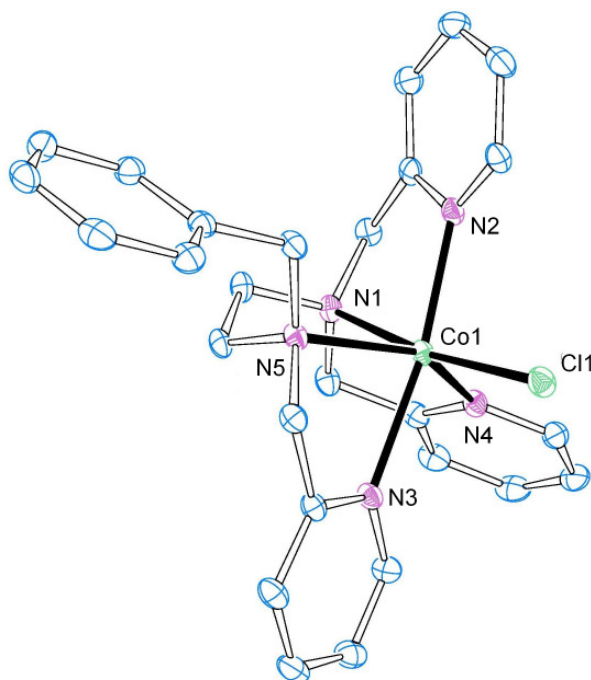


Figure 3-4: Ortep plot of the complex cation [Co(bztpen)Cl]⁺ (**3**). The thermal ellipsoids are shown at 30% probability. Hydrogen atoms are omitted for clarity.

Two bztpen, [Co(bztpen)Cl]BF₄ (**3**) and [Co(bztpen)OAc]BPh₄ (**4**) and one metpen, [Co(metpen)Cl]SbF₆ (**5**) cobalt(II) complexes were isolated. The molecular structure of the cation of **3** is shown in Figure 3-4, the molecular structure of the cation of **4** is shown in Figure 3-5 and the molecular structure of the cation of **5** is shown in Figure 3-6. (crystallographic data for the compounds **3** are reported in Tables 3-1 and 3-2, crystallographic data for the compounds **4** and **5** are reported in Tables 3-3 and 3-4).

Table 3-1: structure and refinement data for the compounds **1 - 3**

	1	2	3
Empirical formula	C ₂₇ H ₂₉ N ₅	C ₅₃ H ₅₂ BF ₆ FeN ₅ O ₂	C ₂₇ H ₂₈ BClCoF ₄ N ₅
Formula weight [g mol ⁻¹]	423.55	857.66	603.73
Crystal system	monoclinic	triclinic	orthorhombic
Space group	C2/c	P-1	P/bca
a [Å]	26.242(5)	13.243(3)	16.309(3)
b [Å]	6.2333(12)	13.507(3)	17.791(4)
c [Å]	17.286(4)	13.992(3)	18.066(4)
α [°]	90	96.03(3)	90
β [°]	123.39(3)	114.15(3)	90
γ [°]	90	101.42(3)	90
V [Å ³]	2360.8(8)	2189.5(8)	5241.9(18)

Chapter 3

Z	4	2	8
D _{calc} [gcm ⁻³]	1.192	1.301	1.530
T [K]	193(2)	193(2)	193(2)
μ(MoKα) [mm ⁻¹]	0.072	0.393	0.813
Crystal size [mm]	0.80 x 0.36 x 0.20	0.16 x 0.16 x 0.16	0.36 x 0.36 x 0.48
F(000)	904	904	2480
θ range [°]	3.40 - 28.06	2.64 - 28.22	2.55 - 28.09
	-32 ≤ h ≤ 34	-17 ≤ h ≤ 17	-21 ≤ h ≤ 20
Index ranges	-8 ≤ k ≤ 8	-17 ≤ k ≤ 17	-22 ≤ k ≤ 23
	-21 ≤ l ≤ 22	-18 ≤ l ≤ 18	-23 ≤ l ≤ 23
Reflections collected	10191	20022	44894
Unique reflections	2748	9774	6334
R _{int}	0.1232	0.0679	0.0684
Refinement method	Full-matrix least-squares on F ²	Full-matrix least-squares on F ²	Full-matrix least-squares on F ²
Data/constraints/parameters	2748 / 0 / 205	9774 / 0 / 560	6334 / 0 / 492
Godness-of-fit on F ²	1.007	0.882	0.973
Final R indices[I > 2σ(I)]	R ₁ = 0.0571 wR ₂ = 0.1448	R ₁ = 0.0552 wR ₂ = 0.1239	R ₁ = 0.0457 wR ₂ = 0.1314
R indices (all data)	R ₁ = 0.0801 wR ₂ = 0.1590	R ₁ = 0.1079 wR ₂ = 0.1442	R ₁ = 0.0622 wR ₂ = 0.1449
Largest diff. peak/hole [e ⁻ Å ⁻³]	0.262 to -0.252	0.562 to -0.620	0.903 to -1.193

Table 3-2: selected distances [Å] and angles [°] for the compounds **2** and **3**

2					
Fe(1)-O(1)	2.068(3)	C(52)-O(2)	1.237(5)	N(1)-Fe(1)-N(4)	76.82(9)
Fe(1)-O(2)	2.579(2)	O(1)-Fe(1)-N(1)	150.37(9)	N(1)-Fe(1)-N(5)	101.83(10)
Fe(1)-N(1)	2.306(3)	O(1)-Fe(1)-N(2)	94.48(11)	N(2)-Fe(1)-N(3)	101.87(10)
Fe(1)-N(2)	2.193(3)	O(1)-Fe(1)-N(3)	83.80(10)	N(2)-Fe(1)-N(4)	95.21(10)
Fe(1)-N(3)	2.226(3)	O(1)-Fe(1)-N(4)	132.30(9)	N(2)-Fe(1)-N(5)	169.16(11)
Fe(1)-N(4)	2.321(3)	O(1)-Fe(1)-N(5)	93.37(11)	N(3)-Fe(1)-N(4)	138.68(9)
Fe(1)-N(5)	2.224(3)	N(1)-Fe(1)-N(2)	74.54(10)	N(3)-Fe(1)-N(5)	86.40(10)
C(52)-O(1)	1.256(4)	N(1)-Fe(1)-N(3)	72.09(10)	N(4)-Fe(1)-N(5)	73.96(10)
3					
Co(1)-Cl(1)	2.3408(8)	Cl(1)-Co(1)-N(2)	94.14(6)	N(1)-Co(1)-N(5)	80.68(7)
Co(1)-N(1)	2.189(2)	Cl(1)-Co(1)-N(3)	88.77(6)	N(2)-Co(1)-N(3)	170.70(8)
Co(1)-N(2)	2.142(2)	Cl(1)-Co(1)-N(4)	103.78(7)	N(2)-Co(1)-N(4)	102.99(8)
Co(1)-N(3)	2.260(2)	Cl(1)-Co(1)-N(5)	102.73(6)	N(2)-Co(1)-N(5)	96.08(8)
Co(1)-N(4)	2.110(2)	N(1)-Co(1)-N(2)	77.58(8)	N(3)-Co(1)-N(4)	84.84(7)
Co(1)-N(5)	2.2093(19)	N(1)-Co(1)-N(3)	99.76(8)	N(3)-Co(1)-N(5)	74.64(7)
Cl(1)-Co(1)-N(1)	171.41(6)	N(1)-Co(1)-N(4)	76.24(8)	N(4)-Co(1)-N(5)	145.89(8)

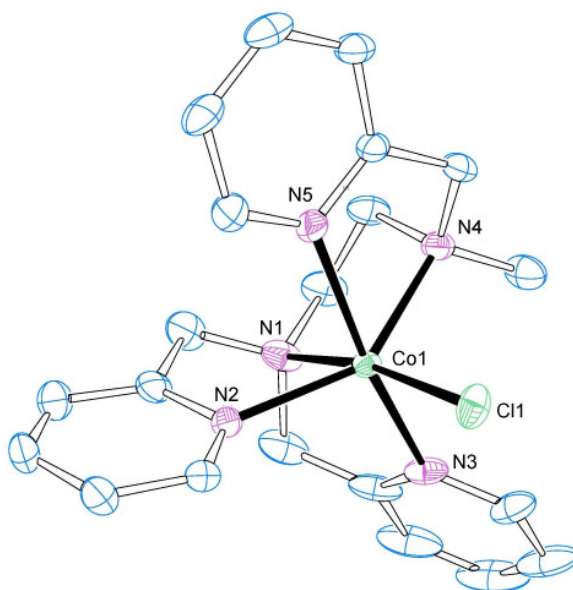


Figure 3-5: Ortep plot of the complex cation $[\text{Co}(\text{metpen})\text{Cl}]^+$ (**4**). The thermal ellipsoids are shown at 30% probability. Hydrogen atoms are omitted for clarity.

The structures of the three cobalt(II) are similar and unremarkable. The geometry around the cobalt(II) ions are distorted octahedral and coordinated by the 5 N donor atoms of the bztpen ligand. The sixth coordination site is occupied either by a chloride ion or a monodentate acetate ligand. Again significant deviation is observed in the cis and trans Co-ligand bonds. The structures of the cations in $[\text{Fe}(\text{bztpen})\text{OAc}]\text{BPh}_4$ and $[\text{Co}(\text{bztpen})\text{OAc}]\text{BPh}_4$ are essentially superimposable. The cell dimensions are almost identical.

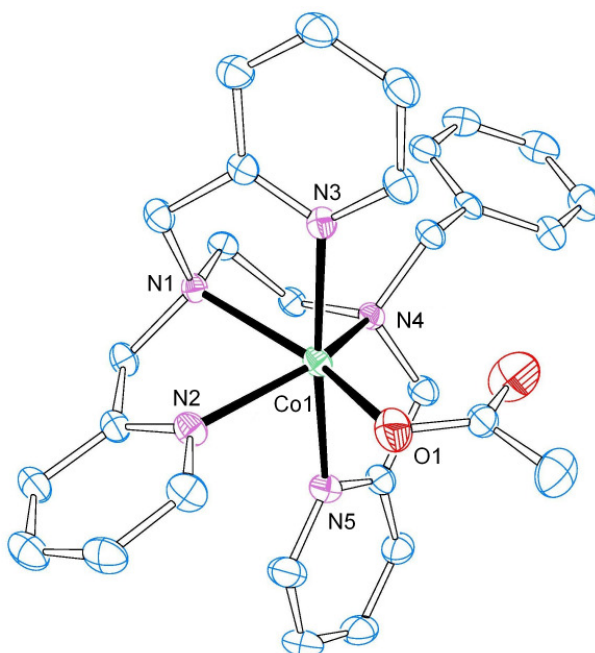


Figure 3-6: Ortep plot of the complex cation $[\text{Co}(\text{bztpen})\text{OAc}]^+$ (**5**). The thermal ellipsoids are shown at 30% probability. Hydrogen atoms are omitted for clarity.

Chapter 3

Cobalt(II) complexes are well known to form dioxygen adducts when exposed to dioxygen or hydrogen peroxide. However, despite the fact that a color change from light purple to dark purple was observed no hydroperoxido adduct could be isolated.

Table 3-3: structure and refinement data for the compounds **4 - 6**

	4	5	6
Empirical formula	C ₂₁ H ₂₅ ClCoF ₆ N ₅ Sb	C ₅₃ H ₅₂ BCoN ₅ O ₂	C ₂₉ H ₂₉ F ₆ FeN ₆ O ₇ S ₂
Formula weight [g mol ⁻¹]	677.59	860.74	807.55
Crystal system	orthorhombic	triclinic	orthorhombic
Space group	Pca2(1)	P-1	Pbca
a [Å]	18.260(4)	13.234(3)	19.105(4)
b [Å]	9.1630(18)	13.491(3)	17.251(4)
c [Å]	15.057(3)	13.920(3)	19.897(4)
α [°]	90	96.33(3)	90
β [°]	90	114.02(3)	90
γ [°]	90	101.27(3)	90
V [Å ³]	2519.3(9)	2175.8(8)	6558(2)
Z	4	2	8
D _{calc} [g cm ⁻³]	1.787	1.314	1.636
T [K]	193(2)	193(2)	193(2)
μ(MoKα) [mm ⁻¹]	1.901	0.443	0.678
Crystal size [mm]	0.53 x 0.38 x 0.04	0.38 x 0.30 x 0.50	0.24 x 0.12 x 0.08
F(000)	1340	906	3304
θ range [°]	4.24 - 28.05	2.64 - 28.17	2.36 - 25.04
Index ranges	-22 ≤ h ≤ 24 -10 ≤ k ≤ 12 -19 ≤ l ≤ 19	-17 ≤ h ≤ 17 -17 ≤ k ≤ 17 -18 ≤ l ≤ 17	-20 ≤ h ≤ 22 -20 ≤ k ≤ 20 -18 ≤ l ≤ 23
Reflections collected	20623	19812	26467
Unique reflections	6001	9719	5755
R _{int}	0.0573	0.0515	0.1650
Refinement method	Full-matrix least-squares on F ²	Full-matrix least-squares on F ²	Full-matrix least-squares on F ²
Data/constraints/parameters	6001 / 1 / 330	9719 / 0 / 756	5755 / 0 / 460
Godness-of-fit on F ²	1.041	0.946	0.871
Final R indices [I > 2σ(I)]	R ₁ = 0.0357 wR ₂ = 0.0940	R ₁ = 0.0528 wR ₂ = 0.1371	R ₁ = 0.0587 wR ₂ = 0.1168
R indices (all data)	R ₁ = 0.0397 wR ₂ = 0.0971	R ₁ = 0.0856 wR ₂ = 0.1560	R ₁ = 0.1384 wR ₂ = 0.1367
Largest diff. peak/hole [e ⁻ Å ⁻³]	0.552 to -0.481	0.694 to -1.228	0.754 to -0.351

3.4.1.1 Reactivity towards Nitric Oxide

Solutions containing the iron(II) bztpen complex were reacted with dioxygen to see a possible reversible formation of an iron(III) superoxido species. However, no evidence for such a reaction could be found. As described in chapter 3.1, nitric oxide is a good model compound for the reaction of metal complexes with dioxygen. The reaction of the iron(II) bztpen complex with nitric oxide in methanol could be observed spectroscopically. The time resolved spectra for this reaction are depicted in Figure 3-7 and show the formation of the purple nitric oxide complex with an absorbance maximum at 550 nm.

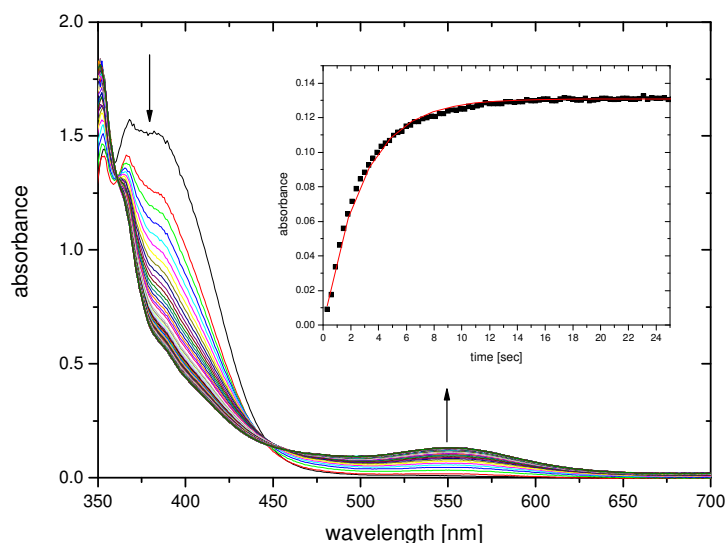


Figure 3-7: Time resolved spectra for the formation of $[\text{Fe}(\text{bztpen})\text{NO}]^{2+}$ in methanol (-40°C , $\Delta t = 300$ ms). Insert: absorbance vs. time trace at 550 nm (data and fit to one exponential function).

The cation of **6** is depicted in Figure 3-8 (crystallographic data are reported in Tables 3-3 and 3-4). The metal center is coordinated in a distorted octahedral geometry by the five nitrogen donors of the ligand molecule. The sixth coordination site is occupied by the nitrogen atom of the nitric oxide molecule. The bond distances for Fe(1)-N(6) (1.733(5) Å) and N(6)-O(1) (1.184(7) Å) and the angle Fe(1)-N(6)-O(1) ($142.8(5)^\circ$) are in a typical range for iron-nitric oxide complexes.¹⁵¹⁻¹⁵⁴

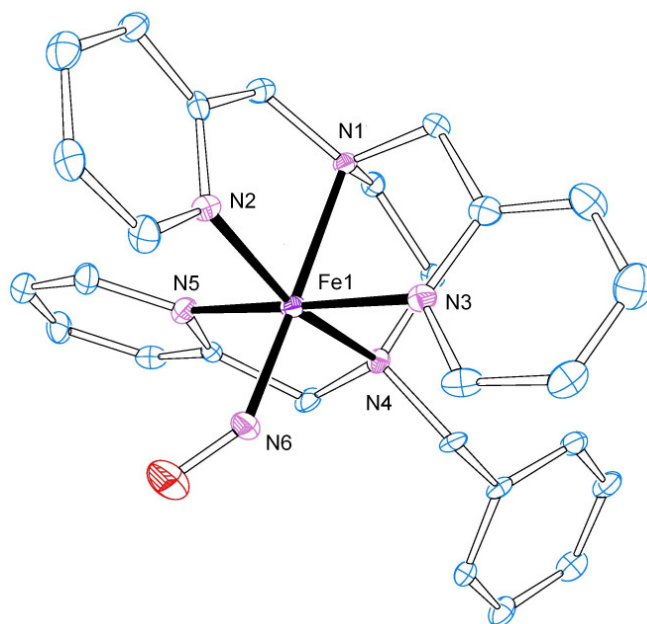


Figure 3-8: Ortep plot of the cation $[\text{Fe}(\text{bztpen})\text{NO}]^+$ (**6**) (30% probability displacement ellipsoids, hydrogen atoms omitted for clarity).

Chapter 3

Table 3-4: selected distances [Å] and angles [°] for compounds **4** - **6**

4					
Co(1)-Cl(1)	2.3271(10)	Cl(1)-Co(1)-N(2)	103.34(9)	N(1)-Co(1)-N(5)	101.36(14)
Co(1)-N(1)	2.203(3)	Cl(1)-Co(1)-N(3)	93.32(10)	N(2)-Co(1)-N(3)	104.22(13)
Co(1)-N(2)	2.106(3)	Cl(1)-Co(1)-N(4)	104.58(10)	N(2)-Co(1)-N(4)	144.33(13)
Co(1)-N(3)	2.134(3)	Cl(1)-Co(1)-N(5)	89.03(9)	N(2)-Co(1)-N(5)	83.02(12)
Co(1)-N(4)	2.165(3)	N(1)-Co(1)-N(2)	75.31(14)	N(3)-Co(1)-N(4)	95.89(12)
Co(1)-N(5)	2.267(3)	N(1)-Co(1)-N(3)	76.82(15)	N(3)-Co(1)-N(5)	171.62(13)
Cl(1)-Co(1)-N(1)	169.20(10)	N(1)-Co(1)-N(4)	81.13(13)	N(4)-Co(1)-N(5)	75.74(13)
5					
Co(1)-O(1)	2.041(3)	C(28)-O(2)	1.179(4)	N(1)-Co(1)-N(4)	79.27(9)
Co(1)-O(2)	2.783(3)	O(1)-Co(1)-N(1)	152.82(10)	N(1)-Co(1)-N(5)	103.66(10)
Co(1)-N(1)	2.228(2)	O(1)-Co(1)-N(2)	84.67(10)	N(2)-Co(1)-N(3)	102.11(9)
Co(1)-N(2)	2.175(2)	O(1)-Co(1)-N(3)	92.90(10)	N(2)-Co(1)-N(4)	141.57(9)
Co(1)-N(3)	2.143(2)	O(1)-Co(1)-N(4)	127.38(11)	N(2)-Co(1)-N(5)	85.30(10)
Co(1)-N(4)	2.243(2)	O(1)-Co(1)-N(5)	90.16(11)	N(3)-Co(1)-N(4)	97.21(8)
Co(1)-N(5)	2.211(3)	N(1)-Co(1)-N(2)	73.48(9)	N(3)-Co(1)-N(5)	172.21(9)
C(28)-O(1)	1.244(4)	N(1)-Co(1)-N(3)	76.52(9)	N(4)-Co(1)-N(5)	75.28(9)
6					
Fe(1)-N(1)	2.102(5)	N(1)-Fe(1)-N(2)	79.1(2)	N(3)-Fe(1)-N(5)	173.15(19)
Fe(1)-N(2)	2.002(5)	N(1)-Fe(1)-N(3)	82.7(2)	N(3)-Fe(1)-N(6)	96.2(2)
Fe(1)-N(3)	1.988(5)	N(1)-Fe(1)-N(4)	84.48(19)	N(4)-Fe(1)-N(5)	83.12(19)
Fe(1)-N(4)	2.077(5)	N(1)-Fe(1)-N(5)	93.1(2)	N(4)-Fe(1)-N(6)	98.7(2)
Fe(1)-N(5)	1.988(5)	N(1)-Fe(1)-N(6)	176.6(2)	N(5)-Fe(1)-N(6)	88.4(2)
Fe(1)-N(6)	1.733(5)	N(2)-Fe(1)-N(3)	92.8(2)	O(1)-N(6)-Fe(1)	142.8(5)
N(6)-O(1)	1.184(7)	N(3)-Fe(1)-N(4)	91.08(19)		

3.4.1.2 Kinetic Studies

When $[\text{Fe}(\text{bztpen})\text{Cl}]\text{ClO}_4$ is reacted with an excess of hydrogen peroxide in a first fast step the iron(II) complex is oxidised to the corresponding iron(III) complex. This reaction could be observed spectroscopically, an example of the time resolved spectra is shown in Figure 3-9. The oxidation of the iron(II) complex could be fitted nicely to a time trace at 393 nm using one exponential function. From these traces rate constants (k_{obs}) were calculated and it was observed that a maximum rate was reached in a plot of k_{obs} vs. $[\text{H}_2\text{O}_2]$ (see Supporting Information). The reason for the saturation kinetics involving hydrogen peroxide should be fast reversible binding of hydrogen peroxide the iron(II) complex followed by rate-determining electron transfer to form the iron(III) complex. This preequilibrium had been postulated previously based on results of ESIMS studies and through studies on the influence of addition of chloride ions on the reaction rates.¹⁰²

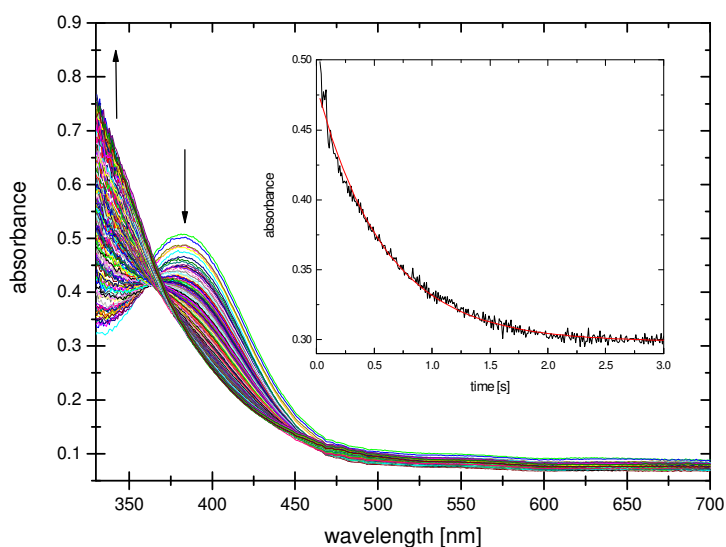


Figure 3-9: Time resolved spectra for the oxidation reaction of $[\text{Fe}(\text{bztpen})(\text{Cl})]\text{ClO}_4$ ($c = 0.2 \text{ mM}$) with hydrogen peroxide ($c = 0.25 \text{ M}$) in methanol ($T = -40^\circ\text{C}$, $\Delta t = 1.5 \text{ ms}$). Insert: absorbance vs. time trace at 393 nm (data and fit to one exponential function). Because of instrument reasons the spectra do not show a clean isosbestic point and some drift at longer wavelengths ($>600 \text{ nm}$).

The oxidation reaction is clearly separated from the formation of the purple hydroperoxido intermediate. Fig. 3-10 shows typical time resolved spectra for this reaction. The formation rate of the hydroperoxido intermediate could be fitted with one exponential function at 540 nm.

We observed that the rate constants obtained were faster by a factor 10 in comparison with our previous investigation.¹⁰² One explanation could be that the concentration of the hydrogen peroxide solutions were not correct due to decomposition before. Both sets of measurements were performed under pseudo first order conditions and the calculated activation parameters are almost the same within the experimental error limits. Previous results: $\Delta H^\ddagger = 53 \pm 2 \text{ kJmol}^{-1}$; $\Delta S^\ddagger = -72 \pm 8 \text{ kJmol}^{-1}\text{K}^{-1}$ vs our new results: $\Delta H^\ddagger = 51 \pm 2 \text{ kJmol}^{-1}$; $-69 \pm 5 \text{ kJmol}^{-1}\text{K}^{-1}$. The negative entropy of activation indicates a higher ordered complex in the transition state. A plausible explanation for this is that the ligand exchange reaction proceeds via the seven coordinated compound, $[\text{Fe}(\text{bztpen})(\text{OMe})(\text{HOOH})]^{2+} \leftrightarrow [\text{Fe}(\text{bztpen})(\text{HOMe})(\text{OOH})]^{2+}\ddagger$; the hydroperoxido and methanolato ligand are both coordinated in the transition state. However, while this result is not unlikely in principle (seven coordinated iron complexes are well known) it is in conflict with previous results.^{103,137,138}

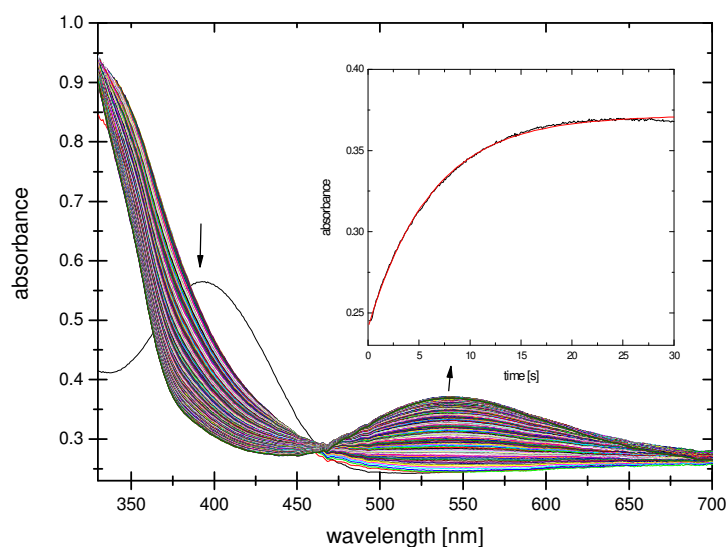


Figure 3-10: Time resolved spectra for the formation of $[\text{Fe}(\text{bztpen})\text{OOH}]^{2+}$ ($c = 0.2$ mM) with hydrogen peroxide ($c = 0.1$ M) in methanol ($T = 25^\circ\text{C}$, $\Delta t = 100$ ms). Inset: absorbance vs. time trace at 550 nm (data and fit to one exponential function). The black line shows the spectrum of the starting complex. Inset: absorbance vs. time trace at 550 nm (data and fit to single exponential function). Because of instrument reasons the spectra do not show a clean isosbestic point and some drift at longer wavelengths (>600 nm).

Activation volumes provide the same information as activation entropies for a mechanism elucidation, however measurements and calculations can be obtained with a greater accuracy. Moreover, in contrast to activation entropies, measurements of the pressure dependence of a reaction most of the time give a clearly answer the question whether a reaction rate is increased or decreased if the pressure is increased (even if the individual rate constants have a large error). Therefore, we performed a high pressure stopped-flow investigation on this reaction. If the negative activation entropy is correct then an increase of reaction rates under pressure would be expected and an interchange associative mechanism would be confirmed. Figure 3-11 shows that this is not true. A plot of the logarithm of the observed rate constants vs pressure does not indicate a dependence on pressure (within the experimental error). Thus the activation volume is close to zero, clearly indicating a pure interchange mechanism: the methanol ligand leaves the complex at the same as the hydroperoxido ligand enters the complex. Thus the mechanism agrees with earlier results on substitution reactions with iron(III) complexes.¹⁰³

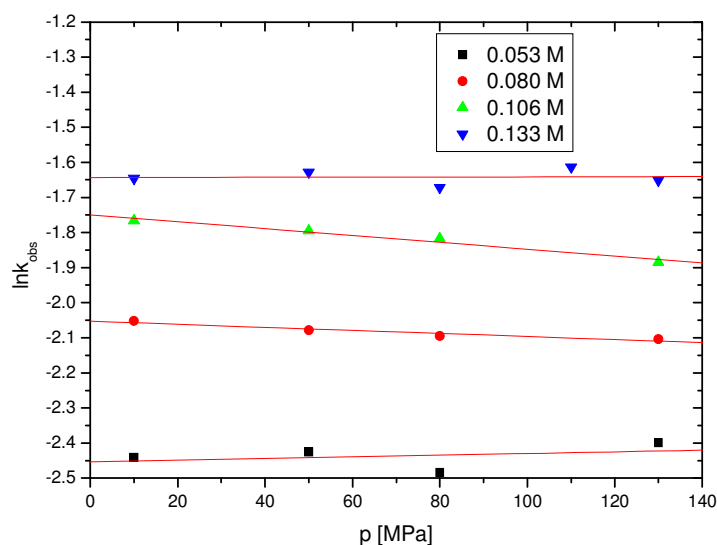


Figure 3-11: Plot of $\ln k_{\text{obs}}$ versus pressure for determination of the activation volume of the formation reaction of $[\text{Fe}(\text{bztpen})\text{OOH}]^{2+}$.

3.5 Conclusion

The single crystal X-ray structures of four new mononuclear iron(II) and cobalt(II) complexes of Rtpen were determined, along with the structure of bztpen. The stability of the iron(II) oxidation state of these complexes is demonstrated by the ease in which the complexes are reisolated after treatment with dihydrogen peroxide. The kinetics of the reaction of $[\text{Fe}(\text{bztpen})\text{Cl}](\text{ClO})_4$ with dihydrogen peroxide in methanol was investigated in detail and was proved to be consistent with the postulated preequilibrium, where dihydrogen peroxide binds to the iron(II) complex to form the reactive species. The activation entropy derived from temperature dependent reaction kinetics has large experimental errors, which can lead to mechanistic misinterpretation. The pressure dependence of the formation rate of the hydroperoxido complex demonstrates the usefulness of activation volumes for explaining reaction mechanism and indicates that the earlier interpretation of temperature dependent kinetics appears to be incorrect.¹⁰²

4 Supporting Information for Chapter 3 and unpublished Results

4.1 Supporting Material for Chapter 3

4.1.1 Oxidation of $[\text{Fe}(\text{bztpen})\text{Cl}]\text{ClO}_4$

Table 4-1: Observed rate constants, k_{obs} (s^{-1}), for the oxidation reaction of $[\text{Fe}(\text{bztpen})\text{Cl}]\text{ClO}_4$ with hydrogen peroxide in methanol calculated from absorbance vs. time traces at 393 nm. Each rate constant is the average of at least three kinetic runs.

$[\text{H}_2\text{O}_2]$ [M]	-40 °C	-35 °C	-30 °C	-25 °C
0.01	0.19 ± 0.02	0.46 ± 0.04	0.8 ± 0.2	0.1 ± 0.1
0.05	0.63 ± 0.02	0.95 ± 0.03	1.47 ± 0.09	2.3 ± 0.1
0.10	1.05 ± 0.02	1.70 ± 0.05	2.43 ± 0.08	4.3 ± 0.1
0.16	1.59 ± 0.04	2.3 ± 0.1	3.4 ± 0.1	5.6 ± 0.2
0.25	1.59 ± 0.06	2.5 ± 0.1		
0.375	1.9 ± 0.2	2.8 ± 0.2		
0.50	2.0 ± 0.4	3.5 ± 0.4	5.4 ± 0.1	10.3 ± 0.3
0.75	2.5 ± 0.5	4.6 ± 0.4	6.2 ± 0.1	15.1 ± 0.5
1.00	3.1 ± 0.5	5.8 ± 0.5	8.2 ± 0.2	16.3 ± 0.5
1.50	3.6 ± 0.3			

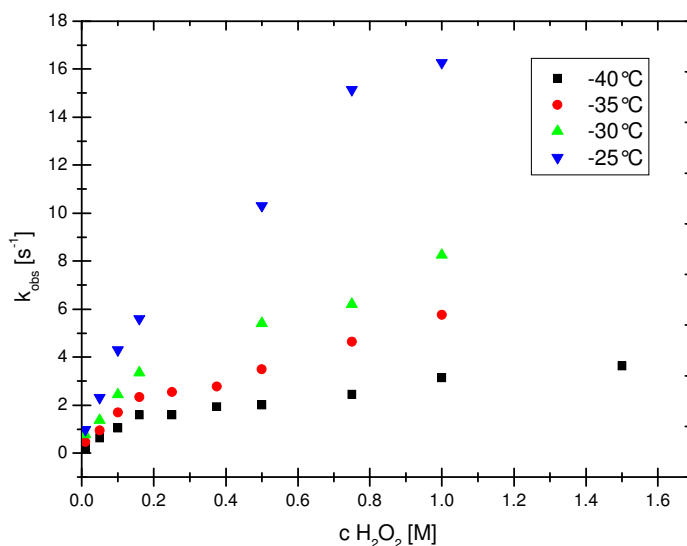


Figure 4-1: k_{obs} vs. $[\text{H}_2\text{O}_2]$ for the oxidation of $[\text{Fe}(\text{bztpen})\text{Cl}]\text{ClO}_4$ by H_2O_2 in methanol.

Chapter 4

Table 4-2: Second order rate constants for the oxidation of $[\text{Fe}(\text{bztpe})\text{Cl}]\text{ClO}_4$ by hydrogen peroxide in methanol, calculated from the initial slopes of the curved plots in 4-1.

Temp. [°C]	k [$\text{M}^{-1} \text{s}^{-1}$]	Intercept [s^{-1}]
-40 °C	9.2 ± 0.3	0.13 ± 0.03
-35 °C	12.8 ± 0.6	0.34 ± 0.06
-30 °C	17.6 ± 0.9	0.57 ± 0.08
-25 °C	31 ± 3	0.8 ± 0.3

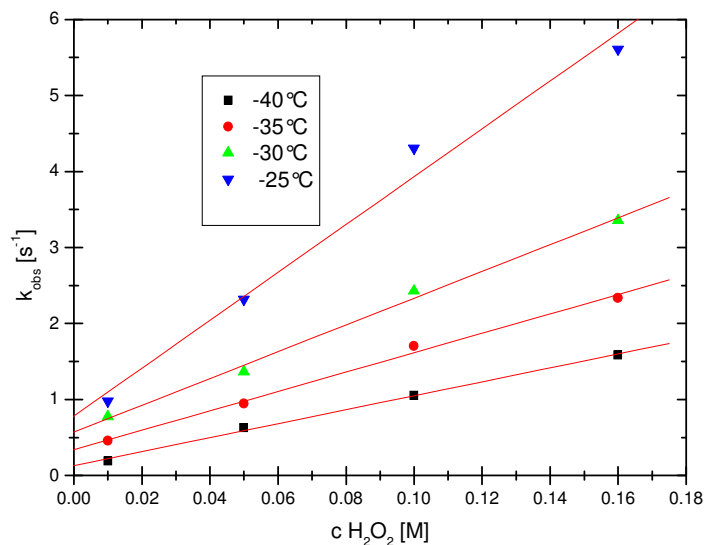


Figure 4-2: k_{obs} vs. $[\text{H}_2\text{O}_2]$ to calculate the initial slopes and intercepts of the curved plots in Figure 4-1.

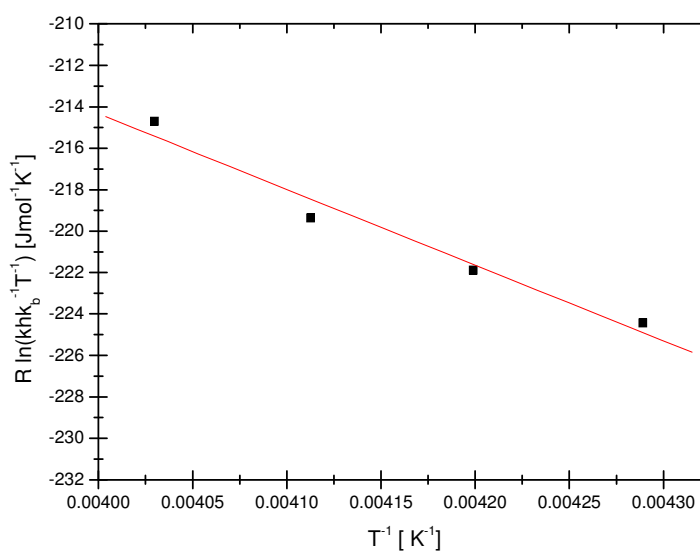


Figure 4-3: “Eyring-Plot” for the oxidation of $[\text{Fe}(\text{bztpe})\text{Cl}]\text{ClO}_4$ in methanol.

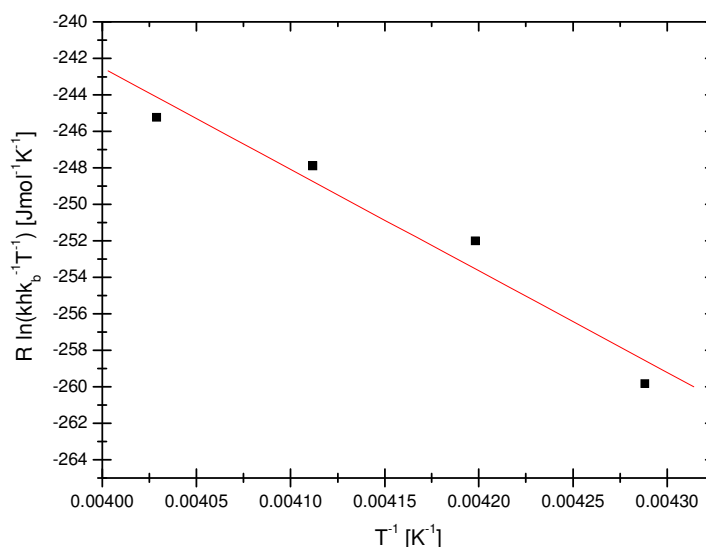


Figure 4-4: “Eyring plot” for the back reaction of the oxidation of $[\text{Fe}(\text{bztpen})\text{Cl}]\text{ClO}_4$ in methanol.

Table 4-3: Activation parameters for the oxidation reaction of $[\text{Fe}(\text{bztpen})\text{Cl}]\text{ClO}_4$ in methanol calculated from the “Eyring plot” in Figure 4-3 and for the back reaction calculated from the “Eyring plot” in Figure 4-4.

	ΔH^\ddagger [kJ mol^{-1}]	ΔS^\ddagger [$\text{J mol}^{-1} \text{K}^{-1}$]
Back reaction	37 ± 5	-68 ± 20
	56 ± 9	-19 ± 37

4.1.2 Formation of $[\text{Fe}(\text{bztpen})\text{OOH}]^{2+}$

Table 4-4: Observed rate constants, k_{obs} (s^{-1}), for the reaction of the formation reaction of $[\text{Fe}(\text{bztpen})\text{OOH}]^{2+}$ in methanol calculated from absorbance vs. time traces at 550 nm. Each rate constant is an average of at least three measurements.

$c \text{H}_2\text{O}_2$ [M]	20 °C	25 °C	30 °C	35 °C	40 °C
0.01	$0.0268 \pm$	$0.0380 \pm$	$0.0575 \pm$	$0.0856 \pm$	$0.1316 \pm$
	0.0001	0.0001	0.0002	0.0003	0.0005
0.02	$0.0365 \pm$	$0.0526 \pm$	$0.0800 \pm$	$0.1173 \pm$	$0.1805 \pm$
	0.0001	0.0002	0.0002	0.0004	0.0004
0.04	$0.0662 \pm$	$0.0927 \pm$	$0.1290 \pm$	$0.1830 \pm$	$0.2725 \pm$
	0.0002	0.0002	0.0004	0.0004	0.0008
0.06	$0.0873 \pm$	$0.1230 \pm$	$0.1772 \pm$	$0.2595 \pm$	$0.3643 \pm$
	0.0002	0.0003	0.0004	0.0006	0.0008
0.08				$0.3433 \pm$	$0.482 \pm$
				0.0007	0.001

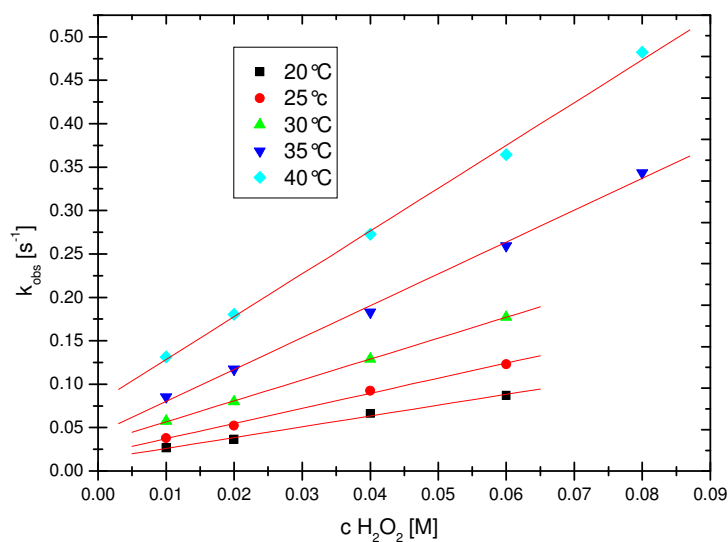


Figure 4-5: k_{obs} vs. $[\text{H}_2\text{O}_2]$ for the formation of $[\text{Fe}(\text{bztpe})\text{OOH}]^{2+}$.

Table 4-5: Second order rate constants for the formation reaction of the iron(III) hydroperoxido complex with hydrogen peroxide in methanol, calculated from slope of the straight lines.

Temp. [°C]	k [$\text{M}^{-1} \text{s}^{-1}$]	Intercept [s^{-1}]
20	1.24 ± 0.07	0.014 ± 0.003
25	1.74 ± 0.08	0.020 ± 0.003
30	2.41 ± 0.01	0.0328 ± 0.0007
35	3.7 ± 0.1	0.044 ± 0.006

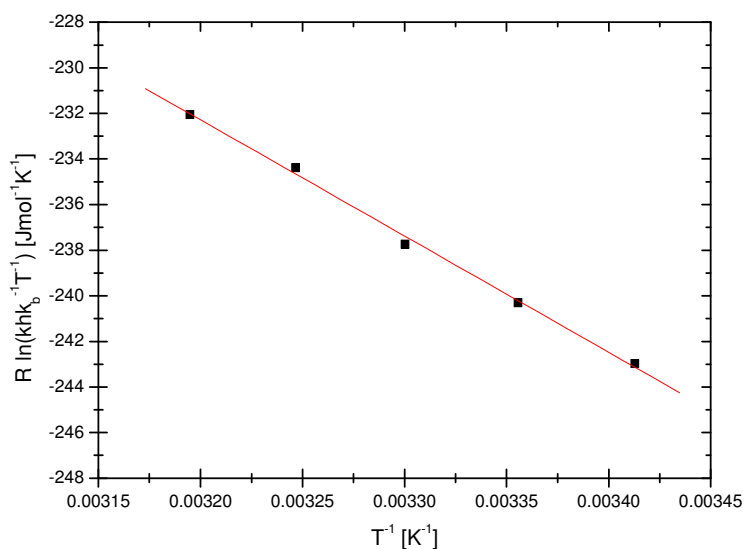


Figure 4-6: “Eyring plot” for the formation of $[\text{Fe}(\text{bztpe})\text{OOH}]^{2+}$.

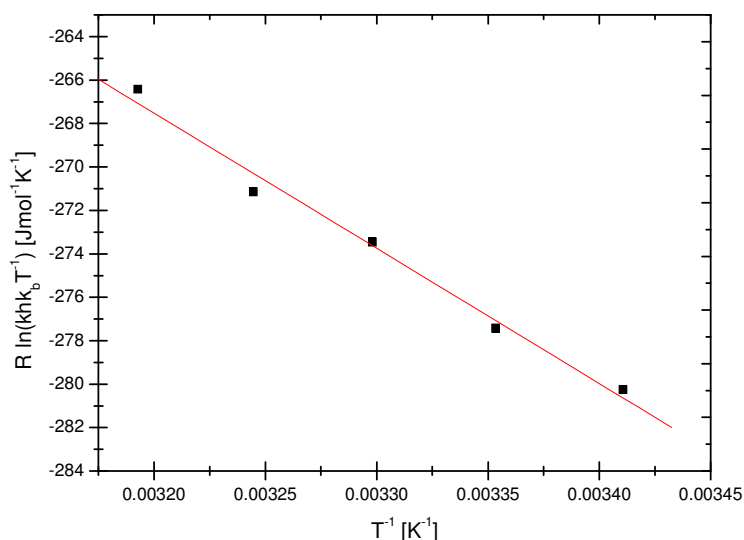


Figure 4-7: “Eyring plot” for the back reaction of the formation of $[\text{Fe}(\text{bztpen})\text{OOH}]^{2+}$.

Table 4-6: Activation parameters for the formation reaction of hydroperoxido complex in methanol calculated from the “Eyring plot” in Figure 4-6 and for the back reaction calculated from the “Eyring plot” in Figure 4-7.

	ΔH^\ddagger [kJ mol^{-1}]	ΔS^\ddagger [$\text{J mol}^{-1} \text{K}^{-1}$]
	51 ± 2	-69 ± 5
Back reaction	62 ± 4	-68 ± 13

4.1.3 High Pressure Kinetics

Table 4-7: Observed rate constants, k_{obs} (s^{-1}), for the formation of $[\text{Fe}(\text{bztpen})\text{OOH}]^{2+}$ in methanol under high pressure conditions at 27°C , calculated from absorbance vs. time traces at 550 nm. Each rate constant is an average of at least three measurements.

$[\text{H}_2\text{O}_2]$ [M]	100 MPa	500 MPa	800 MPa	1100 MPa	1300 MPa
0.053	0.090	0.090	0.080	0.090	
0.080	0.128	0.125	0.123		0.122
0.106	0.171	0.166	0.163		0.152
0.133	0.193	0.197	0.188	0.199	0.192

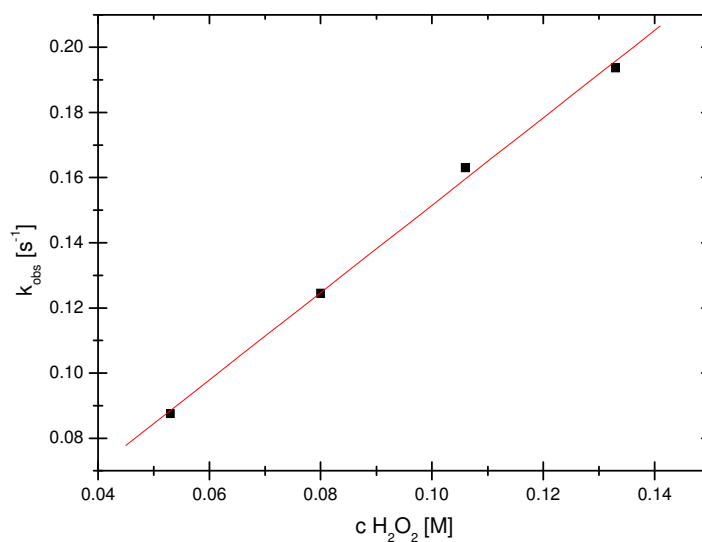


Figure 4-8: k_{obs} vs. $[\text{H}_2\text{O}_2]$ for the formation under high pressure conditions of $\text{Fe}(\text{bztpe})\text{OOH}]^{2+}$ at 27°C (every data point is average over all pressures).

Table 4-8: Second order rate constants for the formation reaction of the iron(III) hydroperoxido complex with hydrogen peroxide in methanol under high pressure conditions calculated from the slope of the straight line.

T [$^\circ\text{C}$]	k [$\text{M}^{-1}\text{s}^{-1}$]	Intercept [s^{-1}]
27	1.34 ± 0.05	0.0017 ± 0.0005

4.2 Unpublished Results related to Chapter 3

4.2.1 Experimental

4.2.1.1 Materials and Reagents

All reagents and solvents were used as obtained without any further purification. Methanol as a solvent for oxygen-sensitive materials was obtained commercially from Acros and was further distilled in argon atmosphere before usage. Handling of oxygen-sensitive compounds and material was carried out in a glove box (M. Braun, Germany, O₂ < 0.1 ppm) under argon atmosphere.

4.2.1.2 Physical Measurement

Single crystal X-ray diffraction studies of the substance **7** and **8** were performed with a STOE IPDS-diffractometer equipped with a low temperature system (Karlsruher Glastechnisches Werk), a graphite monochromator and an IP detector system. Mo-K_α radiation ($\lambda = 0.71069 \text{ \AA}$) was used. The frames were integrated into the STOE software package. No absorption corrections were applied.

ESI-MS studies were performed with a Bruker-Daltronics ESI-HRMS Micro-TOF in the working group of Professor Maison at the Institute for Organic Chemistry of the University of Giessen.

Stopped-flow measurements were performed with a commercially available Hi Tech (Salisbury, GB), SF-61DX2 instrument.

4.2.1.3 Syntheses

4.2.1.3.1 [Fe(bztpen)Cl]OCH₃ x 4 H₂O (**7**)

216.0 mg (0.5 mmol) of bztpen and 101.4 mg (0.5 mmol) FeCl₂ x 4 H₂O were dissolved in 1.5 ml methanol. 1.5 ml 2 M hydrogen peroxide solution in methanol was added carefully to the light brown solution. The color changed to dark brown and the mixture reacted under warming. After cooling down to room temperature, the solution was added to a hot solution 137 mg (0.75 mmol) Na₂S₂O₆ in 1 ml water. After having cooled the solution again, a yellow precipitate formed. Yellow crystalline blocks suitable for X-ray analysis were grown overnight.

4.2.1.3.2 [Co(metpen)Cl]triflate

104.2 mg (0.3 mmol) metpen and 66.6 mg (0.28 mmol) $\text{CoCl}_2 \times 6 \text{H}_2\text{O}$ were dissolved in 1 ml methanol. The resulting brown to violet solution was stirred for 15 min. Then, 22.3 mg (0.14 mmol) lithium triflate dissolved in 1.5 ml methanol was added. A purple crystalline substance was precipitated after having added the complex solution to diethyl ether. The substance was used for ESI-MS studies (see below). All other compounds used for these investigations were synthesized according to the procedures described in Chapter 3.

4.2.1.3.3 Generation of unpurified Nitric Oxide

Nitric oxide was generated by the reaction of an degassed solution of iron(II)sulfate heptahydrate and sulphuric acid with sodium nitrite in argon atmosphere. The nitric oxide was transferred by an argon flow to the complex solutions. As the structure **8** shows, the thus generated nitric oxide contains a massive amount of nitrogen dioxide. For further investigations, the generated gas was purged through a degassed 2 M sodium hydroxide solution to trap the impurities (see chapter 3).

4.2.1.3.4 [Fe(bztpen)NO₂](SbF₆)₂ (**8**)

The nitric oxide evolved as described above, was purged through the iron(II) complex solution. The complex solution was formed by dissolving 42.4 mg (1 mmol) bztpen and 33.6 mg (1 mmol) $\text{Fe}(\text{triflate})_2(\text{CH}_3\text{CN})_2$ in 10 ml absolute methanol in an Argon filled glove box. After reaction with nitric oxide the solution was transferred into the glove box again. 1 ml of this solution was added to 51.7 mg (0.2 mmol) of NaSbF_6 dissolved in 0.5 ml methanol. A relatively slow formation of a precipitate followed. Violet to brown crystals suitable to X-ray analysis were obtained after 24 hours time. ESIMS (CH_3OH) m/z (%), assignment): 524.1 [$\text{Fe}(\text{bztpen})\text{NO}_2\text{-H}^+$]⁺.

4.2.2 Results and Discussion

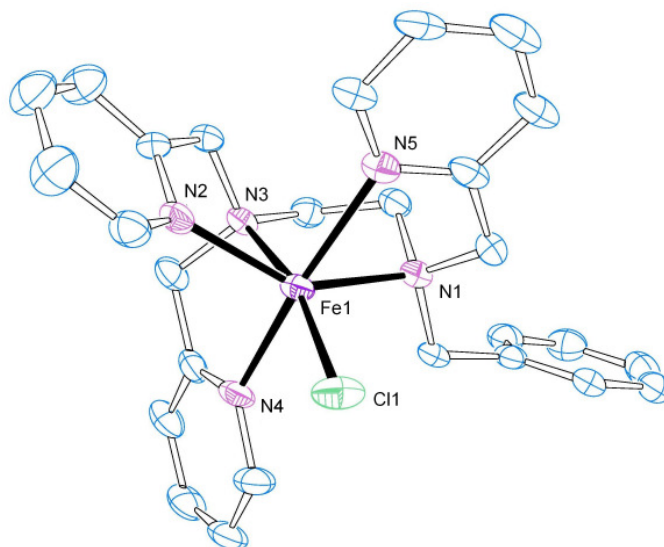
4.2.2.1 Crystal Structure of $[\text{Fe}(\text{bztpen})\text{Cl}]\text{OCH}_3 \times 4 \text{H}_2\text{O}$ (**7**)

Figure 4-9: Ortep plot of the cation $[\text{Fe}(\text{bztpen})\text{Cl}]^+$ (**7**) (30% probability displacement ellipsoids, hydrogen atoms omitted for clarity).

Table 4-9: structure and refinement data for compound **7**.

Empirical formula	$\text{C}_{29}\text{H}_{42}\text{ClFeN}_5\text{O}_5$
Formula weight [g mol^{-1}]	631.98
Crystal system	Monoclinic
Space group	$P2(1)/c$
a [\AA]	9.0285(18)
b [\AA]	22.726(5)
c [\AA]	16.145(3)
α [$^\circ$]	90
β [$^\circ$]	98.83(3)
γ [$^\circ$]	90
V [\AA^3]	3273.5(11)
Z	4
D_{calc} [g cm^{-3}]	1.282
T [K]	193(2)
$\mu(\text{MoK}\alpha)$ mm^{-1}	0.585
Crystal size [mm]	0.1 x 0.15 x 0.2 mm
F(000)	1336
θ range [$^\circ$]	2.20 - 26.03
Index ranges	$-11 \leq h \leq 11$ $-27 \leq k \leq 27$ $-19 \leq l \leq 19$
Reflections collected	23986
Unique reflections	6257
Rint	0.1191
Refinement method	Full-matrix least-squares on F^2
Data/constraints/parameters	6257 / 0 / 373
Godness-of-fit on F^2	1.553
Final R indices [$ I > 2\sigma(I)$]	$R_1 = 0.1462$ $wR_2 = 0.4104$
R indices (all data)	$R_1 = 0.1762$ $wR_2 = 0.4252$
Largest diff. peak/hole [e. \AA^{-3}]	1.906 to -0.946

Table 4-10: Selected distances [Å] and angles [°]

Fe(1)-N(1)	2.251(8)	Cl(1)-Fe(1)-N(2)	104.1(2)	N(1)-Fe(1)-N(5)	73.5(3)
Fe(1)-N(2)	2.141(8)	Cl(1)-Fe(1)-N(3)	166.70(18)	N(2)-Fe(1)-N(3)	75.3(3)
Fe(1)-N(3)	2.232(8)	Cl(1)-Fe(1)-N(4)	91.2(2)	N(2)-Fe(1)-N(4)	101.0(3)
Fe(1)-N(4)	2.219(8)	Cl(1)-Fe(1)-N(5)	94.9(2)	N(2)-Fe(1)-N(5)	86.6(3)
Fe(1)-N(5)	2.276(7)	N(1)-Fe(1)-N(2)	144.6(3)	N(3)-Fe(1)-N(4)	76.0(3)
Fe(1)-Cl(1)	2.319(3)	N(1)-Fe(1)-N(3)	78.9(3)	N(3)-Fe(1)-N(5)	98.3(3)
Cl(1)-Fe(1)-N(1)	106.4(2)	N(1)-Fe(1)-N(4)	95.8(3)	N(4)-Fe(1)-N(5)	168.8(3)

The iron(II) ion is coordinated by three pyridyl arms and two amine nitrogen donors in a distorted octahedral geometry. The sixth coordination site is occupied by a chloride ion. A $[\text{Fe}(\text{bztpen})\text{Cl}]^+$ complex with hexafluorophosphate as the counterion was reported by Hazell et al. in 2002.

4.2.2.2 Stopped Flow Investigation on the Reaction of $[\text{Co}(\text{bztpen})\text{Cl}]\text{BF}_4$ with Hydrogen Peroxide

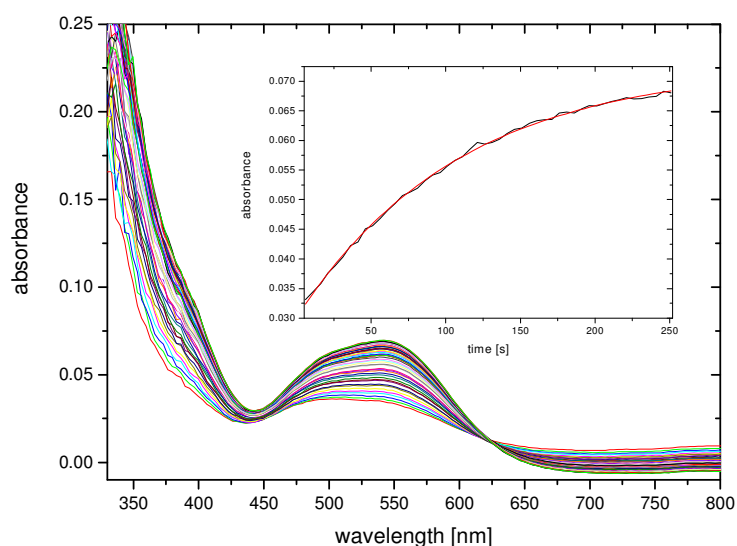


Figure 4-10: Reaction of 1 mM solution of $[\text{Co}(\text{bztpen})\text{Cl}]^+$ with 1 M hydrogen peroxide in methanol at -40°C . Insert: time trace at 550 nm measurement data and fit to one exponential function.

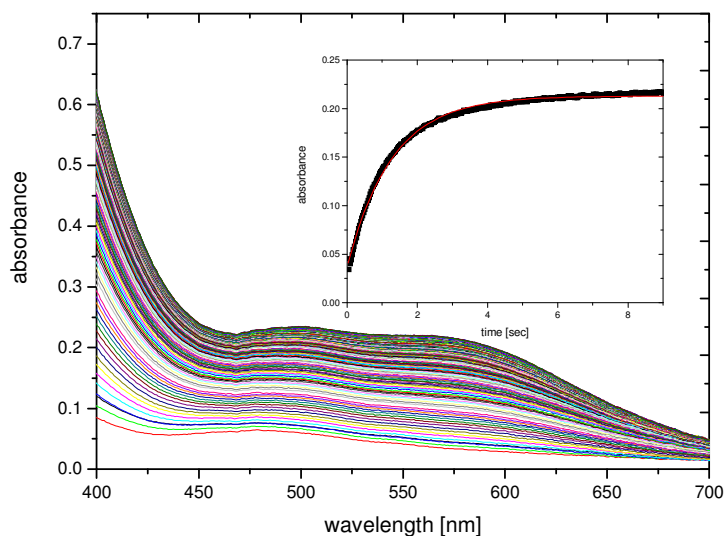


Figure 4-11: Reaction of a 2 mM solution of $\text{Co}(\text{BF}_4)_2 \times 6 \text{H}_2\text{O}$ and bztpen in methanol with 0,2 M hydrogen peroxide in methanol at 24 °C. Insert: time trace at 560 nm measurement data and fit to one exponential function.

Figure 4-10 shows the reaction of a solution of $[\text{Co}(\text{bztpen})\text{Cl}]^+$ with hydrogen peroxide in methanol. The insert shows the absorbance-time trace at 550 nm. The time resolved spectra show the shift of the absorbance maximum from 510 nm to 550 nm.

Figure 4-11 shows the spectral changes caused by the reaction of a solution of $\text{Co}(\text{BF}_4)_2 \times 6 \text{H}_2\text{O}$ and bztpen with hydrogen peroxide in methanol at room temperature. The observed spectral changes show evidence of the formation of a cobalt(III) hydroperoxido species. However, more investigations should be carried out to confirm this outcome. Even already published UV/ Vis spectra have not been able to explain the formation of Cobalt(III) hydroperoxido complexes unambiguously.¹⁵⁵

4.2.2.3 ESIMS Solution Studies of Cobalt Rtpen Complexes and their Reaction with Hydrogen Peroxide

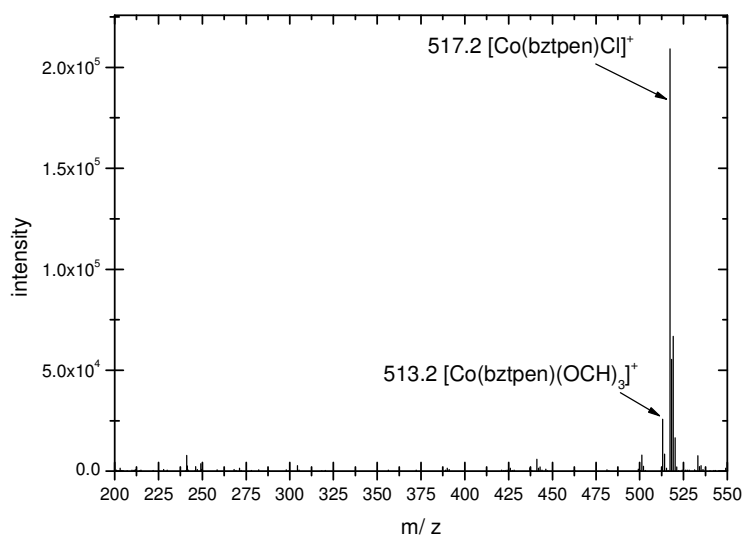


Figure 4-12: ESIMS of a solution of [Co(bztpen)Cl]BF₄ in methanol

Figure 4-12 shows the ESIMS spectrum of a solution of [Co(bztpen)Cl]BF₄ in methanol. In contrast to the iron(II) bztpen complex solution in methanol,¹⁰² in which the chlorido ligand is exchanged by methanolate, the dominant peak in the mass spectrum at $m/z = 517.2$ can be assigned to the cobalt(II) complex cations which contains chloride as co-ligand. Only a small peak at $m/z = 513.2$ shows the formation of a methanolate coordinated complex by a ligand exchange reaction.

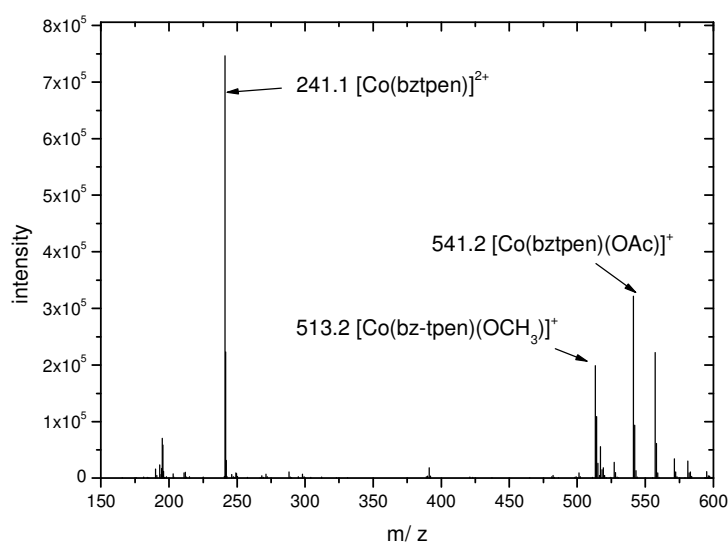


Figure 4-13: ESIMS spectrum of [Co(bztpen)(OAc)]ClO₄ in methanol.

Figure 4-13 shows the mass spectrum of $[\text{Co}(\text{bztpen})(\text{OAc})]\text{ClO}_4$ in a methanol solution. The dominant peak in the mass spectrum is $[\text{Co}(\text{bztpen})]^{2+}$ at $m/z = 241.1$. In this case, the peak for $[\text{Co}(\text{bztpen})(\text{OAc})]^+$ at $m/z = 541.2$ and for $[\text{Co}(\text{bztpen})(\text{OCH}_3)]^+$ at $m/z = 513.2$ have almost the same intensity. This demonstrates the decreased bonding strength of the acetate ion in contrast to the chlorido ligand.

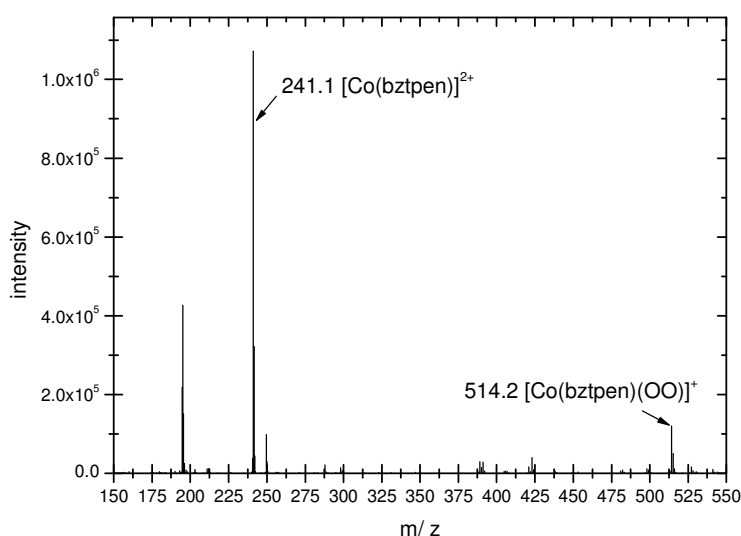


Figure 4-14: ESIMS spectrum of $[\text{Co}(\text{bztpen})(\text{OAc})]\text{ClO}_4$ with an excess of hydrogen peroxide in methanol.

The ESIMS spectrum of the reaction of $[\text{Co}(\text{bztpen})(\text{OAc})](\text{ClO}_4)$ with an excess of hydrogen peroxide in methanol solution is depicted in Figure 4-14. The mass peak at $m/z = 514.2$ could be assigned to the cobalt(III) peroxido species. But the intensity of this peak is visibly lower compared to the dominant peak at $m/z = 241.1$, which is the signal of the cobalt(II) complex $[\text{Co}(\text{bztpen})]^{2+}$.

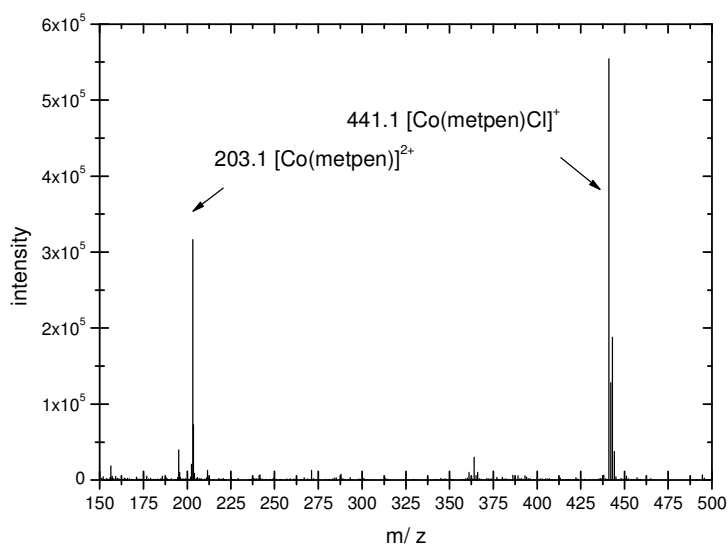


Figure 4-15: ESIMS spectrum of $[\text{Co}(\text{metpen})\text{Cl}]\text{SbF}_6$ in methanol

Figure 4-15 shows the ESIMS spectrum of $[\text{Co}(\text{metpen})\text{Cl}]\text{SbF}_6$ in methanol. The most dominant peak at $m/z = 441.1$ could be assigned to $[\text{Co}(\text{metpen})\text{Cl}]^+$. In contrast to the bztpen complex solutions, no evidence for the formation of a methanolato species was found but the signal at $m/z = 203.1$ could be assigned to $[\text{Co}(\text{metpen})]^{2+}$ and showed the dissociation of the chloride containing complex.

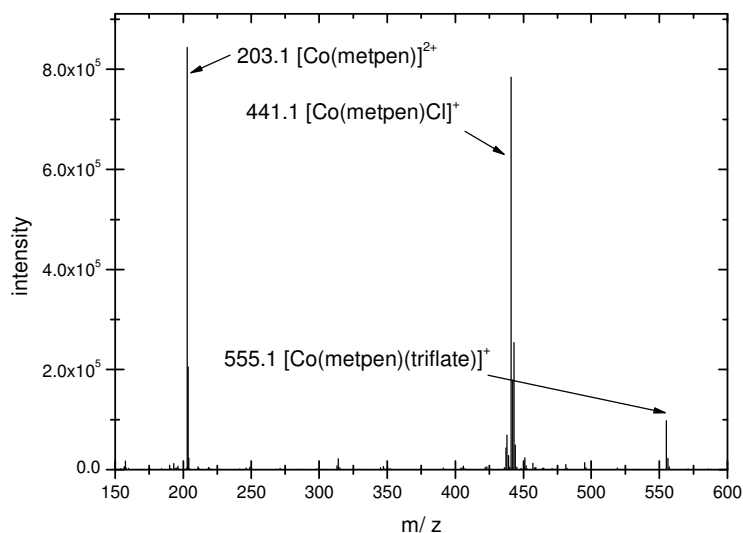


Figure 4-16: ESIMS spectrum of $[\text{Co}(\text{metpen})\text{Cl}]\text{triflate}$ in methanol.

The ESIMS spectrum of a solution of $[\text{Co}(\text{metpen})\text{Cl}]\text{triflate}$ is shown in Figure 4-16. The two dominant peaks in the spectrum are the signals of the chlorido complex $[\text{Co}(\text{metpen})\text{Cl}]^+$ at $m/z = 441.1$, and of the dissociated species $[\text{Co}(\text{metpen})]^+$ at m/z

= 203.1. The signal at $m/z = 555.1$ could be assigned to the cation $[\text{Co}(\text{metpen})(\text{triflate})]^+$.

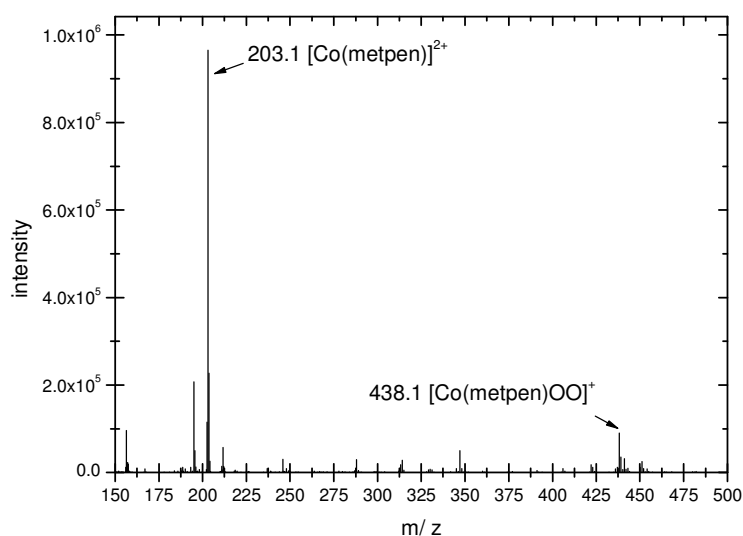


Figure 4-17: ESIMS spectrum of $[\text{Co}(\text{metpen})\text{Cl}]\text{triflate}$ in methanol with an excess of hydrogen peroxide.

Figure 4-17 shows the ESIMS spectrum of a solution of $[\text{Co}(\text{metpen})\text{Cl}]\text{triflate}$ in methanol with an excess of hydrogen peroxide. Like the reaction of the cobalt bztpen complex the signal that could be assigned to the cobalt(III) peroxido complex at $m/z = 438.1$ is relatively small. The most intensive signal at $m/z = 203.1$ could be assigned to $[\text{Co}(\text{metpen})]^{2+}$.

4.2.2.4 Reactions of Iron(II) and Cobalt(II) Bztpen Complexes with Nitric Oxide

4.2.2.4.1 Crystal Structure of $[\text{Fe}(\text{bztpen})\text{NO}_2](\text{SbF}_6)_2$

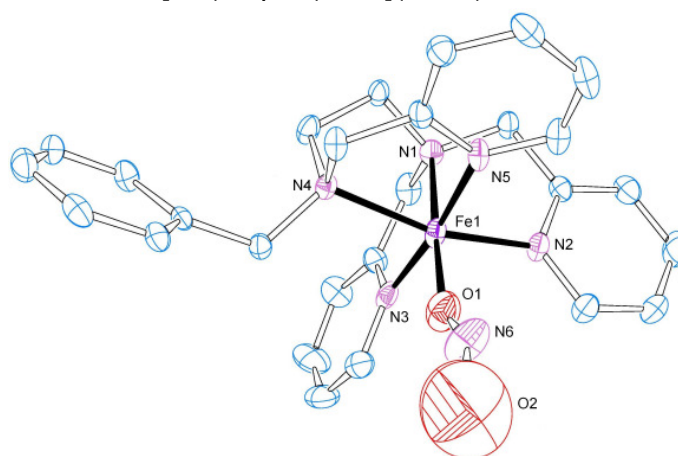


Figure 4-18: Ortep plot of the cation $[\text{Fe}(\text{bztpen})\text{NO}_2]^{2+}$ (**8**) (30% probability displacement ellipsoids, hydrogen atoms omitted for clarity).

Chapter 4

The cation of **8** is depicted in Figure 4-18. The iron(III) cation is coordinated by the five nitrogen donors of the ligand bztpen in a distorted octahedral geometry. The sixth coordination site is occupied by a oxygen atom of nitrite. The distance between Fe(1)-O(1) is 1.823(8) Å, which is in a typical range for an iron(III) nitrite bond.^{153,156} The angle O(1)-N(6)-O(2) is 154.0(16)° which is wider than those reported for related structures. This fact could be caused by the large thermal displacement of the oxygen atom O(2).

Table 4-11: structure and refinement data for compound **8**.

Empirical formula	C ₂₇ H ₂₉ F ₁₂ FeN ₆ O ₂ Sb ₂
Formula weight [g mol ⁻¹]	996.91
Crystal system	orthorhombic
Space group	Pbca
a [Å]	17.735(4)
b [Å]	19.504(4)
c [Å]	19.757(4)
α [°]	90
β [°]	90
γ [°]	90
V [Å ³]	6834(2)
Z	8
D _{calc} [g cm ⁻³]	1.938
T [K]	193(2)
μ(MoKα) [mm ⁻¹]	2.091
Crystal size [mm]	0.08 x 0.16 x 0.48
F(000)	3880
θ range [°]	2.30 to 25.92
Index ranges	-21 ≤ h ≤ 21 23 ≤ k ≤ 23 24 ≤ l ≤ 24
Reflections collected	45074
Unique reflections	6626
R _{int}	0.1346
Refinement method	Full-matrix least-squares on F ²
Data/constraints/parameters	6626 / 0 / 461
Godness-of-fit on F ²	0.889
Final R indices [I > 2σ(I)]	R ₁ = 0.0653 wR ₂ = 0.1604
R indices (all data)	R ₁ = 0.1312 wR ₂ = 0.1830
Largest diff. peak/hole [e. Å ⁻³]	1.548 to -1.008

Table 4-12: selected distances [Å] and angles [°] for compound **8**.

Fe(1)-O(1)	1.823(8)	O(1)-Fe(1)-N(1)	177.6(3)	N(1)-Fe(1)-N(5)	92.9(3)
Fe(1)-N(1)	2.064(7)	O(1)-Fe(1)-N(2)	97.2(3)	N(2)-Fe(1)-N(3)	92.9(3)
Fe(1)-N(2)	1.996(7)	O(1)-Fe(1)-N(3)	96.3(4)	N(2)-Fe(1)-N(4)	164.4(3)
Fe(1)-N(3)	1.978(9)	O(1)-Fe(1)-N(4)	97.4(3)	N(2)-Fe(1)-N(5)	91.6(3)
Fe(1)-N(4)	2.096(6)	O(1)-Fe(1)-N(5)	87.5(4)	N(3)-Fe(1)-N(4)	91.1(3)
Fe(1)-N(5)	1.996(8)	N(1)-Fe(1)-N(2)	80.4(3)	N(3)-Fe(1)-N(5)	173.7(3)
N(6)-O(1)	1.144(11)	N(1)-Fe(1)-N(3)	83.4(3)	N(4)-Fe(1)-N(5)	83.4(3)
N(6)-O(2)	1.52(3)	N(1)-Fe(1)-N(4)	85.0(3)	O(1)-N(6)-O(2)	154.0(16)

4.2.2.5 Stopped Flow Investigations on the Reactions of Cobalt(II) Bztpen Complex Solutions with Nitric Oxide

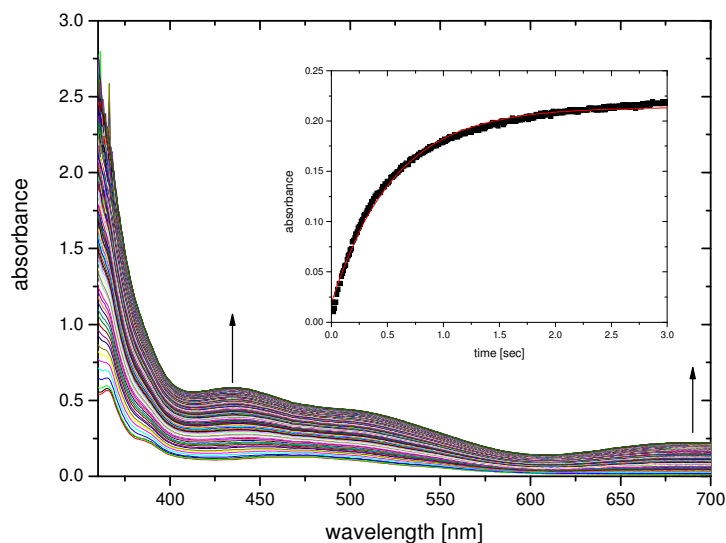


Figure 4-19: Time resolved spectra of the reaction of 2 mM solution of $\text{Co}(\text{BF}_4)_2 \times 6 \text{H}_2\text{O}$ and bztpen with a saturated solution of nitric oxide in methanol ($T = -40^\circ\text{C}$, $\Delta t = 10 \text{ ms}$). Insert: absorbance vs. time trace at 675 nm (data and fit to one exponential function).

Figure 4-19 shows the reaction of the cobalt(II) bztpen complex with nitric oxide in methanolic solution. The time resolved spectra show the formation of an absorbance maximum at 435 nm, a shoulder at 500 nm and an absorbance maximum at 700 nm.

5 Iron Complexes with the bridging Ligands bz-b-tpen and pC-b-tpen

5.1 Experimental

5.1.1 Materials and Reagents

All reagents and solvents were used as obtained without any further purification. Methanol as solvent for oxygen sensitive materials was obtained commercially from Acros and further distilled in argon atmosphere before usage. Handling of all oxygen-sensitive compounds and material was carried out in a glove box (M. Braun, Germany, $O_2 < 0.1$ ppm) within argon atmosphere.

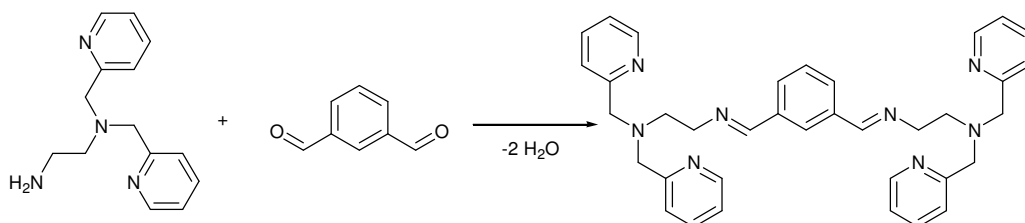
5.1.2 Physical Measurements

1H -NMR spectra were recorded with a Bruker-Aspect 2000/3000 400MHz.

UV/ Vis spectra were obtained using an Agilent 8453 spectrophotometer.

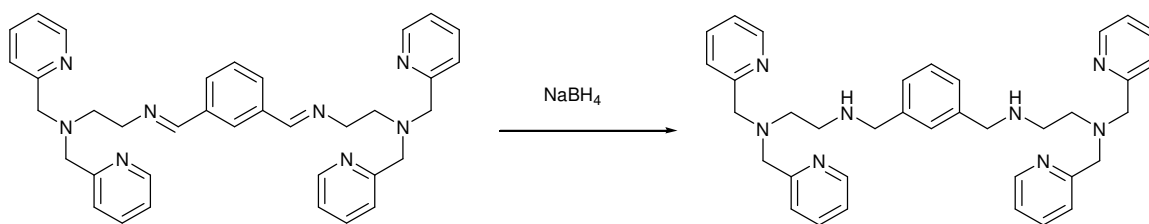
5.1.3 Syntheses of the Ligand bz-b-tpen

5.1.3.1 Formation of the Schiff-Base



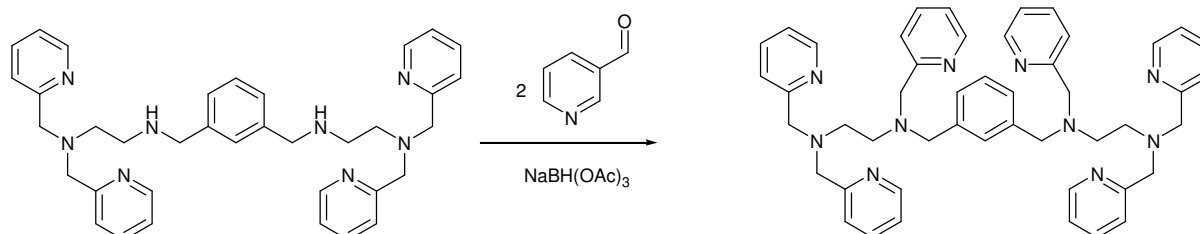
A solution of 5.10 g (22 mmol) uns-penp in 20 ml of methanol was added to a solution of 1.44 g (11 mmol) in absolute methanol. 5 g of mol sieves 3 Å were added to the yellow solution under inert conditions. The color changed immediately to a brown color. This mixture was stirred for 3 h at r.t.. Then the mole sieves were filtered and washed several times with dichloromethane. The organic phases were combined and the solvents were removed to yield a yellow oil. Yield 6.25 g 97 %. 1H NMR ($CDCl_3$, 400 MHz): δ 8.50 (d, 4 H) 8.27 (s, 2 H), 8.10 (s, 1 H), 7.77 (d, 2 H), 7.63-7.40 (m 12 H), 7.14-7.05 (m, 4 H) 3.92 (s, 4 H), 3.82 (t, 4 H), 2.97 (t, 4 H).

5.1.3.2 Reduction of the Schiff-Base



2.74 g (5 mmol) of the Schiff-Base were diluted in 50 ml dichloromethane. The solution was cooled with ice and 3.2 g (85 mmol) of NaBH_4 were added in small portions. The solution was stirred at r.t. for 1.5 h. Then the reaction was stopped by adding 25 ml of 2m aqueous sodium hydroxide solution. The phases were separated and the inorganic phase was washed 3 times with dichloromethane. The combined organic phases were dried over anhydrous Na_2SO_4 . Finally the solvent was evaporated to yield a yellow oil. Yield 2.31 g 78,8 %. $^1\text{H NMR}$ (CDCl_3 , 400 MHz): δ 8.45 (d, 4 H) 7.60-7.28 (m, 12 H) 7.11-7.02 (m, 4 H,) 3.79 (s, 4 H) 3.64 (s, 4 H) 2.92-2.42 (m, 16 H), 1.38 (s, 2 H).

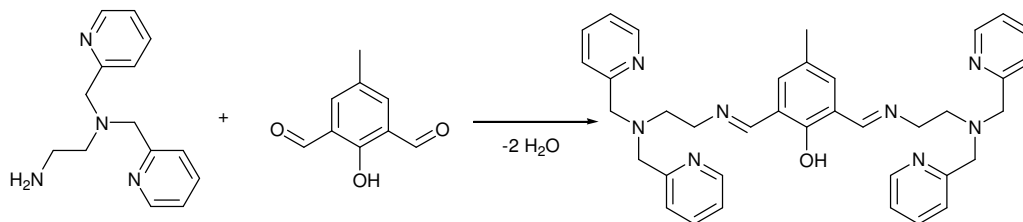
5.1.3.3 Reductive Amination



0.82 g (8 mmol) of pyridine-2-aldehyde diluted in 20 ml of 1,2-dichloroethane were added to 2.24 g (4 mmol) of the amine which had been solved in 20 ml of 1,2-dichloroethane. 2.5 g (20 mmol) of sodium triacetoxyborohydride were slowly added. The mixture was stirred at r.t. for 70 h under argon atmosphere. The reaction was stopped by adding 100 ml of 2 m aqueous sodium hydroxide solution. The phases were separated and the inorganic phase was extracted three times with dichloromethane. The combined organic phases were dried over anhydrous Na_2SO_4 . The solvents were evaporated to yield a yellow oil. Yield 2.52 g 82.5 %. $^1\text{H NMR}$ (CDCl_3 , 400 MHz): δ 8.46 (d, 6 H), 7.72-7.34 (m, 18 H), 7.21-7.01 (m, 4 H), 3.71 (s, 12 H) 3.51 (s, 4 H) 2.78-2.62 (m, 8 H).

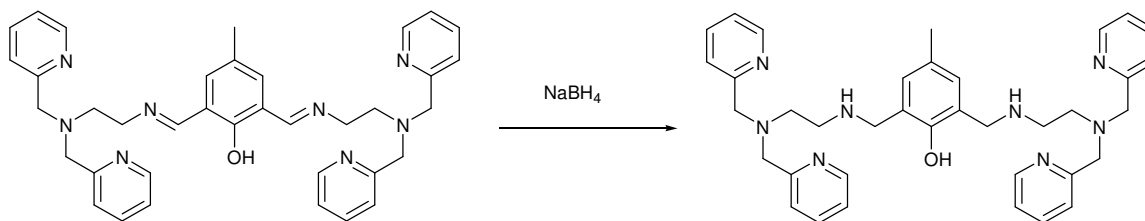
5.1.4 Syntheses of the Ligand pC-b-tpen

5.1.4.1 Formation of the Schiff-Base



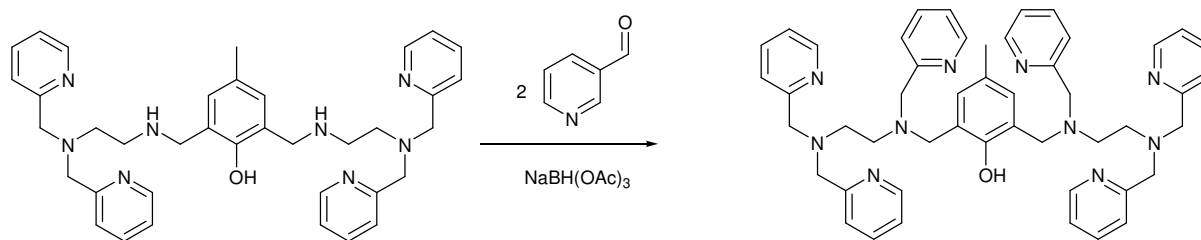
0.483 g (2.9 mmol) of p-Cresol-2,5-dialdehyde and 1.425g (5.9 mmol) of uns-penp were solved in 100 ml of dichloromethane. 4.3 g of anhydrous MgSO_4 were added and the mixture was stirred for 24 h at r.t.. The drying agent was filtered and the solvent was removed to yield a yellow oil. Yield 1.63 g (2.7 mmol) 93.1%. $^1\text{H-NMR}$ (CDCl_3 , 400 MHz): δ 13.90 (s, 1 H); 8.53-8.49 (m, 4 H); 7.70 - 7.08 (m, 12 H); 4.00 - 3.86 (m, 8 H); 3.84 - 3.74 (m, 4 H); 3.00-2.87 (m, 4 H); 2.30 (t, 3 H).

5.1.4.2 Reduction of the Schiff-base



1.63 g (2.7 mmol) of the Schiff-base were solved in 60 ml of dichloromethane and cooled with ice. 0.485 g (12.8 mmol) of NaBH_4 were added in small portions. The mixture was stirred at r.t. for 75 min. The reaction was stopped by adding 50 ml of 2 m NaOH . The phases were separated, and the inorganic phase was extracted three times with dichloromethane. The combined organic phases were dried over anhydrous Na_2SO_4 . Removing of the solvent yielded a yellow to brown oil. Yield 1.53 g (2.48 mmol) 93.6 %. $^1\text{H-NMR}$ (CDCl_3 , 400 MHz): δ 8.57-8.33 (m, 4 H); 7.71-7.07 (m, 12 H); 3.86-3.45 (m, 8 H), 3.05-2.47 (m, 8 H); 2.22-2.14 (m, 3 H).

5.1.4.3 Reductive Amination



0.73 g (1.2 mmol) of the amine were solved in 10 ml 1,2 -dichloroethane and 0.258 g (2.4 mmol) pyridine-2-aldehyde solved in 10 ml 1,2-dichloroethane were added to the solution. Then, 0.86 g (4.1 mmol) of sodium triacetoxyborohydride were added in small portion. The mixture was stirred for 12 h at r.t. under argon atmosphere. The reaction was stopped by adding 100 ml of 2 m aqueous sodium hydroxide solution. The phases were separated and the inorganic phase was extracted three times with dichloromethane. The combined organic phases were dried over anhydrous Na_2SO_4 . Removing of the solvents yielded a brown oil. Yield 0.94 g 99.7 % (crude product). $^1\text{H-NMR}$: (CDCl_3 , 400 MHz): δ 8.58 - 8.44 (m, 6 H); 7.7 - 7.1 (m, 20 H) 3.93 - 3.47 (m, 16 H); 2.79-2.59 (m, 8 H) 2.15 (m, 3 H).

5.1.5 Syntheses of the Complexes

5.1.5.1 $[\text{Fe}_2(\text{bz-b-tpen})](\text{SbF}_6)_4$

200 mg (0.26 mmol) of bz-b-tpen were dissolved in 5 ml absolute methanol. This solution was added to 362 mg (0.47 mmol) $\text{Fe}(\text{CH}_3\text{CN})_6(\text{SbF}_6)_2$ in 3 ml absolute methanol. Immediately, a yellow-orange solid precipitated out of the solution. The deposition was completed by adding anhydrous diethyl ether. The solid was filtered, washed with diethyl ether and dried in vacuum, to yield a beige powder.

5.1.5.2 $[\text{Fe}_2(\text{bz-b-tpen})](\text{PF}_6)_4$

95.6 mg (0.12 mmol) of bz-b-tpen were dissolved in 0.5 ml of absolute methanol. 99,8 mg of $[\text{Fe}(\text{CH}_3\text{CN})_6](\text{BF}_4)_2$ (0.21 mmol) dissolved in 0.5 ml absolute methanol were added. The reddish brown complex solution was stirred for 15 min. Formation of a precipitate followed, which was completed by adding 1 ml of diethyl ether. The precipitate was filtered and washed with small portions of diethyl ether. The yellow brown powder was dried in vacuum.

5.1.5.3 $[\text{Fe}_2(\text{bz-b-tpen})](\text{BPh}_4)_4$

58.7 mg (0.08 mmol) of the ligand were dissolved in 1 ml methanol. A solution of 44.5 mg (0.16 mmol) $\text{Fe}(\text{CH}_3\text{CN})_6(\text{BF}_4)_2$ in 1ml methanol was added. 75.7 mg (0.2 mmol)

of NaBPh₄ were dissolved in 1 ml methanol and added to the reddish brown complex solution. A precipitate was formed immediately. The precipitate was filtered and washed several times with small portions of diethyl ether, followed by drying in vacuum. A yellow powder was obtained.

5.1.5.4 $[Fe_2(bz-b-tpen)](triflate)_4$

A solution of 60 mg (0.08 mmol) of bz-b-tpen in 1 ml methanol was mixed with a solution of 62.2 mg (0.14 mmol) of $[Fe(MeCN)_2(triflate)_2]$ in methanol. The reddish-brown coloured solution was stirred for 15 min. Further, the complex solution was added to an excess of diethyl ether. The precipitate was filtered and dried in vacuum. A yellow powder was obtained.

5.1.5.5 $[Fe_2(bz-b-tpen)](BF_4)_4$

58.8 mg (0.08 mmol) of the ligand were dissolved in 1 ml methanol and mixed with 61.4 mg (0.13 mmol) of $Fe(MeCN)_6(BF_4)_2$ in 1 ml methanol. The reddish brown solution was stirred for 15 min. Further, the complex solution was dropped into an excess of diethyl ether. The precipitate was filtered and washed several times with diethyl ether. A yellow powder was obtained.

5.1.5.6 $[Fe_2(bz-b-tpen)](ClO_4)_4$

79 mg (0.10 mmol) of bz-b-tpen were dissolved in 1 ml of methanol. To this solution 82.2 mg of $Fe(MeCN)_6(BF_4)_2$ in 1 ml methanol were added. A reddish brown complex solution resulted. After stirring for 15 min 60 mg (0.5 mmol) of NaClO₄ dissolved in 1 ml methanol were added. Precipitation occurred and was completed by adding of 1 ml of diethyl ether. The yellow brown precipitate was filtered and washed several times with diethyl ether. A yellow powder was obtained.

5.1.5.7 $[Fe_2(pC-b-tpen)Cl_2](ClO_4)_2$

25 mg (0.03 mmol) of pC-bztpen were dissolved in 1 ml methanol and 12.3 mg (0.06 mmol) $FeCl_2 \times 4 H_2O$ dissolved in 1 ml methanol were added. 12 mg (0.09 mmol) NaClO₄ were added to the yellow solution. Dropping in diethyl ether yielded a yellow oxygen sensitive powder, which was removed by filtration and dried in argon atmosphere.

5.1.5.8 $[Fe_2(pC-b-tpen)Cl_2](ClO_4)_4$

25 mg (0.03 mmol) of the ligand were dissolved in 1 ml methanol and 10 mg FeCl₃ (0.06 mmol) dissolved in 1 ml methanol were added. 12 mg (0.09 mmol) NaClO₄

were added to the intensive blue solution. Dropping into an excess of diethyl ether yielded a dark blue powder, which was removed by filtration and dried on air.

5.2 Results

5.2.1 Synthesis of the Iron(II) complexes.

Iron complexes of the ligands bz-b-tpen and pC-b-tpen could be synthesized by reaction with iron precursor compounds in methanol solutions. Many attempts were made but, unfortunately no single crystals suitable for X-ray analysis could be obtained.

5.2.2 Reaction with of Iron (II) and Iron(III) bz-b-tpen Complex Solutions with Hydrogen Peroxide / Triethylamine

The iron(II) complex solutions are not stable when exposed to air. Thus by air contact, they were oxidized to iron(III). The iron(III) complex solution in methanol shows an absorption shoulder at 350 nm. The UV/ Vis spectrum of this complex solution is depicted in Figure 5-1 (green line). The wavelength is in the same range as those found for iron(III) bztpen species.¹³⁴ The iron(II) and iron(III) species react with hydrogen peroxide in methanol solution to a purple hydroperoxido complex. The UV/ Vis spectrum for the reaction of iron(III) complex with an excess of hydrogen peroxide in methanol at r.t. is shown in Figure 5-1 (black line). The charge transfer band has a maximum at 534 nm which is in the same range as those found for the mononuclear iron Rtpen complexes.¹⁰² The addition of bases such as triethylamine to the purple complex solution leads to a transient blue coloured species. The blue species is an iron(III) peroxido complex, like those described for iron(III) Rtpen complexes.¹⁰⁰ The difference of the maximum assigned to the peroxido complex is caused by the increased donor strength of the peroxido ligand compared to the hydroperoxido ligand. The absorbance maximum at 744 nm is in the same range as those found for the mononuclear iron(III) peroxido species. Both species, the hydroperoxido complex and the peroxido complex, were stable for several minutes at r.t.. Compared to the mononuclear species, an additional stabilisation of the hydroperoxido or peroxido intermediates was not observed.

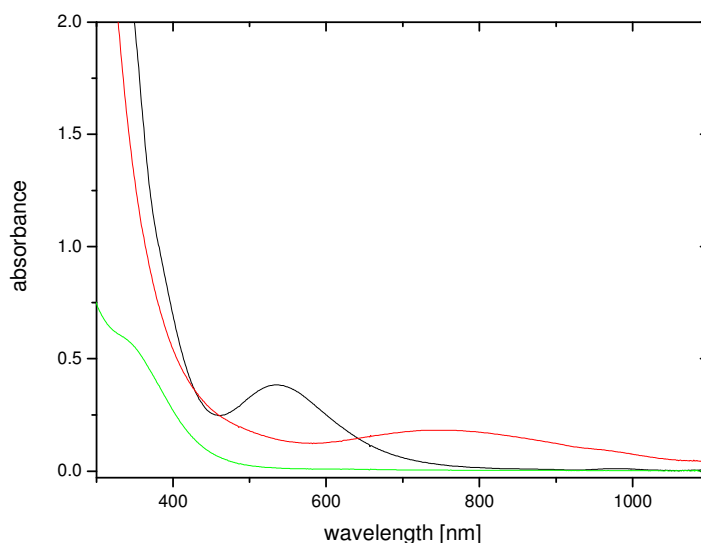


Figure 5-1: UV/ Vis-spectra of the iron(III)bz-b-tpen complex in methanol (green line) and after reaction with hydrogen peroxide (black line) and hydrogen peroxide/ triethylamine (red line) r.t..

5.2.3 Reaction of the Iron(II) pC-b-tpen Complex with Air

The ligand pC-b-tpen was synthesized as a model compound for potential hydroxylation of the phenyl ring by intramolecular reaction of an iron-bz-b-tpen hydroperoxido or peroxido species. Unfortunately, no single crystals of an iron(II) or an iron(III) complex with this ligand could be isolated. Interestingly, the iron(II) complex solution is exceptionally air sensitive. When exposed to air the yellow iron(II) complex solution, changes immediately into an intensive blue. The UV/ Vis spectra for the complex solution under inert conditions (black line) and after reaction with air (red line) are depicted in Figure 5-2. The iron(II) complex has an absorbance maximum at 389 nm. The blue iron(III) complex has an absorbance maximum at 592 nm, which is within the typical range for charge-transfer iron(III)phenolate complexes.¹⁵⁷ Reactions of the iron(II) complex solutions at -80 °C in several solvents with dioxygen also produced the iron(III) species. No iron-oxygen intermediate could be observed.

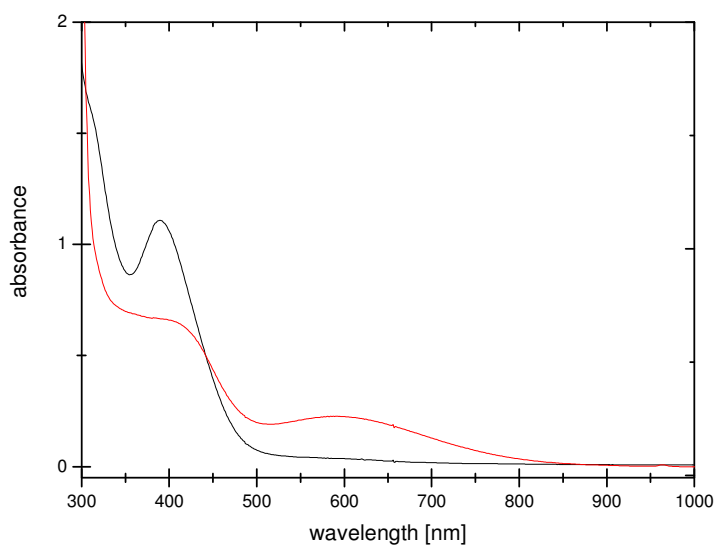


Figure 5-2: UV/ Vis spectra of iron(II)-pC-b-tpen in methanol (black line) and after reaction with air (red line) at r.t..

6 Iron and Cobalt Complexes with the Ligand (2-aminoethyl)-bis(2-pyridylmethyl)amine (uns-penp) and Derivatives

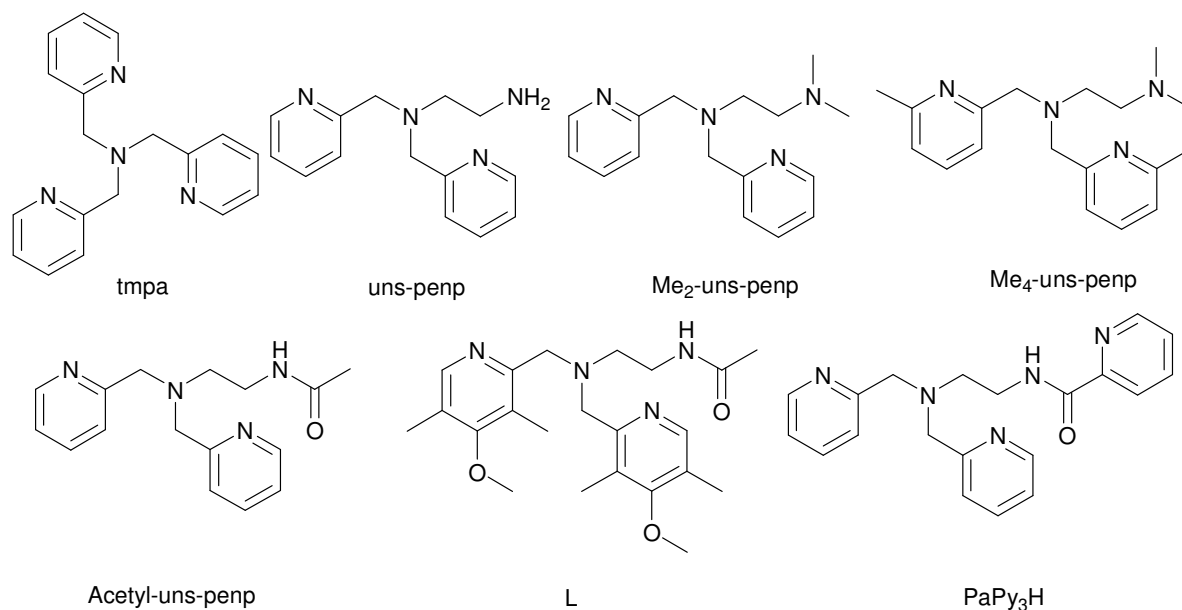
This chapter has been submitted for publication in *Inorganica Chimica Acta*
Thomas Nebe, Jing-Yuan-Xu, Alexander Beitat, Christian Würtele, Olaf Walter,
Michael Serafin and Siegfried Schindler

6.1 Abstract

A series of iron (II)/(III) and cobalt(II)/(III) complexes with the tetradentate tripodal ligands (2-aminoethyl)bis(2-pyridylmethyl)amine (uns-penp), its methylated derivatives Me₂-uns-penp and Me₄-uns-penp as well as the amide ligand N-acetyl-N,N-bis[(2-pyridyl)methyl]ethylenediamine (acetyl-uns-penp) were synthesized and structurally characterized. Complexes of this type seem to have a high potential to be useful in the activation of dioxygen for selective oxidation reactions of organic substrates.

6.2 Introduction

A wide range of chemical reactions is catalyzed by metallo enzymes. We are particularly interested in dioxygen activation at non-heme iron active sites. This is observed in a large number of iron based enzymes such as lipoxygenases, α -keto acid-dependent enzymes, catechol dioxygenases, methane monooxygenases or the anti-tumor drug bleomycin.^{83,121,158} Low molecular weight coordination compounds have been used to functionally model different types of enzymes.^{4,83,158} An important ligand in that context is tris[(2-pyridyl)-methyl]amine (tmpa, also abbreviated as tpa, Scheme 6-1), a tetradentate tripodal ligand which provides four N donor atoms.⁷⁷ Tmpa/tpa proved to be very useful in the bioinorganic chemistry of copper^{3,51,83} and has been successfully used in a large number of experimental studies to model iron enzymes such as catechol dioxygenases.^{4,158,159}



Scheme 6-1: the ligand uns-penp and derivatives.

Substitution of one pyridyl arm of tmpa by an aliphatic ethylamino group leads to the related ligand (2-aminoethyl)bis(2-pyridylmethyl)amine (uns-penp, Scheme 6-1). This compound was first introduced by Mandel et al. who used it as a ligand for copper and cobalt complexes.^{88,91} Uns-penp is particularly interesting in regard to its facile modification. During the synthesis of uns-penp the amide *N*-acetyl-*N*, *N*-bis[(2-pyridyl)methyl]ethylenediamine (acetyl-uns-penp, Scheme 6-1) needs to be prepared.^{86,91} We used uns-penp as well as acetyl-uns-penp for the synthesis and investigation of copper and iron complexes.^{83,160} For instance we tested the iron complexes for their catechol dioxygenase activity, however we could not observe a higher activity compared to the already known iron/tmpa system.^{160,161} Acetyl-uns-penp is related to the ligand *N*-pyridine-2-carboxamide (PaPy₃H, Scheme 6-1). Instead of the methyl group in acetyl-uns-penp, PaPy₃H contains an additional coordinating pyridyl unit. Using this ligand, Mascharak and co-workers have investigated rich in detail the structures and properties of Fe(II)/Fe(III) complexes. They were particularly interested in the formation and characterization of iron nitric oxide complexes, which show photolability of the NO ligands due to the coordination properties of the carboxamido group.¹⁶² Quite surprisingly, the iron(III) complex with the PaPy₃H ligand described by Mascharak and co-workers is completely different to the iron(III) complex with the acetyl-uns-penp ligand described by us.^{160,162}

Furthermore, most recently Que and co-workers presented the crystal structure of a μ -oxido-diiron(III) complex with the ligand L shown in Scheme 1 which is a closely

related derivative of acetyl-uns-penp.¹⁶³ The molecular structure of this complex is nearly identical to the μ -oxido diiron(III) complex with the acetyl-uns-penp ligand has been already published by us previously.⁹¹ The most striking feature of the complex reported by the Que group was the electrochemical formation of a highly potent oxidative dinuclear iron(IV) species from the μ -oxido-diiron(III) precursor.

Subsequent methylation of the ligand uns-penp leads to Me₂-uns-penp (Scheme 1). This ligand had already been used by us previously in copper coordination chemistry for the stabilisation of a copper peroxido complex.^{164,165} Furthermore, it has also been used by us and others (abbreviated as iso-bpmen) in iron coordination chemistry and for catalytic studies on hydrogen peroxide activation.¹⁶⁶

Methylation of the pyridine rings in ortho-position of the ligand uns-penp leads to Me₄-uns-penp (Scheme 1).

In our efforts to gain better understanding of the reactions of iron complexes with dioxygen, nitric oxide or hydrogen peroxide, we have investigated iron complexes with the ligands uns-penp, acetyl-uns-penp, Me₂-uns-penp and Me₄-uns-penp. Furthermore, we have started to investigate the according cobalt complexes with these ligands. Unfortunately, so far we have not been able to observe new iron/cobalt "oxygen or NO adduct" complexes using these ligands. However, during our studies we obtained new interesting iron and cobalt compounds that are reported here and that most likely will be useful for our further investigations.

6.3 Experimental

6.3.1 Materials

Commercially available materials were used without further purification. FeCl₂, [Fe(DMF)₆](ClO₄)₃ as well as [Fe(CH₃CN)₂(triflate)₂] were prepared according to literature procedures.^{141,142,167} Iron(II) in [Fe(CH₃CN)₂(triflate)₂] was determined by manganometric titrations. The absence of water was controlled with ATR-IR-spectroscopy.

6.3.2 Physical Measurements

Single crystal X-ray diffraction studies of the Substance **9**, **11**, **13-21** were performed with a STOE IPDS-diffractometer equipped with a low temperature system (Karlsruher Glastechnisches Werk), a graphite monochromator and IP detector

system used. Mo-K α radiation ($\lambda = 0.71069 \text{ \AA}$) was used. The frames were integrated with the STOE software package. No absorption corrections were applied.

Single crystal X-ray diffraction studies of the substances **10** and **12** were performed with a Siemens SMART CCD 1000 diffractometer equipped with a graphite monochromator and a CCD detector. Mo-K α radiation ($\lambda = 0.7103 \text{ \AA}$) was used. The collected reflections were corrected for absorption effects (SADABS, Siemens Area Detector Absorption Correction, Siemens, Forschungszentrum Karlsruhe ITC-CPV). All structures were solved by direct methods and refined by using fullmatrix least squares in SHELX software package.^{147,148} All non hydrogen atoms were refined anisotropically. All hydrogen atoms were positioned geometrically.

Caution! The perchlorate salts used in this study are potentially explosive and should be handled with care.

6.3.3 Syntheses

6.3.3.1 Ligand Syntheses

The ligands uns-penp, Me₂-uns-penp and acetyl-uns-penp were prepared according to literature procedures.⁸⁶ The ligand Me₄-uns-penp was synthesized by reductive amination of N,N-dimethylethylenediamine using sodium triacetoxyborohydride and 6-methylpyridine-2-carbaldehyde.

6.3.3.2 [Co(uns-penp)Cl₂]SbF₆ x C₃H₆O (**9**)

71 mg (3.0 mmol) of uns-penp and 67 mg (2.8 mmol) CoCl₂ x 6 H₂O were dissolved in 1 ml methanol. 60 mg (2.3 mmol) NaSbF₆ dissolved in 0.5 ml methanol were added to the resulting purple solution. The crude product precipitated by adding the complex solution dropwise into an excess of diethyl ether. Decanting and drying in vacuum yielded a dark purple oil. The crude product was further redissolved in 1.5 ml acetone and decanted from undissolved oily impurities. Purple needles suitable for X-ray analysis were obtained by vapor diffusion of diethyl ether into the complex solution at room temperature.

6.3.3.3 [Fe(Me₂-uns-penp)Cl₂]ClO₄ (**10**)

While stirring, a solution of 163 mg (0.4 mmol) Me₂-uns-penp in 5 ml methanol was added to 93 mg (0.2 mmol) Fe(ClO₄)₃ x H₂O and 65 mg (0.4 mmol) FeCl₃ dissolved in 10 ml methanol. A dark greenish brown solution resulted and some dark oil precipitated. The solution was stirred overnight and the resulting brown slurry was

filtered off. The precipitate was washed with small portions of methanol and diethyl ether. Redissolving of the substance in acetonitrile and vapor diffusion of diethyl ether into the solution led to formation of red prismatic single crystals of **10** which were suitable for X-ray analysis.

6.3.3.4 $[Fe_2(Me_2\text{-uns-penp})_2Cl_2O](BPh_4)_2$ (**11**)

A solution of 136 mg (0.5 mmol) $Me_2\text{-uns-penp}$ and 81 mg (0.5 mmol) anhydrous $FeCl_3$ in 10 ml methanol was mixed with a solution of 177 mg (0.5 mmol) $NaBPh_4$ in 10 ml methanol. A reddish brown slurry was formed which was stirred for 1 h and filtered off. The precipitate was washed with small portions of methanol and diethyl ether and dried in vacuum. Vapor diffusion of diethyl ether into a solution of the complex salt in dimethyl formamide led to the formation of brown cube shaped single crystals.

6.3.3.5 $[Fe(Me_2\text{-uns-penp})Cl(CH_3CN)]BPh_4$ (**12**)

The synthesis of **12** was carried out under argon atmosphere. 100 mg (0.5 mmol) of $FeCl_2 \times 4 H_2O$ and 136 mg (0.5 mmol) $Me_2\text{-uns-penp}$ were dissolved in 5 ml dry acetonitrile while stirring. A light brown solid precipitated after addition of a solution of 177 mg (0.5 mmol) $NaBPh_4$ in 3 ml acetonitrile. The slurry was stirred over night and filtered off. Redissolving the precipitate in acetonitrile and vapor diffusion of diethyl ether into the solution led to yellow cube shaped single crystals suitable for X-ray studies.

6.3.3.6 $[Co(Me_2\text{-uns-penp})Cl]ClO_4$ (**13**)

171 mg (0.6 mmol) $Me_2\text{-uns-penp}$ and 151 mg $CoCl_2 \times 6 H_2O$ (0.6 mmol) were dissolved in 6 ml methanol. After stirring for 15 min, 35 mg (0.3 mmol) $NaBF_4$ were added to 3 ml of the dark green complex solution. A green powder precipitated after the addition of an excess of diethyl ether. After redissolving the substance in acetone, filtration and addition of sodium perchlorate, vapor diffusion of diethyl ether at $-30^\circ C$ yielded dark green block shaped single crystals suitable for X-ray analysis after three months time.

6.3.3.7 $[Co(Me_4\text{-uns-penp})Cl]BF_4$ (**14**)

391 mg (1.3 mmol) of $Me_4\text{-uns-penp}$ and 318 mg (1.3 mmol) $CoCl_2 \times 6 H_2O$ were dissolved in 2 ml methanol. The resulting dark green solution was stirred for 15 min and 5 ml of 146 mg (1.3 mmol) $NaBF_4$ dissolved in 5 ml hot methanol were added. Adding the complex solution dropwise into an excess of diethyl ether yielded a grey

to green solid which was decanted and washed with diethyl ether and dried in air. The crude product was redissolved in acetone. The solution was filtered to remove unsolvable impurities. The dark green block-shaped single crystals were obtained by vapor diffusion of diethyl ether into the solution at room temperature.

6.3.3.8 $[Fe_2(acetyl-uns-penp)_2Cl_2(CH_3OH)_2](ClO_4)_2 \times 2 CH_3OH$ (**15**)

Under inert atmosphere 20 mg (0.1 mmol) $FeCl_2 \times 4 H_2O$ in 1 ml dry methanol were added to a solution of 28 mg (0.1 mmol) acetyl-uns-penp in 1 ml dry methanol. The mixture was stirred for 15 min. After that 28 mg (0.2 mmol) of $NaClO_4$ were added to the intensive yellow colored solution. The solution was layered with diethyl ether and stored at $-36^\circ C$. After a few days yellow crystals of **15** suitable for X-ray analysis were obtained.

6.3.3.9 $[Co_2(acetyl-uns-penp)_2Cl_2](BF_4)_2 \times C_3H_6O$ (**16**)

341 mg (1.2 mmol) acetyl-uns-penp and 286 mg (1.2 mmol) $CoCl_2 \times 6 H_2O$ were dissolved in 5 ml methanol. The resulting purple complex solution was stirred for 15 minutes. 132 mg (1.2 mmol) $NaBF_4$ dissolved in hot methanol were added. The complex solution was added dropwise into an excess of diethyl ether. The complex salt was precipitated as a dark purple oil. The crude product was redissolved in a small amount of acetone. The solution was filtered to remove undissolved impurities. The complex was precipitated by vapor diffusion of diethyl ether into the solution at room temperature. Dark purple prismatic crystals suitable for X-ray analysis, were obtained after one week.

6.3.3.10 $[Fe_2(acetyl-uns-penp)_2(triflate)_2(CH_3OH)_2](ClO_4)_2$ (**17**)

100 mg (0.35 mmol) of acetyl-uns-penp in 1 ml dry methanol were mixed with 140 mg (0.3 mmol) $Fe(CH_3CN)_2(triflate)_2$ in 1 ml dry methanol and stirred for 15 min. 86 mg (0.7 mmol) $NaClO_4$ in 1 ml dry methanol were then added to the reddish-brown colored solution. This mixture was added to dry diethyl ether and an orange-brown oil was precipitated. The separated oil was layered with dry diethyl ether and after a few weeks, orange crystalline needles adequate for X-ray structure analysis were obtained.

6.3.3.11 $[Fe_2(acetyl-uns-penp)_2OH](ClO_4)_2 \times 3 C_3H_6O$ (**18**)

In an argon atmosphere glove box 28 mg (0.1 mmol) of acetyl-uns-penp in 1 ml of dry acetone were mixed with 40 mg (1 mmol) of a NaH / mineral oil dispersion (60 %). Gas development was observed and the color of the solution changed from yellow to

dark red. 13 mg (0.1 mmol) FeCl₂ dissolved in 1 ml dry acetone were added and resulted in a strawberry red solution. This solution was filtered to remove undissolved residues. Addition of 28 mg NaClO₄ (0.2 mmol) led to precipitation of an orange solid which was redissolved by addition of dry acetone. The saturated solution was stored at room temperature. After one week red to orange colored, air sensitive crystals suitable for X-ray structure analysis were obtained.

6.3.3.12 $[Fe_2(acetyl-uns-penp)_2(DMF)_2O](ClO_4)_4 \times CH_3CN$ (**19**)

The synthesis of the complex compound was carried out in an argon-filled glovebox. 317 mg (0.4 mmol) Fe(DMF)₆(ClO₄)₃ and 114 mg (0.4 mmol) acetyl-uns-penp were dissolved in 10 ml of dry acetonitrile and stirred for 30 min. The resulting dark brown solution was filtered. Vapor diffusion of diethyl ether into the filtrate led to the formation of dark red block shaped crystals suitable for X-ray diffraction studies.

6.3.3.13 $[Co(acetyl-uns-penp)Cl(H_2O)]Cl \times H_2O$ (**20**)

A solution of 28 mg (0.1 mmol) acetyl-uns-penp and 24 mg (0.1 mmol) CoCl₂ x 6 H₂O in 1 ml methanol was cooled down to -80 °C and one drop of hydrogen peroxide solution (35 %) was added. After warming to room temperature, vapor diffusion of diethyl ether led to precipitation of a dark brown oil which contained some violet to brown single crystals suitable for X-ray analysis.

6.3.3.14 $[Co(acetyl-uns-penp)CO_3]$ (**21**)

28 mg (0.1 mol) acetyl-uns-penp and 24 mg (0.1 mmol CoCl₂ x 6 H₂O) were dissolved in 1 ml methanol. After cooling down to -80 °C one drop of triethylamine was added. The color of the solution changed immediately from violet to brown. Warming to room temperature did not have an effect on the colour. Brown crystals of **21** were obtained by diffusion of diethyl ether into the solution at room temperature.

6.4 Results and Discussion

As described in the introduction we are interested in the reactivity of iron complexes towards dioxygen and/or hydrogen peroxide with the final goal to use these compounds in selective oxidation reactions of organic substrates such as hydrocarbons. Therefore, it is important to gain a better understanding of the reactive intermediate species so called "oxygen adduct" complexes. So far, only few of these intermediates could be isolated in non-heme iron chemistry.^{4,5,68} Uns-penp and its derivatives are interesting ligands in regard and have been used by us and others to

investigate these reactions in more detail. In this respect, the application of the ligand bztpen has been a real success so far.^{100,102,134} This ligand can be easily prepared from uns-penp by reacting it with 2-pyridine aldehyde followed by reductive amination. The iron(II) complex with this ligand forms iron(III) hydroperoxide and peroxido complexes. These complexes can react further to form an iron(IV) oxido complex that can be used in selective oxidation reactions of cycloalkanes.¹³³

6.4.1 Uns-penp

Uns-penp itself can be easily prepared according to the procedure described previously by Mandel and co-workers.⁸⁷ Different research groups have started to use this versatile ligand for the coordination of different metal ions, using modified synthetic procedures.^{86-88,90,161,168,169} Unfortunately most authors do not refer to the original synthesis of the ligand by Mandel and co-workers. Recently, we described the characterization and reactivity of iron(III) complexes with uns-penp as a ligand. Because of the difficulty to isolate and characterize iron "oxygen adduct" complexes we performed our investigations parallel with the according cobalt complexes. Here, we hoped to have a better chance to obtain these species because related cobalt "oxygen adduct" complexes are well known in the literature and usually can be prepared quite easily. Unfortunately, this was not the case. However, we obtained crystals of $[\text{Co}(\text{uns-penp})\text{Cl}_2]\text{SbF}_6 \times \text{C}_3\text{H}_6\text{O}$ (**9**) suitable for crystallographic analysis. The molecular structure of this complex is shown in Figure 6-1. Crystallographic data are presented in tables 6-1 and 6-2.

6.4.1.1 $[\text{Co}(\text{uns-penp})\text{Cl}_2]\text{SbF}_6 \times \text{C}_3\text{H}_6\text{O}$ (**9**)

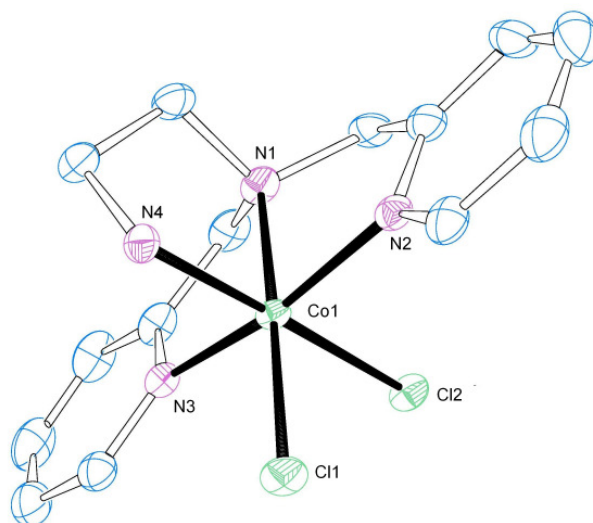


Figure 6-1: Molecular structure of the cation of **9** with hydrogen atoms omitted for clarity. Thermal ellipsoids are shown at 30 % probability levels.

Chapter 6

The unit cell consists of four complex cations. The positive charge is balanced by hexafluoroantimonate anions. The unit cell also contains four solvent molecules. The cobalt(III) cation is coordinated by the four N-donors of uns-penp and two chloride ions in a slightly distorted octahedral geometry. This is represented by the trans

Table 6-1: structural and refinement data for compounds **9** - **11**

	9	10	11
Empirical formula	C ₁₇ H ₂₄ Cl ₂ CoF ₆ N ₄ OSb	C ₁₆ H ₂₂ Cl ₃ FeN ₄ O ₄	C ₈₀ H ₈₄ B ₂ Cl ₂ Fe ₂ N ₈ O
Formula weight [g mol ⁻¹]	665.98	496.58	1377.77
Crystal system	monoclinic,	monoclinic	triclinic
Space group	P2(1)/c	P2(1)/c	P-1
a [Å]	7.9367(16)	10.2465(11)	14.5070(13)
b [Å]	11.029(2)	15.2903(16)	14.8754(14)
c [Å]	27.112(5)	13.6617(15)	17.8164(16)
α [°]	90	90	103.514(11)
β [°]	91.07(3)	104.3270(10)	97.178(11)
γ [°]	90	90	106.903(11)
V [Å ³]	2372.8(8)	2073.8(4)	3499.0(6)
Z	4	4	2
D _{calc} [g cm ⁻³]	1.864	1.590	1.308
T [K]	193(2)	200(2)	193(2)
μ(MoKα) [mm ⁻¹]	2.127	1.144	0.544
Crystal size [mm]	0.10 x 0.15 x 0.35	0.80 x 0.30 x 0.30	0.24 x 0.28 x 0.32
F(000)	1312	1020	1448
θ range [°]	1.99 - 24.05	2.03 - 28.34	2.86 - 28.03
	-9 ≤ h ≤ 9	-13 ≤ h ≤ 13	-19 ≤ h ≤ 19
Index ranges	-11 ≤ k ≤ 12	-20 ≤ k ≤ 20	-19 ≤ k ≤ 19
	-31 ≤ l ≤ 30	-18 ≤ l ≤ 18	-23 ≤ l ≤ 22
Reflections collected	12479	23720	31694
Unique reflections	3703	5026	15485
R _{int}	0.0618	0.0248	0.0354
Refinement method	Full-matrix least-squares on F ²	Full-matrix least-squares on F ²	Full-matrix least-squares on F ²
Data/constraints/parameters	3703 / 0 / 331	5026 / 0 / 259	15485 / 0 / 1195
Godness-of-fit on F ²	1.021	1.040	0.858
Final R indices [I > 2σ(I)]	R ₁ = 0.0465 wR ₂ = 0.1272	R ₁ = 0.0253 wR ₂ = 0.0632	R ₁ = 0.0346 wR ₂ = 0.0688
R indices (all data)	R ₁ = 0.0568 wR ₂ = 0.1332	R ₁ = 0.0314 wR ₂ = 0.0661	R ₁ = 0.0738 wR ₂ = 0.0781
Largest diff. peak/hole [e ⁻ Å ⁻³]	0.881 to -0.971	0.377 to -0.312	0.284 to -0.248

(167.57(17)°), N(1)-Co(1)-Cl(1) (176.78(13)°) and N(4)-Co(1)-Cl(2) (178.30(16)°). The angle between Cl(1)-Co(1)-Cl(2) (90.09(5)°) is very close to the ideal 90°. Compared to the iron(III) complex with uns-penp as a ligand published previously, the geometry of the cobalt(III) complex is closer to an ideal octahedron.⁹¹ Mandel and co-workers described the synthesis and characterization of some cobalt complexes with uns-penp as a ligand, however no crystal structures were reported. More recently, crystal structures of cobalt(III) uns-penp complexes were reported with NO₂⁻, phen and CO₃²⁻ as co-ligands.^{170,171} The bond lengths and angles of **9** are comparable to those reported for the analogous cobalt(III) tmpa complex.^{170,172} Furthermore, it is

interesting to note that uns-penp has a strong tendency to bind a proton. The first complex with the ligand uns-penp characterized crystallographically was a copper(II) complex containing a protonated amine arm.⁸⁸

6.4.2 Me₂-uns-penp

Protons that are available in the solvent or the ligand can be problematic during investigations of the formation of metal "dioxygen adduct" complexes because hydrogen peroxide might be formed instead. In our previous studies on copper complexes with this ligand we therefore preferred to use the methylated form of uns-penp. Using the ligand Me₂-uns-penp in our iron coordination chemistry we could synthesize and crystallographically characterize the iron(III) complex [Fe(Me₂-uns-penp)Cl₂](ClO₄) (**10**). Its molecular structure is presented in Figure 6-2. Crystallographic data are presented in tables 6-1 and 6-2.

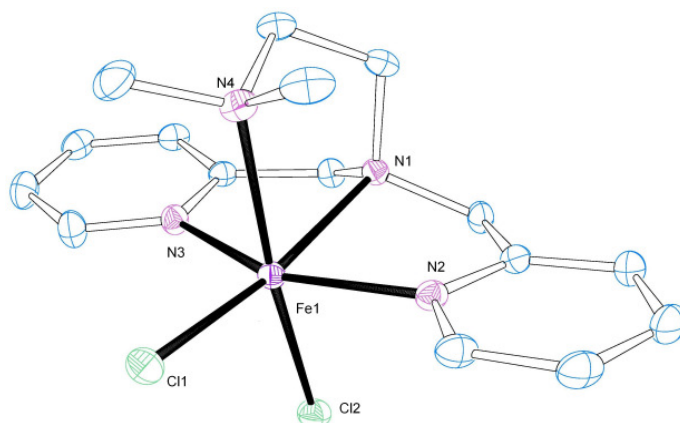


Figure 6-2: Molecular structure of the cation of **10** with hydrogen atoms omitted for clarity. Thermal ellipsoids are shown at 30 % probability levels.

6.4.2.1 [Fe(Me₂-uns-penp)Cl₂](ClO₄) (**10**)

In this case the iron(III) ion is coordinated in a distorted octahedral geometry. This is demonstrated by the trans ligand angle N(2)-Fe(1)-N(3) with 154.17(5)° which significantly differs from 180°. The structure is distorted towards the tertiary nitrogen atom N1. The angles N(1)-Fe(1)-N(2) (76.33(4)°), N(1)-Fe(1)-N(3) (78.01(4)°) and N(1)-Fe(1)-N(4) (79.14(5)°) are significantly smaller than in an ideal octahedron. The

Table 6-2: Selected distances [Å] and angles [°] for compounds **9** - **11**.

9					
Co(1)-Cl(1)	2.2538(13)	Cl(1)-Co(1)-N(1)	176.78(13)	Cl(2)-Co(1)-N(4)	178.30(16)
Co(1)-Cl(2)	2.2615(13)	Cl(1)-Co(1)-N(2)	95.84(12)	N(1)-Co(1)-N(2)	83.38(18)
Co(1)-N(1)	1.950(4)	Cl(1)-Co(1)-N(3)	96.59(13)	N(1)-Co(1)-N(3)	84.22(18)
Co(1)-N(2)	1.952(4)	Cl(1)-Co(1)-N(4)	89.68(14)	N(1)-Co(1)-N(4)	87.22(18)
Co(1)-N(3)	1.948(4)	Cl(2)-Co(1)-N(1)	93.04(13)	N(2)-Co(1)-N(3)	167.57(17)
Co(1)-N(4)	1.933(4)	Cl(2)-Co(1)-N(2)	90.61(12)	N(2)-Co(1)-N(4)	91.09(19)
Cl(1)-Co(1)-Cl(2)	90.09(5)	Cl(2)-Co(1)-N(3)	89.21(12)	N(3)-Co(1)-N(4)	89.14(19)

Chapter 6

10					
Fe(1)-N(1)	2.2519(18)	N(1)-Fe(1)-N(4)	79.85(6)	N(4)-Fe(1)-Cl(1)	92.70(5)
Fe(1)-N(3)	2.1597(19)	N(3)-Fe(1)-N(4)	94.97(7)	N(2)-Fe(1)-Cl(1)	106.15(6)
Fe(1)-N(4)	2.3116(18)	N(1)-Fe(1)-N(2)	77.28(7)	N(2)-Fe(1)-N(5)	87.47(7)
Fe(1)-N(2)	2.1446(19)	N(3)-Fe(1)-N(2)	151.23(8)	N(3)-Fe(1)-N(5)	84.17(7)
Fe(1)-N(5)	2.228(2)	N(4)-Fe(1)-N(2)	88.34(7)	N(1)-Fe(1)-N(5)	89.82(6)
Fe(1)-Cl(1)	2.3065(7)	N(1)-Fe(1)-Cl(1)	171.79(5)	N(5)-Fe(1)-Cl(1)	97.72(5)
Cl(1)-Fe(1)-Cl(2)	98.395(17)	N(5)-Fe(1)-N(4)	169.49(7)	C(1)-N(1)-Fe(1)	108.67(13)
N(1)-Fe(1)-N(3)	75.22(7)	N(3)-Fe(1)-Cl(1)	102.24(6)		
11					
Fe(1)-O(1)	1.7923(4)	O(1)-Fe(1)-N(3)	92.86(5)	N(3)-Fe(1)-N(4)	154.22(6)
Fe(1)-Cl(3)	2.2816(6)	O(1)-Fe(1)-N(4)	87.62(5)	N(3)-Fe(1)-N(6)	75.94(7)
Fe(1)-N(3)	2.1600(17)	O(1)-Fe(1)-N(6)	93.55(5)	N(3)-Fe(1)-N(7)	91.95(7)
Fe(1)-N(4)	2.1261(17)	O(1)-Fe(1)-N(7)	168.90(5)	N(4)-Fe(1)-N(6)	78.31(7)
Fe(1)-N(6)	2.2134(15)	Cl(3)-Fe(1)-N(3)	99.08(5)	N(4)-Fe(1)-N(7)	83.72(7)
Fe(1)-N(7)	2.3647(19)	Cl(3)-Fe(1)-N(4)	106.00(5)	N(6)-Fe(1)-N(7)	77.93(6)
Fe(1)...Fe(1)#1	3.585	Cl(3)-Fe(1)-N(6)	163.66(5)		
O(1)-Fe(1)-Cl(3)	102.30(2)	Cl(3)-Fe(1)-N(7)	86.80(5)		

bond Fe(1)-Cl(1) (2.2452(5) Å) in trans position to N(1) is shorter than the iron(III) chloride bond between Fe(1)-Cl(1) (2.3177(5) Å) trans to N(4). The bond lengths are comparable to the reported structure of [Fe(uns-penp)Cl₂]⁺, except for the bond distance of Fe(1)-N(4).⁹¹ With 2.2942(13) Å this bond distance is significantly larger than the 2.172(2) Å observed in [Fe(uns-penp)Cl₂]⁺. This is easily explained by the steric effect of the two methyl groups on the tertiary amine donor atom compared to the primary amine group in [Fe(uns-penp)Cl₂]⁺.

6.4.2.2 [Fe₂(Me₂-uns-penp)₂Cl₂O](BPh₄)₂ (**11**)

The formation of μ-oxido bridged iron(III) complexes is a well known synthetic problem for the preparation of iron(III) complexes. These reactions were described previously for the iron complexes with the ligands tmpa uns-penp and acetyl-uns-penp.^{91,173,174} Therefore, it was not surprising that we could also prepare and structurally characterize the iron oxido bridged complex with the ligand Me₂-uns-penp. The molecular structure of [Fe₂(Me₂-uns-penp)₂Cl₂O](BPh₄)₂ (**11**) is shown in Figure 6-3. Crystallographic data are presented in tables 6-1 and 6-2.

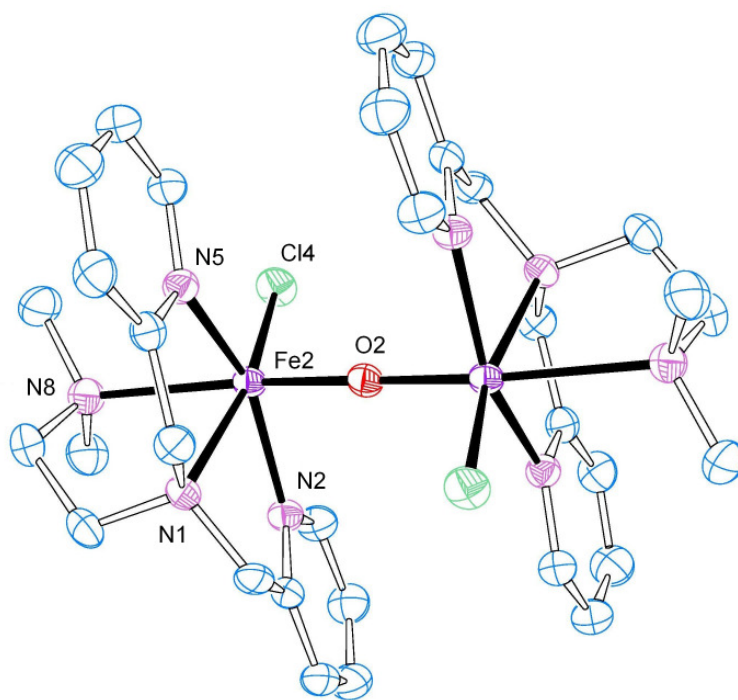


Figure 6-3: Molecular structure of the cation of **11** with hydrogen atoms omitted for clarity. Thermal ellipsoids are shown at 30 % probability levels.

The cation of **11** shows two crystallographically equivalent iron(III) centres coordinated by a CIN₄O donor set in a distorted octahedral geometry. The metal centers are bridged by one oxido group, leading to an intramolecular Fe-Fe distance of 3.585 Å and Fe-O-Fe angle of 180°. These parameters are almost identical to those found for the related uns-penp complex and are typical for such oxido bridged iron(III) centers.¹⁷⁵ As observed previously for the analogous iron uns-penp complex the chloride ions are situated trans to the tertiary amine nitrogen N(1) on each iron center and anti to each other relative to the Fe-O-Fe axis.⁹¹

6.4.2.3 $[Fe(Me_2\text{-uns-penp})Cl(CH_3CN)]BPh_4$ (**12**)

In our efforts to obtain iron "oxygen adduct" complexes we also investigated the reaction of dioxygen with a wide series of iron(II) complexes. During the course of this study we obtained an iron(II) complex with Me₂-uns-penp as a ligand. The molecular structure of the cation of this oxygen sensitive complex is shown in Figure - 6-4. Crystallographic data are presented in tables 6-3 and 6-4.

The iron(II) ion is in a distorted octahedral environment with the tetradentate tripodal Me₂-uns-penp ligand, one acetonitrile molecule and one chloride ion in the coordination sphere. The chloride ion occupies the remaining sixth coordination site

Chapter 6

Table 6-3: structural and refinement data for the compounds **12** - **14**.

	12	13	14
Empirical formula	C ₄₂ H ₄₅ BClFeN ₅	C ₃₂ H ₄₄ Cl ₄ Co ₂ N ₈ O ₈	C ₁₈ H ₂₆ ClCoF ₄ N ₄
Formula weight [g mol ⁻¹]	721.94	928.41	479.62
Crystal system	orthorhombic	monoclinic	monoclinic
Space group	P2(1)2(1)2(1)	P2(1)/c	P2(1)/n
a [Å]	11.9724(10)	9.4443(19)	8.1644(16)
b [Å]	12.5853(11)	32.397(7)	16.963(3)
c [Å]	25.165(2)	13.780(3)	15.962(3)
α [°]	90	90	90
β [°]	90	109.91	95.73(3)
γ [°]	90	90	90
V [Å ³]	3791.8(6)	3964.3(14)	2199.6(8)
Z	4	4	4
D _{calc} [g cm ⁻³]	1.265	1.556	1.448
T [K]	200(2)	193(2)	193(2)
μ(MoKα)[mm ⁻¹]	0.505	1.165	0.946
Crystal size [mm]	0.4 x 0.20 x 0.10	0.16 x 0.28 x 0.052	0.27 x 0.27 x 0.30
F(000)	1520	1912	988
θ range [°]	1.62 - 28.30	2.01 - 23.28	2.72 - 28.10
Index ranges	-15 ≤ h ≤ 15	-9 ≤ h ≤ 9	-10 ≤ h ≤ 10
	-16 ≤ k ≤ 16	-35 ≤ k ≤ 35	-22 ≤ k ≤ 22
	-33 ≤ l ≤ 33	-14 ≤ l ≤ 15	-19 ≤ l ≤ 19
Reflections collected	45759	15396	19242
Unique reflections	9231	5463	5038
R _{int}	0.0599	0.0517	0.0565
Refinement method	Full-matrix least-squares on F ²	Full-matrix least-squares on F ²	Full-matrix least-squares on F ²
Data/constraints/parameters	9231 / 0 / 460	5463 / 0 / 491	5038 / 0 / 359
Godness-of-fit on F ²	0.933	1.077	1.066
Final R indices [I > 2σ(I)]	R ₁ = 0.0349	R ₁ = 0.0462	R ₁ = 0.0517
	wR ₁ = 0.0694	wR ₂ = 0.1297	wR ₂ = 0.1488
R indices (all data)	R ₂ = 0.0685	R ₁ = 0.0582	R ₁ = 0.0725
	wR ₂ = 0.0779	wR ₂ = 0.1369	wR ₂ = 0.1619
Largest diff. peak/hole [e ⁻ Å ⁻³]	0.222 to -0.305	0.723 to -0.846	0.707 to -1.543

to complete the distorted octahedral coordination geometry for the iron(II) ion. Quite surprisingly, one chloride anion and one acetonitrile solvent molecule are coordinated. In our opinion it would have been more likely that either two chloride ions or two acetonitrile ligands were coordinated. Coordination of two triflate ions as co-ligands has been observed previously by Britovsek et al. in [Fe(Me₂-uns-penp)(triflate)₂]. However this complex is much more distorted compared to the ideal octahedron due to the space requirement of the bulky triflate anions.¹⁶⁶

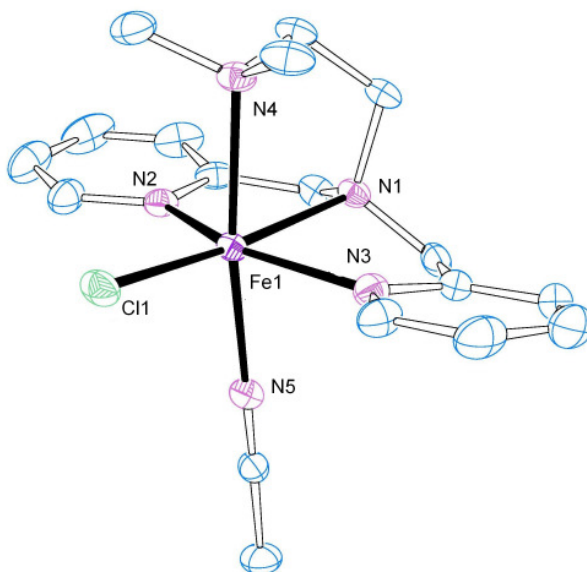


Figure 6-4: Molecular structure of the cation of **12** with hydrogen atoms omitted for clarity. Thermal ellipsoids are shown at 30% probability levels.

6.4.2.4 $[Co(Me_2\text{-uns-penp})Cl]ClO_4$ (**13**)

As expected, the analogous Co(II) complex with the ligand $Me_2\text{-uns-penp}$ is five-fold coordinated and the molecular structure of the cation in $[Co(Me_2\text{-uns-penp})Cl]ClO_4$ (**13**) is presented in Figure 6-5. Crystallographic data are presented in tables 6-3 and 6-4.

The cobalt(II) ion is penta-coordinated by the four nitrogen donors of the $Me_2\text{-uns-penp}$ ligand and one chloride ion. According to the τ -value, the coordination geometry is best described as trigonal bipyramidal ($\tau = 0.867$). The τ -value is a geometric factor introduced into coordination chemistry by Addison et al. and its value can be between 0 (perfect square pyramidal coordination) and 1 (perfect trigonal bipyramidal coordination).¹⁷⁶ The result for the cobalt(II) complex is in contrast to the results for the penta-coordinated copper(II) complex, which can be best described as a square pyramidal coordination environment in its solid state. The lengths of the Co(II)- N_{pyridine} (average = 2.064 Å) bonds are shorter than the Co(II)- N_{amine} (average = 2.162 Å) bonds. In contrast to the copper(II) complex where the two bonds have the same range, the bond Co(1)-N(1) is longer than Co(1)-N(4).

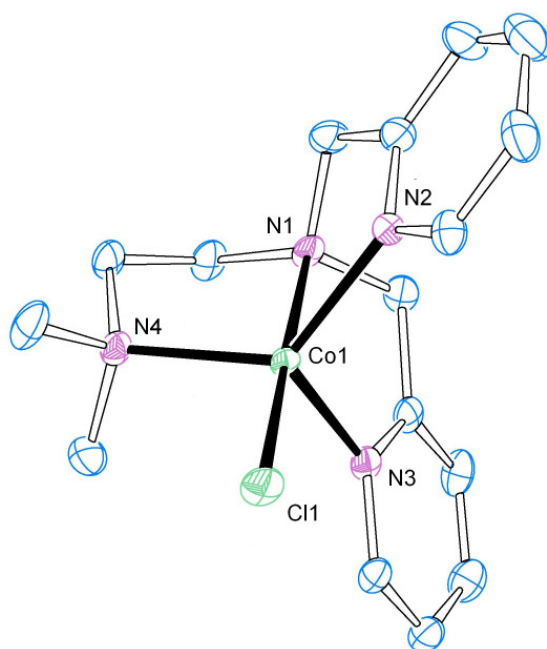


Figure 6-5: Molecular structure of the cation of **13** with hydrogen atoms omitted for clarity. Thermal ellipsoids are shown at 30 % probability levels.

Table 6-4: Selected distances [Å] and angles [°] for the compounds **12** - **14**.

12					
Fe(1)-N(1)	2.2519(18)	N(1)-Fe(1)-N(4)	79.85(6)	N(4)-Fe(1)-Cl(1)	92.70(5)
Fe(1)-N(3)	2.1597(19)	N(3)-Fe(1)-N(4)	94.97(7)	N(2)-Fe(1)-Cl(1)	106.15(6)
Fe(1)-N(4)	2.3116(18)	N(1)-Fe(1)-N(2)	77.28(7)	N(2)-Fe(1)-N(5)	87.47(7)
Fe(1)-N(2)	2.1446(19)	N(3)-Fe(1)-N(2)	151.23(8)	N(3)-Fe(1)-N(5)	84.17(7)
Fe(1)-N(5)	2.228(2)	N(4)-Fe(1)-N(2)	88.34(7)	N(1)-Fe(1)-N(5)	89.82(6)
Fe(1)-Cl(1)	2.3065(7)	N(1)-Fe(1)-Cl(1)	171.79(5)	N(5)-Fe(1)-Cl(1)	97.72(5)
N(1)-Fe(1)-N(2)	98.395(17)	N(5)-Fe(1)-N(4)	169.49(7)	C(1)-N(1)-Fe(1)	108.67(13)
N(1)-Fe(1)-N(3)	75.22(7)	N(3)-Fe(1)-Cl(1)	102.24(6)		
13					
Co(1)-Cl(1)	2.2882(12)	Cl(1)-Co(1)-(N1)	179.00(10)	N(1)-Co(1)-N(3)	78.22(14)
Co(1)-N(1)	2.214(3)	Cl(1)-Co(1)-(N2)	102.34(11)	N(1)-Co(1)-N(4)	81.18(14)
Co(1)-N(2)	2.067(4)	Cl(1)-Co(1)-(N3)	101.39(10)	N(2)-Co(1)-N(3)	113.92(14)
Co(1)-N(3)	2.060(4)	Cl(1)-Co(1)-(N4)	99.82(11)	N(2)-Co(1)-N(4)	126.94(14)
Co(1)-N(4)	2.109(3)	N(1)-Co(1)-N(2)	77.03(15)	N(3)-Co(1)-N(4)	107.89(15)
14					
Co(1)-Cl(1)	2.272(4)	Cl(1)-Co(1)-(N1)	159.4(2)	N(1)-Co(1)-N(3)	80.87(10)
Co(1)-N(1)	2.148(2)	Cl(1)-Co(1)-(N2)	96.9(2)	N(1)-Co(1)-N(4)	79.88(12)
Co(1)-N(2)	2.158(3)	Cl(1)-Co(1)-(N3)	119.4(2)	N(2)-Co(1)-N(3)	96.07(10)
Co(1)-N(3)	2.072(3)	Cl(1)-Co(1)-(N4)	96.5(3)	N(2)-Co(1)-N(4)	143.93(12)
Co(1)-N(4)	2.199(4)	N(1)-Co(1)-N(2)	75.85(10)	N(3)-Co(1)-N(4)	106.02(12)

6.4.3 Me₄-uns-penp

6.4.3.1 [Co(Me₄-uns-penp)Cl]BF₄ (**14**)

Introducing methyl groups into the tmpa ligand (α -position) to provide sterical shielding, had a dramatic effect on the stabilization of copper "dioxygen adduct" complexes.¹⁷⁷ Therefore, a mixed effect, could be expected using this strategy for the Me₂-uns-penp ligand leading to Me₄-uns-penp. With Me₂-uns-penp under comparable reaction conditions a cobalt(II) complex was formed. Thus we, obtained [Co(Me₄-uns-

penp)Cl]BF₄ (**14**) and the molecular structure of its cation is presented in Figure 6-6. Crystallographic data are presented in tables 6-3 and 6-4.

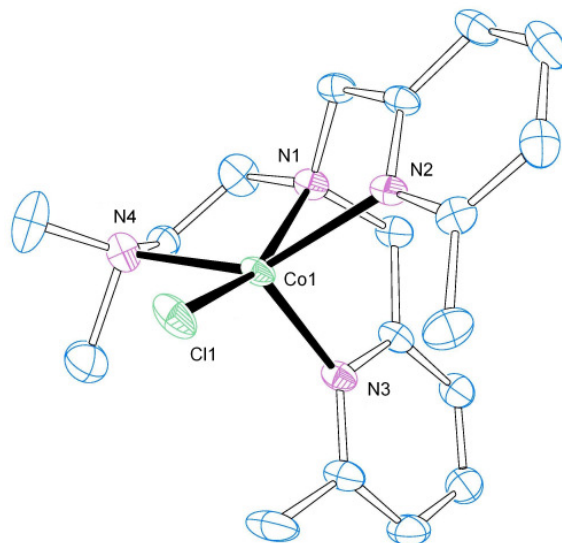


Figure 6-6: Molecular structure of the cation of **14** with hydrogen atoms omitted for clarity. Thermal ellipsoids are shown at 30 % probability levels.

In contrast to the coordination geometry of [Co(Me₂-uns-penp)Cl]⁺ (**13**), the coordination geometry of the complex cation could be best described by using the τ -value as square pyramidal. ($\tau = 0.258$) This fact may be caused by the steric effects of the additional methyl groups.

6.4.4 Acetyl-uns-penp

As described in the introduction, acetyl-uns-penp is an amide which is prepared during the syntheses of uns-penp. We have described the crystal structure of this compound previously and have pointed out that this amide should be an interesting ligand in bioinorganic chemistry.^{86,91} Such compounds are especially interesting in gaining a better understanding of metal peptide binding.¹⁷⁸ Acetyl-uns-penp is quite similar to ligands based on pyridine-2-carboxamide frameworks. Mascharak and co-workers have reported important results of their investigations on metal complexes with PaPy₃H as a ligand (see introduction and Scheme 6-1).^{165,179-186} In contrast and despite the facile synthesis of acetyl-uns-penp, this amide was not been used as a ligand in coordination chemistry prior to our work. However, our statement on the interesting properties of acetyl-uns-penp as a ligand was supported by important results reported by Que and co-workers using L (Scheme 6-1) as a ligand, a slightly modified derivative of acetyl-uns-penp.¹⁶³ It forms a highly reactive diiron(IV) species which has a high potential to attack aliphatic C-H-bonds. This species was directly

formed by electrochemical oxidation from an oxido-bridged diiron(III) precursor in solution.

6.4.4.1 $[Fe_2(\text{acetyl-uns-penp})_2Cl_2(CH_3OH)_2](ClO_4)_2 \times 2 CH_3OH$ (**15**)

Reacting iron(II) chloride in an inert atmosphere with acetyl-uns-penp led to the formation of a dimeric complex. The molecular structure of $[Fe_2(\text{acetyl-uns-penp})_2Cl_2(CH_3OH)_2](ClO_4)_2 \times 2 CH_3OH$ (**15**) is presented in Figure 6-7. Crystallographic data are presented in tables 6-5 and 6-6.

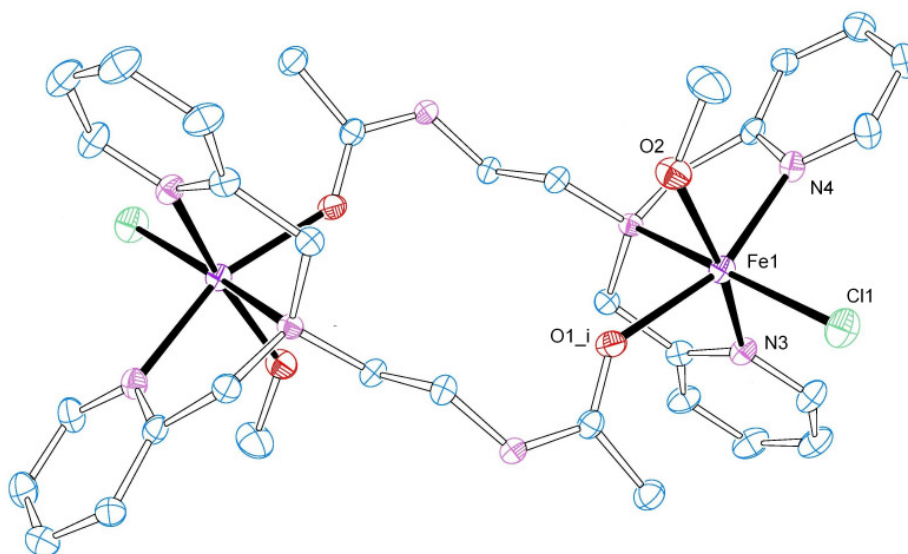


Figure 6-7: Molecular structure of the cation of **15** with hydrogen atoms omitted for clarity. Thermal ellipsoids are shown at 30 % probability levels.

The iron(II) centers are coordinated by the two pyridyl nitrogen atoms and the tertiary amine nitrogen atom of the acetyl-uns-penp ligand, by a chloride ion and by the oxygen donor atom of a methanol molecule as a co-ligand. The two metal centers are linked by the two coordinating amide oxygen atoms (O(1) and O(1)#) of the amide ligand arms, leading to an intramolecular Fe-Fe distance of 7.833 Å. The iron centers are coordinated in a distorted octahedral geometry, as represented by the trans ligand angles 168.86° for Cl(1)-Fe(1)-N(1) and 159.83° for N(4)-Fe(1)-O(1)#. Furthermore the angle for N(1)-Fe(1)-N(3) is 74.86°, which is notably smaller than 90°.

6.4.4.2 $[Co_2(\text{acetyl-uns-penp})Cl_2](BF_4)_2 \times C_3H_6O$ (**16**)

Similar to the iron(II) complex, the binuclear $[Co_2(\text{acetyl-uns-penp})Cl_2](BF_4)_2 \times C_3H_6O$ (**16**) was obtained when cobalt(II) chloride was reacted with acetyl-uns-penp. The molecular structure of the cation of this compound is shown in Figure 6-8. Crystallographic data are presented in tables 6-5 and 6-6.

Chapter 6

Table 6-5: Structural and refinement data for the compounds **15** - **17**.

	15	16	17
Empirical formula	C ₃₆ H ₅₆ N ₈ O ₁₄ Cl ₄ Fe	C ₃₅ H ₄₆ B ₂ C ₁₂ Co ₂ F ₈ N ₈ O ₃	C ₃₆ H ₄₈ Cl ₂ F ₆ N ₈ O ₁₈ S ₂ Fe ₂
Formula weight [g mol ⁻¹]	1078.38	989.18	1241.54
Crystal system	monoclinic	monoclinic	monoclinic
Space group	P2(1)/c	Cc	P2(1)/c
a [Å]	9.8951(8)	26.650(5)	16.060(3)
b [Å]	15.9255(14)	9.1963(18)	17.413(4)
c [Å]	15.6861(13)	17.357(4)	9.2789(19)
α [°]	90	90	90
β [°]	103.063(10)	94.15	102.05(3)
γ [°]	90	90	90
V [Å ³]	2407.9(4)	4242.7(15)	2537.7(9)
Z	4	4	4
D _{calc} [g cm ⁻³]	1.487	1.549	1.625
T [K]	193(2)	193(2)	193(2)
μ(MoKα) [mm ⁻¹]	0.893	0.989	0.859
Crystal size [mm]	0.30 x 0.20 x 0.10	0.38 x 0.15 x 0.08	0.60 x 0.15 x 0.15
F(000)	1120	2024	1272
θ range [°]	2.57 - 28.13	2.90 - 28.15	2.53 - 26.02
Index ranges	-12 ≤ h ≤ 13 -12 ≤ k ≤ 20 -20 ≤ l ≤ 20	-35 ≤ h ≤ 34 -12 ≤ k ≤ 12 -22 ≤ l ≤ 22	-18 ≤ h ≤ 19 -20 ≤ k ≤ 21 -11 ≤ l ≤ 11
Reflections collected	13527	18429	18032
Unique reflections	5490	9611	4927
R _{int}	0.0605	0.0577	0.0925
Refinement method	Full-matrix least-squares on F ²	Full-matrix least-squares on F ²	Full-matrix least-squares on F ²
Data/constraints/parameters	5490/0/301	9611 / 2 / 563	4927 / 0 / 337
Godness-of-fit on F ²	0.851	1.005	1.030
Final R indices [I > 2σ(I)]	R ₁ = 0.0453 wR ₂ = 0.0942	R ₁ = 0.0480 wR ₂ = 0.1333	R ₁ = 0.0856 wR ₂ = 0.2381
R indices (all data)	R ₁ = 0.0976 wR ₂ = 0.1070	R ₁ = 0.0788 wR ₂ = 0.1509	R ₁ = 0.1320 wR ₂ = 0.2716
Largest diff. peak/hole [e ⁻ Å ⁻³]	0.478 to -0.432	0.603 to -0.796	0.714 to -0.796

Similar to the iron(II) complexes **15** and **17**, the cobalt(II) centers are linked by the amide oxygen atoms of the acetyl-uns-penp molecules. However, as expected in contrast to the octahedral iron complexes, the cobalt(II) ions in **16** are only coordinated by five donor atoms. Each cobalt(II) ion is coordinated by the nitrogen donors of one acetyl-uns-penp ligand molecule, a chloride ion and the oxygen atom of the linking amide function. The coordination sphere of the cobalt(II) ion is best described as trigonal bipyramidal using the τ -value. ($\tau = 0.904$) The intramolecular Co-Co distance is 7.427 Å. Thus, it is slightly shorter than the intramolecular Fe-Fe distances in the complexes **15** and **17**. The cobalt centers should be crystallographically identical. However, the structure had to be solved in space group Cc, caused by the highly mobile acetone molecules in the unit cell.

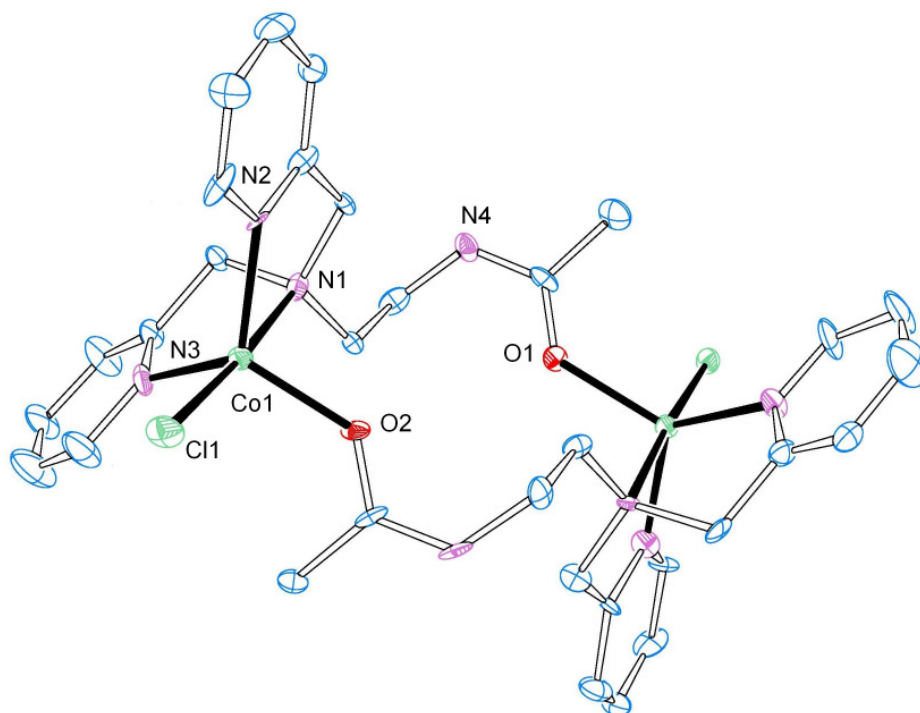


Figure 6-8: Molecular structure of the cation of **16** with hydrogen atoms omitted for clarity. Thermal ellipsoids are shown at 30 % probability levels.

Table 6-6: Selected distances [Å] and angles [°] for the compounds **15** -**17**.

15					
Fe(1)-O(1)#1	2.162(2)	O(1)#1-Fe(1)-N(1)	86.66(8)	N(1)-Fe(1)-N(3)	74.86(9)
Fe(1)-O(2)	2.131(3)	O(1)#1-Fe(1)-N(3)	95.93(10)	N(1)-Fe(1)-N(4)	77.38(9)
Fe(1)-N(1)	2.292(2)	O(1)#1-Fe(1)-N(4)	159.83(9)	N(1)-Fe(1)-Cl(1)	168.86(7)
Fe(1)-N(3)	2.181(3)	O(1)#1-Fe(1)-Cl(1)	100.01(6)	N(3)-Fe(1)-N(4)	91.76(10)
Fe(1)-N(4)	2.170(3)	O(2)-Fe(1)-N(1)	92.87(10)	O(2)-Fe(1)-N(4)	87.96(11)
Fe(1)-Cl(1)	2.3380(9)	O(2)-Fe(1)-N(3)	167.46(10)	N(1)-Fe(1)-Cl(1)	168.86(7)
Fe(1)...Fe(1)#1	7.833	O(2)-Fe(1)-N(4)	87.96(11)	N(3)-Fe(1)-Cl(1)	95.45(7)
O(1)#1-Fe(1)-O(2)	80.51(10)	O(2)-Fe(1)-Cl(1)	97.00(8)	N(4)-Fe(1)-Cl(1)	97.78(7)
16					
Co(1)-Cl(1)	2.330(3)	Cl(1)-Co(1)-O(2)	97.2(2)	O(2)-Co(1)-N(3)	121.3(4)
Co(1)-O(2)	1.940(8)	Cl(1)-Co(1)-N(1)	175.6(3)	N(1)-Co(1)-N(2)	78.3(4)
Co(1)-N(1)	2.243(10)	Cl(1)-Co(1)-N(2)	99.8(3)	N(1)-Co(1)-N(3)	77.0(4)
Co(1)-N(2)	2.083(8)	Cl(1)-Co(1)-N(3)	100.6(3)	N(2)-Co(1)-N(3)	118.4(4)
Co(1)-N(3)	2.069(10)	O(2)-Co(1)-N(1)	87.2(3)		
Co(1)...Co(2)	7.427	O(2)-Co(1)-N(2)	112.8(3)		
17					
Fe(1)-O(1)	2.053(5)	O(1)#1-Fe(1)-O(6)	87.1(2)	O(6)-Fe(1)-N(2)	93.9(2)
Fe(1)-O(3)	2.138(5)	O(1)#1-Fe(1)-N(2)	92.22(18)	O(6)-Fe(1)-N(3)	171.4(2)
Fe(1)-O(6)	2.064(5)	O(1)#1-Fe(1)-N(3)	97.69(19)	O(6)-Fe(1)-N(4)	90.8(3)
Fe(1)-N(2)	2.252(5)	O(1)#1-Fe(1)-N(4)	169.3(2)	N(2)-Fe(1)-N(3)	78.9(2)
Fe(1)-N(3)	2.204(6)	O(3)-Fe(1)-O(6)	93.0(2)	N(2)-Fe(1)-N(4)	77.4(2)
Fe(1)-N(4)	2.179(6)	O(3)-Fe(1)-N(2)	168.3(2)	N(3)-Fe(1)-N(4)	83.1(2)
Fe(1)...Fe(1)#1	7.602	O(3)-Fe(1)-N(3)	93.4(2)		
O(1)#1-Fe(1)-O(3)	97.5(2)	O(3)-Fe(1)-N(4)	93.1(2)		

6.4.4.3 $[Fe_2(\text{acetyl-uns-penp})_2(\text{triflate})_2(\text{CH}_3\text{OH})_2](\text{ClO}_4)_2$ (**17**)

Trying to avoid strong coordinating co-ligands such as chloride we also reacted acetyl-uns-penp with an iron(II) triflate salt. Again, we obtained a binuclear iron(II) complex. The molecular structure of the cation of $[Fe_2(\text{acetyl-uns-}$

penp)₂(triflate)₂(CH₃OH)₂](ClO₄)₂ (**17**) is shown in Figure 6-9. Crystallographic data are presented in tables 6-5 and 6-6.

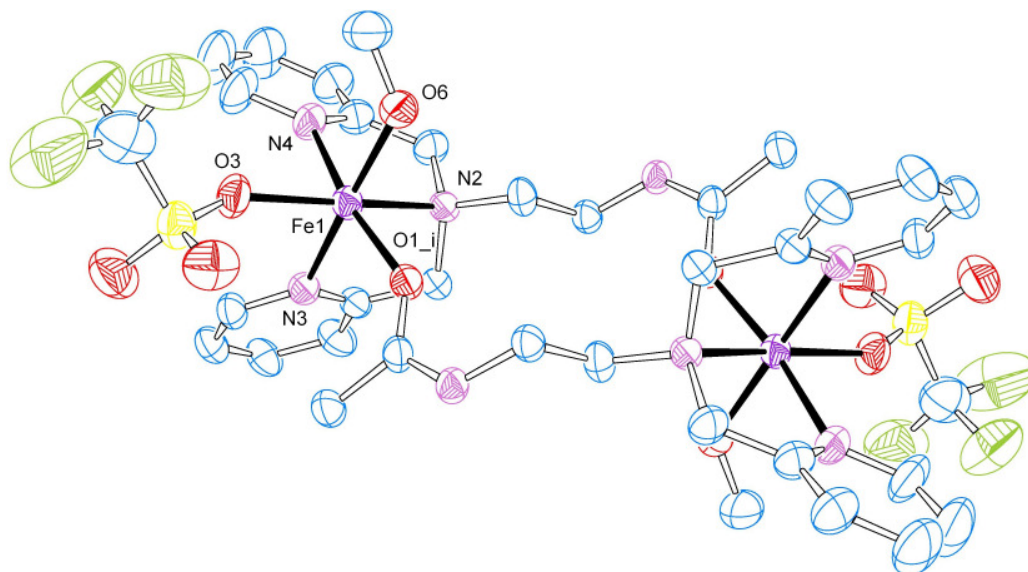


Figure 6-9: Molecular structure of the cation of **17** with hydrogen atoms omitted for clarity. Thermal ellipsoids are shown at 30 % probability levels.

Complex **17** is quite similar to **15**. The main difference is the coordinated chloride ions in **15** are replaced with coordinating triflate ions in **17**. In both compounds, the metal centers are linked by the amide oxygen atoms of the acetyl-uns-penp ligand. The internal Fe-Fe distance (7.833 Å) in **17** is slightly larger than in **15** (7.602 Å). The iron(II) centers are coordinated by a N3O3 donor set. The nitrogen donors are provided by the acetyl-uns-penp ligand. The oxygen donors are provided by coordinating methanol, triflate and the amide oxygen of the linking acetyl-uns-penp ligand. The bond angles show a distorted octahedral coordination geometry. The trans angles are 169.26° for O(1#)-Fe(1)-N(4) 168.30° for O(3)-Fe(1)-N(2) and 171.39° for the O(6)-Fe(1)-N(3). The angle N(2)-Fe(1)-N(4) is 77.39° which is noticeably smaller than 90°. Like in case of **15** the Fe-N_{Py}-bonds (average 2.192 Å) are shorter than the Fe_{amine}-bond (2.252 Å).

6.4.4.4 [Fe₂(acetyl-uns-penp)₂OH](ClO₄)₂ × 3 C₃H₆O (**18**)

Due to the fact that the oxido-bridged iron(III) dimer with acetyl-uns-penp/L is capable (once it is electrochemically transferred into the iron(IV) state) to selectively oxidize C-H bonds, we were interested to investigate the reaction of the iron(II) complex with dioxygen. Therefore, we reacted acetyl-uns-penp, FeCl₂, NaH and NaClO₄ in anhydrous acetone under inert conditions in an argon-filled glove box. We expected to obtain a mononuclear iron(II) acetyl-uns-penp complex with a deprotonated

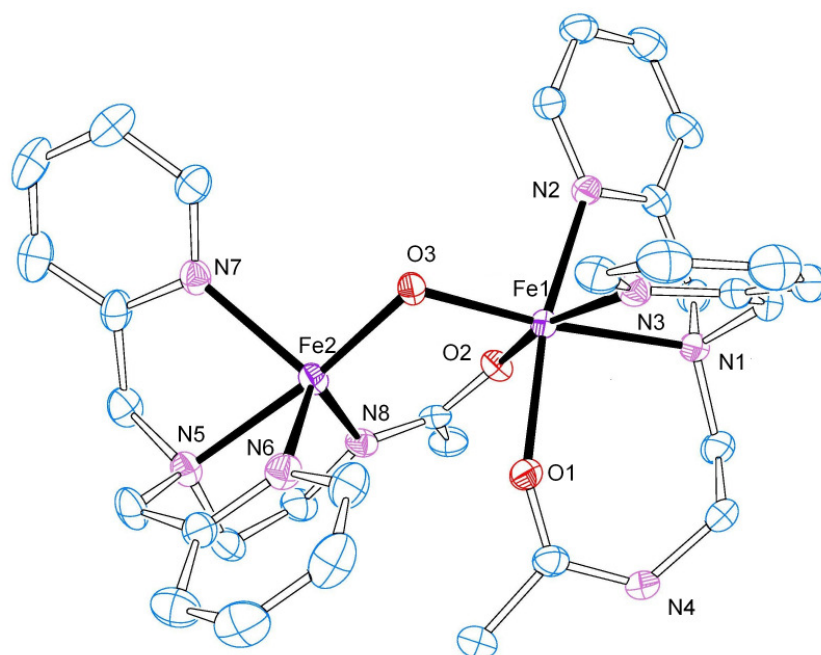


Figure 6-10: Molecular structure of the cation of **18** with hydrogen atoms omitted for clarity. Thermal ellipsoids are shown at 30 % probability levels.

Table 6-7: Structural and refinement data for the compounds **18** - **20**.

	18	19	20
Empirical formula	C ₃₉ H ₅₄ Cl ₂ Fe ₂ N ₈ O ₁₆	C ₄₀ H ₅₇ Cl ₄ Fe ₂ N ₁₁ O ₂₁	C ₁₆ H ₂₃ Cl ₂ CoN ₄ O ₃
Formula weight [g mol ⁻¹]	1069.55	1281.47	449.21
Crystal system	triclinic	triclinic	orthorhombic
Space group	P -1 (2)	P-1	P 2(1)2(1)2(1)
a [Å]	10.610(2)	11.344(2)	8.4839(17)
b [Å]	11.876(2)	12.732(3)	13.984(3)
c [Å]	20.374(4)	12.797(3)	15.971(3)
α [°]	78.68(3)	116.96(3)	90
β [°]	82.79(3)	107.40(3)	90
γ [°]	79.05(3)	96.86(3)	90
V [Å ³]	2461.1(9)	1499.6(5)	1894.8(7)
Z	2	1	4
D _{calc} [g cm ⁻³]	1.443	1.419	1.575
T [K]	193(2)	193(2)	193(2)
μ(MoKα)[mm ⁻¹]	0.768	0.739	1.212
Crystal size [mm]	0.48 x 0.12 x 0.08	0.48 x 0.60 x 0.76	0.48 x 0.24 x 0.2
F(000)	1116	662	928
θ range [°]	2.20 - 25.95	2.57 - 28.17	2.94 - 28.10
	-13 ≤ h ≤ 12	-15 ≤ h ≤ 14	-11 ≤ h ≤ 11
Index ranges	-14 ≤ k ≤ 14	-16 ≤ k ≤ 16	-18 ≤ k ≤ 18
	-24 ≤ l ≤ 24	-16 ≤ l ≤ 16	-21 ≤ l ≤ 19
Reflections collected	18120	13968	17205
Unique reflections	8888	6711	4572
R _{int}	0.0822	0.0573	0.0705
Refinement method	Full-matrix least-squares on F ²	Full-matrix least-squares on F ²	Full-matrix least-squares on F ²
Data/constraints/parameters	8888 / 30 / 655	6711 / 0 / 404	4572 / 0 / 252
Godness-of-fit on F ²	0.802	0.949	1.021
Final R indices [I > 2σ(I)]	R ₁ = 0.0506 wR ₂ = 0.1030	R ₁ = 0.0643 wR ₂ = 0.1860	R ₁ = 0.0383 wR ₂ = 0.1022
R indices (all data)	R ₁ = 0.1164 wR ₂ = 0.1270	R ₁ = 0.0993 wR ₂ = 0.2111	R ₁ = 0.0447 wR ₂ = 0.1092
Largest diff. peak/hole [e. Å ⁻³]	0.374 to -0.342	1.482 to -1.322	0.764 to -0.839

acetyl-uns-penp as the main ligand. To our great surprise, we obtained a hydroxido bridged iron dimer. Crystallographic data are presented in tables 6-7 and 6-8. The molecular structure of the cation of this complex is presented in Figure 6-10. Its positive charge is balanced by two perchlorate ions.

The cation consists of two non-identical iron(II) centers with different coordination numbers. The iron cations are bridged by one deprotonated amide function of one acetyl-uns-penp ligand and a linking hydroxido ligand. The distances Fe(1)-O(3) (1.986(3) Å) and Fe(2)-O(3) (1.958(3) Å) and the angle Fe(1)-O(3)-Fe(2) (112.40(16)°) are comparable for related hydroxido-bridged diiron(II) complexes previously described in the literature.¹⁸⁷⁻¹⁹¹ One iron(II) center is coordinated in a distorted octahedral geometry, with the N_{amine}, N_{pyridine} and amide O donors of a acetyl-uns-penp ligand with protonated amide function. The other coordination sites are occupied by the linking hydroxide ion and the linking amide function of the other acetyl-uns-penp molecule. The amide function of this molecule is deprotonated and shows an unusual pentadentate binding mode with a carboxamido NCO bridging group which involves the delocalisation of the π -bond (C(31)-O(2) = 1.279 Å, C(31)-N(8) = 1.310 Å). This coordination mode for acetyl-uns-penp had been reported before by Xu et al., but in a different iron(III) complex.⁹¹ The deprotonated acetyl-uns-penp molecule coordinates the second iron(II) center in a trigonal bipyramidal geometry ($\tau = 0.872$). The intramolecular Fe-Fe-Distance is 3.277 Å, comparable to μ -hydroxido- μ -caboxylato-linked iron(II) complexes described in literature.¹⁸⁹⁻¹⁹¹

Complex **18** is sensitive towards dioxygen. However, so far we have not analysed the reaction and could not isolate and characterize either reaction intermediates or reaction products. Nevertheless, as described above, complex **18** was not expected as a product in our syntheses. Especially, we do not understand where the hydroxido ligand comes from. We had worked under inert conditions and had excluded water. Therefore, the formation of complex **18** should not taken place. Currently, we suspect water in one of our starting materials or solvents. However, all chemicals have been thoroughly dried prior to use. Most interestingly we could repeat the synthesis and obtained the same complex cation from the reaction of acetyl-uns-penp, [Fe(CH₃CN)₂(triflate)₂] and NaH in acetone. We detected water in the crystal structure which supports our assumption of the presence of water in one of our starting materials. (see compound **22** in Chapter 7).

6.4.4.5 $[Fe_2(\text{acetyl-uns-penp})_2(\text{DMF})_2O](\text{ClO}_4)_2 \times \text{CH}_3\text{CN}$ (**19**)

Furthermore, we tried to synthesize the iron(III) acetyl-uns-penp complex without the oxido bridge. Therefore, we reacted an iron(III) salt with acetyl-uns-penp under inert conditions. Again, we were surprised. Despite working under inert conditions in a glove box we obtained an oxido-bridged dimer. The cation of this complex is shown in Figure 6-11. Crystallographic data are presented in tables 6-7 and 6-8.

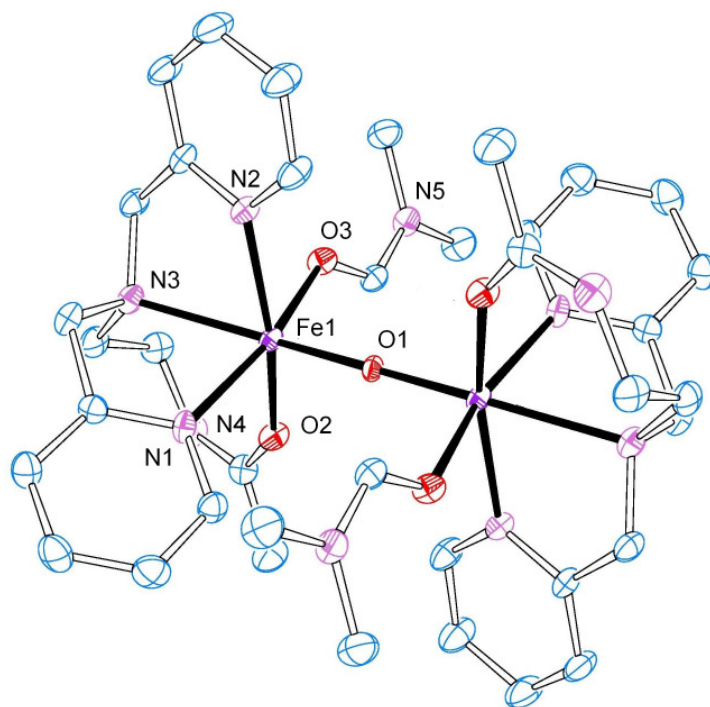


Figure 6-11: Molecular structure of the cation of **19** with hydrogen atoms omitted for clarity. Thermal ellipsoids are shown at 30 % probability levels.

19 consists of two crystallographically identical iron(III) centers which are mono bridged by one oxido group. This group is located in a symmetry centre. One half of the complex cation is generated by inversion. The intramolecular Fe-Fe distance is 3.593 Å and the Fe-O-Fe angle is 180°. Each iron center is coordinated in a distorted octahedral geometry, by the two pyridyl nitrogen, the amine nitrogen and the amide oxygen atom of the acetyl-uns-penp ligand. The sixth coordination site is occupied by the amide oxygen atom of dimethylformamide. The negative charge of the oxido group leads to a significant shorter Fe(1)-O(1) bond (1.763 Å) which is caused by the trans effect (a weakening of the opposite Fe(1)-N(3) bond (2.304 Å)). All cis angles around O(1) are larger than the ideal 90°.

At the moment we do not understand how water was introduced into our mixture of reagents. Work is in progress to clarify this. However, we did not find the solution for

Chapter 6

this problem so far. The obtained molecular structure is quite interesting, because here the amide ligand arms are not deprotonated and instead two DMF molecules, thus an external amide ligand is coordinated. Comparison of the molecular structure of **19** to the oxido-bridged iron(III) complexes with acetyl-uns-penp reported by Xu et. al. shows that the distance between the two iron(III) (3,592 Å) cations are in the same range as found for the oxido-bridged complex with tetrachlorocatechol as a co-ligand (3.586 Å).⁹¹ As expected, the distance is much larger compared to the triply bridged oxido-acetyl-uns-penp complexes described by us as well as by Que and co-workers where an extremely short distance of approximately 3 Å was observed.^{91,163}

Table 6-8: Selected distances [Å] and angles [°] for the compounds **18** - **20**.

18					
Fe(1)-O(1)	2.158(3)	O(1)-Fe(1)-O(3)	91.20(13)	N(2)-Fe(1)-N(3)	91.82(14)
Fe(1)-O(2)	2.099(3)	O(1)-Fe(1)-N(1)	93.49(13)	O(3)-Fe(2)-N(5)	170.47(16)
Fe(1)-O(3)	1.986(3)	O(1)-Fe(1)-N(2)	166.82(15)	O(3)-Fe(2)-N(6)	100.03(15)
Fe(1)-N(1)	2.254(4)	O(1)-Fe(1)-N(3)	90.50(13)	O(3)-Fe(2)-N(7)	98.30(14)
Fe(1)-N(2)	2.206(4)	O(2)-Fe(1)-O(3)	95.53(14)	O(3)-Fe(2)-N(8)	111.33(16)
Fe(1)-N(3)	2.185(4)	O(2)-Fe(1)-N(1)	88.85(14)	N(5)-Fe(2)-N(6)	75.86(15)
Fe(2)-O(3)	1.958(3)	O(2)-Fe(1)-N(2)	87.12(14)	N(5)-Fe(2)-N(7)	75.22(15)
Fe(2)-N(5)	2.269(4)	O(2)-Fe(1)-N(3)	165.88(15)	N(5)-Fe(2)-N(8)	78.09(16)
Fe(2)-N(6)	2.152(4)	O(3)-Fe(1)-N(1)	173.73(13)	N(6)-Fe(2)-N(7)	108.01(17)
Fe(2)-N(7)	2.173(4)	O(3)-Fe(1)-N(2)	101.28(15)	N(6)-Fe(2)-N(8)	118.15(16)
Fe(2)-N(8)	2.059(4)	O(3)-Fe(1)-N(3)	98.49(16)	N(7)-Fe(2)-N(8)	117.79(16)
Fe(1)...Fe(2)	3.277	N(1)-Fe(1)-N(2)	74.39(14)	Fe(1)-O(3)-Fe(2)	112.40(16)
O(1)-Fe(1)-O(2)	87.47(13)	N(1)-Fe(1)-N(3)	77.32(16)		
19					
Fe(1)-O(1)	1.7963(13)	O(1)-Fe(1)-O(3)	99.46(10)	O(3)-Fe(1)-N(1)	164.57(13)
Fe(1)-O(2)	2.030(3)	O(1)-Fe(1)-N(1)	95.29(10)	O(3)-Fe(1)-N(2)	80.95(13)
Fe(1)-O(3)	2.048(3)	O(1)-Fe(1)-N(2)	98.17(10)	O(3)-Fe(1)-N(3)	91.04(14)
Fe(1)-N(1)	2.116(4)	O(1)-Fe(1)-N(3)	165.41(10)	N(1)-Fe(1)-N(2)	101.49(14)
Fe(1)-N(2)	2.146(3)	O(2)-Fe(1)-O(3)	87.47(13)	N(1)-Fe(1)-N(3)	75.32(14)
Fe(1)-N(3)	2.304(4)	O(2)-Fe(1)-N(1)	85.94(14)	N(2)-Fe(1)-N(3)	73.36(14)
O(1)-Fe(1)#1	1.7963(13)	O(2)-Fe(1)-N(2)	161.25(13)	Fe(1)#1-O(1)-Fe(1)	180.00(4)
O(1)-Fe(1)-O(2)	98.25(9)	O(2)-Fe(1)-N(3)	92.27(13)		
20					
Co(1)-Cl(1)	2.2729(11)	Cl(1)-Co(1)-N(1)	92.80(10)	O(1)-Co(1)-N(4)	92.78(13)
Co(1)-O(1)	1.911(3)	Cl(1)-Co(1)-N(2)	90.15(9)	N(1)-Co(1)-N(2)	83.34(13)
Co(1)-N(1)	1.928(3)	Cl(1)-Co(1)-N(3)	89.11(10)	N(1)-Co(1)-N(3)	85.90(13)
Co(1)-N(2)	1.926(3)	Cl(1)-Co(1)-N(4)	175.10(10)	N(1)-Co(1)-N(4)	86.74(13)
Co(1)-N(3)	1.926(3)	O(1)-Co(1)-N(1)	175.07(13)	N(2)-Co(1)-N(3)	169.16(13)
Co(1)-N(4)	1.949(3)	O(1)-Co(1)-N(2)	91.81(12)	N(2)-Co(1)-N(4)	94.64(13)
Cl(1)-Co(1)-O(1)	88.09(10)	O(1)-Co(1)-N(3)	98.97(13)	N(3)-Co(1)-N(4)	85.99(14)

6.4.4.6 [Co(acetyl-uns-penp)Cl(H₂O)]Cl x H₂O (**20**)

When a cobalt(II) chloride complex with acetyl-uns-penp was reacted together with hydrogen peroxide at low temperatures, no "oxygen adduct" complex could be isolated. Instead at higher temperature a Co(III) complex with deprotonated acetyl-uns-penp was obtained. The molecular structure of the cation of this complex is presented in Figure 6-12. Crystallographic data are presented in tables 6-7 and 6-8.

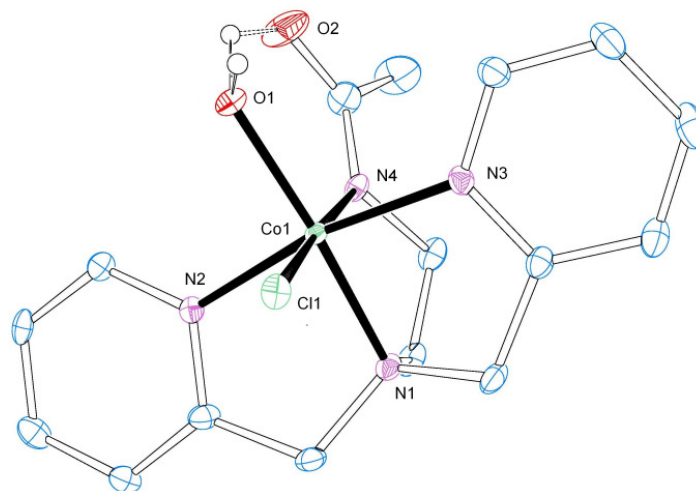


Figure 6-12: Molecular structure of **20** with hydrogen atoms omitted for clarity, except the hydrogen atoms of the coordinated water molecule. Thermal ellipsoids are shown at 30 % probability levels.

The cobalt(III) ion is coordinated in an octahedral geometry by the four nitrogen donor atoms of the acetyl-uns-penp molecule, a chloride ion and a water molecule. The bond lengths and angles demonstrate that the octahedral coordination geometry of **20** is only weakly distorted. It is interesting to note that deprotonation of the acetyl-uns-penp has occurred during the oxidation and that a water molecule instead of a chloride ion is coordinated. Both findings might be a consequence of the hydrogen bonding between the coordinated water molecule and the oxygen atom of the amide group.

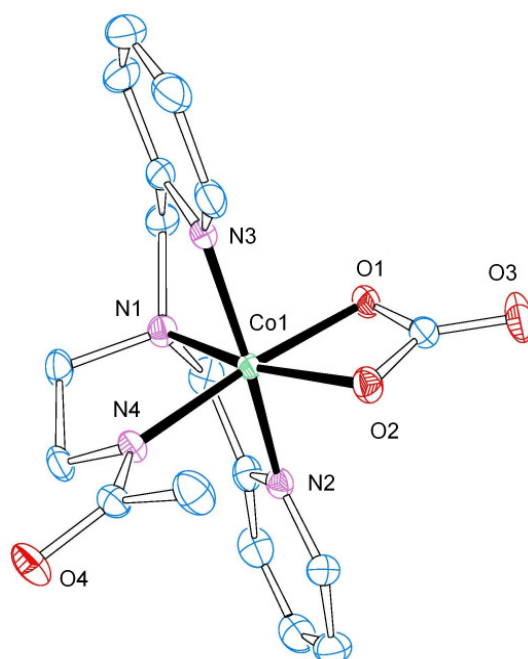
6.4.4.7 $[Co(\text{acetyl-uns-penp})CO_3]$ (**21**)

It is well known that binuclear cobalt peroxido complexes can form in basic aqueous solutions when oxidized in air.¹⁵ Therefore, we also reacted a basic solution of cobalt(II) chloride and acetyl-uns-penp with air. In contrast to our expectations the mononuclear Co(III) carbonate complex $[Co(\text{acetyl-uns-penp})CO_3]$ was obtained. The molecular structure of this complex is presented in Figure 6-13. Crystallographic data are presented in tables 6-9 and 6-10.

The charge of the metal ion is compensated by the carbonate ion and the deprotonated amide function of acetyl-uns-penp. The cobalt(III) ion is coordinated in a distorted octahedral geometry by four nitrogen donor atoms of acetyl-uns-penp and by two oxygen donors of the carbonate ion. Chelated carbonato metal complexes have been well known for a long time in literature,¹⁹² but these species are still rare. Some cobalt carbonato complexes with tripodal ligands based on tmpa were published by Blackman et al. in the past.^{171,193,194}

Table 6-9: Structural and refinement data for the compound **21**.

21	
Empirical formula	C ₁₇ H ₂₅ CoN ₄ O ₇
Formula weight [g mol ⁻¹]	456.34
Crystal system	monoclinic
Space group	P2(1)/n
a [Å]	8.2982(17)
b [Å]	14.207(3)
c [Å]	16.786(3)
α [°]	90
β [°]	100.38(3)
γ [°]	90
V [Å ³]	1946.6(7)
Z	4
D _{calc} [g cm ⁻³]	1.557
T [K]	193(2)
μ(MoKα) [mm ⁻¹]	0.930
Crystal size [mm]	0.84 x 0.56 x 0.32
F(000)	952
θ range [°]	2.88 - 28.09
Index ranges	-10 ≤ h ≤ 10 -18 ≤ k ≤ 18 -21 ≤ l ≤ 22
Reflections collected	16914
Unique reflections	4522
R _{int}	0.0720
Refinement method	Full-matrix least-squares on F ²
Data/constraints/parameters	4522 / 0 / 361
Godness-of-fit on F ²	1.053
Final R indices [I > 2σ(I)]	R ₁ = 0.0375 wR ₂ = 0.1023
R indices (all data)	R ₁ = 0.0433 wR ₂ = 0.1112
Largest diff. peak/hole [e. Å ⁻³]	0.611 to -0.504

**Figure 6-13:** Molecular structure of **21** with hydrogen atoms omitted for clarity. Thermal ellipsoids are shown at 30 % probability levels.

Chapter 6

Table 6-10: Selected distances (Å) and angles (°) for the compound **21**

21					
Co(1)-O(1)	1.9033(12)	O(1)-Co(1)-N(1)	96.51(7)	O(2)-Co(1)-N(4)	107.37(6)
Co(1)-O(2)	1.9111(14)	O(1)-Co(1)-N(2)	89.38(6)	N(1)-Co(1)-N(2)	85.49(7)
Co(1)-N(1)	1.9313(18)	O(1)-Co(1)-N(3)	90.29(6)	N(1)-Co(1)-N(3)	84.64(7)
Co(1)-N(2)	1.9123(15)	O(1)-Co(1)-N(4)	174.73(6)	N(1)-Co(1)-N(4)	87.41(7)
Co(1)-N(3)	1.9229(15)	O(2)-Co(1)-N(1)	165.17(6)	N(2)-Co(1)-N(3)	170.02(7)
Co(1)-N(4)	1.9449(15)	O(2)-Co(1)-N(2)	93.88(7)	N(2)-Co(1)-N(4)	87.41(6)
O(1)-Co(1)-O(2)	68.67(6)	O(2)-Co(1)-N(3)	95.30(7)	N(3)-Co(1)-N(4)	93.60(6)

The bond lengths Co(1)-O(1) (1.9033 Å) and Co(1)-O(2) (1.9111) are in the same range as reported for the cobalt(III) uns-penp carbonato complex.¹⁷¹ Also, the angle O(1)-Co(1)-O(2) (68.68°) is significantly smaller than the angle N(1)-Co(1)-N(4) (87.42°) in trans position. All bond lengths and angles are very close to the reported structure of the cobalt(III) carbonato complex with the ligand uns-penp.¹⁷¹

6.5 Conclusion

This work, together with previous investigations, has shown that the ligand uns-penp and its derivatives are interesting ligands in the coordination chemistry/ bioinorganic chemistry of iron and cobalt complexes. While uns-penp and its methylated analogues are similar to other tripodal tetradentate amines such as tmpa, the acetyl-uns-penp derivative is a very interesting amide ligand. From our findings and recent results by the Que group we presume that especially this ligand is a promising candidate for complexes that will be involved in selective oxidation reactions of organic substrates. However, as our results for the coordination chemistry of the acetyl-uns-penp ligand show we have no full understanding of its complexes so far. Despite these problems our crystallographic characterization of the iron(II) acetyl-uns-penp complex **18** demonstrates that it should be possible to use such compounds to activate and transfer dioxygen.

6.6 Supplementary Material

CCDC Nos. 763298 (**9**), 763302 (**10**), 763291 (**11**), 763303 (**12**), 763299 (**13**), 763297 (**14**), 763292 (**15**), 763296 (**16**), 763294 (**17**), 763295 (**18**), 763295 (**19**), 763302 (**20**) and 763300 (**21**) contain the supplementary data for this paper. These data can be obtained free of charge from The Cambridge Crystallographic Data Centre via www.ccdc.cam.ac.uk/data_request/cif [or on application to CCDC, 12 Union Road, Cambridge CB2 1EZ, UK; fax: int. code +44(1223)336 033; e-mail: deposit@ccdc.cam.ac.uk].

7 Unpublished Results related to Chapter 6

7.1 Experimental

7.1.1 Reagents and Materials

All reagents and solvents were used as obtained without any further purification. Solvents for oxygen sensitive materials were obtained commercially from Acros and distilled in argon atmosphere before further usage. All handling of the oxygen sensitive compounds and material was carried out in a glove box (M. Braun, Germany, O₂ < 0.1 ppm) within an argon atmosphere.

7.1.2 Physical Measurements

Single crystal X-Ray diffraction studies of the substances **22** and **23** were performed with a STOE IPDS-diffractometer equipped with a low temperature system (Karlsruher Glastechnisches Werk), a graphite monochromator and IP detector system. Mo-K_α radiation ($\lambda = 0.71069 \text{ \AA}$) was used. The frames were integrated into the STOE software package. No absorption corrections were applied.

ESI-MS studies were performed with a Bruker-Daltronics ESI-HRMS Micro-TOF in the working group of Professor Maison at the Institute for Organic Chemistry of the University of Giessen.

UV/ Vis-spectra were obtained using an Agilent 8453 diode array spectrophotometer. ATR-IR spectra were gained using a Bruker Optics ISF48 spectrometer with ATR unit ("golden gate", diamond, one reflexion).

7.1.3 Syntheses

7.1.3.1 $[Fe_2(\text{acetyl-uns-penp})_2(OH)](\text{triflate})_2 \times C_3H_6O \times H_2O$ (**22**)

In an argon glove box 200 mg (0.7 mmol) acetyl-uns-penp were dissolved in 5 ml absolute acetone. Then 28 mg (700 mmol) of a 60% dispersion of NaH in mineral oil were added. The suspension was stirred for 15 min and a gas formation could be observed. Adding of 307 mg $[Fe(CH_3CN)_2(\text{triflate})_2]$ (0.9 mmol) led to formation of a dark red complex solution. Dark orange air sensitive single crystals suitable for X-ray analysis were obtained by diffusion of diethyl ether at -40 °C.

7.1.3.2 $[Fe_2(uns-penp)_2Cl_2O]S_2O_6 \times 2 H_2O$ (**23**)

30 mg (0.13 mmol) uns-penp and 25 mg (0.13 mmol) $FeCl_2 \times 4 H_2O$ were dissolved in 0.5 ml methanol. This solution was mixed with 43 mg (0.21 mmol) $Na_2S_2O_6$ in 0.5 ml hot water. The mixture was filtered while warm, cooled down and stored at 6 °C. After three months some dark brown block shaped single crystals were formed.

7.1.3.3 Complexes used for ESI-MS and UV/ Vis Studies

The compounds **9**, **14** and **16** were synthesized as described in chapter 6. $[Co(Me_2-uns-penp)Cl]BF_4$ was synthesized according to the procedure described for compound **15** in chapter 6.

7.1.3.4 $[Fe(CH_3CN)_2(triflate)_2]$

Iron(II) triflate hexahydrate was synthesized by dissolving a small excess of pure iron chips in a trifluoromethanesulfonic acid/water mixture (1:1) under argon atmosphere. Concentrating the solvent yielded a turquoise crystalline product which was separated by filtration. The yield of Iron(II) was evaluated by titration with potassium permanganate. The product was dried in vacuum at 90° C for 12 h to yield a white powder. The iron(II) content was again quantified permanganometric. ATR-IR-spectroscopy was used to be sure of the anhydrous character of the product.

The iron(II) triflate was further dissolved in anhydrous acetonitrile under argon atmosphere. Activated molecular sieves (3 Å) were added to the turquoise solution. After two hours the solution was filtrated under an inert atmosphere to remove the molecular sieves. The solvent was removed in vacuum. The residue was dissolved in anhydrous acetonitrile and precipitated by adding the solution dropwise to an excess of diethyl ether. The turquoise product was filtrated and dried in vacuum for 30 min. to yield a white, free flowing powder. The iron(II) content was controlled by titration with potassium permanganate. ATR-IR-spectroscopy was used to be sure of the anhydrous character of the product and coordination of acetonitrile.

7.1.3.5 $[Fe(CH_3CN)_6](BF_4)_2$

Iron(II) tetrafluoroborate hexahydrate was synthesized by dissolving a small excess of iron powder p.a. in tetrafluoroboric acid (50% solution in water) under argon atmosphere. After the development of hydrogen gas had stopped, the solvent was removed by carefully warming in vacuum. A turquoise, crystalline product was obtained. The Iron(II) content was quantified by permanganometric titration.

5 g of (14.8 mmol) $\text{Fe}(\text{BF}_4)_2 \times 6 \text{H}_2\text{O}$ were dissolved in 60 ml anhydrous acetonitrile in a round-bottom schlenk-flask assembled with a soxlett extractor filled with 16 g of activated molecular sieves (3 Å). Furthermore, a condenser was attached to the extractor under an argon atmosphere to exclude oxygen. The acetonitrile solution was refluxed for 5 d. The solution was concentrated and 100 ml of anhydrous diethyl ether were added via a canula through a septum. A turquoise product precipitated and was filtered under inert conditions. The product was dried in vacuum to yield a slightly turquoise adhesive powder. The product was still containing water as shown in ATR-IR-spectroscopy. Repeating the procedure yielded a white, free flowing powder. ATR-IR spectroscopy showed the anhydrous character of the product and the coordination of acetonitrile. The yield of iron(II) was verified by titration with potassium permanganate.

7.1.3.6 $[\text{Fe}(\text{CH}_3\text{CN})_6](\text{SbF}_6)_2$

$[\text{Fe}(\text{MeCN})_y](\text{SbF}_6)_2 \times z\text{H}_2\text{O}$ was synthesized by dissolving 2.5 g (44.7 mmol) iron powder p.a. (excess) in a solution of $\text{HSbF}_6 \times 6 \text{H}_2\text{O}$ in acetonitrile. The acidic solution was prepared by dissolving 25 g (72.5 mmol) of hexafluoroantimonic acid hexahydrate in 5 ml acetonitrile p.a.. Under argon atmosphere, the acidic solution slowly poured into the iron powder. A slow gas development was observed. After five days a turquoise solution evolved. The solvent was removed in vacuum to obtain a slightly blue, adhesive powder.

10 g of the product were dissolved in 130 ml of anhydrous acetonitrile in a round-bottom schlenk-flask. The flask was equipped with a Soxlett extractor filled with 16 g of activated molecular sieves (3 Å). Under an inert atmosphere a refluxer was assembled. The solution was refluxed for 22 days under argon atmosphere. A brown solution was formed. The solvent was removed in vacuum to yield a beige powder. The residue was redissolved in anhydrous actonitrile. The product was precipitated by adding the solution dropwise into an excess of anhydrous diethyl ether. The product was filtrated and dried in vacuum to yield 6.76 g of a free flowing, white powder.

Alternatively, 1 g of the water containing-product was dissolved in 12 ml acetonitrile and 3 g of activated molecular sieves (3 Å) where added. After two weeks, the solution was filtered and added dropwise into an excess of anhydrous diethyl ether to

precipitate a white powder. The product was filtrated and dried in vacuum to yield 0.4 g of a free flowing, white powder.

7.2 Results and Discussion

7.2.1 Acetyl-uns-penp

7.2.1.1 Crystal Structure of $[Fe_2(\text{acetyl-uns-penp})_2(OH)](\text{triflate})_2 \times C_3H_6O \times H_2O$ (**22**)

As described for substance **18** in chapter 6 our attempts to isolate an mononuclear iron(II) complex with the deprotonated acetyl-uns-penp ligand failed. We could only isolate a dinuclear hydroxido-bridged iron(II) complex. In this attempt, we could repeat the isolation of this species with mixed coordination spheres for both iron(II) ions. The crystal structure of **18** is depicted in Figure 7-1. Crystallographic data are presented in table 7-1 and 7-2.

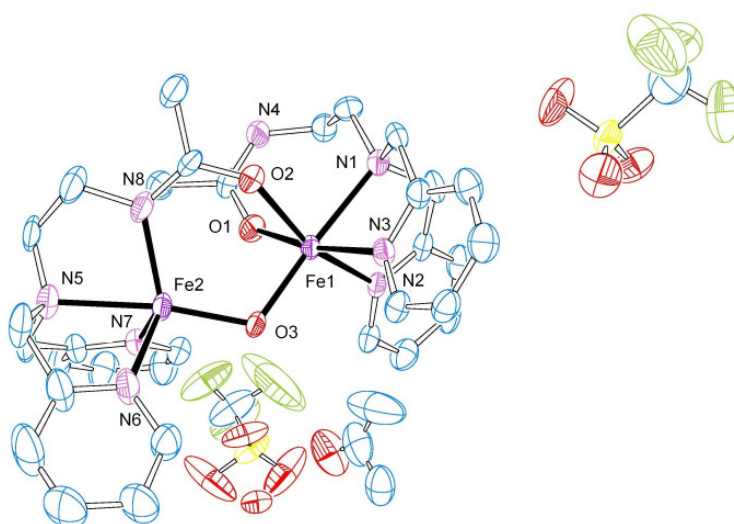


Figure 7-1: Crystal structure of **22** with hydrogen atoms omitted for clarity. Thermal ellipsoids are shown at 30 % probability levels.

Crystals of **22** were obtained by reacting deprotonated acetyl-uns-penp with $[Fe(CH_3CN)_2(\text{triflate})_2]$ in absolute acetone. The unit cell consist of four dinuclear complex cations, eight triflate anions and four acetone and four water molecules. The fact that we found water in the crystal structure supports our assumption that water was present in one of our starting materials. The bond lengths and angles are almost identical to those found for compound **18**.

Chapter 7

Table 7-1: Crystal structure and refinement data for **23**.

Empirical formula	C ₃₇ H ₄₈ F ₆ Fe ₂ N ₈ O ₁₁ S ₂
Formula weight [g mol ⁻¹]	1070.65
Crystal system	monoclinic
Space group	P2(1)/n
a [Å]	10.394(2)
b [Å]	17.854(4)
c [Å]	25.027(5)
α [°]	90
β [°]	92.64
γ [°]	90
V [Å ³]	4639.4(16)
Z	4
D _{calc} [g cm ⁻³]	1.533
T [K]	193(2)
μ(MoKα) [mm ⁻¹]	0.804
Crystal size [mm]	0.20 x 0.24 x 0.40
F(000)	2208
θ range [°]	2.16 - 24.99
	-11 ≤ h ≤ 12
Index ranges	-21 ≤ k ≤ 21
	-29 ≤ l ≤ 29
Reflections collected	28406
Unique reflections	8120
R _{int}	0.0858
Refinement method	Full-matrix least-squares on F ²
Data/constraints/parameters	8120 / 1 / 616
Godness-of-fit on F ²	1.053
Final R indices [I > 2σ(I)]	R ₁ = 0.0925
	wR ₂ = 0.2437
R indices (all data)	R ₁ = 0.1297
	wR ₂ = 0.2597
Largest diff. peak/hole [e. Å ⁻³]	1.086 to -0.607

Table 7-2: Selected distances [Å] and angles [°] for **23**

Fe(1)-O(1)	2.169(6)	Fe(2)-N(8)	2.082(7)	O(2)-Fe(1)-N(3)	91.0(2)
Fe(1)-O(2)	2.099(6)	Fe(1)...Fe(2)	3.304	O(3)-Fe(1)-N(1)	174.4(3)
Fe(1)-O(3)	1.978(7)	O(1)-Fe(1)-O(2)	87.9(2)	O(3)-Fe(1)-N(2)	103.4(3)
Fe(1)-N(1)	2.277(7)	O(1)-Fe(1)-O(3)	90.7(3)	O(3)-Fe(1)-N(3)	99.2(3)
Fe(1)-N(2)	2.178(6)	O(1)-Fe(1)-N(1)	94.9(2)	N(1)-Fe(1)-N(2)	76.9(2)
Fe(1)-N(3)	2.188(6)	O(1)-Fe(1)-N(2)	85.1(2)	N(1)-Fe(1)-N(3)	75.2(2)
Fe(2)-O(3)	1.943(7)	O(1)-Fe(1)-N(3)	170.0(2)	N(2)-Fe(1)-N(3)	92.8(2)
Fe(2)-N(5)	2.310(6)	O(2)-Fe(1)-O(3)	94.5(3)	O(3)-Fe(2)-N(5)	171.6(3)
Fe(2)-N(6)	2.159(8)	O(2)-Fe(1)-N(1)	85.9(2)		
Fe(2)-N(7)	2.138(8)	O(2)-Fe(1)-N(2)	160.8(2)		

7.2.2 Uns-penp

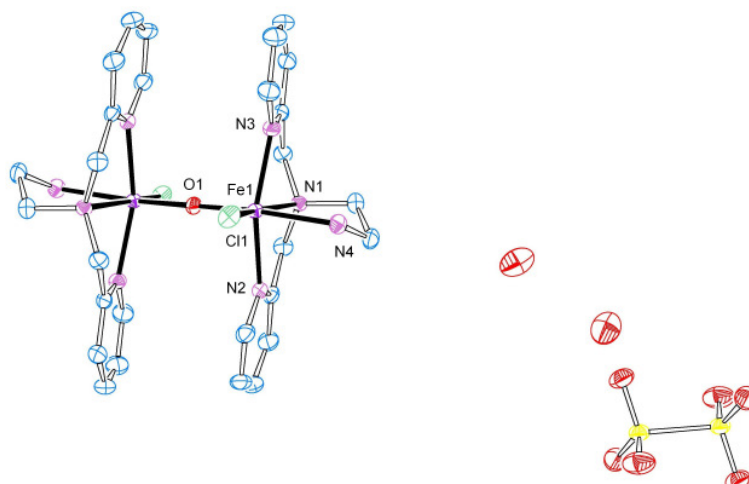
7.2.2.1 Crystal Structure of $[Fe(uns-penp)_2Cl_2O]S_2O_6 \times 2 H_2O$ (**23**)

Figure 7-2: Crystal structure of **23** with hydrogen atoms omitted for clarity. Thermal ellipsoids are shown at 30 % probability levels.

The molecular structure of **23** is presented in figure 7-2. The complex cation of **23** consist of two crystallographic identical iron(III) centers, linked by a bridging oxido group. The positive charge is balanced by a dithionate anion. The structure of the complex cation is identical to the oxido-bridged diiron(III) uns-penp complex published by Xu et al..⁹¹

Table 7-3: Crystal structure and refinement data for **24**.

Empirical formula	$C_{28}H_{44}Cl_2Fe_2N_8O_{11}S_2$
Formula weight [$g\text{mol}^{-1}$]	915.43
Crystal system	monoclinic
Space group	$P2(1)/c$
a [\AA]	11.446(2)
b [\AA]	9.2443(18)
c [\AA]	18.151(4)
α [$^\circ$]	90
β [$^\circ$]	96.85(3)
γ [$^\circ$]	90
V [\AA^3]	1499.6(5)
Z	2
D_{calc} [$g\text{cm}^{-3}$]	1.594
T [K]	193(2)
$\mu(\text{MoK}\alpha)$ [mm^{-1}]	0.71073
Crystal size [mm]	0.36 x 0.12 x 0.24
F(000)	948
θ range [$^\circ$]	2.48 - 25.98
Index ranges	$-14 \leq h \leq 14$ $-10 \leq k \leq 11$ $-22 \leq l \leq 22$
Reflections collected	13515
Unique reflections	3700
R_{int}	0.0653
Refinement method	Full-matrix least-squares on F^2
Data/constraints/parameters	3700 / 0 / 275

Godness-of-fit on F^2	0.967
Final R indices [$I > 2\sigma(I)$]	$R_1 = 0.0378$ $wR_2 = 0.0979$
R indices (all data)	$R_1 = 0.0500$ $wR_2 = 0.1018$
Largest diff. peak/hole [$e. \text{ \AA}^{-3}$]	0.533 to -0.360

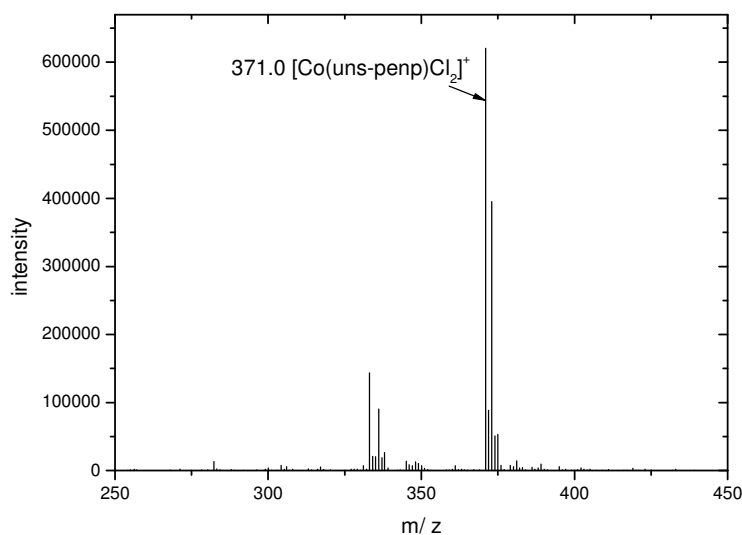
Table 7-4: Selected distances [\AA] and angles [$^\circ$] for **24**.

Fe(1)-Cl(1)	2.3196(9)	O(1)-Fe(1)-N(2)	88.44(6)	N(2)-Fe(1)-N(3)	154.64(9)
Fe(1)-O(1)	1.8026(4)	O(1)-Fe(1)-N(3)	94.32(6)	N(2)-Fe(1)-Cl(1)	104.34(6)
Fe(1)-N(1)	2.207(2)	O(1)-Fe(1)-N(4)	169.02(6)	N(2)-Fe(1)-N(3)	154.64(9)
Fe(1)-N(2)	2.139(2)	N(1)-Fe(1)-Cl(1)	164.39(6)	N(2)-Fe(1)-N(4)	84.21(8)
Fe(1)-N(3)	2.129(2)	N(1)-Fe(1)-N(2)	78.12(8)	N(3)-Fe(1)-Cl(1)	99.59(7)
Fe(1)-N(4)	2.201(2)	N(1)-Fe(1)-N(3)	76.58(9)	N(3)-Fe(1)-N(4)	88.91(9)
O(1)-Fe(1)-Cl(1)	102.98(3)	N(1)-Fe(1)-N(4)	78.08(9)	N(4)-Fe(1)-Cl(1)	86.79(7)
O(1)-Fe(1)-N(1)	92.44(6)	N(2)-Fe(1)-Cl(1)	104.34(6)	Fe(1)-O(1)-Fe(1)#1	180.00(4)

7.3 Solution Studies of Cobalt Complexes with Uns-penp, Acetyl-uns-penp, Me₂-uns-penp and Me₄-uns-penp and their Reactions with hydrogen peroxide.

7.3.1 ESI-MS Solution Studies

7.3.1.1 $[\text{Co}(\text{uns-penp})\text{Cl}_2]\text{SbF}_6$ (**9**)

**Figure 7-3:** ESIMS of a solution of $[\text{Co}(\text{uns-penp})\text{Cl}_2]\text{SbF}_6$ (**9**) in methanol.

The ESIMS of a solution of $[\text{Co}(\text{uns-penp})\text{Cl}_2]\text{SbF}_6$ in methanol is depicted in Figure 7-3. The most prominent signal at $m/z = 371.0$ could be assigned to $[\text{Co}(\text{uns-penp})\text{Cl}_2]^+$. The addition of an excess of hydrogen peroxide showed no evidence for the formation of a peroxido intermediate.

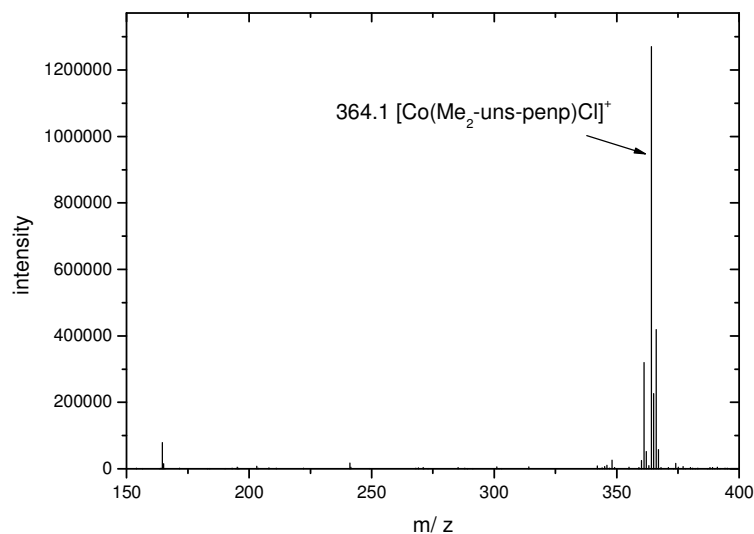
7.3.1.2 $[\text{Co}(\text{Me}_2\text{-uns-penp})\text{Cl}]\text{BF}_4$ 

Figure 7-4: ESIMS of a solution of $[\text{Co}(\text{Me}_2\text{-uns-penp})\text{Cl}]\text{BF}_4$ in methanol.

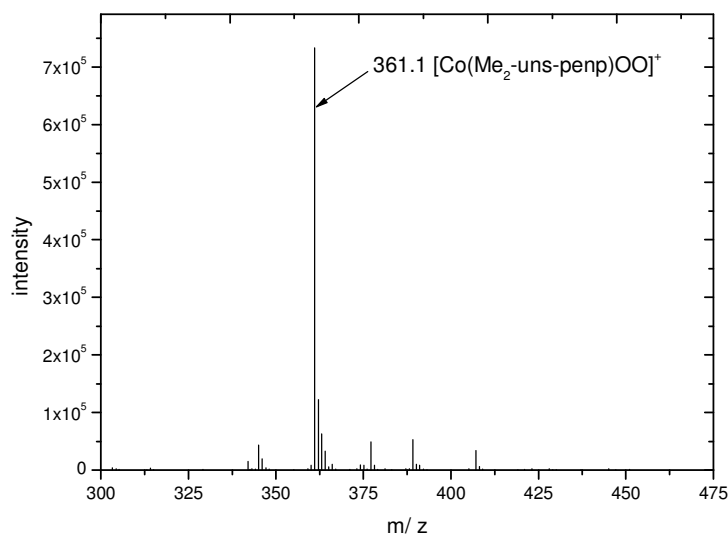


Figure 7-5: ESIMS of a solution of $[\text{Co}(\text{Me}_2\text{-uns-penp})\text{Cl}]\text{BF}_4$ in methanol with an excess of hydrogen peroxide.

The ESIMS of a solution of $[\text{Fe}(\text{Me}_2\text{-uns-penp})\text{Cl}]\text{BF}_4$ in methanol is depicted in Figure 7-4 and shows the signal of the chloride containing complex $[\text{Co}(\text{Me}_2\text{-uns-penp})\text{Cl}]^+$ at $m/z = 364.1$.

Figure 7-5 shows the mass spectrum of the complex solution after adding an excess of hydrogen peroxide. The most prominent peak is at $m/z = 361.1$ and can be assigned to the peroxido complex $[\text{Co}(\text{Me}_2\text{-uns-penp})(\text{OO})]^+$.

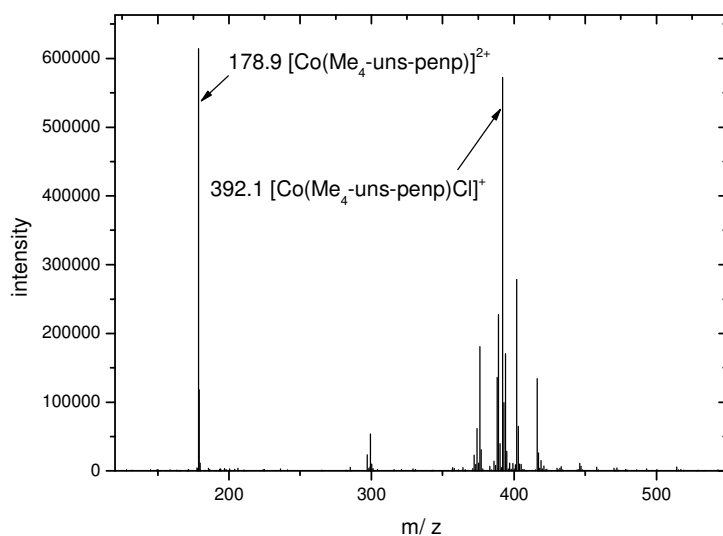
7.3.1.3 $[\text{Co}(\text{Me}_4\text{-uns-penp})\text{Cl}]\text{BF}_4$ (**14**)

Figure 7-6: ESIMS of a solution of **14** in methanol.

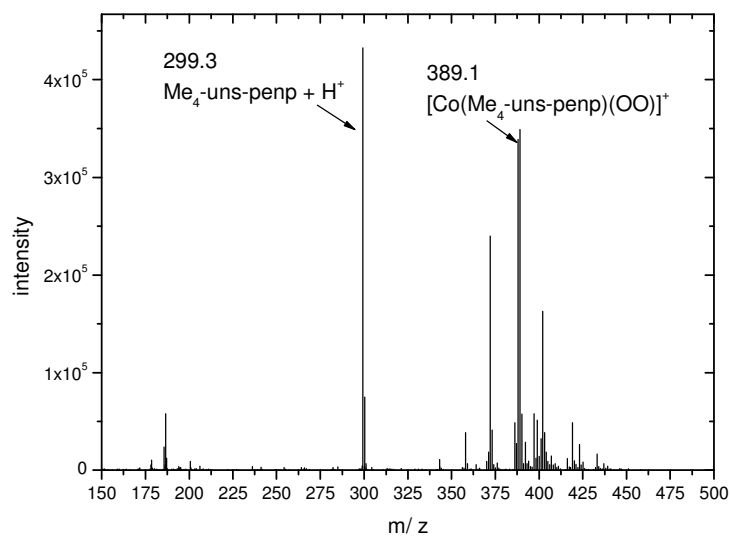


Figure 7-7: ESIMS of a solution of **14** in methanol with an excess of hydrogen peroxide.

The ESIMS of compound **14** is depicted in Figure 7-6. There are two prominent signals in the mass spectrum. The signal at $m/z = 178.9$ could be assigned to $[\text{Co}(\text{Me}_4\text{-uns-penp})]^{2+}$ and the signal at $m/z = 392.1$ to $[\text{Co}(\text{Me}_4\text{-uns-penp})\text{Cl}]^+$. After the addition of a large excess of hydrogen peroxide as Figure 7-7 shows one signal at $m/z = 389.1$. This peak could be assigned to a mononuclear cobalt(III) peroxido complex $[\text{Co}(\text{Me}_4\text{-uns-penp})\text{OO}]^+$.

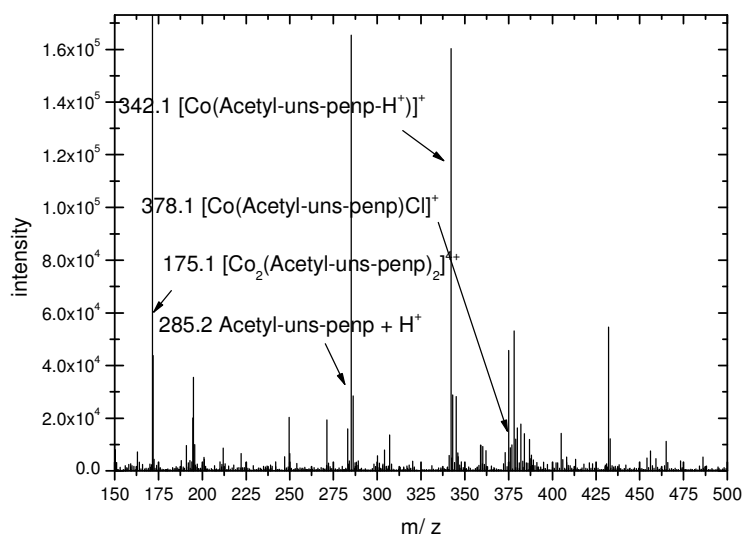
7.3.1.4 $[\text{Co}_2(\text{acetyl-uns-penp})_2\text{Cl}_2](\text{BF}_4)_2 \times \text{C}_3\text{H}_6\text{O}$ (**16**)

Figure 7-8: ESIMS of a solution of $[\text{Co}_2(\text{acetyl-uns-penp})_2\text{Cl}_2](\text{BF}_4)_2$ (**16**) in methanol.

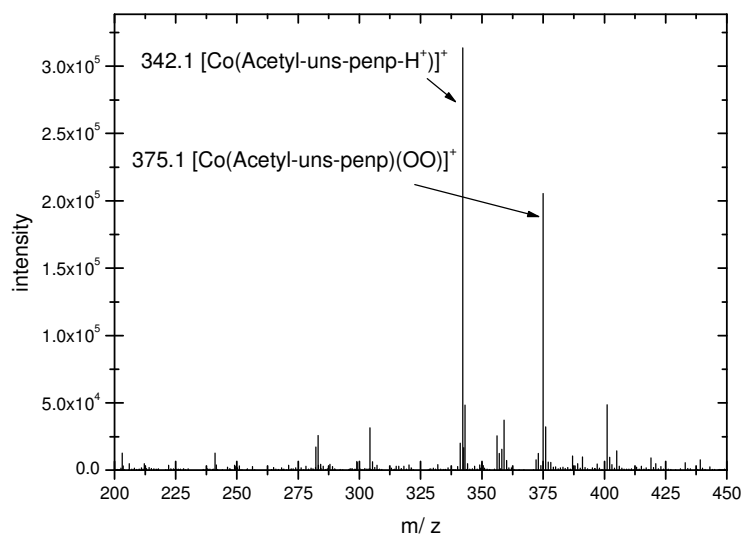


Figure 7-9: ESIMS of a solution of $[\text{Co}_2(\text{acetyl-uns-penp})_2\text{Cl}_2](\text{BF}_4)_2$ (**16**) in methanol with an excess of hydrogen peroxide.

Compound **16** was diluted in methanol. The ESI mass spectrum of the cobalt(II) complex solution is depicted in Figure 7-8 and shows a mixture of different species. The peak at $m/z = 171.5$ can be assigned to a dimeric complex species $[\text{Co}_2(\text{acetyl-uns-penp})_2]^{4+}$ and the peak at $m/z = 342.1$ to deprotonated $[\text{Co}(\text{acetyl-uns-penp})]^+$. The peak at $m/z = 378.1$ can be assigned to the chloride containing species

$[\text{Co}(\text{acetyl-uns-penp})\text{Cl}]^+$. Another signal at $m/z = 285.2$ can be assigned to the uncoordinated ligand cation $[(\text{acetyl-uns-penp})+\text{H}^+]$.

The mass spectrum after the reaction with an excess of hydrogen peroxide is depicted in Figure 7-9 and shows a prominent peak at $m/z = 375.1$. This peak can be assigned to the cobalt(III) peroxido complex $[\text{Co}(\text{acetyl-uns-penp})\text{OO}]^+$.

7.3.2 UV/ Vis Studies on the Reaction of Cobalt Complexes with Hydrogen Peroxide

7.3.2.1 $[\text{Co}(\text{Me}_2\text{-uns-penp})\text{Cl}]\text{BF}_4$

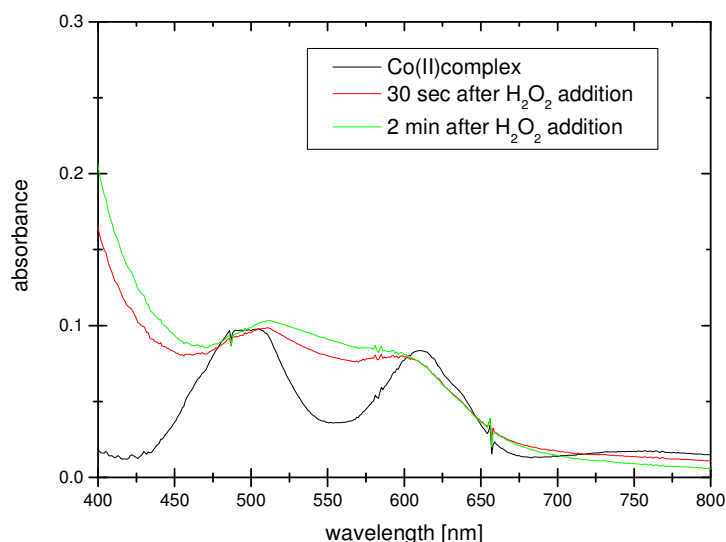


Figure 7-10: UV/ Vis spectra of a solution of $[\text{Co}(\text{Me}_2\text{-uns-penp})\text{Cl}]\text{BF}_4$ in methanol (black line) and after addition of hydrogen peroxide (red and green lines).

The UV/ Vis spectrum of a solution of $[\text{Co}(\text{Me}_2\text{uns-penp})\text{Cl}]\text{BF}_4$ in methanol is depicted in Figure 7-10. The UV/ Vis spectrum of the cobalt(II) complex shows two bands with absorbance maxima at 496 nm and 609 nm. After the addition of a large excess of hydrogen peroxide (> 10000 fold) a new band with a maxima at 511 nm and a shoulder at 598 nm was formed.

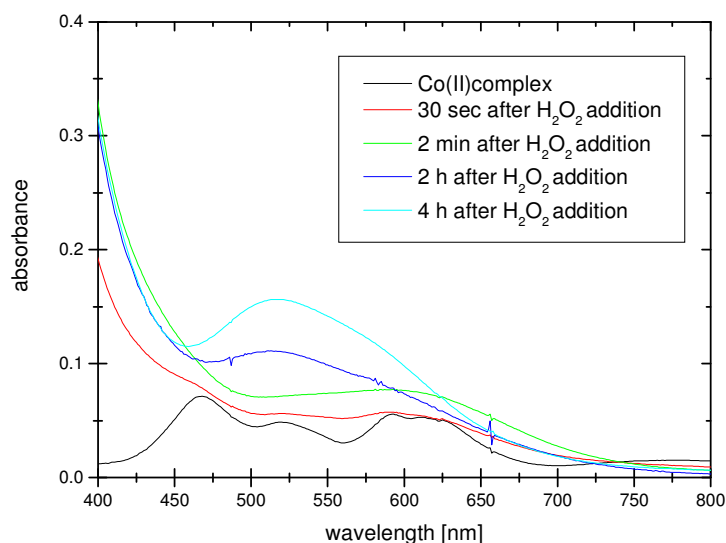
7.3.2.2 $[\text{Co}(\text{Me}_4\text{-uns-penp})\text{Cl}]\text{BF}_4$ (**14**)

Figure 7-11: UV/ Vis spectra of a solution of **14** in methanol (black line) and after addition of hydrogen peroxide (red, green, blue and turquoise lines).

The UV/ Vis spectrum of a solution of **14** in methanol is depicted in Figure 7-11. The UV/ Vis spectrum shows three overlapping bands with absorbance maxima at 468 nm, 520 nm, 592 nm and a shoulder at 610 nm. Having added a large excess of hydrogen peroxide (> 10000 fold) a new band with a maxima at 592 nm appeared (red and green lined spectra). After four hours a new band with a maximum at 516 nm (blue and turquoise lined spectra) was detected.

7.3.3 ATR-IR Spectroscopy of the Iron(II) Acetonitrile Complexes

The absence of water and the coordination of acetonitrile in the products could be proven by ATR-IR spectroscopy. The infrared data was compared with literature data for the vibrational wavenumbers.^{142,195-197}

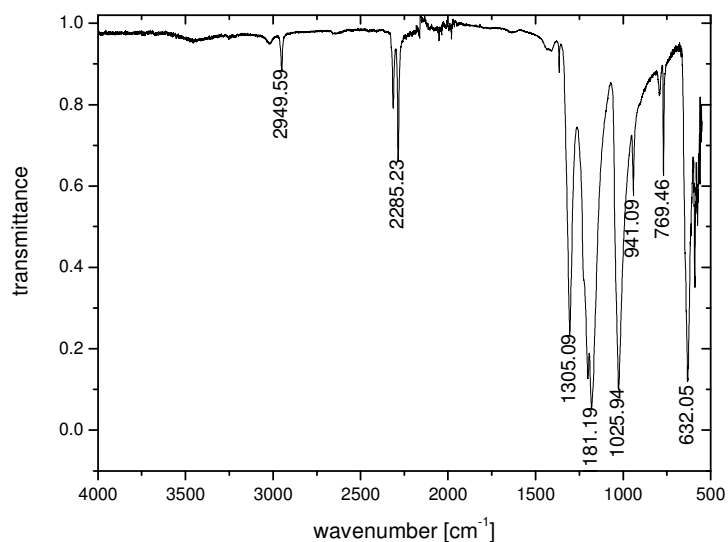


Figure 7-12: ATR-IR-spectrum of $[\text{Fe}(\text{CH}_3\text{CN})_2(\text{triflate})_2]$.

3019 ν_{CH} ; 2950 ν_{CH} ; 2314 ν_{CN} ; 2285 ν_{CN} ; 1365 ($\delta_{\text{C-H}} + \delta_{\text{CN}}$); 1181 ν_{asCF_3} ; 1026 ν_{sSO_3} ; 769 $\delta_{\text{sCF}_3} + \nu_{\text{(C-S)}}$; 632 $\delta_{\text{as SO}_3}$.

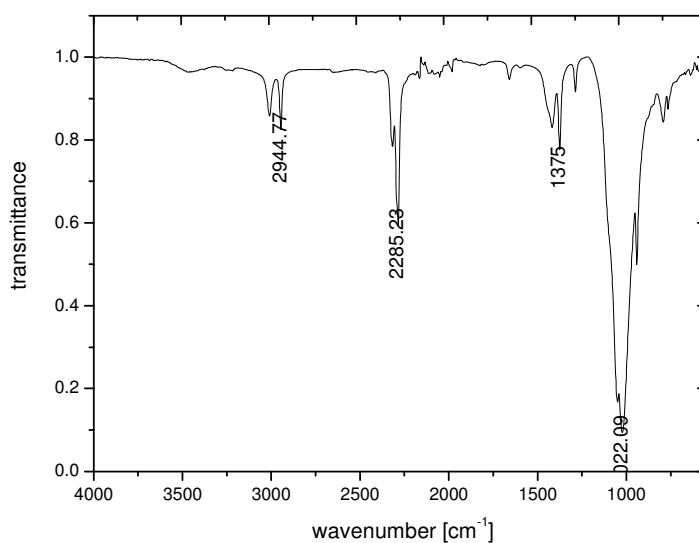


Figure 7-13: ATR-IR-spectrum of $[\text{Fe}(\text{CH}_3\text{CN})_6](\text{BF}_4)_2$.

3010 ν_{CH} ; 2945 ν_{CH} ; 2314 ν_{CN} ; 2285 ν_{CN} ; 1417 $\delta_{\text{C-H}}$; 1375 ($\delta_{\text{C-H}} + \delta_{\text{CN}}$); 1022 ν_{BF_4} .

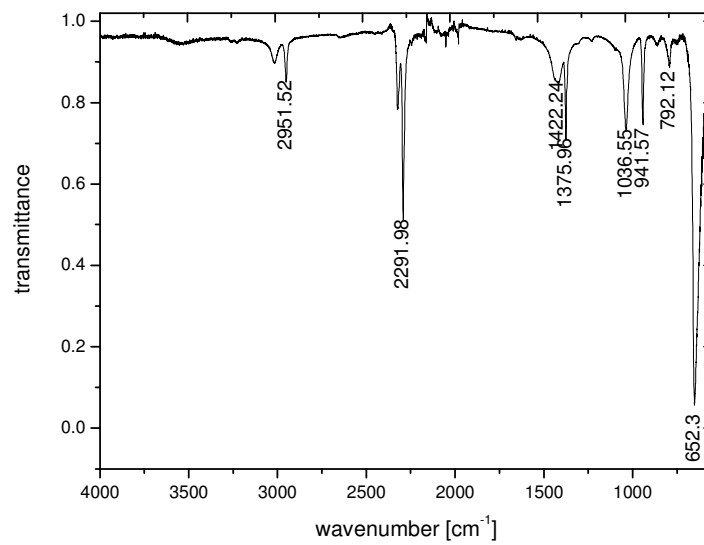


Figure 7-14: ATR-IR-spectrum, of $[\text{Fe}(\text{CH}_3\text{CN})_6](\text{SbF}_6)_2$.

3015 νCH ; 2952 νCH ; 2324 νCN ; 2292 νCN ; 1417 $\delta\text{C-H}$; 1375 ($\delta\text{C-H} + \delta\text{CN}$); 652 νSbF_6 .

8 Summary

In this work, model complexes for iron-containing enzymes like methane monooxygenase were investigated. The most important part is the analysis of the formation of so called „oxygen-adducts“.

In the first part of this thesis synthetic and reaction kinetics investigations on iron complexes of the ligand N-benzyl-N,N',N'-tris(2-pyridylmethyl)ethylenediamin (bztpen) depicted in figure 8-1 were carried out.

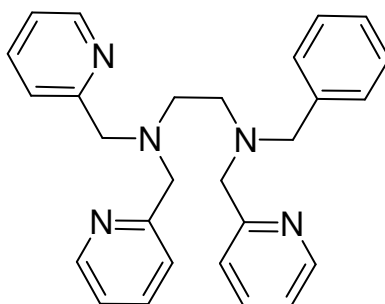


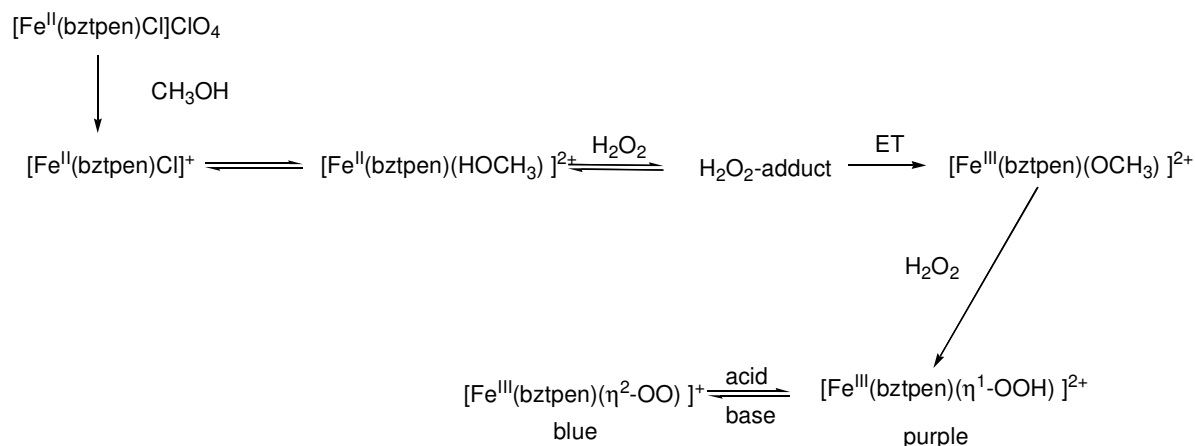
Figure 8-1: The ligand bztpen.

Before the beginning of this work it had been known, that iron(II) and iron(III) complexes of this ligand react with hydrogen peroxide to form hydroperoxido- and peroxido complexes. In the past it was pointed out that the iron oxido complexes could oxidize relatively inert alkanes like cyclohexane. Due to this fact, kinetic research on these complexes seemed to be particularly interesting in order to gain a more detailed knowledge of the reaction mechanism. In the past, there had already been investigations of the temperature dependency of the iron(III) bztpen complex in reaction with hydrogen peroxide in the Schindler group. They had the result that reaction proceeds with an associative character. This means that the reaction has a seven-fold coordinated transition state. This was justified with the determination of a negative activation entropy. ($\Delta S^\ddagger = -72 \pm 8 \text{ Jmol}^{-1}\text{K}^{-1}$). These results were reproduced successfully in this thesis.

However, it is known that temperature dependent kinetic investigations often have a large error in the allocation of the activation entropy. Due to this fact, high pressure experiments for determination of activation volumes were performed at the van Eldik group (University of Erlangen). Activation volumes can be determined more exactly compared to activation entropies, yet they provide the same details of reaction

SUMMARY

mechanisms. Using high-pressure „stopped-flow“-experiments it was observed that the reaction is not dependent on the pressure. The activation volume is close to zero. This means that the reaction proceeds via a mere interchange mechanism in with the ligands substitute simultaneously. For the reaction with hydrogen peroxide including the additional investigations mentioned the mechanism can be depicted as follows:



Scheme 8-1

Another goal of this thesis was the structural characterization of the formed hydroperoxido and peroxido complex. Unfortunately, many experiments on crystallisation of these compounds were unsuccessful. This was not unexpected, as such complexes are relatively unstable, and other working groups had not been successful in doing so either. Additional experiments to isolate an iron superoxido complex from iron(II) bztpen and dioxygen had no results. In this context, an iron-nitric oxide complex could be isolated and characterized by X-ray crystallography (Figure 8-2, left), a compound which is also not easy to isolate. Surprisingly, the formation of this complex could be monitored by „stopped-flow“-measurements spectroscopically (Figure 8-2, right). Due to its electronic character, nitric oxide is a good model compound for „oxygen adducts“ and supplies useful structural informations.

SUMMARY

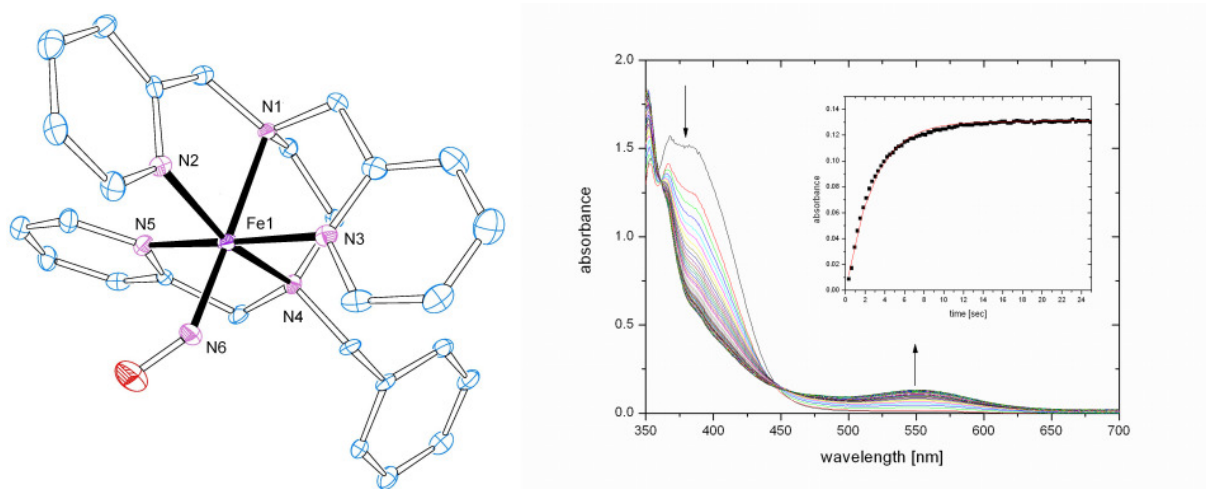


Figure 8-2: left: molecular structure of the cation $[\text{Fe}(\text{bztpen})\text{NO}]^{2+}$ (**6**) right: time-resolved UV/ Vis Spectra for the reaction of iron(II) bztpen complex with nitric oxide in methanol at $-40\text{ }^\circ\text{C}$. (insert: absorbance vs. time at 550 nm and fit to one exponential function).

It is well known that cobalt complexes form peroxido complexes very easily. Based on this fact, in this work it was tried to investigate the cobalt-bztpen complexes additional to the analogous iron-bztpen complexes. Unfortunately, neither cobalt hydroperoxido nor cobalt peroxido-complex could be isolated and crystallographically characterized. Even UV/ Vis spectroscopy and mass spectrometric investigations did not have any unambiguous results. Still several new cobalt(II) complexes with the ligands bztpen and metpen could be structurally characterized.

In this work, the new bridging ligand 1,3-bis(N,N,N'-tris(2-pyridylmethyl-))diaminoethyl-benzol (bz-b-tpen) could be synthesized. The lifetime of the iron(III) hydroperoxido and peroxido complexes could not be extended by this ligand as expected by secondary interactions (chapter 5). The formation of these complexes could be monitored by UV/ Vis-spectroscopy. However, no stabilization of the intermediates was observed.

The ligand bztpen can be derivated and synthesized from the tripodal ligand (2-amino-ethyl)-bis(2-pyridylmethyl)amine (uns-penp). This ligand, depicted in Figure 8-3 and its derivatives themselves are also very interesting ligands for the coordination chemistry of iron.

SUMMARY

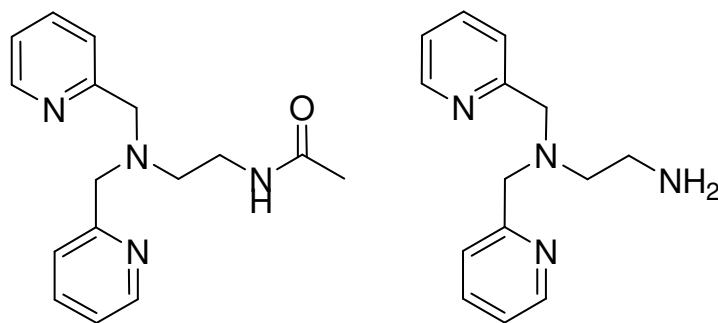


Figure 8-3: The ligands acetyl-uns-penp (left) and uns-penp (right).

Based on former investigations of the Schindler group, who had already worked with of these compounds as model complexes for catechol dioxygenases, several new iron(II)/ iron(III) and the analogous cobalt(II)/ cobalt(III) complexes could be synthesized and characterized in this work. These compounds are described in detail in chapter 6 and 7. Particularly interesting is the crystal structure of the complex $[\text{Fe}_2(\text{acetyl-uns-penp})_2(\text{OH})](\text{ClO}_4)_2$ as depicted in Figure 8-4.

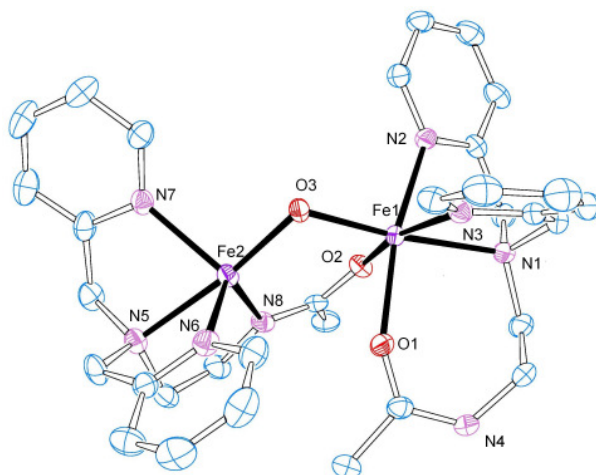


Figure 8-4: molecular structure of the cation of $[\text{Fe}_2(\text{acetyl-uns-penp})_2(\text{OH})](\text{ClO}_4)_2$ (**18**).

This complex was obtained while trying to synthesize the mononuclear iron(II) complex $[(\text{Fe}(\text{acetyl-uns-penp}))\text{ClO}_4]$ (with a deprotonated acetyl-uns-penp ligand), the reactivity towards dioxygen was supposed to be analyzed. Surprisingly, the dinuclear ligand as depicted above could be isolated instead. Here, both iron(II) ions are linked by a hydroxido ligand and only one amide function is deprotonated and functions as a second bridging ligand.

Concluding the facts this work contributes important knowledge for the understanding of the reactions of iron complexes with hydrogen peroxide as well as with dioxygen. It demonstrates that such compounds can be used in oxidation catalysis in the future.

SUMMARY

Especially the ligand acetyl-uns-penp seems to have a high potential for such reactions as current results of Que et al. had shown. Based on these facts, there will be further investigations on this system in the Schindler group, in the next future.

9 Zusammenfassung

Im Rahmen der hier vorliegenden Arbeit wurden Modellkomplexe für Eisenenzyme, wie z. B. die in der Einleitung beschriebenen Methanmonooxygenase, untersucht. Hierbei spielte die Analyse der Ausbildung sogenannter „Sauerstoffaddukt-Komplexe“ eine wesentliche Rolle.

Dazu wurden im ersten Teil dieser Arbeit synthetische und reaktionskinetische Untersuchungen mit Eisenkomplexen des in Abbildung 9-1 gezeigten Liganden N-benzyl-N, N',N'-tris(2-pyridylmethyl)ethyldiamin (bztpen) durchgeführt.

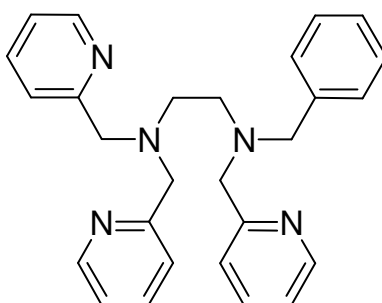
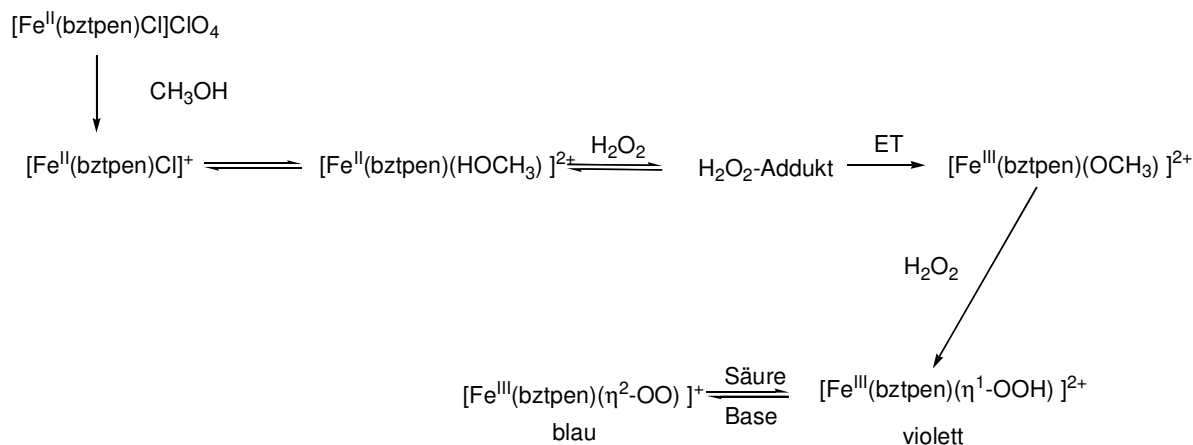


Abbildung 9-1: Der Ligand bztpen.

Zu Beginn dieser Arbeit war bereits bekannt, dass die Eisen(II)- bzw. Eisen(III)komplexe dieses Liganden mit Wasserstoffperoxid zu dem entsprechenden Hydroperoxido- und Peroxidokomplexen umgesetzt werden können. Gezeigt wurde dabei, dass die Eisenoxidokomplexe mit dem bztpen-Liganden in der Lage sind reaktionsträge Kohlenwasserstoffen wie z. B. Cyclohexan zu oxidieren. Vor diesem Hintergrund war die kinetische Untersuchung solcher Komplexe interessant, um Aufschluss über den detaillierten Reaktionsmechanismus zu erlangen. Eine vorausgegangene Untersuchung der Temperaturabhängigkeit der Reaktion des Eisen(III) bztpen Komplexes mit Wasserstoffperoxid im Arbeitskreis Schindler hatte ergeben, dass die Bildung des Hydroperoxidokomplexes nach einem Mechanismus mit assoziativen Charakter abläuft, welcher über ein siebenfach koordinierten Übergangszustand verläuft. Begründet wurde dies durch die Bestimmung einer negativen Aktivierungsentropie von $\Delta S^\ddagger = -72 \pm 8 \text{ Jmol}^{-1}\text{K}^{-1}$. Diese Untersuchungen konnten zunächst im Rahmen der hier vorliegenden Arbeit erfolgreich reproduziert werden. Da aber bekannt ist, dass temperaturabhängige reaktionskinetische Untersuchungen oftmals mit einem großen Fehler bei der Bestimmung der Aktivierungsentropie verbunden sind, wurden hier zusätzlich wesentlich

ZUSAMMENFASSUNG

aussagekräftigere Hochdruckuntersuchungen im Arbeitskreis von Prof. Rudi van Eldik (Universität Erlangen) zur Bestimmung des Aktivierungsvolumens durchgeführt. Aktivierungsvolumina lassen sich genauer als Aktivierungsentropien bestimmen und geben die gleichen Hinweise auf den Reaktionsmechanismus. Mit Hilfe von Hochdruck-"Stopped-Flow"-Messungen wurde beobachtet, dass die Reaktion druckunabhängig ist und somit ein Aktivierungsvolumen von nahezu 0 vorliegt. Das bedeutet, dass die Reaktion nach einem reinen Interchange-Mechanismus abläuft, bei welchem die Liganden simultan ausgetauscht werden. Für die Reaktion mit Wasserstoffperoxid ergibt sich somit, zusammen mit weiteren zusätzlichen Untersuchungsergebnissen der in Schema 9-1 gezeigte Mechanismus:



Schema 9-1

Ein weiteres Ziel dieser Arbeit war in diesem Zusammenhang die strukturelle Charakterisierung der gebildeten Hydroperoxido- bzw. Peroxidokomplexe. Leider waren die Versuche diese Verbindungen zu kristallisieren trotz zahlreicher Versuche nicht erfolgreich. Dies war nicht gänzlich unerwartet, da es sich bei beiden Komplexen um recht instabile Verbindungen handelt und hier auch andere Arbeitsgruppen bislang kein Glück hatten. Auch Versuche einen Eisen-Superoxido-Komplex aus dem Eisen(II) bztpen und Sauerstoff zu erhalten waren nicht erfolgreich.

Dafür konnte aber im Rahmen dieser Untersuchungen ein Eisen-Stickstoffmonoxid-Komplex isoliert und durch Kristallstrukturanalyse charakterisiert werden (siehe Abbildung 9-2 links), eine Verbindung, die ebenfalls nicht ganz einfach zu erhalten ist. Die Bildung dieses Komplexes konnte sogar überraschenderweise mit „Stopped-Flow“-Messungen spektroskopisch verfolgt werden (siehe Abbildung 9-2 rechts).

ZUSAMMENFASSUNG

Durch seine elektronischen Eigenschaften ist Stickstoffmonoxid eine gute Modellspezies für „Sauerstoffaddukt-Komplexe“ und lieferte damit wertvolle strukturelle Informationen.

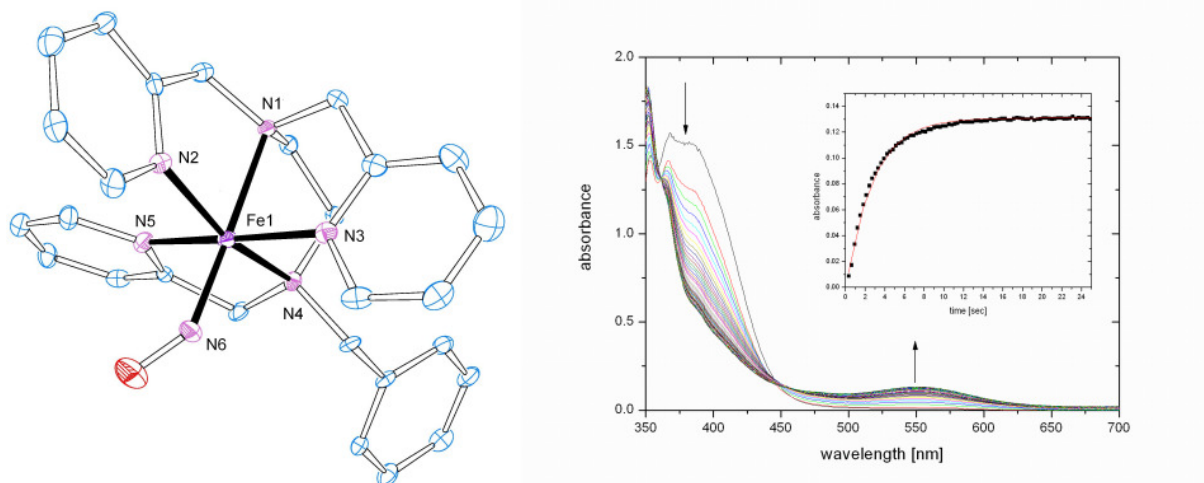


Abbildung 9-2: links: Molekülstruktur des Kations $[\text{Fe}(\text{bztpen})\text{NO}]^{2+}$ (6) rechts: zeitaufgelöste UV/ Vis-Spektren der Reaktion des Eisen(II)-bztpen-Komplexes mit Stickstoffmonoxid in Methanol bei $-40\text{ }^{\circ}\text{C}$. (Einschub: Extinktions-Zeit-Schnitt bei 550 nm und Anpassung an eine Exponentialfunktion).

Da Kobaltkomplexe bekanntermaßen sehr leicht Peroxidkomplexe bilden sollte im Rahmen dieser Arbeit auch versucht werden, analog zum Eisen-bztpen auch die entsprechenden Kobalt-bztpen Komplexe genauer zu untersuchen. Leider gelang es auch hier nicht, die entsprechenden Cobalt-Hydroperoxido/Peroxido-Komplexe zu isolieren und kristallographisch zu charakterisieren. Selbst UV/ Vis-spektroskopische und massenspektrometrische Untersuchungen (Kapitel 4) lieferten dabei keine eindeutigen Ergebnisse. Es gelang jedoch neue Cobalt(II)komplexe mit dem Liganden bztpen erfolgreich strukturell zu charakterisieren.

Im Rahmen dieser Arbeit konnte weiterhin der verbrückende neue Ligand 1,3-bis(N,N,N'-tris(2-pyridylmethyl-))diaminoethyl-benzol (bz-b-tpen) synthetisiert werden, mit welchem die Lebensdauer der Eisen(III)hydroperoxido- und -peroxido-Komplexe verlängert werden sollte (Kapitel 5). Die Bildung dieser Komplexe konnte durch UV/Vis-spektroskopische Untersuchungen bestätigt werden. Leider zeigte sich allerdings, dass der erhoffte Stabilisierungseffekt ausblieb.

Der Ligand bztpen kann aus dem tripodalen Liganden (2-amino-ethyl)-bis(2-pyridylmethyl)amin (uns-penp) abgeleitet, sowie daraus synthetisiert werden. Das in

ZUSAMMENFASSUNG

Abbildung 9-3 gezeigte uns-penp und seine Derivate sind aber selbst bereits sehr interessante Liganden für die Koordinationschemie des Eisens.

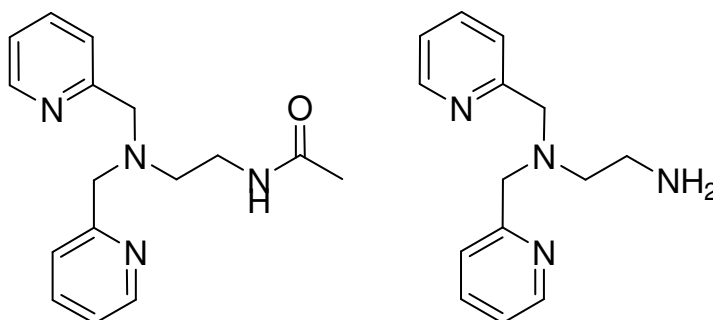


Abbildung 9-3: Die Liganden acetyl-uns-penp (links) und uns-penp (rechts).

Ausgehend von früheren Untersuchungen im Arbeitskreis Schindler, die sich mit diesen Komplexen als Modellverbindungen für Catecholdioxygenasen befassten, konnten im Rahmen der hier vorliegenden Arbeit Eisen(II)/Eisen(III)-Komplexe, sowie die analogen Cobalt(II)/Cobalt(III)-Komplexe synthetisiert und kristallographisch charakterisiert werden. Die einzelnen Verbindungen wurden in den Kapiteln 6 und 7 ausführlich beschrieben. Besonders interessant war dabei die Kristallstruktur des in Abbildung 9-4 gezeigten Komplexes $[\text{Fe}_2(\text{acetyl-uns-penp})_2(\text{OH})](\text{ClO}_4)_2$.

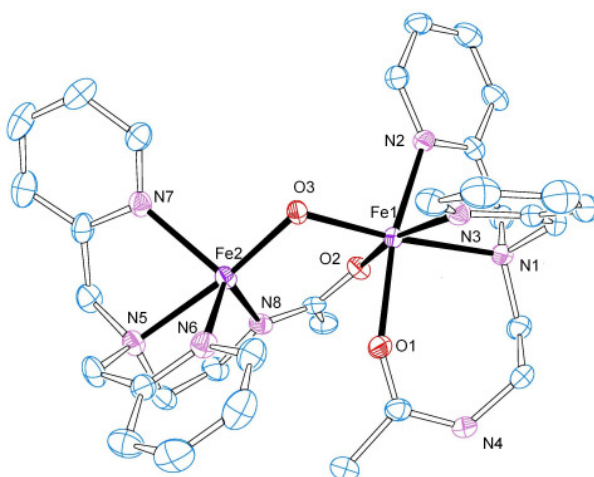


Abbildung 9-4: Molekülstruktur des Kations von $[\text{Fe}_2(\text{acetyl-uns-penp})_2(\text{OH})](\text{ClO}_4)_2$ (18).

Dieser Komplex wurde bei Versuchen gebildet, den einfachen mononuklearen Eisen(II)-Komplex $[\text{Fe}(\text{acetyl-uns-penp})]\text{ClO}_4$ (mit deprotoniertem acetyl-uns-penp) zu erhalten, um dessen Reaktion gegenüber Sauerstoff zu analysieren. Erstaunlicherweise wurde statt diesem Komplex der obige zweikernige Eisen(II)-Komplex gebildet. Hier sind die beiden Eisen(II)-Ionen über einen Hydroxido-

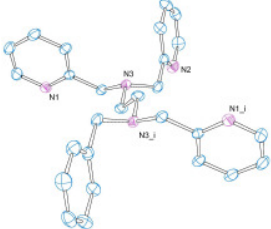
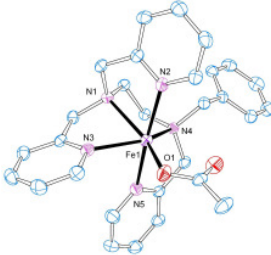
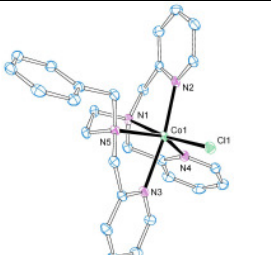
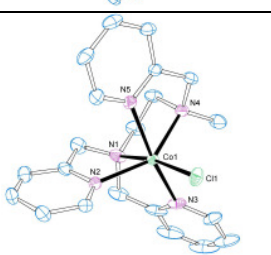
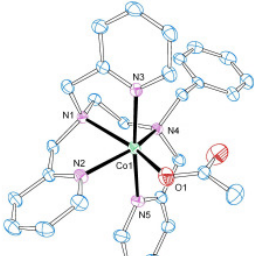
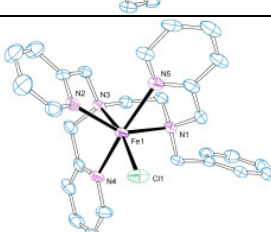
ZUSAMMENFASSUNG

Liganden verbrückt und nur eine der beiden Amidgruppen ist deprotoniert und wirkt als zweiter Brückenligand.

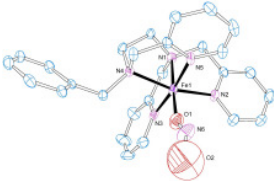
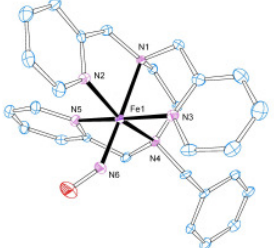
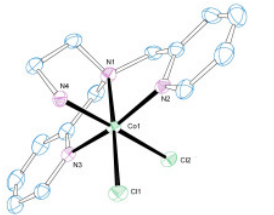
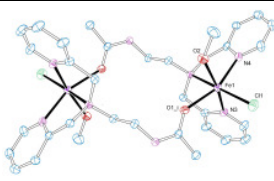
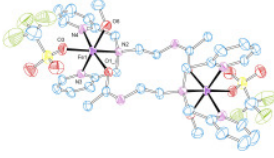
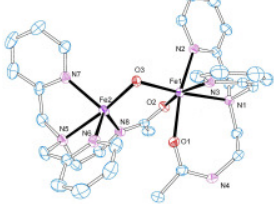
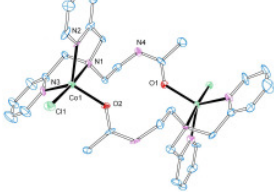
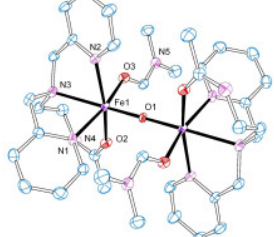
Abschließend kann gesagt werden, dass diese Arbeit wichtige Beiträge zum besseren Verständnis der Reaktion von Eisenkomplexen mit Wasserstoffperoxid, bzw. Sauerstoff geleistet hat und Möglichkeiten aufzeigt, wie diese Verbindungen in der Oxidationskatalyse in Zukunft besser nutzbar gemacht werden können. Insbesondere der Ligand Acetyl-uns-penp scheint, wie auch aktuelle Untersuchungen von Que et al. gezeigt haben, ein großes Potential für solche Reaktionen zu besitzen. Daher wird es aufbauend auf diese Arbeit im Arbeitskreis Schindler weitere Untersuchungen an diesem System geben.

List of Crystal Structures

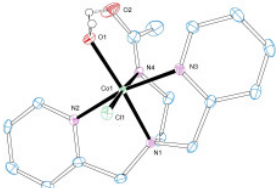
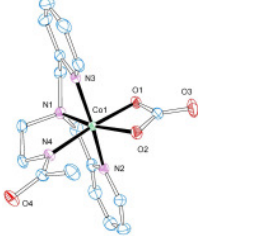
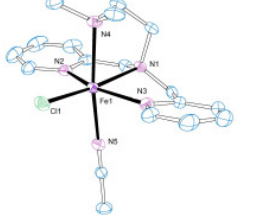
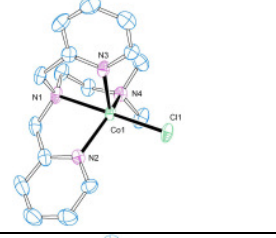
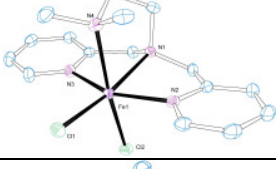
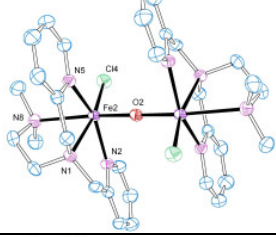
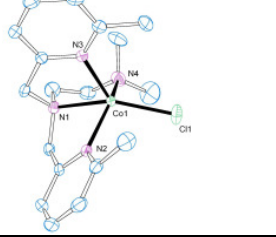
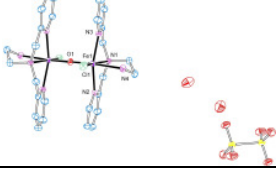
List of Crystal Structures

Ortep plot	Compound, Name, Formula, Formula weight [g mol ⁻¹]	Crystal system, space group	Cell dimensions [Å] Angles [°], Volumes [Å ³]
	1 bztpen C ₂₇ H ₂₉ N ₅ 423.55	monoclinic C2/c	[a, b, c] = [26.242(5), 6.2333(12), 17.286(4)] [α, β, γ] = [90, 123.39(3), 90] V = 2360.8(8)
	2 [Fe(bztpen)(OAc)]BPh ₄ C ₅₃ H ₅₂ BF ₄ N ₅ O ₂ 857.66	triclinic P-1	[a, b, c] = [13.243(3), 13.507(3), 13.992(3)] [α, β, γ] = [96.03(3), 114.15(3), 101.42(3)] V = 2189.5(8)
	3 [Co(bztpen)Cl]BF ₄ C ₂₇ H ₂₈ BClCoF ₄ N ₅ 603.73	orthorhombi c P/bca	[a, b, c] = [16.309(3), 17.791(4), 18.066(4)] [α, β, γ] = [90, 90, 90] V = 5241.9(18)
	4 [Co(metpen)Cl]SbF ₆ C ₂₁ H ₂₅ ClCoF ₆ N ₅ Sb 677.59	orthorhombi c Pca2(1)	[a, b, c] = [18.260(4), 9.1630(18), 15.057(3)] [α, β, γ] = [90, 90, 90] V = 2519.3(9)
	5 [Co(bztpen)(OAc)]BPh ₄ C ₅₃ H ₅₂ BCoN ₅ O ₂ 860.74	triclinic P-1	[a, b, c] = [13.234(3), 13.491(3), 13.920(3)] [α, β, γ] = [96.33(3), 114.02(3), 101.27(3)] V = 2175.8(8)
	6 [Fe(bztpen)Cl]OCH ₃ x 4 H ₂ O C ₂₉ H ₄₂ ClFeN ₅ O ₅ 631.98	monoclinic P2(1)/c	[a, b, c] = [9.0285(18), 22.726(5), 16.145(3)] [α, β, γ] = [90, 98.83(3), 90] V = 3273.5(11)

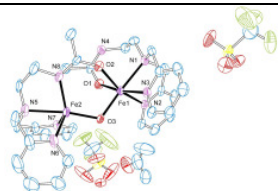
List of Crystal Structures

	7 [Fe(bztppen)NO ₂](SbF ₆) ₂ C ₂₇ H ₂₉ F ₁₂ FeN ₆ O ₂ Sb ₂ 996.91	orthorhombic Pbca	[a, b, c] = [17.735(4), 19.504(4), 19.757(4)] [α, β, γ] = [90, 90, 90] V = 6834(2)
	8 [Fe(bztppen)NO](SO ₃ CF ₃) ₂ C ₂₉ H ₂₉ F ₆ FeN ₆ O ₇ S ₂ 807.55	orthorhombic Pbca	[a, b, c] = [19.105(4), 17.251(4), 19.897(4)] [α, β, γ] = [90, 90, 90] V = 6558(2)
	9 [Co(uns-penp)Cl ₂](SbF ₆) C ₁₇ H ₂₄ Cl ₂ CoF ₆ N ₄ OSb 665.98	monoclinic P2(1)/c	[a, b, c] = [7.9367(16), 11.029(2), 27.112(5)] [α, β, γ] = [90, 91.07(3), 90] V = 2372.8(8)
	10 [Fe ₂ (acetyl-uns-penp) ₂ Cl ₂ (HOCH ₃) ₂](ClO ₄) ₂ C ₁₈ H ₂₈ N ₄ O ₇ Cl ₂ Fe 539.19	monoclinic P2(1)/c	[a, b, c] = [9.8951(8), 15.9255(14), 15.6861(13)] [α, β, γ] = [90, 103.063(10), 90] V = 2407.9(4)
	11 [Fe ₂ (acetyl-uns-penp) ₂ (SO ₃ CF ₃) ₂ (HOCH ₃) ₂](ClO ₄) ₂ C ₁₈ H ₂₄ ClF ₃ N ₄ O ₉ SFe 620.77	monoclinic P2(1)/c	[a, b, c] = [16.060(3), 17.413(4), 9.2789(19)] [α, β, γ] = [90, 102.05(3), 90] V = 2537.7(9)
	12 [Fe ₂ (acetyl-uns-penp) ₂ OH](ClO ₄) x 3 C ₃ H ₆ O C ₄₁ H ₅₈ Cl ₂ Fe ₂ N ₈ O ₁₄ 1069.55	triclinic P-1	[a, b, c] = [10.610(2), 11.876(2), 20.374(4)] [α, β, γ] = [78.68(3), 82.79(3), 79.05(3)] V = 2461.1(9)
	13 [Co ₂ (acetyl-uns-penp) ₂ Cl ₂] C ₃₅ H ₄₆ B ₂ C ₁₂ Co ₂ F ₈ N ₈ O 989.18	monoclinic Cc	[a, b, c] = [26.650(5), 9.1963(18), 17.357(4)] [α, β, γ] = 90, 94.15, 90 V = 4242.7(15)
	14 [Fe ₂ (acetyl-uns-penp) ₂ (DMF) ₂ O](ClO ₄) ₄ C ₄₀ H ₅₇ Cl ₄ Fe ₂ N ₁₁ O ₂₁ 1281.47	triclinic P-1	[a, b, c] = [11.344(2), 12.732(3), 12.797(3)] [α, β, γ] = 116.96(3), 107.40(3), 96.86(3) V = 1499.6(5)

List of Crystal Structures

	15 [Co(acetyl-uns-penp)Cl(H ₂ O)]Cl ₂ C ₁₆ H ₂₃ Cl ₂ CoN ₄ O ₃ 449.21	orthorhombic P2(1)2(1)2(1)	[a, b, c] = [8.4839(17), 13.984(3), 15.971(3)] [α, β, γ] = [90, 90, 90] V = 1894.8(7)
	16 [Co(acetyl-uns-penp)CO ₃] C ₁₇ H ₂₅ CoN ₄ O ₇ 456.34	monoclinic P2(1)/n	[a, b, c] = [8.2982(17), 14.207(3), 16.786(3)] [α, β, γ] = [90, 100.38(3), 90] V = 1946.6(7)
	17 [Fe(Me ₂ -uns-penp)(CH ₃ CN)Cl]BPh ₄ C ₄₂ H ₄₅ BClFeN ₅ 721.94	orthorhombic P2(1)2(1)2(1)	[a, b, c] = [11.9724(10), 12.5853(11), 25.165(2)] [α, β, γ] = [90, 90, 90] V = 3791.8(6)
	18 [Fe(Me ₂ -uns-penp)Cl]ClO ₄ C ₃₂ H ₄₄ Cl ₄ Co ₂ N ₈ O ₈ 928.41	monoclinic P2(1)/c	[a, b, c] = [9.4443(19), 32.397(7), 13.780(3)] [α, β, γ] = [90, 109.91, 90] V = 3964.3(14)
	19 [Fe(Me ₂ -uns-penp)Cl ₂]ClO ₄ C ₁₆ H ₂₂ Cl ₃ FeN ₄ O ₄ 496.58	monoclinic P2(1)/c	[a, b, c] = [10.2465(11), 15.2903(16), 13.6617(15)] [α, β, γ] = [90, 104.3270(10), 90] V = 2073.8(4)
	20 [Fe ₂ (Me ₂ -uns-penp) ₂ Cl ₂ O](BPh ₄) ₂ C ₈₀ H ₈₄ B ₂ Cl ₂ Fe ₂ N ₈ O 1377.77	triclinic P-1	[a, b, c] = [14.5070(13), 14.8754(14), 17.8164(16)] [α, β, γ] = [103.514(11), 97.178(11), 106.903(11)] V = 3499.0(6)
	21 [Co(Me ₄ -uns-penp)Cl]BF ₄ C ₁₈ H ₂₆ BClCoF ₄ N ₄ 479.62	monoclinic P2(1)/n	[a, b, c] = 8.1644(16), 16.963(3), 15.962(3) [α, β, γ] = 90, 95.73(3), 90 V = 2199.6(8)
	22 [Fe ₂ (uns-penp) ₂ Cl ₂ O]S ₂ O ₆ × 2 H ₂ O C ₃₇ H ₄₈ F ₆ Fe ₂ N ₈ O ₁₁ S ₂ 915.43	monoclinic P2(1)/c	[a, b, c] = [11.446(2), 9.2443(18), 18.151(4)] [α, β, γ] = [90, 96.85(3), 90] V = 1499.6(5)

List of Crystal Structures



23

[Fe₂(acetyl-uns-
penp)₂OH](SO₃CF₃) x 2 H₂O
C₂₈H₄₄Cl₂Fe₂N₈O₁₁S₂
915.43

monoclinic
P2(1)/c

[a, b, c] = [11.446(2),
9.2443(18), 18.151(4)]
[α, β, γ] = [90, 96.85(3), 90]
V = 1499.6(5)

**Der Lebenslauf wurde aus der elektronischen
Version der Arbeit entfernt.**

**The curriculum vitae was removed from the
electronic version of the paper.**

Publications

- Nebe, T.; Xu, J. Y.; Schindler S. in *Activating Unreactive Substrates*, Bolm C.; Hahn, E. (editors), Wiley VCH, Weinheim, **2009**, 39-51
- Nebe, T., Beitat A., Würtele C., Dücker-Benfer C., van Eldik, R., McKenzie C. J., Schindler S.; Dalton Transactions; *submitted*
- Nebe, T, Xu, J. Y.; Beitat, A.; Würtele, C.; Walter, O.; Serafin, M.; Schindler S.; Inorganica Chimica Acta; *submitted*

Presentations

- Poster presentation: GdCh-Wissenschaftsforum Ulm (2007/09)
“Iron hydroperoxo and peroxo complexes”
- Poster presentation: Koordinationchemietagung Universität Nürnberg-Erlangen (2009/02)
“Reactions of Iron-bztpen complex with hydrogen peroxide”
- Poster presentation: GdCh-Wissenschaftsforum Frankfurt/ Main (2009/09)
“Kinetic investigations on hydroperoxido complex formation”

Bibliography

- (1) Balasubramanian, R.; Rosenzweig, A. *Acc. Chem. Res.* **2007**, *40*, 573-580.
- (2) Murray, L.; Lippard, S. *Acc. Chem. Res.* **2007**, *40*, 466-474.
- (3) Costas, M.; Mehn, M. P.; Jensen, M. P.; Que, L. *Chem. Rev.* **2004**, *104*, 939-986.
- (4) Tshuva, E. Y.; Lippard, S. J. *Chem. Rev.* **2004**, *104*, 987-1011.
- (5) Kryatov, S. V.; Rybak-Akimova, E. V.; Schindler, S. *Chem. Rev.* **2005**, *105*, 2175-2226.
- (6) Korendovych, I.; Kryatov, S.; Rybak-Akimova, E. *Acc. Chem. Res.* **2007**, *40*, 510-521.
- (7) Hollemann, A. F.; Wiberg, E. *Lehrbuch der Anorganischen Chemie*; 101 ed.; Walter der Gruyter & Co.: Berlin, **1995**.
- (8) Lippard, S. J.; Berg, J. M. *Bioanorganische Chemie*; 1 ed.; Spektrum Akademischer Verlag: Heidelberg Berlin Oxford, **1995**.
- (9) Busch, D. H.; Jackson, P. J.; Kojima, M.; Chmielewski, P.; Matsumoto, N.; Stevens, J. C.; Wu, W.; Nosco, D.; Herron, N. *Inorg. Chem.* **1994**, *33*, 910-923.
- (10) Hanzlik, R. P.; Williamson, D. *J. Am. Chem. Soc.* **1976**, *98*, 6570-6573.
- (11) Reetz, M. T.; Töllner, K. *Tetrahedron lett.* **1995**, *36*, 9461-9464.
- (12) Jain, S. L.; Sain, B. *Angew. Chem. Int. Ed.* **2003**, *42*, 1265-1267.
- (13) Reinaud, O. M.; Yap, G. P. A.; Rheingold, A. L.; Theopold, K. H. *Angew. Chem. Int. Ed. Engl.* **1995**, *34*, 2051-2052.
- (14) Müller, J.; Würtele, C.; Walter, O.; Schindler, S. *Angew. Chem. Int. Ed.* **2007**, *46*, 7775-7777.
- (15) Niederhoffer, E. C.; Timmons, J. H.; Martell, A. E. *Chem. Rev.* **1984**, *84*, 137-203.
- (16) Werner, A.; Mylius, A. *Z. anorg. Chem.* **1898**, *16*, 245-267.
- (17) Werner, A. *Ann. Chem.* **1910**, *375*, 1-144.
- (18) Thewalt, U.; Marsh, R. E. *J. Am. Chem. Soc.* **1967**, *89*, 6364-6365.
- (19) Christoph, G. G.; Marsh, R. E.; Schaefer, W. P. *Inorg. Chem.* **1969**, *8*, 291-297.

BIBLIOGRAPHY

- (20) Tsumaki, T. *Bull. Chem. Soc. J.* **1938**, *13*, 252-260.
- (21) Wilmarth, W. K.; Aranoff, S.; Calvin, M. *J. Am. Chem. Soc.* **1946**, *68*, 2263-2266.
- (22) Calligaris, M.; Nardin, G.; Randaccio, L.; Ripamonti, A. *J. Chem. Soc. A* **1970**, 1069 - 1074.
- (23) Appleton, T. G. *J. Chem. Edu.* **1977**, *54*, 443-444.
- (24) Calvin, M.; Bailes, R. H.; Wilmarth, W. K. *J. Am. Chem. Soc.* **1946**, *68*, 2254-2256.
- (25) Barkelew, C. H.; Calvin, M. *J. Am. Chem. Soc.* **1946**, *68*, 2257-2262.
- (26) Calvin, M.; Barkelew, C. H. *J. Am. Chem. Soc.* **1946**, *68*, 2267-2273.
- (27) Cini, R.; Orioli, P. *J. Chem. Soc.-Chem. Commun.* **1981**, 196-198.
- (28) Carre, F.; Corriu, R. J. P.; Lancelle-Beltran, E.; Mehdi, A.; Reye, C.; Guilard, R.; Sykora, J.; Lee, A. v. d. *Dalton Trans.* **2003**, 3211-3215.
- (29) Terry, N. W.; Amma, E. L.; Vaska, L. *J. Am. Chem. Soc.* **1972**, *94*, 653-655.
- (30) Brown, L. D.; Raymond, K. N. *Inorg. Chem.* **1975**, *14*, 2595-2601.
- (31) Halpern, J.; Goodall, B. L.; Khare, G. P.; Lim, H. S.; Pluth, J. J. *J. Am. Chem. Soc.* **1975**, *97*, 2301-2303.
- (32) Crump, D. B.; Stepaniak, R. F.; Payne, N. C. *Can. J. Chemistry* **1976**, *55*, 438-446.
- (33) Gall, R. S.; Rogers, J. F.; Schaefer, W. P.; Christoph, G. G. *J. Am. Chem. Soc.* **1976**, *98*, 5135-5144.
- (34) Gall, R. S.; Schaefer, W. P. *Inorg. Chem.* **1976**, *15*, 2758-2763.
- (35) Jameson, G. B.; Robinson, W. T.; Rodley, G. A. *Dalton Trans.* **1978**, 191-196.
- (36) Schaefer, W. P.; Huie, B. T.; Kurilla, M. G.; Ealick, S. E. *Inorg. Chem.* **1980**, *19*, 340-344.
- (37) Martell, A. E. *Acc. Chem. Res.* **1982**, *15*, 155-162.
- (38) Ohishi, T.; Kashiwabara, K.; Fujita, J.; Ohba, S.; Ishii, T.; Saito, T. *Bull. Chem. Soc. J.* **1986**, *59*, 385-393.
- (39) Egan, J. W.; Haggerty, B. S.; Rheingold, A. L.; Sendlinger, S. C.; Theopold, K. H. *J. Am. Chem. Soc.* **1990**, *112*, 2445-2446.
- (40) Hohenester, E.; Kratky, C.; Krautler, B. *J. Am. Chem. Soc.* **1991**, *113*, 4523-4530.

BIBLIOGRAPHY

- (41) Hikichi, S.; Akita, M.; Moro-oka, Y. *Coord. Chem. Rev.* **2000**, *198*, 61-87.
- (42) Hu, X. L.; Castro-Rodriguez, I.; Meyer, K. *J. Am. Chem. Soc.* **2004**, *126*, 13464-13473.
- (43) Rahman, A.; Jackson, W. G.; Willis, A. C. *Inorg. Chem.* **2004**, *43*, 7558-7560.
- (44) Guzei, I. A.; Bakac, A. *Inorg. Chem.* **2001**, *40*, 2390-2393.
- (45) Feig, A. L.; Lippard, S. J. *Chem. Rev.* **1994**, *94*, 759-805.
- (46) Momenteau, M.; Reed, C. A. *Chem. Rev.* **1994**, *94*, 659-698.
- (47) Meunier, B.; de Visser, S. P.; Shaik, S. *Chem. Rev.* **2004**, *104*, 3947-3980.
- (48) Burger, R. M. *Chem. Rev.* **1998**, *98*, 1153-1169.
- (49) Bukowski, M. R.; Zhu, S. R.; Koehntop, K. D.; Brennessel, W. W.; Que, L. *J. Biol. Inorg. Chem.* **2004**, *9*, 39-48.
- (50) Sono, M.; Roach, M. P.; Coulter, E. D.; Dawson, J. H. *Chem. Rev.* **1996**, *96*, 2841-2887.
- (51) Lieberman, R. L.; Rosenzweig, A. C. *Nature* **2005**, *434*, 177-182.
- (52) Liu, K. E.; Valentine, A. M.; Wang, D. L.; Huynh, B. H.; Edmondson, D. E.; Salifoglou, A.; Lippard, S. J. *J. Am. Chem. Soc.* **1995**, *117*, 10174-10185.
- (53) Merckx, M.; Kopp, D. A.; Sazinsky, M. H.; Blazyk, J. L.; Muller, J.; Lippard, S. J. *Angew. Chem. Int. Ed.* **2001**, *40*, 2782-2807.
- (54) Dalton, H. *Phil. Trans. Royal Soc. B* **2005**, *360*, 1207-1222.
- (55) Hanson, R. S.; Hanson, T. E. *Microbiol. Rev.* **1996**, *60*, 439-+.
- (56) Rosenzweig, A. C.; Brandstetter, H.; Whittington, D. A.; Nordlund, P.; Lippard, S. J.; Frederick, C. A. *Proteins* **1997**, *29*, 141-152.
- (57) Rosenzweig, A. C.; Frederick, C. A.; Lippard, S. J.; Nordlund, P. *Nature* **1993**, *366*, 537-543.
- (58) Rosenzweig, A. C.; Lippard, S. J. *Acc. Chem. Res.* **1994**, *27*, 229-236.
- (59) Rosenzweig, A. C.; Nordlund, P.; Takahara, P. M.; Frederick, C. A.; Lippard, S. J. *Chem. Biol.* **1995**, *2*, 409-418.
- (60) Whittington, D. A.; Lippard, S. J. *J. Am. Chem. Soc.* **2001**, *123*, 827-838.

BIBLIOGRAPHY

- (61) Whittington, D. A.; Sazinsky, M. H.; Lippard, S. J. *J. Am. Chem. Soc.* **2001**, *123*, 1794-1795.
- (62) Woodland, M. P.; Dalton, H. *J. Biol. Chem.* **1984**, *259*, 53-59.
- (63) Liu, K. E.; Valentine, A. M.; Qiu, D.; Edmondson, D. E.; Appelman, E. H.; Spiro, T. G.; Lippard, S. J. *J. Am. Chem. Soc.* **1995**, *117*, 4997-4998.
- (64) Lund, J.; Woodland, M. P.; Dalton, H. *Eur. J. Biochem.* **1985**, *147*, 297-305.
- (65) Brazeau, B. J.; Lipscomb, J. D. *Biochem.* **2000**, *39*, 13503-13515.
- (66) Valentine, A. M.; Stahl, S. S.; Lippard, S. J. *J. Am. Chem. Soc.* **1999**, *121*, 3876-3887.
- (67) Lee, S. K.; Nesheim, J. C.; Lipscomb, J. D. *J. Biol. Chem.* **1993**, *268*, 21569-21577.
- (68) Que, L. *Acc. Chem. Res.* **2007**, *40*, 493-500.
- (69) Hayashi, Y.; Suzuki, M.; Uehara, A.; Mizutani, Y.; Kitagawa, T. *Chem. Lett.* **1992**, 91-94.
- (70) Menage, S.; Brennan, B. A.; Juarez-Garcia, C.; Munck, E.; Que, L. *J. Am. Chem. Soc.* **1990**, *112*, 6423-6425.
- (71) Brennan, B. A.; Chen, Q.; Juarez-Garcia, C.; True, A. E.; O'Connor, C. J.; Que, L. *Inorg. Chem.* **1991**, *30*, 1937-1943.
- (72) Dong, Y. H.; Fujii, H.; Hendrich, M. P.; Leising, R. A.; Pan, G. F.; Randall, C. R.; Wilkinson, E. C.; Zang, Y.; Que, L.; Fox, B. G.; Kauffmann, K.; Munck, E. *J. Am. Chem. Soc.* **1995**, *117*, 2778-2792.
- (73) Feig, A. L.; Lippard, S. J. *J. Am. Chem. Soc.* **1994**, *116*, 8410-8411.
- (74) Feig, A. L.; Becker, M.; Schindler, S.; van Eldik, R.; Lippard, S. J. *Inorg. Chem.* **1996**, *35*, 2590-2601.
- (75) Westerheide, L.; Muller, F. K.; Than, R.; Krebs, B.; Dietrich, J.; Schindler, S. *Inorg. Chem.* **2001**, *40*, 1951-1961.
- (76) Nizova, G. V.; Krebs, B.; Süss-Fink, G.; Schindler, S.; Westerheide, L.; Gonzalez, L. G.; Shul'pin, G. B. *Tetrahedron* **2002**, *58*, 9231.
- (77) Blackman, A. G. *Polyhedron* **2005**, *24*, 1-39.
- (78) Schindler, S. *Eur. J. Inorg. Chem.* **2000**, 2311-2326.
- (79) Mirica, L. M.; Ottenwaelder, X.; Stack, T. D. P. *Chem. Rev.* **2004**, *104*, 1013-1045.
- (80) Lewis, E. A.; Tolman, W. B. *Chem. Rev.* **2004**, *104*, 1047-1076.

BIBLIOGRAPHY

- (81) Jang, H. G.; Cox, D. D.; Que, L. *J. Am. Chem. Soc.* **1991**, *113*, 9200-9204.
- (82) Weitzer, M.; Schatz, M.; Hampel, F.; Heinemann, F. W.; Schindler, S. *Dalton Trans.* **2002**, 686-694.
- (83) Merkel, M.; Pascaly, M.; Krebs, B.; Astner, J.; Foxon, S. P.; Schindler, S. *Inorg. Chem.* **2005**, *44*, 7582-7589.
- (84) Schatz, M.; Becker, M.; Thaler, F.; Hampel, F.; Schindler, S.; Jacobson, R. R.; Tyeklar, Z.; Murthy, N. N.; Ghosh, P.; Chen, Q.; Zubieta, J.; Karlin, K. D. *Inorg. Chem.* **2001**, *40*, 2312-2322.
- (85) Foxon, S. P.; Walter, O.; Schindler, S. *Eur. J. Inorg. Chem.* **2002**, 111-121.
- (86) Schatz, M.; Leibold, M.; Foxon, S. P.; Weitzer, M.; Heinemann, F. W.; Hampel, F.; Walter, O.; Schindler, S. *Dalton Trans.* **2003**, 1480-1487.
- (87) Mandel, J. B.; Maricondi, C.; Douglas, B. E. *Inorg. Chem.* **1988**, *27*, 2990-2996.
- (88) Mandel, J. B.; Douglas, B. E. *Inorg. Chim. Acta* **1989**, *155*, 55-69.
- (89) Matouzenko, G. S.; Bousseksou, A.; Lecocq, S.; vanKoningsbruggen, P. J.; Perrin, M.; Kahn, O.; Collet, A. *Inorg. Chem.* **1997**, *36*, 2975-2981.
- (90) Davies, C. J.; Fawcett, J.; Shutt, R.; Solan, G. A. *Dalton Trans.* **2005**, 2630-2640.
- (91) Xu, J. Y.; Astner, J.; Walter, O.; Heinemann, F. W.; Schindler, S.; Merkel, M.; Krebs, B. *Eur. J. Inorg. Chem.* **2006**, 1601-1610.
- (92) Patra, A. K.; Afshar, R. K.; Rowland, J. M.; Olmstead, M. M.; Mascharak, P. K. *Angew. Chem. Int. Ed.* **2003**, *42*, 4517-4521.
- (93) Shan, X.; Que, L., *Proc. Natl. Acad. Sci. U. S. A.* **2005**, *102*, 5340-5345.
- (94) Würtele, C.; Gaoutchenova, E.; Harms, K.; Holthausen, M. C.; Sundermeyer, J.; Schindler, S. *Angew. Chem.* **2006**, *118*, 3951-3954.
- (95) Cramer, C.; Tolman, W. *Acc. Chem. Res.* **2007**, *40*, 601-608.
- (96) Bukowski, M. R.; Comba, P.; Lienke, A.; Limberg, C.; de Laorden, C. L.; Mas-Balleste, R.; Merz, M.; Que, L. *Angew. Chem. Int. Ed.* **2006**, *45*, 3446-3449.
- (97) Rosenthal, J.; Nocera, D. *Acc. Chem. Res.* **2007**, *40*, 543-553.
- (98) Wada, A.; Harata, M.; Hasegawa, K.; Jitsukawa, K.; Masuda, H.; Einaga, H. *J. Inorg. Biochem.* **1997**, *67*, 73.

BIBLIOGRAPHY

- (99) McBeth, C. E.; Golombek, A. P.; Young, V. G. J.; Yang, C.; Kuczera, K.; Hendrich, M. P.; Borovik, A. S. *Science* **2000**, *289*, 938.
- (100) Jensen, K. B.; McKenzie, C. J.; Nielsen, L. P.; Pedersen, J. Z.; Svendsen, H. M. *Chem. Commun.* **1999**, 1313-1314.
- (101) Bernal, I.; Jensen, I. M.; Jensen, K. B.; McKenzie, C. J.; Toftlund, H.; Tuchagues, J. P. *Dalton Trans.* **1995**, 3667-3675.
- (102) Hazell, A.; McKenzie, C. J.; Nielsen, L. P.; Schindler, S.; Weitzer, M. *Dalton Trans.* **2002**, 310-317.
- (103) Than, R.; Schrodtr, A.; Westerheide, L.; van Eldik, R.; Krebs, B. *Eur. J. Inorg. Chem.* **1999**, 1537-1543.
- (104) Berry, J. F.; Bill, E.; Bothe, E.; George, S. D.; Mienert, B.; Neese, F.; Wieghardt, K. *Science* **2006**, *312*, 1937-1941.
- (105) de Oliveira, F. T.; Chanda, A.; Banerjee, D.; Shan, X. P.; Mondal, S.; Que, L.; Bominaar, E. L.; Munck, E.; Collins, T. J. *Science* **2007**, *315*, 835-838.
- (106) Krebs, C.; Galonic, x; Fujimori, D.; Walsh, C.; Bollinger, J. *Acc. Chem. Res.* **2007**, *40*, 484-492.
- (107) Shaik, S.; Hirao, H.; Kumar, D. *Acc. Chem. Res.* **2007**, *40*, 532-542.
- (108) Nam, W. *Acc. Chem. Res.* **2007**, *40*, 522-531.
- (109) Rohde, J. U.; In, J. H.; Lim, M. H.; Brennessel, W. W.; Bukowski, M. R.; Stubna, A.; Munck, E.; Nam, W.; Que, L. *Science* **2003**, *299*, 1037-1039.
- (110) Bukowski, M. R.; Comba, P.; Limberg, C.; Merz, M.; Que, L.; Wistuba, T. *Angew. Chem.* **2004**, *116*, 1303-1307.
- (111) Pestovsky, S.; Bominaar, O.; Emile, S. L.; Shan, X.; MÜNCK, E.; Que, L.; Bakac, A. *Angew. Chem.* **2005**, *117*, 7031-7034.
- (112) Bautz, J.; Bukowski, M. R.; Kerscher, M.; Stubna, A.; Comba, P.; Lienke, A.; Munck, E.; Que, L. *Angew. Chem. Int. Ed.* **2006**, *45*, 5681-5684.
- (113) Klinker, E. J.; Kaizer, J.; Brennessel, W. W.; Woodrum, N. L.; Cramer, C. J.; Que, L. *Angew. Chem. Int. Ed.* **2005**, *44*, 3690-3694.
- (114) England, J.; Martinho, M.; Farquhar, E. R.; Frisch, J. R.; Bominaar, E. L.; MÜNCK, E.; Que, L. *Angew. Chem. Int. Ed.* **2009**, *48*, 3622-3626.
- (115) Shan, X. P.; Que, L. *Proc. Natl. Acad. Sci. U. S. A.* **2005**, *102*, 5340-5345.
- (116) Lange, S. J.; Que, L. *Curr. Opin. Chem. Biol.* **1998**, *2*, 159-172.

BIBLIOGRAPHY

- (117) Jensen, M. P.; Costas, M.; Ho, R. Y. N.; Kaizer, J.; Payeras, A. M. I.; Munck, E.; Que, L.; Rohde, J. U.; Stubna, A. *J. Am. Chem. Soc.* **2005**, *127*, 10512-10525.
- (118) Kim, C.; Dong, Y.; Que, L. *J. Am. Chem. Soc.* **1997**, *119*, 3635-3636.
- (119) Hsu, H.-F.; Dong, Y.; Shu, L.; Young, V. G.; Que, L. *J. Am. Chem. Soc.* **1999**, *121*, 5230-5237.
- (120) Costas, M.; Rohde, J. U.; Stubna, A.; Ho, R. Y. N.; Quaroni, L.; Munck, E.; Que, L. *J. Am. Chem. Soc.* **2001**, *123*, 12931-12932.
- (121) Ghosh, A.; de Oliveira, F. T.; Yano, T.; Nishioka, T.; Beach, E. S.; Kinoshita, I.; Munck, E.; Ryabov, A. D.; Horwitz, C. P.; Collins, T. J. *J. Am. Chem. Soc.* **2005**, *127*, 2505-2513.
- (122) Xue, G. Q.; Wang, D.; De Hont, R.; Fiedler, A. T.; Shan, X. P.; Munck, E.; Que, L. *Proc. Natl. Acad. Sci. U. S. A.* **2007**, *104*, 20713-20718.
- (123) Polster, J. *Reaktionskinetische Auswertung spektroskopischer Messdaten*; Vieweg: Braunschweig/ Wiesbaden, **1995**.
- (124) Jordan, R. B. *Mechanismen anorganischer und metallorganischer Reaktionen*; Teubner Studienbücher Chemie: Stuttgart, **1994**.
- (125) Espenson, J. H. *Chemical Kinetics and Reaction Mechanisms*; McGraw-Hill: New York, **1995**.
- (126) Wilkins, R. G. *Kinetics and Mechanism of Reactions of Transition Metal Complexes*; 2 ed.; VCH: Weinheim, **1991**.
- (127) Que, L.; Ho, R. Y. N. *Chem. Rev.* **1996**, *96*, 2607-2624.
- (128) Kim, J.; Larka, E.; Wilkinson, E. C.; Que, L. *Angew. Chem.- Int. Ed. Engl.* **1995**, *34*, 2048-2051.
- (129) Zang, Y.; Elgren, T. E.; Dong, Y.; Que, L. *J. Am. Chem. Soc.* **1993**, *115*, 811-813.
- (130) Nielsen, A.; Larsen, F. B.; Bond, A. D.; McKenzie, C. J. *Angew. Chem.- Int. Ed.* **2006**, *45*, 1602-1606.
- (131) Park, M. J.; Lee, J.; Suh, Y.; Kim, J.; Nam, W. *J. Am. Chem. Soc.* **2006**, *128*, 2630-2634.
- (132) Rohde, J. U.; Torelli, S.; Shan, X. P.; Lim, M. H.; Klinker, E. J.; Kaizer, J.; Chen, K.; Nam, W. W.; Que, L. *J. Am. Chem. Soc.* **2004**, *126*, 16750-16761.
- (133) Kaizer, J.; Klinker, E. J.; Oh, N. Y.; Rohde, J. U.; Song, W. J.; Stubna, A.; Kim, J.; Munck, E.; Nam, W.; Que, L. *J. Am. Chem. Soc.* **2004**, *126*, 472-473.

BIBLIOGRAPHY

- (134) Duelund, L.; Hazell, R.; McKenzie, C. J.; Nielsen, L. P.; Toftlund, H. *Dalton Trans.* **2001**, 152-156.
- (135) Horner, O.; Jeandey, C.; Oddou, J. L.; Bonville, P.; McKenzie, C. J.; Latour, J. M. *Eur. J. Inorg. Chem.* **2002**, 3278-3283.
- (136) Hirao, H.; Que, L.; Nam, W.; Shaik, S. *Chem.-Eur. J.* **2008**, *14*, 1740-1756.
- (137) Fish, L. L.; Crumbliss, A. L. *J. Am. Chem. Soc.* **1985**, *24*, 2198-2204.
- (138) Brink, C. P.; Crumbliss, A. L. *Inorg. Chem.* **1984**, *23*, 4708-18.
- (139) Hayton, T. W.; Legzdins, P.; Sharp, W. B. *Chem. Rev.* **2002**, *102*, 935-992.
- (140) Eisenberg, R.; Meyer, C. D. *Acc. Chem. Res.* **1975**, *8*, 26-34.
- (141) Heyn, B.; Hipler, B.; Kreisel, G.; Schreer, H.; Walther, D. *Anorganische Synthesechemie*; Springer Verlag: Berlin, **1990**; Vol. 2.
- (142) Heintz, R. A.; Smith, J. A.; Szalay, P. S.; Weisgerber, A.; Dunbar, K. R. in *Inorg. Synth.*, Vol 33; John Wiley & Sons Inc: New York, **2002**; Vol. 33, p 75-83.
- (143) van Eldik, R.; Gaede, W.; Wieland, S.; Kraft, J.; Spitzer, M.; Palmer, D. A. *Rev. Sci. Instrum.* **1993**, *64*, 1355.
- (144) 3.1 ed.; Hi-Tec Scientific: **2003**.
- (145) On-line Instruments Inc.: Bogart, GA, USA, **1990**.
- (146) 6.0 ed.; Microcal Software: Northhampton MA, USA, **1999**.
- (147) Sheldrick, G. M.; University Göttingen: **1997**.
- (148) 6.1 ed.; Bruker AXS: Madison, WI, USA, **2000**.
- (149) Ortega-Villar, N.; Ugalde-Saldivar, V. M.; Munoz, M. C.; Ortiz-Frade, L. A.; Alvarado-Rodriguez, J. G.; Real, J. A.; Moreno-Esparza, R. *Inorg. Chem.* **2007**, *46*, 7285-7293.
- (150) Jensen, M. P.; Payeras, A. M. I.; Fiedler, A. T.; Costas, M.; Kaizer, J.; Stubna, A.; Munck, E.; Que, L. *Inorg. Chem.* **2007**, *46*, 2398-2408.
- (151) Siri, O.; Tabard, A.; Pullumbi, P.; Guillard, R. *Inorg. Chim. Acta* **2003**, *350*, 633-640.
- (152) Grapperhaus, C. A.; Patra, A. K.; Mashuta, M. S. *Inorg. Chem.* **2002**, *41*, 1039-1041.
- (153) Hauser, C.; Glaser, T.; Bill, E.; Weyhermuller, T.; Wieghardt, K. *J. Am. Chem. Soc.* **2000**, *122*, 4352-4365.

BIBLIOGRAPHY

- (154) Schweitzer, D.; Ellison, J. J.; Shoner, S. C.; Lovell, S.; Kovacs, J. A. *J. Am. Chem. Soc.* **1998**, *120*, 10996-10997.
- (155) Wang, W. D.; Bakac, A.; Espenson, J. H. *Inorg. Chem.* **1995**, *34*, 4049-4056.
- (156) Arulsamy, N.; Bohle, D. S.; Hansert, B.; Powell, A. K.; Thomson, A. J.; Wocadlo, S. *Inorg. Chem.* **1998**, *37*, 746-750.
- (157) Jewett, S. L.; Egging, S.; Geller, L. *J. Inorg. Biochem.* **1997**, *66*, 165-173.
- (158) Sastri, C. V.; Lee, J.; Oh, K.; Lee, Y. J.; Lee, J.; Jackson, T. A.; Ray, K.; Hirao, H.; Shin, W.; Halfen, J. A.; Kim, J.; Que, L.; Shaik, S.; Nam, W. *Proc. Natl. Acad. Sci. U. S. A.* **2007**, *104*, 19181-19186.
- (159) Legros, J.; Bolm, C. *Angew. Chem. Int. Ed.* **2004**, *43*, 4225-4228.
- (160) Rowe, G. T.; Rybak-Akimova, E. V.; Caradonna, J. P. *Chem.-Eur. J.* **2008**, *14*, 8303-8311.
- (161) Incarvito, C.; Lam, M.; Rhatigan, B.; Rheingold, A. L.; Qin, C. J.; Gavrilova, A. L.; Bosnich, B. *Dalton Trans.* **2001**, 3478-3488.
- (162) Singh, A. K.; Mukherjee, R. *Inorg. Chem.* **2005**, *44*, 5813-5819.
- (163) Wang, D.; Farquhar, E. R.; Stubna, A.; Münck, E.; Que, L. *Nat. Chem.* **2009**, *1*, 145-150.
- (164) Nebe, T.; Beitat, A.; Würtele, C.; van Eldik, R.; Schindler, S. *Dalton Trans.* **2009**.
- (165) Patra, A. K.; Afshar, R.; Olmstead, M. M.; Mascharak, P. K. *Angew. Chem. Int. Ed.* **2002**, *41*, 2512-2515.
- (166) Britovsek, G. J. P.; England, J.; White, A. J. P. *Inorg. Chem.* **2005**, *44*, 8125-8134.
- (167) Hodgkinson, J.; Jordan, R. B. *J. Am. Chem. Soc.* **1973**, *95*, 763-768.
- (168) Horner, O.; Anxolabehere-Mallart, E.; Charlot, M. F.; Tchertanov, L.; Guilhem, J.; Mattioli, T. A.; Boussac, A.; Girerd, J. J. *Inorg. Chem.* **1999**, *38*, 1222-1232.
- (169) Hanaoka, K.; Kikuchi, K.; Urano, Y.; Nagano, T. *Perkin Trans. 2* **2001**, 1840-1843.
- (170) Otter, C. A.; Hartshorn, R. M. *Dalton Trans.* **2004**, 150-156.
- (171) McClintock, L. F.; Bagaria, P.; Kjaergaard, H. G.; Blackman, A. G. *Polyhedron* **2009**, *28*, 1459-1468.
- (172) Failes, T. W. *Acta Cryst. Sect. E* **2003**, *59*, m616-m617.

BIBLIOGRAPHY

- (173) Yang, X. F.; Guo, X. Q. *Analyst* **2001**, *126*, 928-932.
- (174) Norman, R. E.; Yan, S.; Que, L.; Backes, G.; Ling, J.; Sanders-Loehr, J.; Zhang, J. H.; O'Connor, C. J. *J. Am. Chem. Soc.* **1990**, *112*, 1554-1562.
- (175) Musie, G.; Lai, C. H.; Reibenspies, J. H.; Sumner, L. W.; Darensbourg, M. Y. *Inorg. Chem.* **1998**, *37*, 4086-4093.
- (176) Addison, A. W.; Rao, T. N.; Reedijk, J.; van Rijn, J.; Verschoor, G. C. *Dalton Trans.* **1984**, 1349 - 1356.
- (177) Kodera, M.; Katayama, K.; Tachi, Y.; Kano, K.; Hirota, S.; Fujinami, S.; Suzuki, M. *J. Am. Chem. Soc.* **1999**, *121*, 11006-11007.
- (178) Sigel, H.; Martin, R. B. *Chem. Rev.* **1982**, *82*, 385-426.
- (179) Rowland, J. M.; Olmstead, M.; Mascharak, P. K. *Inorg. Chem.* **2001**, *40*, 2810-2817.
- (180) Patra, A. K.; Rowland, J. M.; Marlin, D. S.; Bill, E.; Olmstead, M. M.; Mascharak, P. K. *Inorg. Chem.* **2003**, *42*, 6812-6823.
- (181) Afshar, R. K.; Patra, A. K.; Olmstead, M. M.; Mascharak, P. K. *Inorg. Chem.* **2004**, *43*, 5736-5743.
- (182) Rowland, J. M.; Olmstead, M. M.; Mascharak, P. K. *Inorg. Chem.* **2002**, *41*, 2754-2760.
- (183) Guajardo, R. J.; Hudson, S. E.; Brown, S. J.; Mascharak, P. K. *J. Am. Chem. Soc.* **1993**, *115*, 7911-7977.
- (184) Guajardo, R. J.; Chavez, F.; Farinas, E. T.; Mascharak, P. K. *J. Am. Chem. Soc.* **1995**, *117*, 3883-3884.
- (185) Ghosh, K.; Eroy-Reveles, A. A.; Avila, B.; Holman, T. R.; Olmstead, M. M.; Mascharak, P. K. *Inorg. Chem.* **2004**, *43*, 2988-2997.
- (186) Noveron, J. C.; Olmstead, M. M.; Mascharak, P. K. *J. Am. Chem. Soc.* **2001**, *123*, 3247-3259.
- (187) López, J. P.; Kämpf, H.; Grunert, M.; Gütlich, P.; Heinemann, F. W.; Prakash, R.; Grohmann, A. *Chem. Commun.* **2006**, 1718-1720.
- (188) He, C.; Barrios, A. M.; Lee, D.; Kuzelka, J.; Davydov, R. M.; Lippard, S. J. *J. Am. Chem. Soc.* **2000**, *122*, 12683-12690.
- (189) Mizoguchi, T. J.; Lippard, S. J. *J. Am. Chem. Soc.* **1998**, *120*, 11022-11023.
- (190) Chaudhury, P.; Wieghardt, K.; Nuber, B.; Weiss, J. *Angew. Chem. Int. Ed. Engl.* **1985**, *24*, 778-779.

BIBLIOGRAPHY

- (191) Cohen, J. D.; Payne, S.; Hagen, K. S.; Sanders-Loehr, J. *J. Am. Chem. Soc.* **1997**, *119*, 2960-2961.
- (192) Yoshida, T.; Thorn, D. L.; Okano, T.; Ibers, J. A.; Otsuka, S. *J. Am. Chem. Soc.* **1979**, *101*, 4212.
- (193) McClintock, L. F.; Cavigliasso, G.; Stranger, R.; Blackman, A. G. *Dalton Trans.* **2008**, 4984-4992.
- (194) Cheyne, S. E.; McClintock, L. F.; Blackman, A. G. *Inorg. Chem.* **2006**, *45*, 2610-2618.
- (195) Manewa, M. *Monatsh. Chem.* **1976**, 337-343.
- (196) Boumizane, K.; Herzog-Cance, M. H.; Jones, D. J.; Pascal, J. L.; Potier, J.; Roziere, J. *Polyhedron* **1991**, *10*, 2757-2769.
- (197) Gantar, D.; Rahten, A. *J. Therm. Anal.* **1990**, *36*, 553-558.